

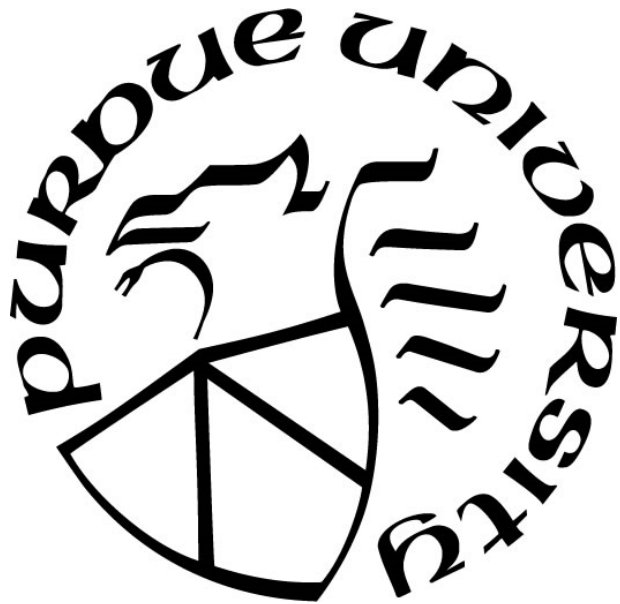
**A SEQUENTIAL APPROACH FOR ACHIEVING SEPARATE SENSIBLE
AND LATENT COOLING**

by
Jie Ma

A Dissertation

*Submitted to the Faculty of Purdue University
In Partial Fulfillment of the Requirements for the degree of*

Doctor of Philosophy



Lyles School of Civil Engineering

West Lafayette, Indiana

August 2021

**THE PURDUE UNIVERSITY GRADUATE SCHOOL
STATEMENT OF COMMITTEE APPROVAL**

Dr. W. Travis Horton, Chair

Lyles School of Civil Engineering

Dr. Ming Qu

Lyles School of Civil Engineering

Dr. James E. Braun

School of Mechanical Engineering

Dr. Eckhard A. Groll

School of Mechanical Engineering

Approved by:

Dr. Dulcy M. Abraham

BENCH OF CONTENTS

LIST OF TABLES.....	6
LIST OF FIGURES	7
ABSTRACT.....	11
1. INTRODUCTION	12
1.1 Background and Motivation	12
1.2 Overall Objective and Approach	14
1.3 Thesis Outline	17
2. LITERATURE REVIEW	19
2.1 Review of Previously Developed SSLC System	19
2.1.1 Vapor-compression Cycle with Liquid/Solid Desiccant	19
2.1.2 Vapor-compression Cycle with Desiccant Wheel	21
2.1.3 Parallel Vapor Compression Systems.....	22
2.1.4 Variable Speed Direct Expansive A/C Unit	23
2.1.5 Discussion.....	24
2.2 Review of Temperature and Humidity Control	25
2.2.1 Multiple Sub-systems	26
2.2.2 SHR Matching Control.....	27
2.2.3 Variable Speed DX A/C System.....	29
2.3 System Performance Model for Variable Speed A/C Units	30
2.3.1 Integrated Component Models	30
2.3.2 Polynomial Model	34
2.3.3 Neural Network Models	36
2.3.4 Summary.....	36
2.4 Review of Component Models of Vapor Compression Cycle.....	37
2.4.1 Compressor Model.....	37
2.4.2 Heat Exchanger Model	39
2.5 Co-simulation Approaches Combining Building and HVAC Systems	44
2.6 Summary and Contributions of the Current Work.....	45

3.	MODEL DEVELOPMENT.....	47
3.1	SSLC Model Development.....	47
3.1.1	Compressor Model.....	48
3.1.2	Condenser Model.....	49
3.1.3	Expansion Valve Model	53
3.1.4	Evaporator Model	53
3.1.5	Integrated SSLC System Model	55
3.1.6	Re-evaporation Model	58
3.2	Residential Building Model Development.....	60
3.2.1	Building Characteristics.....	61
3.2.2	Simulation in TRNSYS	64
3.3	Residential Building Model Simplification	65
3.3.1	Thermal Model Simplification	65
3.3.2	Moisture Model Simplification.....	69
3.3.3	Simplified Residential Building Model Training	70
3.4	Summary.....	76
4.	EXPERIMENTS AND MODEL VALIDATION.....	77
4.1	Experimental Description	77
4.1.1	Experiment Set-up	77
4.1.2	Testing Conditions.....	81
4.1.3	Test Data Calculation and Uncertainty Analysis.....	83
4.2	SSLC system Model Validation.....	85
4.2.1	Compressor Model Validation.....	86
4.2.2	Evaporator Model Validation	88
4.2.3	SSLC System Model Validation.....	90
4.2.4	Re-evaporation model validation.....	92
4.3	Modeling Results and Energy Saving Potential.....	94
4.3.1	Modeling Results under Special Boundary Conditions.....	94
4.3.2	Energy Saving Potential	97
4.4	SSLC Model Simplification with Artificial Neural Network.....	99
4.4.1	Initial Neural Network Generation	100

4.4.2	ANN Model Training	103
4.4.3	ANN Model Training Results.....	104
4.5	Summary.....	107
5.	SSLC CONTROL STRATEGIES.....	108
5.1	Baseline Simulation	108
5.2	Co-Simulation of Cooling System and Building under SSLC Control Strategies.....	112
5.3	Control Strategy 1 – Mode Switch with Constant Equipment Speeds	114
5.3.1	Compressor Speed and Supply Fan Speed Determination	115
5.3.2	Thermostat Priority Control.....	118
5.3.3	Humidistat Priority Control	123
5.4	Control Strategy 2 – Load Prediction Control with Variable Equipment Speeds	127
5.4.1	Sensible Load Estimation	128
5.4.2	Compressor and Supply Fan Speed Determination.....	131
5.4.3	Simulation Results.....	135
5.5	Summary.....	138
6.	ENERGY PERFORMANCE AND COMFORT DELIVERY ANALYSIS.....	139
6.1	Case Study for Cool and Humid Clime Zone — Indianapolis	139
6.2	Case Study for Cool and Dry Clime Zone — Denver	145
6.3	Case study for Hot and Humid Clime Zone — Miami.....	149
6.4	Case study for Hot and Dry Clime Zone — Phoenix	153
6.5	Case study for Marine Climate Zone—Seattle.....	157
6.6	Summary.....	161
7.	SUMMARY AND FUTURE WORK.....	163
7.1	Summary.....	163
7.2	Future Work.....	166
	REFERENCES	168

LIST OF TABLES

Table 2.1. Model input–output forms.	31
Table 3.1. Fin-tube geometry information for condenser and evaporator.	50
Table 3.2. Heat transfer correlations in condenser and evaporator model.....	50
Table 3.3. Building envelope material data.	62
Table 3.4. Building window data.....	62
Table 3.5. Specific leakage area.	63
Table 3.6. Non-zero element in matrix A	68
Table 3.7. Non-zero element in matrix B	68
Table 4.1. The model and uncertainty of measurement sensors.	81
Table 4.2. Values of parameters used in compressor model.....	86
Table 4.3. Neural network training accuracy for different numbers of hidden layers and neural nodes.	104
Table 6.1. Energy performance under different control strategies in Indianapolis throughout summer.....	140
Table 6.2. Comfort Delivery under different control strategies in Indianapolis throughout summer.	141
Table 6.3. Energy performance under different control strategies in Denver throughout summer.	145
Table 6.4. Comfort Delivery under different control strategies in Denver throughout summer.	146
Table 6.5. Energy performance under different control strategies in Miami throughout summer.	150
Table 6.6. Comfort Delivery under different control strategies in Miami throughout summer.	150
Table 6.7. Energy performance under different control strategies in Phoenix throughout summer.	154
Table 6.8. Comfort Delivery under different control strategies in Phoenix throughout summer.	154
Table 6.9. Energy performance under different control strategies in Seattle throughout summer.	158
Table 6.10 Comfort Delivery under different control strategies in Seattle throughout summer.	158

LIST OF FIGURES

Figure 1.1. Two typical A/C unit operation modes for sequential SSLC system: (a) Low SHR mode (Deep dehumidification); (b) Sensible only mode.....	15
Figure 2.1. A hybrid solar air conditioning system realizing SSLC.....	20
Figure 2.2. Two Parallel SSLC system : (a) Serial configuration; (b) Parallel configuration.....	23
Figure 2.3. Traditional A/C system temperature and humidity control procedure.....	26
Figure 2.4. Direct expansion cooling mode system.....	33
Figure 2.5. Fin-tube geometry sketch.	41
Figure 3.1. Program flow chart of integrated SSLC system.	57
Figure 3.2. Prototype residential building generated in SketchUp.	61
Figure 3.3. Building sensible and latent internal heat gain.....	64
Figure 3.4. Thermal network for the prototypical residential building.....	66
Figure 3.5. Moisture network for building model.....	69
Figure 3.6. U.S. climate zones and cities chosen to calibrate simplified building model.	72
Figure 3.7. Indoor temperature comparison for state-space thermal model and TRNSYS in Phoenix, Miami, Indianapolis and Denver.....	73
Figure 3.8. Indoor humidity ratio comparison for state-space moisture model and TRNSYS in Phoenix, Miami, Indianapolis and Denver.	74
Figure 4.1. Testing system set-up at the refrigerant side.	78
Figure 4.2. Location of sensors at refrigerant line: pressure transducer, thermocouple and mass flow meter.	78
Figure 4.3. Experiment set-up on the air side.	80
Figure 4.4. Sensors location on the air side: thermogrid for drybulb temperature, dew-point hygrometer.	80
Figure 4.5. Testing conditions on the psychometric chart.	82
Figure 4.6. Compressor model validation of mass flow rate.	87
Figure 4.7. Compressor model validation of compressor power.....	87
Figure 4.8. Evaporator model validation of cooling capacity.....	89
Figure 4.9. Evaporator model validation of SHR.	89
Figure 4.10. Evaporator model validation of air out-flowing temperature.....	90

Figure 4.11. Integrated SSLC model validation of cooling capacity.....	91
Figure 4.12. Integrated SSLC model validation of SHR.	91
Figure 4.13. Integrated SSLC model validation of COP	92
Figure 4.14. Re-evaporation model calibration.	93
Figure 4.15. One case of developed SSLC model simulation for cooling capacity.	95
Figure 4.16. One case of developed SSLC model simulation for SHR.....	96
Figure 4.17. One case of developed SSLC model simulation for COP.....	96
Figure 4.18. Energy consumption with different dehumidification times.....	99
Figure 4.19. Neural network structure of developed SSLC system.....	101
Figure 4.20. Comparison of validating data between ANN model and physical-based SSLC model for cooling capacity.....	105
Figure 4.21. Comparison of validating data between ANN model and physical-based SSLC model for SHR.	106
Figure 4.22. Comparison of validating data between ANN model and physical-based SSLC model for total power input.....	106
Figure 5.1. Building and SSLC system co-simulation framework of baseline.....	109
Figure 5.2. Indoor temperature and relative humidity simulation of baseline on July 4 th	111
Figure 5.3. Indoor temperature and relative humidity simulation of baseline on July 26 th	112
Figure 5.4. Co-simulation structure connecting SSLC system and prototype building under SSLC control strategies.	114
Figure 5.5. Sensible and latent hourly average load of prototype building throughout summer under Indianapolis weather conditions.	116
Figure 5.6. Sensible load line generation.....	116
Figure 5.7. Total capacity and SHR contour under full ranges of compressor speed ratio and supply air flow rate.	117
Figure 5.8. Control logic framework for thermostat priority control.	119
Figure 5.9. Indoor temperature and absolute humidity response to thermostat priority control on July 4 th	121
Figure 5.10. A/C unit performance under thermostat priority control on July 4 th	121
Figure 5.11. Indoor temperature and absolute humidity response to thermostat priority control on July 26 th	122
Figure 5.12. A/C unit performance under thermostat priority control on July 26 th	123
Figure 5.13. Control logic framework for humidistat priority control.	124

Figure 5.14. Indoor temperature and absolute humidity response to humidistat priority control on July 4 th	125
Figure 5.15. A/C system performance under humidistat priority control on July 4 th	126
Figure 5.16. Indoor temperature and absolute humidity response to humidistat priority control on July 26 th	127
Figure 5.17. A/C system performance under humidistat priority control on July 26 th	127
Figure 5.18. Total capacity and SHR contour under full ranges of equipment speeds in the situation that no SHR equals to 1.	134
Figure 5.19. Total capacity and SHR contour under full ranges of equipment speeds in the situation that larges region shows SHR equals to 1.....	134
Figure 5.20. Indoor temperature and absolute humidity response to load prediction control on July 4 th	136
Figure 5.21. A/C system performance under load prediction control on July 4 th	136
Figure 5.22. Indoor temperature and absolute humidity response to load prediction control on July 26 th	137
Figure 5.23. A/C system performance under load prediction control on July 26 th	137
Figure 6.1. Indoor temperature and humidity simulation for baseline in Indianapolis.....	143
Figure 6.2. Indoor temperature and humidity response to thermostat priority control in Indianapolis.	143
Figure 6.3. Indoor temperature and humidity response to humidistat priority control in Indianapolis.	144
Figure 6.4. Indoor temperature and humidity response to SSLC control strategy 2 in Indianapolis.	144
Figure 6.5. Indoor temperature and humidity simulation for baseline in Denver.....	147
Figure 6.6. Indoor temperature and humidity response to thermostat priority control in Denver.	148
Figure 6.7. Indoor temperature and humidity response to humidistat priority control in Denver.	148
Figure 6.8. Indoor temperature and humidity response to SSLC control strategy 2 in Denver..	149
Figure 6.9. Indoor temperature and humidity simulation for baseline in Miami.....	151
Figure 6.10. Indoor temperature and humidity response to thermostat priority control in Miami.	152
Figure 6.11. Indoor temperature and humidity response to humidistat priority control in Miami.	152

Figure 6.12. Indoor temperature and humidity response to SSLC control strategy 2 in Miami.	153
Figure 6.13. Indoor temperature and humidity simulation for baseline in Phoenix.	155
Figure 6.14. Indoor temperature and humidity response to thermostat priority control in Phoenix.	156
Figure 6.15. Indoor temperature and humidity response to humidistat priority control in Phoenix.	156
Figure 6.16. Indoor temperature and humidity response to SSLC control strategy 2 in Phoenix.	157
Figure 6.17. Indoor temperature and humidity simulation for baseline in Seattle.	159
Figure 6.18. Indoor temperature and humidity response to thermostat priority control in Seattle.	160
Figure 6.19. Indoor temperature and humidity response to humidistat priority control in Seattle.	160
Figure 6.20. Indoor temperature and humidity response to SSLC control strategy 2 in Seattle.	161

ABSTRACT

Current air conditioning systems generally operate with a relatively fixed moisture removal capacity, and indoor humidity conditions are usually not actively controlled in most buildings. If we focus only on sensible heat removal, an air conditioning system could operate with a fairly high evaporating temperature, and consequently a high coefficient of performance (COP). However, to provide an acceptable level of dehumidification, air conditioners typically operate with a much lower evaporating temperature (and lower COP) to ensure that the air is cooled below its dew point to achieve dehumidification. The latent (moisture related) loads in a space typically only represent around 20-30% of the total load in many environments; however, the air conditioning system operates 100% of the time at a low COP to address this small fraction of the load. To address issues associated with inadequate dehumidification and high energy consumption of conventional air conditioning systems, the use of a separate sensible and latent cooling (SSLC) system can dramatically increase system COP and provide active humidity control. Most current SSLC approaches that are reported in the literature require the installation of multiple components or systems in addition to a conventional air conditioner to separately address the sensible and latent loads. This approach increases the overall system installation and maintenance costs and complicates the controller design.

A sequential SSLC system is proposed and described in this work takes full advantage of readily available variable speed technology and utilizes independent speed control of both the compressor and evaporator fan, so that a single direct expansion (DX) air-conditioning (A/C) system can be operated in such a way to separately address the sensible and latent loads in a highly efficient manner. In this work, a numerical model of DX A/C system is developed and validated through experiential testing to predict the performance under varied equipment speeds and then used to investigate the energy saving potential with the implementation of the proposed sequential SSLC system. To realize the sequential SSLC system approach, various corresponding control strategies are proposed and explained in this work that minimizes energy consumption while provides active control over both space temperature and relative humidity. At the end of this document, the benefits of applying the SSLC system in a prototype residential building under different typical climate characteristics are demonstrated.

1. INTRODUCTION

1.1 Background and Motivation

Improving the energy efficiency of air-conditioning systems has recently become an important topic. According to the annual energy outlook (EIA, 2019), space cooling by mechanical air-conditioning systems for residential and commercial buildings accounted for 16% and 11% of the sector electricity consumption, respectively in 2019; and these percentages are anticipated to continue growing. In building air conditioning systems, significant energy consumption usually occurs in the process of removing the cooling load of a building to meet thermal comfort requirements for the indoor environment, which includes two parts: the sensible load removal and the latent load removal. The sensible load can be removed by cooling down the supply air and then mixing it with the space air; to overcome the latent load, however, the air-conditioner must also remove the water vapor (latent load) in the building. A conventional air conditioning system usually meets these two types of space cooling loads at the same time. Firstly, the return air is cooled to a low temperature (below the dew-point temperature of the space air and much lower than the supply air temperature), and then the supply air is sent back to the building after being re-heated to an appropriate and comfortable temperature level. Such a process in conventional air-conditioning systems is inherently costly and energy inefficient since it cost a great amount of energy to overcool the flowing through air and extra energy for re-heating the supply air under comfortable temperature condition.

Furthermore, most direct expansive (DX) air conditioner (A/C) units are currently equipped with single speed compressors and supply fans, where both cooling and dehumidification processes are conducted in a single cooling coil simultaneously, which makes it impossible to have the sensible and latent capacities being coordinated based on the space requirements. To maintain the space thermal comfort conditions, the DX A/C unit with fixed speed compressor and supply fan relies on the simplest and low-cost approach, on-off cycling compressor, to only control space temperature, which can result in either over or under dehumidified situations.

Even in variable speed equipment that is widely implemented nowadays, the supply fan speed is usually locked with the compressor speed to maintain a fixed equipment sensible heat ratio (SHR), i.e., the ratio of sensible capacity to the total capacity, for the whole cooling system.

The use of this locking mechanism makes it difficult to meet the sensible and latent load of building separately and may lead to over-dehumidification or under-dehumidification in the building depending on the different sensible and latent load characteristics.

Instead of the conventional air conditioning system, a separate sensible and latent cooling (SSLC) system has been proposed to provide an opportunity of mitigating the negative effects of high relative humidity in the space while simultaneously reducing the energy consumption. A number of different SSLC approaches were proposed in previous literature. The first approach is to incorporate a solid/liquid desiccant and a desiccant wheel into a conventional compression-expansive cycle (CX) air-conditioning (A/C) system, in which the CX is used for sensible load removal and the solid or liquid is used to meet the space latent load. However, to address some issues associated with these hybrid systems (such as the additional energy that is required for the desiccant regeneration process, application is limited to locations with hot and humid weather conditions). A second approach was proposed, which adds auxiliary systems to the traditional cooling system, such as a chilled ceiling or radiant panel for auxiliary sensible cooling. It has two parallel vapor-compression sub-systems: one for sensible load removal and one for latent load removal. In most aforementioned SSLC systems, there are two sub-systems: the first sub-system contains a vapor compression cycle that is designed to handle the sensible load only, and that usually involves a high evaporating temperature to increase the system efficiency; and the other sub-system only deals with the latent load and includes another independent cycle, a vapor compression cycle or desiccant-assisted dehumidification cycle. In practice, the fact that a typical SSLC approach requires two vapor-compression systems operating in parallel, however, results in a high initial cost and difficulties in installation (especially for existing building retrofits).

More recently, with the help of existing variable speed equipment and controls, a third type of SSLC approach was proposed. It is found that the required combination of total cooling capacity and equipment SHR (the ratio of sensible capacity to total capacity) can be obtained by changing the compressor and fan speeds simultaneously to match the varying space sensible and latent loads. In details, the increase of the compressor speed leads to the decrease of surface temperature on evaporator coil. Only when coil surface temperature is lower than the dew-point temperature of space air, the water vapor in air stream becomes to condensate on the coil, and the lower the coil surface temperature is, the more moisture is removed from space. When the speed of supply fan decreases, the air flow rate through the evaporator coil decreases and more latent heat transfer can

occurs. Based on experimental data and simulation studies on the characteristics of a variable speed DX A/C unit, a number of studies suggested that better dehumidification can be achieved at a high compressor speed with a low evaporator fan speed. This is because the aforementioned that the lower evaporating temperature, together with a longer resident time of the air in the cooling coil, can facilitate dehumidification.

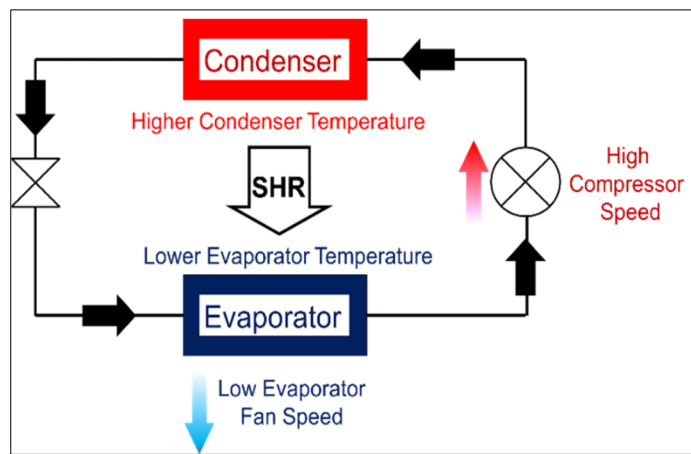
Depending on this A/C unit mechanical characteristics, the method for space temperature and humidity independent control is proposed, which can be realized by varying the compressor to match the total cooling capacity with space cooling load, and changing the speed of supply fan to vary the equipment SHR (the ratio of sensible capacity to total capacity). However, the cooling and dehumidification process taking place in a single coil are coupled and affect each other. Varying both compressor and fan speed independently and simultaneously without considering the coupled effect between cooling and dehumidification will requires more expensive control hardware and tends to suffer from stability problems since the control system needs to continuously vary the equipment speed and run a decoupled MIMO feedback control scheme.

Therefore, a sequential approach for achieving separate sensible and latent cooling (SSLC) could be an appropriate solution to these aforementioned drawbacks. This approach takes the advantage of variable speed technologies and utilizes independent speed control of both the compressor and evaporator fan, so that a single system can be operated in two different conditions sequentially to meet both sensible and latent loads which, in turn can realize energy savings without sacrificing occupant comfort.

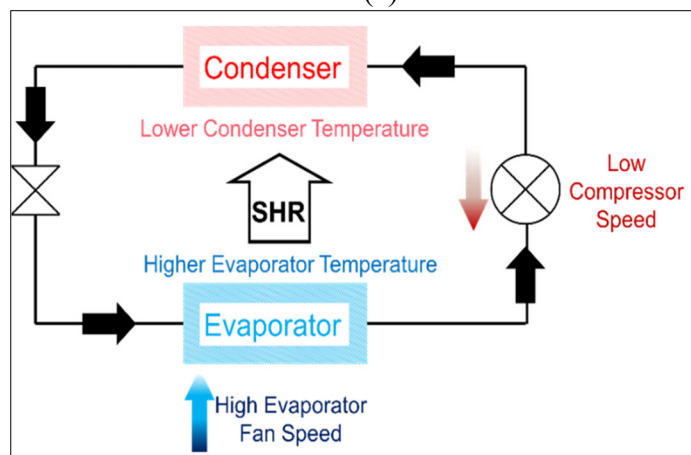
1.2 Overall Objective and Approach

An approach that independently addresses the sensible and latent cooling loads by using only one cooling cycle in a space is a potential methodology for a substantial reduction of cooling energy consumption in residential and commercial buildings. Specifically, the system can be operated in two different modes (shown in Figure 1.1): one is a low-SHR mode (the latent-load removal mode) and the other is a sensible-only mode. The first operating mode is realized by increasing the compressor speed and decreasing the evaporator fan speed, in which the evaporator temperature is much lower than dew-point temperature of the return air to allow moisture to be removed from the air stream effectively. In this operating mode, the evaporator temperature is taken very low and the pressure ratio of the vapor compression cycle is increased. The second

operating mode (i.e., the sensible-load removal mode), on the other hand, requires a low compressor speed and a high evaporator fan speed, which elevates the evaporating temperature to a point higher than the dew-point temperature of space air and reduces the cycle pressure ratio, thus the system has higher efficiency in this mode. Depending on these characteristics of the two modes, there is high energy-savings potential for a separate sensible and latent cooling system that works sequentially by operating most of the time in the sensible-only cooling mode but shifts to the low sensible heat ratio (low-SHR) mode for a short period of time depending on the latent load required to be removed from the space. In fact, when using continuously variable speed cooling equipment, there are an infinite number of strategies for operation that will take care of both the sensible and latent loads in the space.



(a)



(b)

Figure 1.1. Two typical A/C unit operation modes for sequential SSLC system: (a) Low SHR mode (Deep dehumidification); (b) Sensible only mode.

Thus, with a development of appropriate control logic, the sequential SSLC system can be applied as a low-cost and energy-efficient approach for practical HVAC applications. Through carefully controlling the operation of each mode, the following benefits can be achieved:

- the sensible and latent cooling load in a space can be addressed separately and independently using a single vapor-compression cycle, which can reduce the system complexity as well as the initial installation and maintenance cost;
- considerable energy-savings can be achieved by controlling the system to be operated in the sensible-only mode (i.e., the mode with higher efficiency) as long as possible while operating in the low-SHR mode just long enough to meet the required latent load removal;
- the proposed SSLC system shifts the latent load to the low-SHR mode and does not necessarily need to meet the sensible and latent loads in the space during short time intervals, but only integrated across a desirable time horizon. Additionally, the equipment speed varies only when the mode is switched, which can simplify the system controls.

To achieve the aforementioned benefits, the main objectives for this research are to develop a sequential SSLC system, evaluate its performance, and optimize the control strategies of the system for different cooling load conditions:

(1) Develop a numerical SSLC system model to predict A/C system cooling performance in the two operation modes (the latent-load-removal mode and sensible load-removal mode). Since the cooling and dehumidification processes couple with each other and be determined by the speed of compressor and speed of supply fan together with the evaporator inlet air conditions, the characteristics of DX A/C unit performance under equipment speeds and boundary conditions (evaporator inlet air conditions) are required to be verified.

(2) Validate the numerical SSLC system model using experimental data under different combination of equipment speed, as well as indoor and outdoor operating conditions. Conducting the experiments under different evaporator inlet air conditions at a fixed compressor and supply fan speed, or different speed combinations of compressor and supply fan under a fixed evaporator inlet air condition is necessary to observe the performance of A/C unit operating under two proposed SSLC system modes. Furthermore, the experimental data can be used for developed SSLC model training and validation.

(3) Map the variable speed DX A/C unit performance by Artificial Neural Network (ANN) model. The developed physical based SSLC model is very complex and difficult to use in the system control. Thus, simplifying the original SSLC system into an ANN model that only containing multiple parameters can significantly increase the computational speed of SSLC system simulation when it is coupled with building models.

(4) Develop an appropriate control strategy for sequential SSLC systems and compare to a suitable energy consumption baseline. Since application of the proposed SSLC system is depended on the proper A/C system control, two control strategies based on the currently existing control logic are proposed. The simulation coupling the SSLC model and building model is conducted to research the SSLC system performance and the conditioned spaced response.

(5) Investigate SSLC system performance and energy efficiency in different climate zones and evaluate the impact on indoor comfort from the sequential SSLC system.

1.3 Thesis Outline

Based on the above-mentioned objectives, this thesis is organized as follows:

Chapter 1 introduces the background and motivation of proposing the sequential SSLC system with a single vapor compression system, and briefly describes the basic approach and lists the specific objectives of the current work.

In Chapter 2, a comprehensive literature review is presented which covers the current existing SSLC systems, the logic of temperature and humidity independent control, and commonly used numerical models for various components in a vapor compression cycle. Through reviewing the publication, the contributions of this research can be understood more clearly.

Chapter 3 explains the numerical model for the sequential SSLC system, which can, in turn, be used to predict the performance and energy consumption of the two operation modes, the low-SHR mode and the sensible-only mode. Since the performance prediction relies on the targeted building characteristics, a TRNSYS model of a residential building is developed and described in this chapter. However, using the TRNSYS model to calculate the temperature and humidity response of the building requires a computational time that is impractically long for such simulations. Therefore, the building response model used in the presented simulations is a simplified linear steady-state model and it is validated using the results from the TRNSYS model.

Chapter 4 describes the experiments that have been carried out to validate the component models for the compressor, condenser, and evaporator separately as well as the SSLC system model developed in Chapter 3. It is demonstrated that the model predicted performance of the proposed sequential SSLC system is accurate under a reasonably wide range of operating conditions and indoor environments. The energy saving potential of SSLC system application is verified and explained. Furthermore, the original SSLC system is mapped into an ANN model to simplify the model construction and pave the way for further simulation application.

The main work in Chapter 5 is to propose two different control strategies for the sequential SSLC system to reduce energy cost and at the same time improve indoor thermal comfort. The control strategies are implemented on an A/C unit applying SSLC approach, which the numerical model used to predict A/C unit performance is combined with the simplified building thermal and moisture model. In each sequential SSLC control strategy, it is mainly to explain the approach selecting SSLC operation mode (sensible-only mode or deep-dehumidification mode) and determining the compressor speed and indoor fan speed of A/C system at each time step.

After the numerical model for the sequential SSLC system is developed and validated in the Chapter 3 and Chapter 4, and the corresponding control strategies are also proposed and explained in Chapter 5, Chapter 6 is to simulate the energy consumption and comfort delivery for sequential SSLC system implementation in five cities representing various climate characteristics.

2. LITERATURE REVIEW

The purpose for the first part of this chapter is to review different SSLC systems that have been developed and studied in the past. Based on this review, the drawbacks of previously developed SSLC systems are made clear as compared with the proposed sequential SSLC system. A comprehensive literature review presented in the second part is focused on the numerical methods that can be used for modeling the various components in a vapor compression cycle and can provide guidance for developing the sequential SSLC system model. And lastly, a literature review for temperature and humidity control in a space that is presented which can be modified to develop different SSLC control strategies proposed in the current work.

2.1 Review of Previously Developed SSLC System

In the past, many different SSLC systems were proposed to reduce the energy costs of conventional air-conditioners and to improve the resulting thermal comfort in a space. Generally speaking, all these SSLC systems are realized by including another parallel system only for latent cooling in addition to a conventional vapor compression system. The following section introduces some previously proposed hybrid systems to realize separate sensible and latent cooling.

2.1.1 Vapor-compression Cycle with Liquid/Solid Desiccant

Yadav (in 1995) proposed a hybrid solar air conditioning system including two systems: a conventional vapor-compression(V-C) cycle and a liquid-desiccant cycle (shown in Figure 2.1). In this hybrid system, the vapor-compression system uses R-11 as the refrigerant and only handles the sensible load in space. The liquid-desiccant is circulated between the condenser and evaporator, in which water-LiBr is used as the liquid desiccant for latent heat removal. Considering the whole hybrid system, the condenser of the V-C system is used for partial regeneration of the desiccant in an open dehumidification cycle and the V-C's evaporator surface is used as the absorber for the liquid-desiccant cycle. Moreover, another heat-exchanger is added in the liquid desiccant cycle in order to pre-cool the hot desiccant after leaving the regenerator section and pre-heat the desiccant leaving the absorber. Yadav also showed that this hybrid system can achieve an 80% energy-saving

and a 90% latent removal by eliminating the reheat process of the conventional air condition, and is suitable for hot and humid climates or high latent loads spaces.

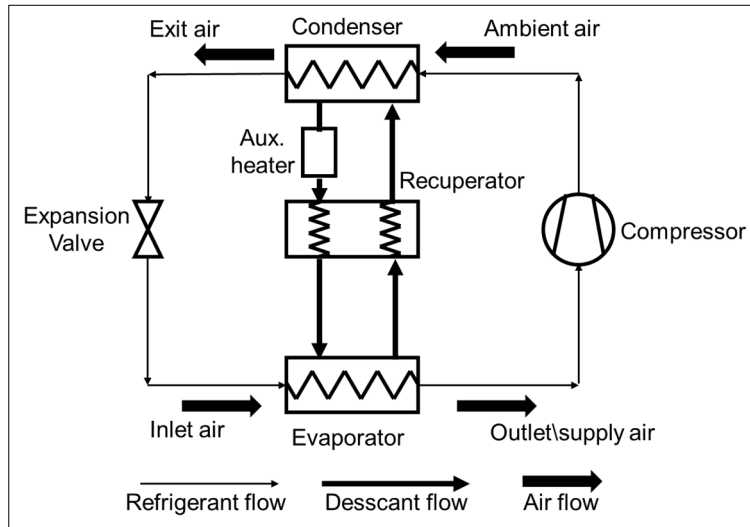


Figure 2.1. A hybrid solar air conditioning system realizing SSLC.

Different from Yadav's liquid desiccant system, Dai et al., (2001) proposed another hybrid system including three cycles. The first one is similar to the conventional V-C cycle which consists of compressor, condenser, expansion valve and evaporator, and is used primarily to remove the sensible heat in space. The second cycle is a liquid desiccant cycle with a dehumidifier, which is used to deal with the latent load of the flow-through air stream. And the last one is a regenerator and cooling water cycle, and it is used to cool down the regenerated liquid desiccant. Based on the experience, they showed that 42.9% energy-saving can be achieved at the compressor side, and the COP of the whole system increases 55.2% under the operating outdoor condition of 35°C, 40% and indoor condition of 35°C, 50.5%. In order to save the energy required by the liquid desiccant regeneration, Katejanekarn & Kumar (2008) applied a solar-regenerated liquid desiccant system for dehumidification of ventilation air. This liquid desiccant assisted system is more suitable for hot and humid climate zones, in which the air stream is dehumidified and then sent to the cooling coils of evaporator. It was also claimed that by carefully selecting the operating parameters for the equipment, the solar-regenerated liquid desiccant system is a significant contributor to the energy savings in dehumidification.

Dhar & Singh (2001) simulated the performance of two different configurations of a hybrid system, which includes a solid desiccant wheel and a vapor compression cycle. This idea is originally proposed by Burn et al., (1985), one of the earliest researchers studying solid desiccant-based hybrid cooling systems. The first configuration of the hybrid system is reformed to a ventilation-condenser cycle, where only fresh air is passed through the dehumidifier, accounting for 10% - 20% of the total supply air. The dehumidified fresh air is indirectly cooled down after flowing out of the dehumidifier and is then mixed with the space return air for further cooling until the mixed air meets the required conditions of the supply air. The second one is named a recirculation-condenser cycle, where the difference is that the fresh air is mixed with the space return-air and then sent to the dehumidifier together. Based on the simulated performance for these different systems, Dhar & Singh (2001) made a conclusion that the maximum energy-saving can reach 63.15% when the hybrid system operates under hot and dry weather conditions with 0.75 load sensible heat ratio (SHR), and there is still energy-savings of around 46.6% with load SHR of 0.35.

In the Dhar & Singh (2001) proposed system, considerable energy is consumed during the regeneration of the desiccant. Thus, renewable energy, such as solar energy or geo-thermal energy, is a good replacement for electric heating for the regeneration process. Khalid et al., (2016) conducted some experimental and simulation studies, based on the weather data of Pakistani cities to study the performance of a solar assisted pre-cooled hybrid desiccant cooling systems and to analyze the life cycle cost of the air collector. It is concluded that only three months of the total seven-month cooling season can apply the solar assisted pre-cooled hybrid desiccant cooling system without any other auxiliary cooling unit. Also, the energy and environmental payback periods of solar collector can be only one year or one-and-half year.

2.1.2 Vapor-compression Cycle with Desiccant Wheel

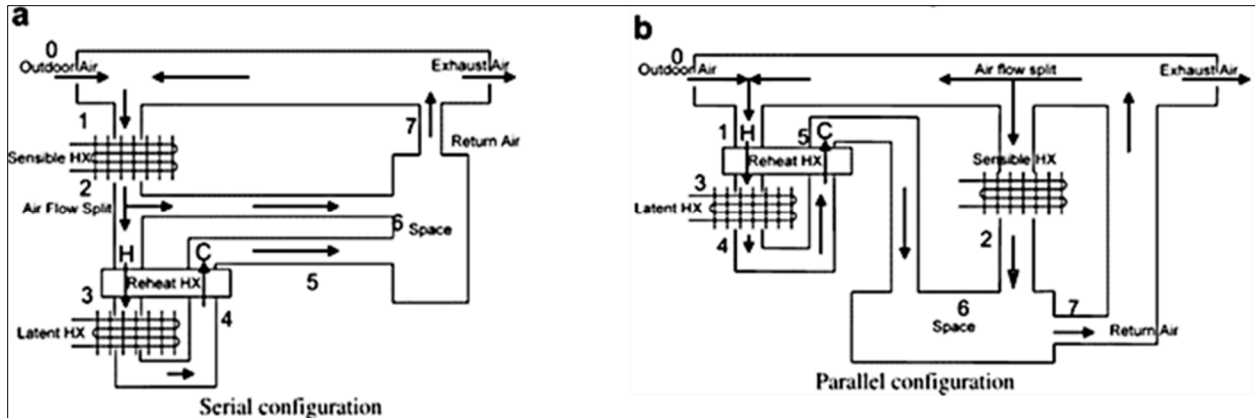
Jia et al., (2007) also carried out some experimental studies of a desiccant wheel (DW) assisted system with various heat sources to provide hot regeneration air. In their experiments, an electric heater and an electro thermal humidifier are used for pretreatment of the air before it enters the desiccant system. Then, the air stream is dehumidified in the desiccant wheel and is sent to the evaporator and cooled down to the needed temperature. Based on the experimental results and the

validated numerical model, it is found that the electric power consumption in the hybrid desiccant system is significantly reduced when the vapor compression system SHR is increased.

The primary challenge of an SSLC system with a desiccant is that the regeneration of the desiccant requires additional energy costs. Thus, Ling et al., (2011) performed the experimental evaluation on the performance of a desiccant wheel assisted SSLC system with low regeneration temperature, which uses CO₂ or R-410A as the refrigerant in the vapor compression cycle. The DW is used to remove the latent load only and is regenerated by the out-flow air from the condenser. It is demonstrated that the resulting energy saving is 7% for both R410a and CO₂ when the DW regeneration temperature is 50°C. The energy savings increase to 32% for CO₂ and 34% for R410a respectively when the DW regeneration temperature is reduced to 45°C.

2.1.3 Parallel Vapor Compression Systems

All above mentioned hybrid SSLC systems, either using a liquid desiccant or a solid rotatory desiccant wheel, need additional energy for the regeneration of the desiccant and they usually involve complicated system structures. Based on these concerns Ling et al., (2010) proposed a new SSLC system which includes two parallel vapor-compression systems as shown in Figure 2.2: one is mainly used for the space sensible load removal and the other handles the space latent load. They designed two different configurations: a serial configuration and a parallel configuration. In the serial configuration, fresh air from the outdoors and return air from space are firstly mixed together and then the mixed air goes through the sensible heat exchanger. After flowing out from the sensible exchanger, it is divided into two air streams, one stream is sent to the space directly; the other one enters the latent heat exchanger and re-heater before going into the space. In the parallel configuration, however, the recirculated air from space is split into two air streams before mixing with the fresh air from the outdoors, one air stream passes through the sensible heat exchanger and the other one mixed with fresh air and goes through latent heat exchanger. For both configurations, the sensible cooling system can be operated at an evaporator temperature higher than that in a conventional air conditioner, resulting in saving more energy and improving the total system COP.



(a)

(b)

Figure 2.2. Two Parallel SSLC system : (a) Serial configuration; (b) Parallel configuration.

In 2013, Ling et al., proposed to use heat recovery wheels (sensible wheel (SW) or enthalpy wheel(EW)) to replace one of the parallel vapor compression systems. The basic operation process for this heat recovery wheel integrated SSLC system is that, taking the EW as an example, the hot and humid ambient air enters the EW first and it exchanges the sensible heat and moisture with the relatively cold and dry return air stream from the space. At this stage, both the sensible load and latent load are partially removed from the air stream before it enters the evaporator of a conventional vapor compression system. For a SW system, it is very similar to the EW, except that only the sensible heat is transferred between the two air streams without any mass transfer.

2.1.4 Variable Speed Direct Expansive A/C Unit

Li and Deng (2007) studied the on the inherence operational characteristics of a direct air condition unit. They did an experiment to vary compressor and supply fan speeds at fixed inlet conditions of 24°C air dry-bulb temperature and 50% relative humidity. It was observed that a lower equipment SHR is achieved at a fixing compressor speed but running a lower supply fan speed, in which situation the dehumidification is more effective. It is also found that SHR is significantly changed through varying the supply fan speed at a given compressor speed, although the total cooling capacity does not change significantly. Based on this paper, it is seen that the equipment SHR can be effectively changed through the compressor speed and supply fan speed, in which way the building environment sensible and latent environment can be well controlled.

Xu et al., (2010) conducted another experiment to study on the inherent correlation between the total cooling capacity and the equipment SHR of a variable speed DX A/C unit. But different from Deng's experiment, Xu conducted the experiments also under different evaporator inlet air at a fixed compressor and supply fan speed, different speed combinations of compressor and supply fan. They found that not only the equipment speed (compressor speed and supply fan speed), but also the indoor inlet conditions (temperature and humidity) also significantly affect the unit total capacity and equipment SHR. They also noticed that the total output capacity and equipment SHR of the variable speed unit are strongly coupled and mutually constrained within a nonlinear relationship. In 2017, Xia et al., conducted a follow up experiment to study on the inherent operational characteristics of a variable DX A/C unit at different combinations of compressor speed and supply fan speed, degree of superheat settings and inlet air states. It showed that, beside the nonlinear relationship between the equipment speeds and total capacity, equipment SHR, the unit operating super heat temperature also impacts the operational stability of the experimental system. A higher compressor speed, a lower supply fan speed, and a lower inlet air temperature or RH all can be result in a system unstable operation.

2.1.5 Discussion

Although the proposed SSLC system can bring about substantial energy-savings and improvement of thermal comfort for a space, as summarized before, the following problems need to be considered in practice:

- For desiccant-assisted hybrid systems, additional energy is needed for the regeneration of the desiccant. For example, another high temperature heat source is necessary to regenerate a silica gel desiccant wheel because of its high regeneration temperature (70°C). Even for some low-temperature regenerators, the regeneration temperature is still around 45°C-50°C, which still results in considerable energy cost for the regeneration process. Although some free heat 12 sources, such as solar energy or CHP waste heat can be used, their applications still suffer from other practical limitations, such as site location.
- Applying a parallel vapor compression system, some sensible load is also removed in the latent load removal coil, which leads to over-cooling in the space. Parallel systems inevitably increase the difficulties in controlling the space temperature and humidity.

- The use of a recovery wheel can pre-cool or pre-dehumidify the fresh air, but does not separate the sensible load and the latent load. This also means that the other vapor compression cycle is still responsible to ensure that the supply air reaches the required temperature and humidity level. Also, the system performance efficiency is limited by the location and weather conditions since it is suitable only for hot and humid weather.

- For all the systems mentioned above, their complicated designs and controls increase the systems installation and maintenance costs; and the use of multiple systems impedes their application for existing building retrofits.

2.2 Review of Temperature and Humidity Control

The main purpose of controlling a HVAC system can be summarized into three aspects: indoor thermal comfort control, indoor air quality control and indoor air pressurization control. Considering the indoor environment comfort, dry-bulb temperature and humidity are two important factors. Most current heat pumps and air conditioners control systems only consider the dry-bulb temperature but leave the indoor humidity free floating with ambient conditions and zone gains. In commercial buildings, the conventional all-air central A/C systems controls the indoor temperature and humidity by cooling, dehumidification and reheat processes. As shown in psychrometric chart in Figure 2.3, the indoor dry temperature is cooled down until it reaches the air dew-point temperature, then the moisture in the air is condensed into liquid state with continuously decreasing the air temperature. Before the conditioned air is sent to the building, it is required to reheat due to its low supply air temperature after dehumidification. However, this air conditioning procedure is not energy friendly. Based on the aforementioned problems, studies on temperature and humidity independent or coupled control were conducted by a number of researchers.

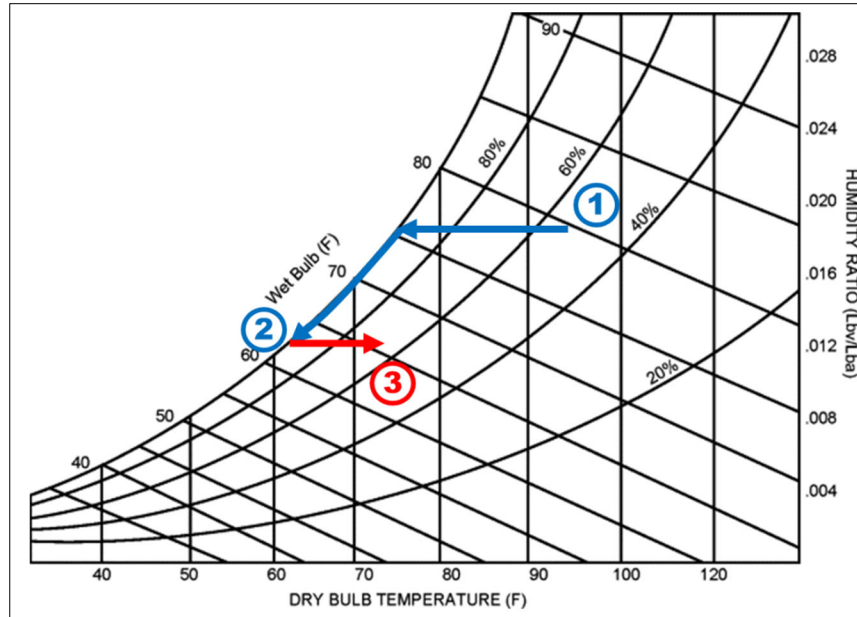


Figure 2.3. Traditional A/C system temperature and humidity control procedure.

2.2.1 Multiple Sub-systems

In the previous section, multiple separate sensible and latent systems are introduced. One of most popular temperature and humidity independent control systems involves dual cooling sources (DCSTHIC). As mentioned in the work conducted by Chen et al., (in 2016), the building sensible load is removed by a high temperature source to control the temperature, and the latent load is removed by a humidity control system. But they also showed that the implementation of a DCSTHIC system requires a limited range of heat moisture ratio and the fresh air ratio. When this limited condition extends the range of heat moisture ratio and the fresh air ratio, the indoor temperature and humidity cannot be controlled well. Han and Zhang (2011) studied a residential temperature-humidity separate control air-conditioner, which includes two evaporating coils: an air cooling evaporator and water cooling evaporator. It concluded that under a certain cooling and dehumidification load ratio, there is a unique set of compressor and refrigerant distribution ratio in air cooling evaporators that can meet both sensible and latent cooling loads in space.

Jiang et al., (2013) proposed a temperature and humidity independent control strategy for a desiccant-assisted air conditioning system. When using a heat pump with a solid or liquid desiccant to handle the latent load, the sensible load is removed separately by the vapor compression (VC) system. For this reason, through controlling the solid or liquid desiccant system

and the VC system, it is possible to realize independent temperature and humidity independent control. In their research, Jiang et al., (2013) conducted some experiments using a variable refrigerant flow (VRF) air conditioning system and heat recovery ventilation system (HRV). The VRF system is used to meet the sensible load in the space and maintain the indoor air dry-bulb temperature, while the HRV system is applied to reduce the moisture in the air stream. Based on the measured data of one month in the summer, it was showed that the indoor humidity can be controlled to be maintained at 11 g/kg, 51% relative humidity.

2.2.2 SHR Matching Control

Some researchers used the sensible heat ratio (SHR) as the control variable, which considers the inherent relation between sensible and latent cooling loads. Li and Deng (2007a) proposed a direct digital control (DDC) algorithm to realize the temperature and humidity separate control which can be implemented on a variable speed direct expansion (DX) air conditioning (A/C) system. Firstly, the control system measures the temperature and RH in the space and predicts the SHR for a conditioned space, which is called the application SHR, by:

$$SHR_{application} = \frac{c_{p,a} \cdot (T_{abd,s} - T_{abd,r})}{h_{a,s} - h_{a,r}} \quad (2-1)$$

where $T_{abd,s}$ and $T_{abd,r}$ are the supply and return air temperature respectively, and $h_{a,s}$ and $h_{a,r}$ are enthalpy of supply and return air. Also, the real-time operating parameters of DX A/C, (such as the pressure of high and low sides, super-heated and sub-cooled temperature), are measured, based on which the equipment SHR can be calculated by:

$$SHR_{equipment} = \frac{c_{p,r} \cdot (T_{evap,out} - T_{evap,in})}{h_{evap,out} - h_{evap,in}} \quad (2-2)$$

here, $h_{evap,in}$ is the refrigerant enthalpy at the evaporator inlet, which is considered to be the same as that at the condenser outlet and can be obtained by measuring the sub-cooled temperature and the condensing pressure; $h_{evap,out}$ is the enthalpy at the evaporator outlet, which can be obtained by measuring the super-heated temperature and evaporating pressure; also the temperature at inlet ($T_{evap,in}$) and outlet ($T_{evap,out}$) of evaporator can be calculated. Finally, the application SHR is forced to match the equipment SHR through varying the compressor speed and supply fan speed.

In 2009, Sekhar and Tan also proposed an SHR matching method to improve cooling and dehumidification performance of over-sized coils. First, the coil performance is evaluated at different operating conditions and for various coil geometries. Then, through changing the effective surface area of the coil in the evaporator, the moisture removal ability can be adjusted, the SHR of the unit and the space cooling load SHR can be controlled to match each other. This method can reduce the unit size, decrease the energy consumption and improve the space humidity control performance to some extent.

Furthermore, Sekhar and Tan (2009) introduced an optimization concept to optimize the energy consumption with thermal comfort as the constraints that ensures the satisfaction of both the sensible and latent load of the space. They developed a simplified and validated simulation DX A/C model to predict the sensible and latent capacity of the unit. Then, five different system control variables are considered: the compressor capacity fraction, condenser fan speed, the supply air flow rate, bypass air around the cooling coil, and the cooling coil face-split circuit. Among these, the first two variables can be controlled to meet the loads according to the outdoor conditions. The last three variables can be controlled to split the sensible and latent load and avoid over-cooling. Moreover, the constraints considered in their work are related to the thermal comfort of the space including indoor set-point of temperature, maximum humidity setpoint, and the minimum and maximum of predicted mean vote (PMV).

The SHR matching control is a good control strategy for meeting both the temperature and humidity set-point of a space and improving the indoor thermal comfort. However, there are some issues that need to be addressed:

- For SHR matching controls, the primary challenge is to simultaneously predict the application SHR and equipment SHR in order to control them to match each other in real time during operation.
- Using SHR as the only control variable may not result in the desired temperature and humidity at the same time, and thus can cause problems such as over-cooling or under dehumidification. This may affect the thermal comfort of the space. Thus, developing a system with multiple control variables and thermal comfort constraints may overcome these drawbacks.
- The SHR matching control is a good strategy that can be applied to sequentially SSLC systems. However, the SHR should not be used as a control variable but the only a parameter indicating the operating mode of the sequentially SSLC system.

2.2.3 Variable Speed DX A/C System

The wide application of variable speed units makes it possible to control the indoor temperature and humidity through varying the equipment speeds (compressor and supply fan). In 2008, Xu et al., proposed a novel control strategy called high-level-low-level control with a variable speed DX A/C unit to overcome the drawbacks of the conventional ON-OFF control. First, the conventional ON-OFF control maintains a fixed equipment SHR leading to insufficient dehumidification for humid and cool indoor conditions; secondly, when the compressor stops but the supply fan keeps running, the evaporator coil becomes an evaporative cooler and carries the condensed water back to building space. While in Xu et al.,'s control strategy, the compressor keeps running at a low speed to avoid a complete shut down when the indoor air temperature is satisfied. However, the evaporator coil may turn from a wet-coil to a dry-coil, and the re-evaporation problem cannot be properly dealt with in this control strategy.

In 1995, Krakow et al., have developed a Proportional Integral Differential (PID) method to control the space temperature and humidity by varying the compressor and indoor fan speed. Two independent PID loops were used: a temperature loop controlled by varying the compressor speed; and a RH loop controlled by varying the supply fan speed. This control strategy maintains both temperature and RH at their set-point in the space by altering the compressor and indoor fan speed to remove variable sensible and latent loads in the space. Krakow et al., (1995) treated the two control loops as two single-input-single-output (SISO) systems and ignored the coupling effect between the two control variables, temperature and humidity, which may result in a poor control performance. However, in Krakow et al.,'s control strategy, the temperature and humidity are treated as two independent control variables and their coupling effect is not considered. To overcome this drawback, Qi and Deng (2009) developed a multiple-input-multiple-output (MIMO) system which considered the coupling effect between the temperature and humidity in space. Through developing a linearized dynamic model of the direct expansion (DX) A/C system based on the principle of energy and mass conservation, the indoor temperature and humidity can be expressed in a state-space form for MIMO control. Different from Qi and Deng's physical based model, Li et al., (2012) realized the temperature and humidity control by a DX A/C system with artificial neural network.

2.3 System Performance Model for Variable Speed A/C Units

System performance models of air conditioners are widely used for system performance prediction, building energy performance assessment and air conditioner model-based control. Nowadays, the wide application of variable speed technologies, which can provide a wide range and varied ratio of sensible and latent cooling capacity through operating compressor and supply fan at different speeds, brings a high demand of performance models for variable speed A/C units. The system performance model for variable speed units is more complicated than the models for single-speed units, since the performance for variable speed A/C systems not only is impacted by the boundary conditions, such as indoor and outdoor temperature and humidity, but also it determined by its operation conditions, the speed of compressor and supply fan.

The performance models of A/C units can be classified into physical models and simplified empirical or semi-empirical models, where physical models include more physical aspects for each component of the air conditioner units, and the simplified empirical or semi-empirical models are simpler and are trained by experimental data, the unknown coefficients are usually determined to achieve the best-fit with experimental observations. Also, both physical models and simplified empirical or semi-empirical models can be classified into either transient or steady-state model. However, a steady-state model can be used for co-simulation with building models, since the dynamic characteristic of a refrigerant cycle is at a much faster time scale than the building thermal and moisture dynamics.

To summarize existing performance models for variable speed A/C units and to compare to the models used in current work, the following models are reviewed.

2.3.1 Integrated Component Models

The integrated model of A/C unit contains different components in the system: compressor, condenser, evaporator and expansion valve an A/C DX (direct expansive) unit. The compressor has a performance map, that can be obtained from manufacturer's website. Also, comprehensive mechanistic (or deterministic) models have been developed to analyze and optimize compressor performance. Bell et al., (2020) and Ziviani et al., (2020) introduced an open-source generalized simulation framework for positive displacement machines (PDSim) and provided a comprehensive overview of several modeling aspects of different conventional and novel compressor types.

Furthermore, the condenser and evaporator can be treated as the heat exchanger in the modeling process and the $\varepsilon - Ntu$ method is used to calculate the heat transfer capacity. The popular methods used for heat transfer area and related coefficients are described in next section.

Take an example, Cai and Braun (2015) applied an integrated A/C model in building co-simulations. The integrated model in their model has three components: compressor, evaporator and condenser. The simulated model is generated based on the energy balance equation where the outdoor unit packaging compressor and condensing coiling provides an equal cooling capacity to what is delivered by the evaporator in given boundary conditions and equipment operation conditions.

$$\begin{cases} q_{tot} + 0.95 \times pow_{comp} = q_{cond} \\ T_{sc} = 15^\circ\text{F} \end{cases} \quad (2-3)$$

The input-output correspondences for models of the three components are listed in Table 2.1, where the evaporating and condensing temperatures (T_{evap} and T_{cond}) are the initial values that need to be calculated iteratively. m_r is the mass flow rate obtained from the compressor performance map. *Stage* is the stage of the compressor ranging from 0 to 0.5. The other quantities are the boundary conditions impacting the system performance, including ambient or outdoor temperature (T_{amb}), dry-bulb temperature ($T_{air,db,evap}$) and web-bulb temperature ($T_{air,wb,evap}$) of air entering evaporator.

Table 2.1. Model input–output forms.

Compressor	$[P_{comp}, m_r] = \text{Comp}(T_{evap}, T_{cond}, Stage)$
Condenser	$q_{cond} = \text{Cond}(T_{cond}, T_{amb}, m_r)$
Evaporator	$[q_{tot}, q_{sen}] = \text{Evap}(T_{evap}, V, T_{air,db,evap}, T_{air,wb,evap})$

Another widely used A/C system model is the ACHP model developed by Bell (2012), which is designed to investigate the direct expansion (DX) cycle by applying detailed physical models of each component to predict the performance of the combined cycle. In ACHP model, two independent variables, saturation temperature of the refrigerant at evaporation (T_{evap}) and

condensation (T_{cond}), are the input variables to each component model to calculate the outputs from each component.

The compressor model of ACHP relies on a compressor map to predict the mass flow rate of refrigerant and compressor power for given saturation temperature of the refrigerant at evaporation and condensation as well as superheat temperature.

$$\begin{aligned}\dot{m}_r &= f_{map}(T_{evap}, T_{cond}, \Delta T_{sh}) \\ \dot{W}_{comp} &= f_{map}(T_{evap}, T_{cond}, \Delta T_{sh})\end{aligned}\quad (2-4)$$

In the condenser, the refrigerant starts from the superheated state at point 3 in Figure 2.4, goes through a two-phase state and finally condenses to a sub-cooled state (point 4 in the figure). The condenser model is based on a moving boundary model to calculate the heat transfer rate between air side and refrigerant side, respectively, where the heat transfer rate on the air side can be expressed as:

$$\dot{Q}_{cond} = \varepsilon_{HX} \frac{V_{ha,cond}}{\rho_{ha}} c_{p,a} (T_{i,a,cond} - T_{cond}) \quad (2-5)$$

where $T_{i,a,cond}$ is the air temperature at the coil inlet and T_{cond} is the condensing temperature of the refrigerant. ε_{HX} is the correlation related to heat transfer calculation obtaining by $\varepsilon - Ntu$ method. The heat transfer rate on the refrigerant side is:

$$\dot{Q}_{cond,\Delta h} = \dot{m}_r (h_{r,o,comp} - h(T_{cond} - \Delta T_{sc}, p_{cond})) \quad (2-6)$$

here, $h_{r,o,comp}$ is the enthalpy of refrigerant at the compressor outlet, $h(T_{cond} - \Delta T_{sc}, p_{cond})$ is the enthalpy of refrigerant at the condenser outlet, which is calculated based on refrigerant saturation temperature at condensation subtracting the sub-cooled temperature.

In ACHP, no expansion device is included. Thus, the expansion device model is assumed as a constant-enthalpy throttling device that expands the refrigerant from high pressure line side to low pressure line side between point 5 and point 6 in Figure 2.4. The equation describing the expansion process is

$$h_{r,i,EX} = h_{r,o,EX} \quad (2-7)$$

The evaporator model is more complicated comparing with the other three models, since it is possible for the evaporator coil to be fully dry, fully wet or partially wet and partially dry. Thus, in the ACHP model, the coil surface temperature at air inlet ($T_{s,a,i}$) and outlet ($T_{s,a,o}$) is compared to the dew-point temperature of entering air (T_{dp}) first, and then the heat transfer rate (\dot{Q}_{evap}) in the evaporator is determined by the following equation:

$$\dot{Q}_{evap} = \begin{cases} \dot{Q}_{evap,dry} & T_{s,a,o} > T_{dp} \\ \dot{Q}_{evap,wet} & T_{s,a,i} < T_{dp} \\ \frac{T_{s,a,o} - T_{dp}}{T_{s,a,o} - T_{s,a,i}} \dot{Q}_{evap,wet} + \left(1 - \frac{T_{s,a,o} - T_{dp}}{T_{s,a,o} - T_{s,a,i}}\right) \dot{Q}_{evap,dry} & T_{s,a,i} > T_{dp} > T_{s,a,o} \end{cases} \quad (2-8)$$

To model the complete cycle, the cycle analysis begins at point 1 in Figure 2.4. To give a good initial guess of two independent variables, saturation temperature of the refrigerant at evaporation and condensation, the mass flow rate of refrigerant is obtained from compressor map and becomes input variable to the other component models. Then, the numerical calculation is conducted for each component, after the outputs of each component in the cycle are calculated sequentially for one loop, the refrigerant properties at point 1 is compared with the starting values of this loop. If the values of initial independent variables are correct, the state the initial guess state at point 1 and the state at the same point obtained after the loop round calculation should be the same. If they are different, the initial guessed values can be updated based on the obtained values after the loop around calculation.

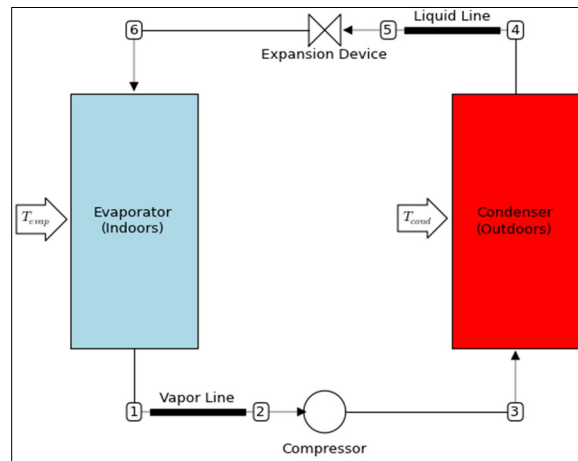


Figure 2.4. Direct expansion cooling mode system.

Since there are two independent initial variables, there needs to be two residuals used to coverage the cycle. One of the residuals is based on the energy balance of the whole cycle, the other residual could be either the charge keeps constrained with an imposed charge, or indirectly the subcooled temperature matches a given value. The two residuals are expressed as:

$$\begin{cases} \vec{\Delta}_1 = \dot{m}_r (h_1 - h_{1'}) \\ \vec{\Delta}_2 = \dot{m}_r - \dot{m}_{r,target} \text{ or } \Delta T_{sc,cond} - \Delta T_{sc,cond,target} \end{cases} \quad (2-9)$$

2.3.2 Polynomial Model

Cheung and Braun (2010) proposed a simple empirical model for a heat pump operating in heating mode. They tested the unit in laboratory and use steady-state testing data for model training and model prediction. The modeling was separated into two parts: 1) modeling the performance at maximum compressor and fan speed and 2) modeling the performance with relative load and fan speed. The power consumption relative to the maximum power consumption is presented using a polynomial model in terms of relative supply fan speed and part-load ratio, then the model is simplified into the following polynomial:

$$\begin{aligned} \frac{W}{W_{max}} = & C_0 + C_1 \frac{Q}{Q_{max}} + C_2 \left(\frac{Q}{Q_{max}} \right)^2 + C_3 \left(\frac{Q}{Q_{max}} \right) \left(\frac{V}{V_{max}} \right) + C_{46} \left(\frac{Q}{Q_{max}} \right)^3 \\ & + C_5 \left(\frac{V}{V_{max}} \right)^3 + C_6 \left(\frac{Q}{Q_{max}} \right) \left(\frac{V}{V_{max}} \right)^2 \end{aligned} \quad (2-10)$$

$$\begin{aligned} \text{Where: } W_{max} &= A_0 + A_1 T_{outdoor} \\ Q_{max} &= A_2 + A_3 T_{outdoor} \end{aligned}$$

Here, A_0, A_1, A_2, A_3 and C_0 to C_6 are the coefficients calculated by linear regression. The r^2 of the trained polynomial model is 99.85%.

Cai and Braun (2018) proposed performance models of a variable speed RTU based on ASHRAE Toolkit model to predict unit cooling capacity, EIR (Energy Input Ratio) under various boundary conditions, compressor speed and supply fan speed. Different from the polynomial proposed by Cheung and Braun (2010), the predicted total cooling capacity polynomial includes the rated cooling capacity, which is extracted from performance data at an ambient dry-bulb temperature of 95°F, an indoor wet-bulb temperature of 66.7°F, and a rated air flow rate of 2300 CFM. Then, the total cooling capacity is predicted as a correlation of dry-bulb temperature (T_{amb}), indoor wet-bulb temperature ($T_{a,ent,wb}$), rated air flow rate (V_{rate}), actual air flow rate (V) and the compressor speed (Sp).

$$\frac{Q_{cap}}{Q_{cap,rat}} = (a_0 + a_1T_{a,ent,wb} + a_2T_{a,ent,wb}^2 + a_3T_{amb} + a_4T_{amb}^2 + a_5T_{amb}T_{a,ent,wb}) (1 + b_1\frac{V}{V_{rate}} + b_2\left(\frac{V}{V_{rate}}\right)^2)(1 + f_1Sp + f_2Sp^2 + f_3Sp^3) \quad (2-11)$$

where Q_{cap} is the total cooling capacity at specific operating conditions.

Similarly, the EIR is predicted as:

$$\frac{EIR}{EIR_{cap,rat}} = (c_0 + c_1T_{a,ent,wb} + c_2T_{a,ent,wb}^2 + c_3T_{amb} + c_4T_{amb}^2 + c_5T_{amb}T_{a,ent,wb}) (1 + d_1\frac{V}{V_{rate}} + d_2\left(\frac{V}{V_{rate}}\right)^2)(1 + e_1Sp + e_2Sp^2 + e_3Sp^3) \quad (2-12)$$

A Levenberg-Marquardt-based non-linear regression algorithm is used to calibrate all the coefficients in Equation (2-11) and (2-12). Training by 545 data points, the root mean square of the relative fitting error is 3.6% and the maximum relative error is 7.8% for total capacity.

Other existing performance models for A/C system performance prediction are more or less similar to the aforementioned two models. The only difference between them is the complexity of model construction, which contains different number of correlation parameters that required to be trained. In Equation (2-13), the polynomial model contains three parts: the outdoor and indoor conditions, the compressor speed ratio and air flow rate of supply fan, where each part can be added or removed based on specific applications. For example, Guo et al., (2017) proposed a polynomial model with 20 coefficients for compressor power prediction considering the frequency of compressor:

$$\begin{aligned} W = & k_1 + k_2T_{evap} + k_3T_{con} + k_4f_{comp} + k_5T_{evap}^2 + k_6T_{con}^2 + k_7f_{comp}^2 \\ & + k_8T_{evap}T_{con} + k_9T_{evap}f_{comp} + k_{10}T_{con}f_{comp} + k_{11}T_{evap}^3 + k_{12}T_{con}^3 \\ & + k_{13}f_{comp}^3 + k_{14}T_{evap}^2T_{con} + k_{15}T_{evap}^2f_{comp} + k_{16}T_{con}^2T_{evap} \\ & + k_{17}T_{con}^2f_{comp} + k_{18}f_{comp}^2T_{evap} + k_{19}f_{comp}^2T_{con} \\ & + k_5T_{evap}T_{con}f_{comp} \end{aligned} \quad (2-13)$$

where f_{comp} is the frequency of compressor, T_{evap} and T_{con} are the evaporating and condensing temperature, respectively.

In the model proposed by Hu et al.,(2020), terms involving air flow rate in the model equation are removed and the polynomial is simplified as:

$$Q^* = \frac{Q}{Q_{rat}} = (a_1 + a_2 T_{in,wb} + a_3 T_{out,db} + a_3 T_{out,db} + a_4 T_{in,wb}^2 + a_5 T_{out,db}^2 + a_6 T_{in,wb} T_{out,db}) \times (1 + b_1 N_{comp} + N_2 N_{comp}^2 + b_3 N_{comp}^3) + \varepsilon_Q \quad (2-14)$$

where $T_{out,db}$ and $T_{in,wb}$ are outdoor dry-bulb temperature and indoor wet-bulb temperature respectively, N_{comp} is the compressor operating frequency.

2.3.3 Neural Network Models

Besides polynomial performance models for the A/C unit, models applying machine learning methods are also another option. For example, artificial neural network (ANN) is applied to predict the performance of a heat pump with different mass ratios (Mohanraj et al., 2012). They developed an ANN model with three input neurons representing three input variables (mixture ratio, refrigerant temperature entering the evaporator and condenser pressure) to predict two outputs, COP and rational efficiency in the output layer. It showed that the network prediction results are close to experimental results with a R^2 of 0.9999.

2.3.4 Summary

There are many numerical models developed to predict the various A/C DX system performance in previous studies. The aforementioned models have different advantages in particular applications. The integrated vapor compression cycle models based on detailed physical component models (i.e., “white-box” models) can provide more physical understanding of the cycle and have been demonstrated to be more suitable for extrapolations. Whereas, when design improvements or new A/C system types are to be investigated, physical-based models are usually employed to system analyses and optimization. However, these models need more detailed system information, such as coiling coil geometry, and heat transfer coefficients in both the condenser and evaporator. Also, the high computational requirement of physical-based models leads to difficulties in cycle convergence and initial guess values.

The polynomial model and ANN model are “black-box” models which are easy to construct and can be applied on various systems. However, due to the absence of physical principles, the correlation in the models is highly relied on experimental data used in training. Thus,

these types of models are more suitable in situations where only general performance characteristics of system are in demand.

2.4 Review of Component Models of Vapor Compression Cycle

The SSLC numerical model used in this work is based on a general vapor compression cycle model, which usually contains four components: compressor, condenser, expansion valve and evaporator. This section provides a literature review on the modeling of some basic components of a vapor compression system: the compressor, and the heat exchangers used in the condenser and evaporator. These models will be applied directly in the work presented in later chapters.

2.4.1 Compressor Model

To evaluate the performance of compressors and predict its performance in vapor compression systems, various compressor models have been developed. As outlined by Cheung and Wang (2018), empirical and semi-empirical models have been widely used to map compressor performance. The compressor model involved in this research is to develop a SSLC system model, which is a vapor compressor cycle including the compressor section. Thus, several popular compressor models are reviewed and compared with each other to select the proper one for following work.

Model 1: 10-coefficient polynomial with superheat adjustment

Several different compressor models representing different levels of applications of empirical coefficients and physical principles are developed to predict the compressor performance. In industry, it is a common practice to apply current ANSI/AHRI Standard 540 (AHRI, 2015) for compressor performance rating and utilize the 10-coefficient cubic polynomial model to predict the mass flow rate and compressor power, as shown in Equation (2-15).

$$\begin{aligned} \dot{m}_{map}[\text{kg/hr}] &= M_1 + M_2 \cdot T_e + M_3 \cdot T_c + M_4 \cdot T_e^2 + M_5 \cdot (T_e \cdot T_c) + M_6 \cdot T_c^2 + M_7 \\ &\quad \cdot T_e^3 + M_8 \cdot (T_e^2 \cdot T_c) + M_9 \cdot (T_e \cdot T_c^2) + M_{10} \cdot T_c^3 \\ \dot{W}_{map}[W] &= P_1 + P_2 \cdot T_e + P_3 \cdot T_c + P_4 \cdot T_s^2 + P_5 \cdot (T_s \cdot T_d) + P_6 \cdot T_d^2 + P_7 \cdot T_s^3 + P_8 \\ &\quad \cdot (T_s^2 \cdot T_d) + P_9 \cdot (T_s \cdot T_d^2) + P_{10} \cdot T_d^3 \end{aligned} \quad (2-15)$$

where $M_1 \cdots M_{10}$ and $P_1 \cdots P_{10}$ are the regression coefficients provided by the manufacturer or can be estimated by linear regression with compressor calorimeter testing data at a rated compression suction and superheated; T_d is the discharge dew point temperature and T_s is the suction dew point temperature.

The Equation (2-15) is used to estimate a rated mass flow rate and compressor power at the given compressor suction and discharge dewpoint temperature. To estimate these two outputs other than the rated value, Dabiri and Rice (1981) presented a technique for correcting the compressor motor input power and refrigerant mass flow rate as below:

$$\begin{aligned} \dot{m}_{r,actual} &= \left[1 + F_v \left(\frac{v_{map}}{v_{actual}} - 1 \right) \right] \dot{m}_{r,map} \\ \dot{W}_{comp,actual} &= \left(\frac{\dot{m}_{r,actual}}{\dot{m}_{r,map}} \right) \left(\frac{\Delta h_{isen,actual}}{\Delta h_{isen,map}} \right) \dot{W}_{comp,map} \end{aligned} \quad (2-16)$$

here, the subscripts *actual*, *map* and *isen* represent the actual superheated conditions, the map superheated conditions, and an isentropic process from estimated suction port conditions to compressor outlet pressure respectively.

Model 2: Volumetric Efficiency Based Model

In most cases, the 10-coefficient polynomial predicts the compressor performance well but does not necessarily provide reliable extrapolations for some operation conditions that are not represented in the compressor calorimeter tests. In 2000, Jahnig et al., investigated a semi-empirical model that based on the concept of volumetric efficiency. And this model is further developed to apply in variable speed compressors (Li, 2013a). In Jahnig's model, the mass flow rate (\dot{m}_r) is expressed as a function of volumetric efficiency (η_v):

$$\begin{aligned} \dot{m}_r &= \eta_v \cdot \frac{V \cdot RPM}{v_{suction} \cdot 60} \\ \eta_v &= 1 - C \left[\left(\frac{P_{dis}}{P_{suc}(1 - \delta p)} \right)^{\frac{1}{k}} - 1 \right] \end{aligned} \quad (2-17)$$

where P_{dis} and P_{suc} are discharge and suction pressure, respectively. δp is suction pressure drop and k here is isentropic coefficient. In this model, only C is unknown variable. For simplification, Li (2013a) set C as a polynomial and reshaped Equation (2-17) as below:

$$\eta_v = b_1 + b_2 \left(\frac{P_{dis}}{P_{suc}(1 - \delta p)} \right)^{\frac{1}{k}} \quad (2-18)$$

A complete of compressor shaft power is organized by Li (2013a):

$$W = P_{suc} \dot{m}_r v_{suc} a_1 \left[\left(\frac{P_{dis}}{P_{suc}} \right)^{a_2 + \frac{k-1}{k}} + \frac{a_3}{P_{dis}} \right] + W_{loss} \quad (2-19)$$

with four parameters a_1, a_2, a_3 and W_{loss} to be calculated by fitting experimental data.

Model 3: Artificial Neural Network

Nowadays, with machine-learning techniques that are widely used in engineering, a number of researchers develop a compressor map applying artificial neural networks (ANN). For instance, Gholamrezaei and Ghorbanian (2010) proposed a feed-forward neural network model to reconstruct the performance map of an axial compressor with limited experimental data. Ziviani et al., (2019) demonstrated that a multi-input multi-out ANN model can achieve higher accuracy with respect to a semi-empirical model to predict the performance of a single-phase and two-phase injected scroll compressor.

2.4.2 Heat Exchanger Model

The ORNL Heat Pump Design Model (Fischer & Rice, 1981) calculates the heat transfer performance of air-to-refrigerant condenser and evaporator by using the $\varepsilon - Ntu$ method. The EVSIM model (Piotr, 1989) (an evaporator simulation model account for refrigerant and one-dimensional air distribution), simulates refrigerant-to-air heat exchanger performance of the evaporator in residential air-conditioners. Moreover, the software EVAP-COND (NIST, 2003) is usually used to simulate the performance of finned-tube evaporator and condenser. Also, in the ACHP model presented and summarized by Bell (2012), the prediction of heat exchanger performance is based on the $\varepsilon - Ntu$ method, which simplifies the heat transfer rate calculation. In the application of the $\varepsilon - Ntu$ method, the heat transfer rate can be calculated by obtaining the various convective heat transfer coefficients, surface areas and the inlet temperature of both streams. Since the ACHP model has been implemented in the development of the SSLC model that will be presented in the later chapter, the details on heat transfer area calculation and the finned-tube cooling coils correlation estimation are reviewed here.

Cooling Coil Heat Transfer Area Calculation

Analysis of the heat exchange process in cooling coils is important for predicting condenser and evaporator performance. For example, in the $\varepsilon - Ntu$ method, the fin-tube area and fin efficiency are important parameters used to find the overall heat transfer conductance. The ACHP model provides a numerical method to calculate heat-exchanger area on both refrigerant side and air side, and to estimate the fin efficiency for a finned-tube heat exchanger. On the refrigerant-side, the average circuit length ($\overline{L_{circuit}}$) is given by:

$$L_{tube,total} = N_{tube/bank} \cdot N_{bank} \cdot L_{tube} \quad (2-20)$$

$$\overline{L_{circuit}} = L_{tube,total} / N_{circuits}$$

where the $L_{tube,total}$ is total length of all tubes, $N_{tube/bank}$ is the number of tubes per bank; the N_{bank} is number of banks of tubes; and L_{tube} [m] is the length of one tube. The refrigerant side surface area is given by:

$$A_{r,total} = \pi \cdot D_i \cdot L_{tube,total} \quad (2-21)$$

where the D_i [m] is the interior diameter of the tubes.

On the air side, the calculation of the heat transfer surface area is more complicated. The total air-side area includes both the tube and the fins, which is given by:

$$A_{a,total} = A_f + N_{tube/bank} \cdot N_{bank} \cdot \pi \cdot D \cdot (L_{tube} - N_{fin} \cdot t) \quad (2-22)$$

Here, A_f is the sum of air side area of all fins, and N_{fin} is the number of fins which is given by:

$$A_f = 2N_{fin}(H \cdot P_l \cdot N_{bank} \cdot \sec \theta - N_{tube/bank} \cdot N_{bank} \cdot \pi \cdot D^2/4) \quad (2-23)$$

where H is fin height. P_l Longitudinal bank-bank pitch (in the flow direction)[m].

$$H = P_t(N_{tube/bank} + 1) \quad (2-24)$$

$$N_{fin} = L_{tube} \cdot FPM$$

The FPM [1/m] here is the pitch per meter; and P_t [m] presents the transverse pitch in Figure 2.5.

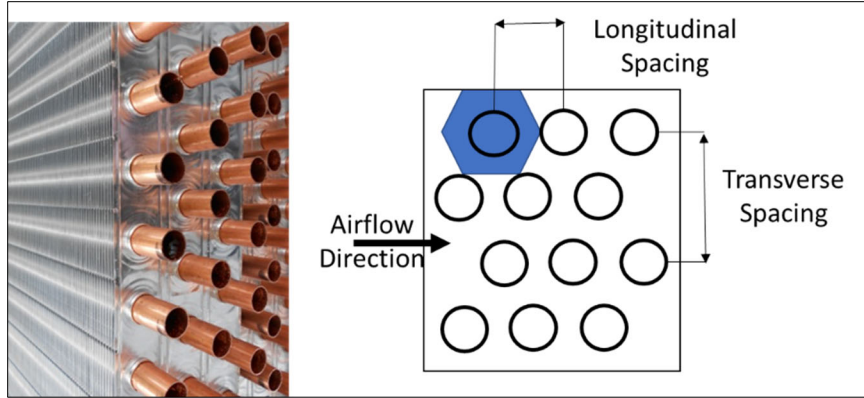


Figure 2.5. Fin-tube geometry sketch.

Fin Efficiency

By adding fins to the coil tubes, the air-side heat transfer area can be significantly increased but at the expense of decreasing the mean temperature difference between the coil surface and the air stream. Fin efficiency (η) is a correlation for the heat transfer performance of the fins. Schmidt, T. E. (1945), provided a way to calculate the fin efficiency based on the fin root radius (r_o) and the equivalent fin tip radius (R). Following the description by McQuiston (1975), two intermediate parameters need to be calculated first:

$$M = \left(\frac{2 \cdot h}{k_f \cdot t} \right)^{0.5} N_{fin} = L_{tube} \cdot FPM \quad (2-25)$$

$$\theta = \left(\frac{R}{r_o} - 1 \right) \left(1 + 0.35 \cdot \ln \left(\frac{R}{r_o} \right) \right)$$

And then the fin efficiency (η) can be expressed in terms of M , θ and the tube outside radius r_o as:

$$\eta = \frac{\tan h(M \cdot r_o \cdot \theta)}{M \cdot r_o \cdot \theta} \quad (2-26)$$

Air-side Heat Transfer Coefficient

In the EVSIM model, a correlation, provided by Gray and Webb (1986) and tested by Wang et al., (1998), is used to calculate the heat transfer coefficient for flat fins. And the correlation provides an average value for the Colburn j-factor, evaluated by the different geometry of plate fins. j_4 is used for the flat fins with four or a greater number of tube depth rows and j_N ($N < 4$) is used for heat exchangers with less than four depth rows, which can be calculated by:

$$\begin{aligned}
Mj_4 &= 0.14 \times Re^{-0.32} \left(\frac{P_t}{P_l}\right)^{-0.502} \left(\frac{s}{D_o}\right)^{0.0312} \\
j_N &= j_4 \times 0.991 \left[2.24 Re^{-0.092} \left(\frac{N}{4}\right)^{-0.031} \right]^{0.607(4-N)}
\end{aligned} \tag{2-27}$$

Then, the convection heat transfer coefficients for dry and wet coil can be expressed by:

$$\begin{aligned}
Mh_{c,o,dry} &= \frac{j \cdot Ga \cdot c_{p,a}}{Pr^{2/3}} \\
h_{c,o,wet} &= \frac{j \cdot Ga \cdot c_{p,a}}{Pr^{2/3}} \cdot \left[1 + \frac{i_{f,g,w} \cdot (\omega_a - \omega_w)}{c_{p,a} \cdot (t_a - t_w)} \right]
\end{aligned} \tag{2-28}$$

where Ga is the air mass flux based with the minimum air flow area. The air side heat transfer correlations for other kind of fins, such as Convex-Louver and Wavy Fin-and-Tube is also studied and validated by Wang et al., (1998).

Condensation Heat Transfer Coefficient on Refrigerant-side

The Shah Condensation Correlation (Shah, 1979) is a commonly-used method to estimate the heat transfer coefficient for condensing flow in the tube of a condenser. The average condensation heat transfer coefficient for the refrigerant with its vapor quality ranging from x_1 to x_2 is calculated as:

$$\overline{h_{2\phi,cond}} = \frac{\int_{x_1}^{x_2} h_{2\phi,cond}(x) dx}{x_2 - x_1} \tag{2-29}$$

where $\overline{h_{2\phi,cond}}$ is the overall heat transfer coefficient for a given quality.

Through analyzing data for different fluids (such as water, Benzene, ethanol and so on) in horizontal, vertical and inclined pipes of diameters from 7mm to 40mm, $h_{2\phi,cond}$ can be expressed as:

$$h_{2\phi,cond}(x) = h_L [(1-x)^{0.8} + \frac{3.8 \cdot x^{0.76} \cdot [0.76 \cdot (1-x)^{0.004}]}{Pr^{0.38}}] \tag{2-30}$$

in which h_L is the heat transfer coefficient assuming the refrigerant being in the liquid phase, is calculated by:

$$h_L = \frac{0.0023 Re_l^{0.8} Pr_l^{0.4} k_l}{D} \tag{2-31}$$

where Re_l Reynolds number, Pr_l is Prandtl number, k_l is the thermal conductivity of fluid and D is the tube diameter.

Evaporation Heat Transfer Coefficient on Refrigerant-side

Gungor and Winterton (1986) developed a general correlation for annular flow regimes in smooth tubes. Depending on the calculation method, the two-phase evaporation heat transfer coefficient ($h_{2\phi, evap}$) can be represented as a weighted average of the convective single-phase heat transfer coefficient (h_l) and the pool boiling heat transfer coefficient (h_{pool}):

$$h_{2\phi, evap} = E \cdot h_l + S \cdot h_{pool}$$

$$E = 1 + 2400 \cdot Bo^{1.16} + 1.37 \cdot \left(\frac{1}{X_{tt}}\right)^{0.86} \quad (2-32)$$

$$S = \frac{1}{1 + 1.15 \times 10^{-6} \cdot E^2 \cdot Re_l^{1.17}}$$

here, Bo is the boiling number; X_{tt} is Martinelli parameter; Re is the Reynold number; Pr is Prandtl number. And the h_{pool} is proposed by Cooper and expressed by:

$$h_{pool} = 55 \cdot Pr^{0.12} (-\log_{10} Pr)^{-0.55} \cdot M^{-0.5} \cdot q^{0.67} \quad (2-33)$$

where M is the molecular weight and q [W/m^2] is heat flux.

Single-phase Heat Transfer Coefficient on Refrigerant-side

In 1977, Churchill developed a coefficient (f) related to the pipe friction loss and heat transfer of fluid flowing in the tube as single phase. This single-phase heat transfer coefficient is also applied in CHPB model named as Churchill correlation and is shown below:

$$h_\phi = \frac{k}{D} \cdot \frac{\frac{f}{8} \cdot (Re - 1000) \cdot Pr}{1 + 12.7 \cdot \left(\frac{f}{8}\right)^{\frac{1}{2}} \cdot (Pr^{\frac{2}{3}} - 1)} \quad (2-34)$$

where Re is the Reynold number; Pr is Prandtl number; and f is a friction coefficient that can be expressed by:

$$f = 8 \left[\left(\frac{8}{Re_d}\right)^{12} + \frac{1}{(A+B)^{1.5}} \right]^{\frac{1}{12}}$$

$$where: A = \left(-2.457 \log \left[\left(\frac{7}{Re}\right)^{0.9} + 0.27 \frac{\epsilon}{D} \right] \right)^{16} \quad (2-35)$$

$$B = \left(\frac{37530.0}{Re} \right)^{16}$$

2.5 Co-simulation Approaches Combining Building and HVAC Systems

To understand the A/C system performance in a building, a number of building and HVAC system integrated performance simulation approaches are developed. In this section, several widely-used simulation software and approaches are reviewed.

One popular building and HVAC system integrated simulation software is Energyplus, in which the heat gain or loss through the building envelop, internal heat gain, infiltration loads as well as loads due to the air exchange with other zones (Trcka et al., 2007) are defined and estimated first, then, the required heating or cooling loads are calculated depending on the set-point temperature and humidity. After the required system loads are obtained, the system component in Energyplus can simulate the performance of A/C system, finally, the deliverable energy from A/C system is input to building component to update the space temperature and humidity.

Energyplus has a good building model in details, which can describe the building information well, such as geometry, envelop, internal gain, infiltration and so on. In addition, the HVAC/R system in EnergyPlus covers most types of components, such as boilers, chiller, coils, pumps, fans, cooling towers and so on (Zhou et al., 2014). However, the HVAC/R system model in EnergyPlus is cumbersome since it requires to define all the pipes and duct loops of the A/C system. Furthermore, the temperature and humidity control in space is highly relied on the “Setpoint Manager” modules, which are one of high-level control structures in Energyplus to access data from any HVAC module and to calculate the setpoint for one or more spaces. This setpoint used as the HVAC control action limits the model flexibility in studying the A/C system control.

Another software reviewed is TRNSYS, which has an extensive library of HVAC/R components but less extensive building model in comparison to EnergyPlus. In TRNSYS, there are multiple modules used for predicting the performance of building and energy systems. For example, the module “Type 56” is a building module, which is used for building characteristic definition.

Besides the co-simulation software, an inverse building model is developed by Cai and Braun (2016) to study the dynamic behavior of the building. In this model, the building model is simplified as a RC network structure to simulate the heat flow through the building envelopes and different heat gain/loss source. Then, Cai and Braun (2016) applied this inverse building model in study of the A/C system control strategy combining with equipment models.

The literature reviews from the current co-simulation approaches indicate that the software like EnergyPlus, TRNSYS provide the possibilities to combine the building model and HVAC/R system model together and to establish the internal communication between them to evaluate both building and HVAC system performance, as well as the influence between them. However, the cumbersome and inflexible nature of these software packages limits their application in system control, novel system optimization and so on. To some extent, the RC-network inverse building model can solve the problems of the co-simulation software, that provide a simplified approach in simulation of building performance with special HVAC systems, although it cannot contain as much detailed building information as EnergyPlus or TRNSYS can.

2.6 Summary and Contributions of the Current Work

As mentioned in Chapter 1, most air-conditioning systems implemented in practice at the present time use indoor temperature as the only thermal comfort indicator to determine the operation strategies of the system, more specifically, to decide the profile of the system on/off, the compressor speed and the fan speed of the condenser and evaporator. This, however, ignores the humidity condition in the space which is another important thermal comfort criterion. Therefore, in the current work, the near-simultaneous satisfaction of the indoor temperature and humidity requirements (i.e., to meet both the sensible and latent cooling load requirements) is primarily focused on when designing an air-conditioning system and proposing the associated control strategies. Although various types of air-conditioning systems have been designed in previous research to realize separate sensible and latent cooling as described in Section 2.1, few of those SSLC systems have considerable potential from a wide-range practical implementation and commercialization point of view. This is due to, as summarized at the end of Section 2.1, the requirement of additional energy sources or equipment, as well as the restriction on the applicable climate zones. Based on these concerns, a sequential SSLC system is proposed in the current work, which utilizes a single variable-speed air-conditioner to perform separate sensible and latent cooling, by operating the single system in either a sensible only cooling mode or a deep dehumidification (low SHR) mode at different time periods. Accordingly, appropriate control strategies are proposed to decide timing of mode switch and the operation profile for each time period, so that the sensible and latent load requirements are satisfied while the energy consumption of the system is optimized. In order to design appropriate control strategies for the proposed SSLC

system to achieve the expected cooling performance under different indoor and outdoor environments, suitable mathematical models need to be constructed to calculate the system's sensible and latent cooling capacity under given speed settings of the equipment, as well as to estimate the building's sensible and latent cooling load under given indoor and outdoor thermal conditions. Based on the previous work summarized in Section 2.2, the heat transfer and thermodynamics models are constructed first for each individual equipment component such as compressor, condenser and evaporator. Then an integrated system model is developed to connect all these components together to predict the sensible and latent cooling capacity under varied input compressor speed and evaporator fan speed. The constructed equipment models are further validated by experiments on each component as well as on the integrated system. A simplified linear steady-state model is used to estimate the indoor temperature and humidity, or to calculate the cooling load of the building under different environments which is then validated by the simulation results from TRNSYS. By combining the SSLC system model and the building model used in the current work, the indoor temperature and humidity can be predicted as a response to an arbitrary speed profile of the compressor and evaporator fan. It is also shown that the models chosen and developed in the current work can be effectively used to design the control strategies due to their accuracies and inexpensive computational load. With suitable equipment models and building models prepared, control strategies for the proposed SSLC system can be investigated for different building and climate characteristics. The resulting system performances and energy consumptions can also be evaluated. The energy efficiency evaluations in the previous works are usually performed based on only the temperature performance requirement, it is not applicable to the system proposed in this research where both the temperature and humidity requirements are presented. Thus, a baseline case is proposed in the current work to evaluate the energy efficiencies for separate sensible and latent cooling systems. Based on this baseline, different control strategies developed in this work can be compared and evaluated. Two control strategies are proposed (listed with the computational complexity from low to high): the mode-switch control with fixed equipment speed in each mode, and the load prediction control with variable equipment speed in each mode. Through comparing the average coefficient of performance (COP) and comfort delivery between these two control strategies with baseline, the performance of two proposed control strategies applying SSLC methodology is evaluated in different climates.

3. MODEL DEVELOPMENT

As mentioned in the introduction in Chapter 1, a sequential SSLC system is developed in this work to realize separate sensible and latent cooling in a single vapor compression cycle by utilizing variable speed technologies. To analyze the SSLC system performance and energy consumption of its two operation modes (i.e., the latent-load-removal mode and the sensible-load-removal mode), a numerical model for the SSLC system is presented in this chapter. The developed SSLC model is a physical-based model containing detailed information of main components of an A/C system. A physical-based model consisting of models for each component is used in the current work because such a model is more helpful in investigating the system performance, especially the system's cooling and dehumidification capacity, under various compressor speed and evaporator fan speed. Additionally, the reliability and extrapolation capability of physical-based model are also better than the "black-model" mentioned in previous chapter.

Furthermore, the system performance and energy consumption of an SSLC system is considerably dependent on the characteristics of the targeted building. Thus, it is difficult to evaluate the actual system performance and the effect of associated control strategies without a suitable building model. For these reasons, a residential building model is also described in this chapter to conduct simulation studies on the performance of the proposed SSLC system and its related control strategies.

3.1 SSLC Model Development

The SSLC system proposed in the current work utilizes a single vapor compression cycle to realize separate sensible and latent cooling. The SSLC model developed is based on an empirical numerical model for a vapor compression cycle, which is validated by experimental heat pump testing in this research. There are four basic components in a vapor compression cycle; the compressor, condenser, expansion valve and evaporator. But the SSLC system model only contains three of them, with the expansion valve excluded. The expansion device is treated as a constant enthalpy throttling device, which expands the refrigerant from the high-pressure of system to low-pressure side of the system. Here, the model for each component is generated based on the ACHP model developed by Bell (I. Bell, 2012), and the heat transfer coefficients related to the

heat exchange process in the cooling coils (i.e., the condenser and evaporator) are obtained from widely-used empirical models. The software used for developing the SSLC system is Matlab combined with Coolprop (Bell et al., 2014) for thermodynamic state point evaluation. The following subsections explain the numerical model development for each component first, and then describes the method that connects all the components together and calculates the performance for the two operation modes: low-SHR and sensible-only modes.

3.1.1 Compressor Model

The compressor model in the SSLC system is used to predict the refrigerant mass flow rate and compressor power input at a given compressor speed. The compressor model described in Li's work (W. Li, 2013b) is applied to the current work, where the mass flow rate (\dot{m}_r) and power input (W) can be estimated as:

$$\dot{m}_r = \eta_v \cdot \frac{V_{disp} \cdot N_{speed}}{v_{suc} \cdot 60} \quad (3-1)$$

$$W = P_{suc} \dot{m}_r v_{suc} a_1 \left[\left(\frac{P_{dis}}{P_{suc}} \right)^{a_2 + \frac{k-1}{k}} + \frac{a_3}{P_{dis}} \right] + W_{loss} \quad (3-2)$$

where, N_{speed} is the compressor speed, V_{disp} is the compressor displacement, P_{dis} and P_{suc} are discharge and suction pressure of compressor, respectively. v_{suc} is the suction specific volume and η_v is the compressor volume efficiency, which can be expressed as:

$$\eta_v = b_1 - b_2 \left(\frac{P_{dis}}{P_{suc}(1 - \delta p)} \right)^{\frac{1}{k}} \quad (3-3)$$

where k is the isentropic coefficient. V_{disp} and k values have been obtained from the manufacturer, which are 8 cm³ and 0.72, respectively. The unknown parameters, a_1, a_2, a_3 and W_{loss} in Equation (3-2), as well as b_1, b_2 and δp in Equation (3-3) are found through experimental data fitting.

3.1.2 Condenser Model

In the cooling coil model (for both condenser and evaporator), the effectiveness– Ntu method is used to conduct the analysis for a counter flow heat exchanger. The heat transfer conductance (UA) between the refrigerant and the air side is found first, which gives the number of thermal units (Ntu) and, in turn, the effectiveness (ε). Finally, the heat transfer rate can be estimated if the inlet temperatures of the refrigerant and air are provided. The calculations involved in this model are summarized in the following equations:

$$\frac{1}{UA_{overall}} = \frac{1}{UA_a} + \frac{1}{UA_r} \quad (3-4)$$

$$UA_a = \eta_{fin,a} \alpha_a A_a; \quad UA_r = \alpha_r A_r \quad (3-5)$$

$$Ntu = \frac{UA}{C_{min}} \quad (3-6)$$

$$C_{min} = \min[\dot{m}_a c_{p,a}, \dot{m}_r c_{p,r}]; \quad C_{max} = \max[\dot{m}_a c_{p,a}, \dot{m}_r c_{p,r}] \quad (3-7)$$

$$\varepsilon = \frac{1 - \exp[-Ntu (1 - \frac{C_{min}}{C_{max}})]}{1 - \frac{C_{min}}{C_{max}} \exp[-Ntu (1 - \frac{C_{min}}{C_{max}})]} \quad (3-8)$$

$$\dot{Q} = \varepsilon C_{min} (T_{h,i} - T_{l,i}) \quad (3-9)$$

Here, A is the heat transfer surface area, α is the convective heat transfer coefficient, and η_{fin} is the fin efficiency. Each of these parameters are calculated based on the fin-tube geometry information listed in Table 3.1 and the ACHP model developed by Bell (Bahman et al., 2018; I. Bell, 2012). C_{min} and C_{max} are the lowest and highest heat capacity rates between the two flow streams. Sub-scripts a and r represent the air side and refrigerant side, respectively. In addition, \dot{m} is the mass flow rate, c_p is the heat capacity, and $T_{h,i}$ and $T_{l,i}$ are the inlet temperature for hot and cool streams.

Table 3.1. Fin-tube geometry information for condenser and evaporator.

	Condenser	Evaporator
Interior diameter of tubes [m]	0.0064	0.0090
Exterior diameter of tubes [m]	0.0071	0.0095
Fin thickness [m]	0.00011	0.00011
Transvers spacing [m]	0.022	0.022
Longitudinal spacing [m]	0.0191	0.025
Fin per inch	20	14.5
Length of one tube [m]	2.0	0.4
Number of tubes per row	41	23
Number of circuits	9	4

In the condenser, the refrigerant enters the coil of the condenser in a superheated state, then passes through its two-phase region to reach a final subcooled state, with a nearly constant pressure, before it enters the expansion valve. Thus, the condenser model is formulated using a moving boundary method according to the refrigerant phases in the condenser and is divided into three lumped regions: super-heated, two-phase, and sub-cooled segments. To determine the interface between the regions, the circuit length fractions for each segment are introduced and estimated based on Bell's work (I. Bell, 2012). By incorporating circuit length fractions into the $\varepsilon - Ntu$ method, the total heat transfer rate can be estimated starting from the super-heated segment by providing the inlet temperature of both the refrigerant and air, then two-phase and sub-cooled sections are calculated one by one (Bahman et al., 2018; I. Bell, 2012).

Table 3.2. Heat transfer correlations in condenser and evaporator model.

	Condenser		Evaporator
Refrigerant-side	Single-phase	Condensing	Evaporating
	Churchill, 1977	Shah, 1979	Gungor and Winterton, 1986
Air-side	Gray and Webb, 1986		

Super-heated Section

In the super-heated section, the refrigerant flows at a single-phase state and the heat transfer coefficient can be calculated by the Churchill correlation (Equation (2-34)). Assuming pure cross flow in the condenser coil, the coil length fraction of super- heated region is obtained by:

$$\omega_{sh} = \frac{\ln(1 - \Psi)}{1 - \exp\left(-\frac{UA_{overall}}{\dot{m}_{c,a}c_{p,a}}\right)} \cdot \frac{\dot{m}_r c_{p,r}}{\dot{m}_{c,a}c_{p,a}} \quad (3-10)$$

The parameter Ψ can be obtained by:

$$\Psi = \frac{T_{c,r,i} - T_{dew,r}}{T_{c,r,i} - T_{c,a,i}} \quad (3-11)$$

where are $T_{dew,r}$ dew-point temperature of refrigerant. The heat transfer rate for the super-heated region can be finally obtained by:

$$\dot{Q}_{sh} = \dot{m}_r c_{p,r} (T_{c,r,i} - T_{dew,r}) \quad (3-12)$$

Two-phase Section

There are two possible states for the refrigerant discharging from the condenser, two-phase or sub-cooled. To determine which state occurs in a particular situation, it is better to assume that the refrigerant goes through the whole two-phase portion and exits with zero vapor quality at first. The heat transfer analysis is based on the $\varepsilon - Ntu$ method for a dry coil and two- phase working fluid. The coil length fraction of two-phase region is:

$$\omega_{2\phi} = \frac{\dot{m}_r h_{fg} (1 - x_{out,2\phi})}{\dot{m}_{c,a} c_{p,a} (T_{c,a,i} - T_{sat,r}) \varepsilon_{2\phi}} \quad (3-13)$$

where the $x_{out,2\phi}$ is the outlet quality of refrigerant for the two-phase portion; h_{fg} is the refrigerant latent heat; and $T_{sat,r}$ is the refrigerant saturation temperature in coil. The heat transfer rate for two-phase region can then be obtained by:

$$\dot{Q}_{2\phi} = \omega_{2\phi} \varepsilon_{2\phi} \dot{m}_{c,a} c_{p,a} (T_{r,sat} - T_{c,a,i}) \quad (3-14)$$

The refrigerant state at condenser outlet can be determined as follows:

- If $\omega_{sh} + \omega_{2\phi} > 1$, there is no sub-cooled segment, and $\omega_{2\phi}$ needs to be updated to $\omega_{2\phi} = 1 - \omega_{sh}$ to further calculate the vapor quality of the refrigerant discharging from condenser.
- If $\omega_{sh} + \omega_{2\phi} = 1$, there is still no sub-cooled segment, but the outlet quality of the condenser does not need to be updated.
- If $\omega_{sh} + \omega_{2\phi} < 1$, there exists a sub-cooled segment, and the outlet vapor quality of refrigerant from two-phase section is equal to zero, and the $\omega_{sc} = 1 - \omega_{2\phi} - \omega_{sh}$.

Sub-cooled Section

The heat transfer process analysis also uses the $\varepsilon - Ntu$ method but there is a slight difference compared with the methods for other segments. The overall UA-value in sub-cooled section is calculated by:

$$UA_{sc} = \frac{\omega_{sc}}{\frac{1}{UA_a} + \frac{1}{UA_r}} \quad (3-15)$$

The minimum and maximum capacity are needed for further calculations and can be obtained by:

$$C_{min} = \min [\omega_{sc}\dot{m}_{c,a}c_{p,a}; \dot{m}_r c_{p,r}] \quad (3-16)$$

Finally, the heat transfer rate in the sub-cooled portion is:

$$\dot{Q}_{sc} = \omega_{sc}C_{min}(T_{r,l} - T_{c,a,i}) \quad (3-17)$$

here, the $T_{r,l}$ is the liquid saturated temperature of refrigerant at condensing pressure.

According to the results of the heat transfer exchange rate in the sub-cooled segment (\dot{Q}_{sc}), the sub-cooled temperature (ΔT_{sc}) can be calculated as:

$$\Delta T_{sc} = \frac{\dot{Q}_{sc}}{\dot{m}_r \cdot c_{p,r}} \quad (3-18)$$

3.1.3 Expansion Valve Model

To simplify the overall system model, the expansion device is modeled as a constant enthalpy throttling device, which expands the refrigerant from the high-pressure to the low-pressure side of the system in an isenthalpic process. It can express numerically that the enthalpy of refrigerant at the outlet of the condenser is equal to the enthalpy of refrigerant at the inlet of the evaporator, as shown in Equation (3-19).

$$h_{c,r,o} = h_{e,r,i} \quad (3-19)$$

3.1.4 Evaporator Model

The evaporator model is developed assuming only two-phase flow on the refrigerant side since the super-heated section is much smaller compared to the two-phase section. According to this assumption, the overall refrigerant side heat transfer rate can be determined by applying Equation (3-9), in which $T_{h,i}$ is modified to the air temperature of the evaporator ($T_{e,a,i}$) and $T_{l,i}$ becomes the evaporating temperature (T_e).

Correspondingly, the refrigerant enthalpy at the evaporator inlet ($h_{e,r,i}$) is obtained as follows:

$$h_{e,r,i} = h_{e,r,o} - \frac{\dot{Q}_{evap}}{\dot{m}_r} \quad (3-20)$$

where \dot{Q}_{evap} is the overall heat transfer rate in the evaporator, and $h_{e,r,o}$ is the enthalpy of the refrigerant at the outlet, which is obtained according to a specified super-heat temperature together with the evaporating temperature.

On the air side of the evaporator, both sensible and latent heat transfer occur in the low-SHR mode, while only sensible heat transfer occurs in the sensible-only mode. The evaporator model is developed under three different situations depending on the surface temperature on the coil: completely dry, completely wet, or partially wet partially dry.

Following the ACHP model (I. Bell, 2012), it is assumed that the cooling coil is completely dry first, so that the overall heat transfer rate (\dot{Q}_{evap}) and air temperature at coil outlet ($T_{e,a,o}$) can be calculated as follows:

$$\dot{Q}_{evap} = \varepsilon_{dry} c_{p,a} (T_{e,a,i} - T_{sat,r}) \quad (3-21)$$

$$T_{e,a,o} = T_{e,a,i} - \frac{\dot{Q}_{evap}}{\dot{m}_{e,a} c_{p,a}} \quad (3-22)$$

here, $T_{sat,r}$ is the refrigerant saturation temperature at evaporating pressure. ε_{dry} is calculated based on $\varepsilon - Ntu$ method.

The interface between the dry and wet sections can be determined by calculating the coil surface temperature at the air inlet ($T_{s,i}$) and outlet ($T_{s,o}$) and then comparing the coil surface temperature with the dew-point temperature of the entering air (T_{dp}):

$$T_{s,i} = \frac{UA_a T_{e,a,i} + UA_r T_e}{UA_a + UA_r} \quad (3-23)$$

$$T_{s,o} = \frac{UA_a T_{e,a,o} + UA_r T_e}{UA_a + UA_r} \quad (3-24)$$

If $T_{s,o} > T_{dp}$, the coil is completely dry. The previous assumption is true and the overall heat transfer rate (\dot{Q}_{evap}) and air temperature at coil outlet ($T_{e,a,o}$) are already calculated in Equation (3-21) and Equation (3-22), respectively.

If $T_{s,i} < T_{dp}$, the coil is completely wet, and the heat transfer rate is based on the completely wet analysis.

$$\dot{Q}_{evap} = \varepsilon_{wet} \dot{m}_{e,a} (h_{e,a,i} - h_{e,a,sat,r,i}) \quad (3-25)$$

Similarly, \dot{m}_{ea} is the air flow rate through the evaporator. $h_{e,a,sat,r,i}$ is the enthalpy of saturated air at refrigerant inlet temperature.

Otherwise, $T_{s,i} > T_{dp} > T_{s,o}$, the coil is partially-wet and partially-dry. It is critical to estimate the interface between the dry and wet sections since the air side heat transfer analysis is conducted in both dry and wet regions to determine the total heat transfer rate and air outlet temperature. In dry coil region, the heat transfer rate is:

$$\dot{Q}_{dry} = \dot{m}_a c_{p,a} (T_{e,a,i} - T_{a,x}) \quad (3-26)$$

where $T_{a,x}$ is air dry-bulb temperature at wet-dry interface can be calculated as follow:

$$T_{a,x} = T_{dp} + \frac{UA_i}{UA_o} (T_{sp} - T_{sat,r}) \quad (3-27)$$

The heat transfer rate in the wet coil region is:

$$\dot{Q}_{wet} = \varepsilon_{wet} \dot{m}_a (h_{e,a,i} - h_{a,sat,r}) \quad (3-28)$$

here, $h_{a,sat,r}$ is the air saturation enthalpy at the refrigerant saturation temperature ($T_{sat,r}$).

Thus, the overall heat transfer occurs on the evaporator coil is:

$$\dot{Q}_{evap} = \dot{Q}_{dry} + \dot{Q}_{wet} \quad (3-29)$$

The sensible cooling capacity can then be obtained from the following relationship:

$$\dot{Q}_{sen} = \dot{m}_{ea} c_{p,a} (T_{e,a,i} - T_{e,a,o}) \quad (3-30)$$

The equipment SHR is introduced here to express the ratio of sensible cooling capacity to the total cooling capacity:

$$SHR = \frac{\dot{Q}_{sen}}{\dot{Q}_{evap}} \quad (3-31)$$

Besides cooling capacity, power input to the evaporator fan is also an important consideration to capture since the evaporator fan speed plays a significant role in setting the operating mode of the SSLC system. In the current work, fan power input is determined based on a fan curve obtained from the equipment manufacturer.

3.1.5 Integrated SSLC System Model

After generating the numerical models for each component, the next step is to combine each component model together to form an integrated SSLC system model. The flow chart for combining the individual components into a complete air conditioning system and solving the overall model is shown in Figure 3.1.

The algorithm is based on a set of inputs, such as boundary conditions, heat exchanger pinch-point temperature differences, equipment speed information (compressor speed ratio and evaporator fan speed ratio) and initial guess values, to achieve convergence of the whole cycle. The boundary conditions include outdoor air temperature, indoor air temperature, and indoor air

relative humidity, which are used to provide air-side thermodynamic properties as it enters the condenser or evaporator.

In terms of SSLC main program, the refrigerant cycle begins from the inlet of compressor. In compressor model, the condensing pressure and evaporating pressure can be obtained from the initial guess variables, i.e., the saturation temperatures of refrigerant at evaporation and condensation. Then, combining the given information (the compressor speed ratio and superheated temperature), the mass flow rate, compressor power and refrigerant state at condenser inlet (at compressor outlet) can be calculated.

$$[\dot{m}_r, \dot{W}_{comp}, T_{c,r,i}] = \text{Comp}(T_{evap}, T_{cond}, \Delta T_{sh}, \gamma_{comp}) \quad (3-32)$$

After the compressor model, the condenser model calculates the process that the refrigerant is condensed from superheated state to subcooled state at the condenser outlet (expansion device inlet) based on the energy balance between refrigerant side and air side. In detail, the model uses boundary condition, i.e., the temperature of air entering the condenser coil ($T_{c,a,i}$), the outputs from compressor model ($\dot{m}_r, T_{c,r,i}$) to estimate the refrigerant subcooled temperature and enthalpy at the condenser outlet (expansion device inlet).

$$[\Delta T_{sc}, h_{c,r,o}] = \text{Cond}(\dot{m}_r, T_{c,r,i}, T_{c,a,i}) \quad (3-33)$$

In evaporation, the refrigerant is heated by the airstream flowing through coil from some two-phase quality to a superheated vapor. In the SSLC model, the evaporator simulates this process in the opposite direction. Since the refrigerant state at the evaporator outlet is known, which is $T_{evap} + \Delta T_{sh}$; the air conditions, including dry-bulb temperature and relative humidity at the coil inlet, as well as air flow rate through evaporator coil (\dot{V}_{ea}) are given, the refrigerant enthalpy at evaporator inlet is obtained. Furthermore, the heat transfer rate between air side and refrigerant side, which is also the cooling capacity of the A/C system, is obtained.

$$[h_{e,r,i}, T_{e,a,o}, \dot{Q}_{cap}, SHR] = \text{Evap}(\dot{m}_r, \Delta T_{sh}, T_{e,a,i}, RH_{e,a,i}, \dot{V}_{ea}) \quad (3-34)$$

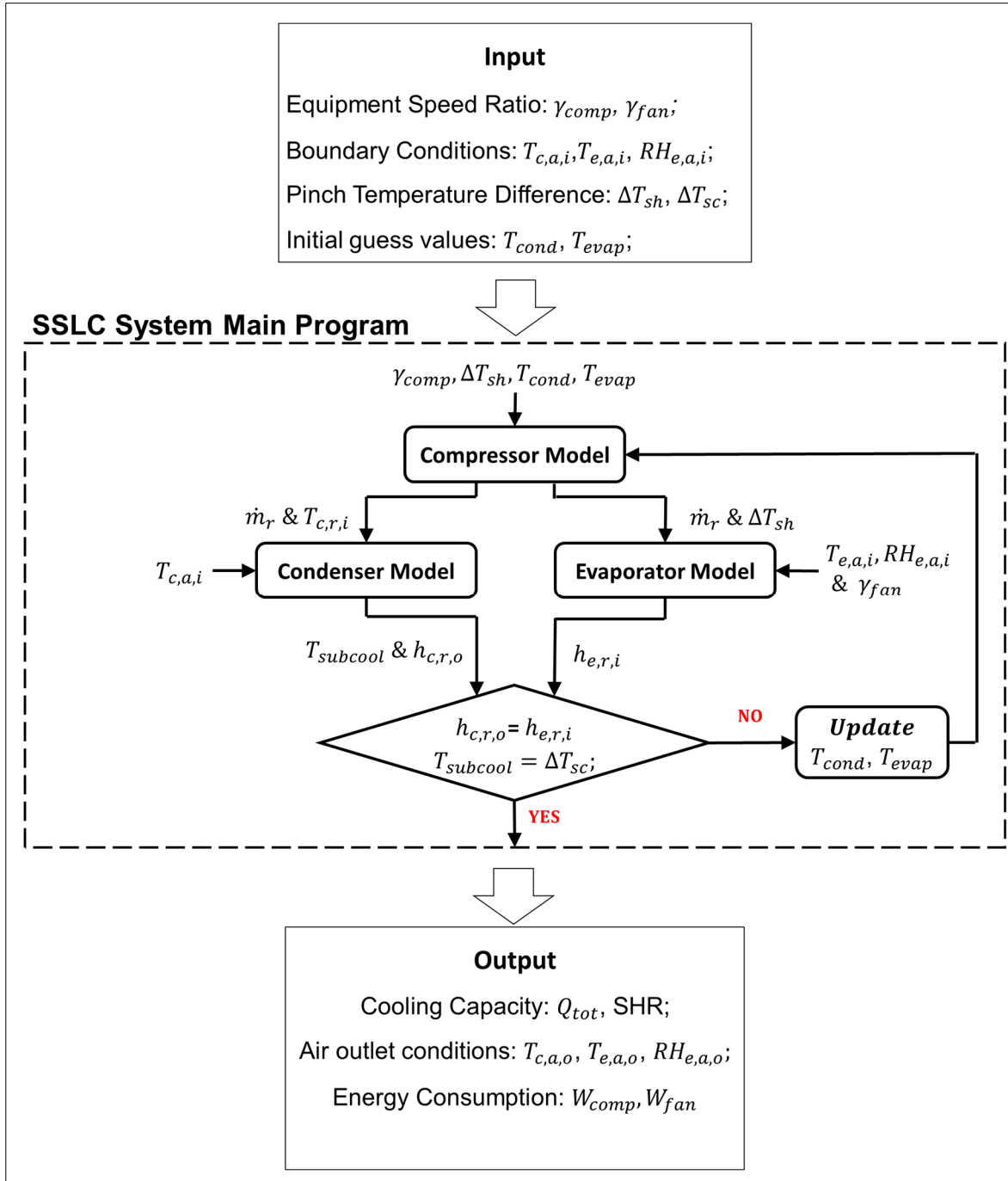


Figure 3.1. Program flow chart of integrated SSLC system.

Once the loop calculation from two directions is accomplished, the first equation in cycle convergence criteria used to update the two initial guess values is based on the aforementioned assumption of an isenthalpic process in the expansion valve:

$$\begin{cases} h_{c,r,o} = h_{e,r,i} \\ \Delta T_{sc,pre} = \Delta T_{sc} \end{cases} \quad (3-35)$$

where, $h_{c,r,o}$ and $h_{e,r,i}$ are enthalpy of refrigerant at the condenser outlet and the evaporator inlet, respectively. The second equation indicates that the subcooling temperature predicted by condenser model is equal to an imposed refrigerant subcooling supplied by the user. A numerical solver called the Trust-Region algorithm in Matlab (Byrd et al., 1988) is used to drive the residual of the equations toward zero through updating from the initial guesses (T_{evap}, T_{cond}).

3.1.6 Re-evaporation Model

During low-SHR mode, the moisture in the air stream condenses on the coil surfaces (including the coil tubes and fins, the condensate pan, and the condensate drain) thanks to the lower evaporating temperature compared to the dew-point air temperature. But when the cooling system is switched to sensible only mode and the coil surface temperature increases, the cooling coil cannot capture moisture at this moment, which leads to the moisture on the coil surface evaporating back into the air stream. As a result, the net dehumidification capacity is lower than what is estimated without considering the re-evaporation phenomenon, and the cooling system spends relatively more time for dehumidification. Therefore, a re-evaporation model is developed to combine with the integrated SSLC system model aimed at estimating the moisture as it evaporates back into the air stream when the cooling system switches from deep dehumidification mode to sensible only mode.

Henderson and Rengarajan (1996) developed a simple model to predict how sensible heat ratio (SHR) varies with runtime for a single-coil that with continuous supply air fan operation. And then, Shirey et al., (2006) improved this model and developed a better on/off cycle moisture evaporation model, which can be applied in the current work. In this re-evaporation model, the evaporator cooling coil can be seen as an evaporative cooler when the re-evaporation occurs, and the evaporation rate can be defined as:

$$q_{evap} = \frac{1.08 \cdot cfm \cdot (DB - WB) \cdot \eta_{evap}}{1060} \quad (3-36)$$

where cfm is the air flow rate through evaporator coil, DB and WB is the dry-bulb and wet-bulb temperature of air entering cooling coil. η_{evap} is defined as the saturation effectiveness of an evaporative cooler, which is calculated as:

$$\eta_{evap} = 1 - e^{-NTU} \quad (3-37)$$

here, NTU is the number of transfer units based on the mass transfer, which can be expressed in Equation (3-38) when an air-water mixture is below 50 °C.

$$NTU = \frac{K \cdot A}{cfm^{0.2}} \quad (3-38)$$

Where K can be obtained by curve fitting and A is the wetted surfaced area, which can be calculated as the ratio of moisture remaining on the coil (M) multiplying the ratio of the fully wetted surface (A_0) to a maximum amount of moisture the coil can hold (M_0).

$$A = \frac{M \cdot A_0}{M_0} \quad (3-39)$$

Besides the evaporation rate, the moisture remaining on the coil is calculated based on amass balance that the rate of moisture evaporation is equal the change of the moisture on the coil surface. The detail mathematical inference is represented in Shirey et al., (2006) work, and the final rearranged equation is:

$$M = \frac{1}{\alpha} \cdot \ln(e^{\alpha\beta t} \cdot (e^{\alpha M_s} - 1) + 1) \quad (3-40)$$

Here, M_s is the amount of moisture in the coil at the end of the dehumidification mode. α and β are correlations introduced to simplify the Equation (3-40).

$$\alpha = \frac{NTU_o}{M_o}; \beta = \frac{1.08 \cdot cfm \cdot (DB - WB)}{1060} \quad (3-41)$$

where M_o is the maximum amount of water hold on the cooling coil surface and NTU_o is calculated at the fully wetted situation.

Recalling all the equations from Equation (3-36) to Equation (3-41), the evaporation rate can be arranged to a function related to time as below:

$$q_{evap} = -\beta \frac{e^{\alpha\beta t} \cdot (e^{\alpha M_s} - 1)}{e^{\alpha\beta t} \cdot (e^{\alpha M_s} - 1) + 1} \quad (3-42)$$

To calculate the re-evaporation rate, the correlation β is determined by dry-bulb and wet-bulb temperature of the air entering the cooling coil, as well as air flow rate, which are obtained from indoor condition measurements. The correlation α is constant in the whole re-evaporation process since the related two correlations (NTU_o and M_o) are only depended on the cooling coil characteristics but not the A/C system boundary conditions.

In this work, the purpose of application of the re-evaporation model is to predict the amount of moisture of water evaporating back to the air stream when the A/C system turns from deep dehumidification mode to sensible only mode. To simplify the problem, there are three assumptions proposed:

- It assumes that no moisture evaporation occurs when the unit is off, since the supply fan does not run to take the moisture back to air.
- A fixed mass of water (M_o) has collected rapidly on the tube and fins surface when the unit is turned from off to deep dehumidification mode, or from sensible only mode to deep dehumidification mode, which means the amount of moisture on the coil surface at the end of the dehumidification mode (M_s) is equal to M_o .
- In Henderson and Rengarajan's re-evaporation model, it ignores the temperature increase of the evaporating coil and the evaporation rate reaches a maximum when the compressor stops running.

The developed re-evaporation model is validated in Chapter 4 based on the experimental testing data.

3.2 Residential Building Model Development

To simulate and investigate how residential buildings respond to different SSLC control strategies and the cooling system operation, a prototypical residential building model is necessary. In the US, there are a wide range of home types and styles, but Huang and Gu (2012) utilized the Residential Energy Consumption Survey (RECS) and the American Home Survey (AHS) to summarize five primary categories of home types throughout the U.S.:

- Single-family detached homes;

- Single-family attached home(duplexes);
- Multi-family residences with four or less units;
- Multi-family residences with five or more units;
- Manufactured homes (mobile home).

The building used in this research is a prototype residential building described by Kneifel, (2012). It is two-stories tall with an integral garage, moderate window area and symmetrical building geometry, and a front-gabled roof. Because the main purpose of constructing the residential building model is to predict the space thermal and moisture system performance, only factors related to the thermal and moisture balance are considered for simplification. Assuming that the building is a system, the factors affecting the thermal balance include the heat transfer from the building envelope, the heat flux due to infiltration and internal heat gains, and the heat removed by the air conditioner. Similarly, for the moisture balance, the factors of moisture flux from infiltration, internal latent heat gain, and condensate removed by the air conditioner are considered.

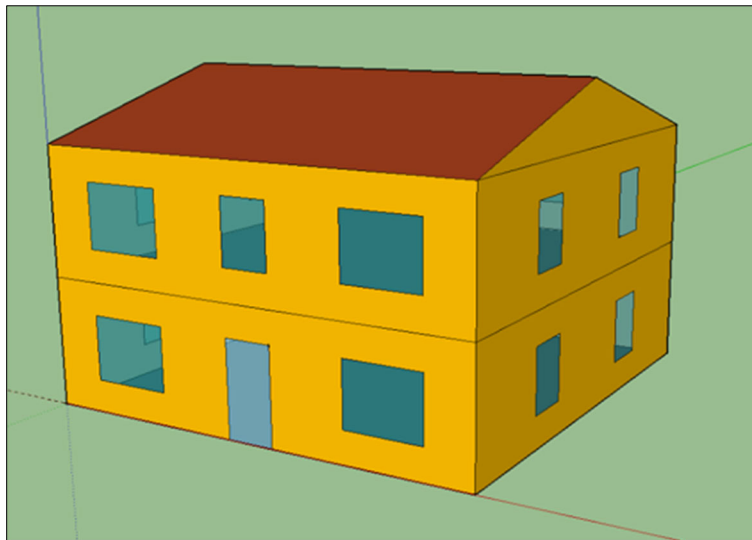


Figure 3.2. Prototype residential building generated in SketchUp.

3.2.1 Building Characteristics

In current work, the simulated building has two floors and with 4 bedrooms is considered as a typical house in the US , the foundation floor area is 1000 ft² (40 ft × 25 ft) and the conditioned floor area is 2000 ft² . And the height is 8 ft for each level and giving a total building

volume of 16000 ft³. The average window area ratio is 12.8%. And the building geometry model in SketchUp is shown in Figure 3.2.

Building Envelope

Here, the characteristics of the building envelope are identified based on the residential building model described by Kneifel (2012). Since the building is treated as a single zone in the simulation, which neglects the temperature difference among different rooms, the material data for internal wall, ceiling (floor) and window is not required in the simulation, other than to account for its impact on building thermal mass. The materials of the external-wall, roof, floor and external-windows are listed in Table 3.3 and Table 3.4 along with their property information.

Table 3.3. Building envelope material data.

	Layers	L [m]	k [kJ/hm K]	c_p [kJ/kg K]	ρ [kg/m ³]
External Wall	Gypsum	0.013	1.26	1.00	1200
	Wall board	0.011	1.69	1.00	1200
	Insulation	0.013	0.54	1.20	800
	Wall board	0.011	1.69	1.00	1200
	Cladding	0.013	0.50	0.90	530
Roof	Plaster board	0.011	0.58	0.84	950
	Insulation	0.012	0.54	1.20	800
	Shingle	0.0095	1.04	1.26	1121
Floor	Capet	0.012	0.187	1.38	560
	Concrete	0.102	4.07	1.00	1400

Table 3.4. Building window data.

Window Type	Layers	U-value [W/m ² K]	SHGC value [-]	Frame U-value [W/m ² K]
1101	Single, glazing	5.68	0.6	10.91

Infiltration heat gain

Based on the method for estimating the infiltration leakage of air between indoor and outdoor environment proposed by Sherman (1987), the general infiltration calculation is a complicated process which is dependent on the various details of the building, indoor and outdoor environment, and the driving force for the leakage. However, in TRNSYS, the type-75a module (Klein et al.,) provides a direct way to calculate infiltration heat gain where the Lawrence Berkeley Laboratory (LBL) infiltration model is applied and envelope leak is assumed to be a simple orifice leak subjected to dynamic wind pressure, buoyancy forces and envelope characteristics. By inputting the outdoor weather data and the effective leakage area (ELA) into TRNSYS, the air change rate (ACH) can be calculated by the software. And the ELA can be calculated by the equation provided by AHRAE 62.2 2004.

$$ELA = A_{sl} \times FAZ \quad (3-43)$$

here, A_{sl} is the specific leakage area constant listed in Table 3.5 and FAZ is the floor area of the zone.

Table 3.5. Specific leakage area.

	Low	Std	High
$A_{sl} [-]$	0.00088	0.00057	0.00036

Then, with a knowledge of the air change rate $ACH [-/hr]$, the total air volume of infiltration $\dot{V}_{inf} [m^3/hr]$, can be presented as the product of building volume V_{bld} and ACH and the heat flux $\dot{Q}_{inf} [kJ/hr]$, caused by infiltration can be presented by the infiltration air-flow multiplied by the temperature difference between ambient temperature (T_a) and the zone temperature (T_z).

$$\begin{aligned} \dot{V}_{inf} &= V_{bld} \cdot ACH \\ \dot{Q}_{inf} &= \dot{V}_{inf} \cdot \rho_{air} \cdot c_p \cdot (T_a - T_z) \end{aligned} \quad (3-44)$$

where ρ_{air} is the density of infiltration air, and c_p is the specific heat of infiltration air.

Internal heat gain

The building internal heat gain should be considered in the calculation of the space-conditioning load and the energy consumption. The internal heat sources include the lighting, people and the equipment. For a single zone, the daily total sensible internal heat gain can be calculated by:

$$I_{gain,sen} = FAE \cdot 15 \left(\frac{Btu}{day} \right) ft^2 + N_{br} \cdot 20000(Btu/day) \quad (3-45)$$

where N_{br} is the number of living units (bedrooms) in building.

Then, the daily total latent internal heat gain can be calculated by:

$$I_{gain,lat} = 0.2 \cdot I_{gain,sen} \quad (3-46)$$

This daily internal heat gain represents the total internal load for a whole day, and the sensible and latent load for each hour (shown in Figure 3.3) is the daily total heat gain multiplied by the corresponding fractions.

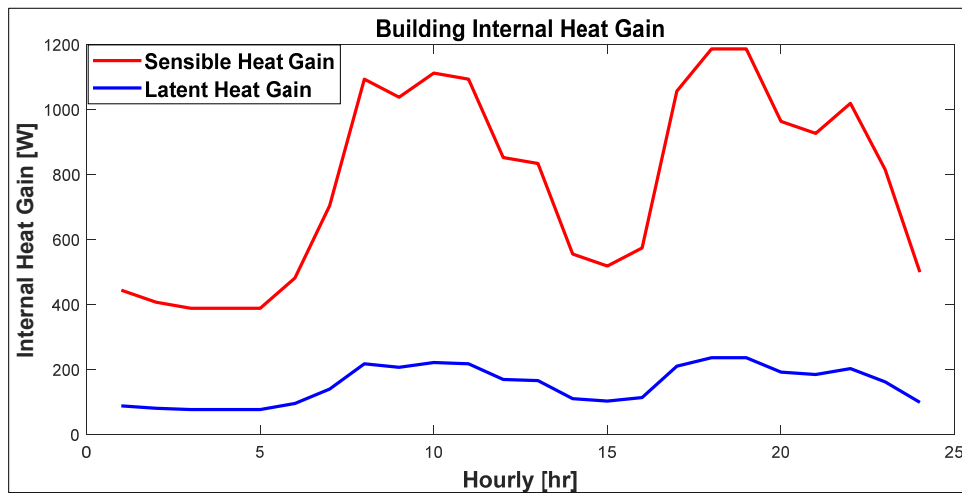


Figure 3.3. Building sensible and latent internal heat gain.

3.2.2 Simulation in TRNSYS

The residential building model is constructed in the TRNSYS. In this research, TRNSYS provides the most convenient way to simulate the prototypical building performance with the input files including:

- Typical Meteorological Year - 3 (TMY-3) weather data.

- Building envelop material data (external-wall, roof, floor and window) (Table 3.3 and Table 3.4).
- Internal heat gain information (daily sensible and latent heat gain and scheduled ratio)(Figure 3.3) .

3.3 Residential Building Model Simplification

The building models generated in commercial software such as TRNSYS and EnergyPlus mainly based on the physical characteristics of a building can accurately simulate the building temperature and humidity performance and calculate the building sensible and latent cooling load. However, when this developed residential building model coupled with the SSLC system model to simulate the building responses to special control strategies, the commercial is time-consuming and the whole co-simulation programming is easy to crash. Furthermore, even if the SSLC could be inserted into the software as a package, the computation time for simulating the coupled building and SSLC system takes an impractically long time.

For this reason, the residential building model used for predicting the building performance needs to be simplified. Furthermore, since the residential building model coupled with the SSLC model is only required to predict the sensible and latent energy flows that impact the indoor space temperature and humidity without considering the physical characteristics, the building model in TRNSYS can be simplified to a thermal model and a moisture model , which can then be used to predict the indoor temperature and humidity fluctuation based on outdoor and indoor disturbance, as well as sensible and latent cooling capacity provided to building by the cooling system.

3.3.1 Thermal Model Simplification

Braun and Chaturvedi (2002) proposed an "Inverse Grey-box Model" to predict the transient building load, with the application of the idea provided by Seem et al., (1989) that the building constructions such as walls, floors and ceilings can be treated as a homogeneous plane and a combination of 3-resistance-2-capacitance (3R2C) to represent the heat transfer rate through it. For further applications, Braun and Chaturvedi (2002) converted a whole building model to an electrical circuit analogy, in which the indoor space is treated as a single air-node, the construction with heat storage as a 3R2C coupled element and the construction without heat storage (such as

window) as a pure resistance element. Then, the thermal network can be easily presented as a state space representation, which can be used to simulate the sensible cooling required to keep the indoor set-point temperature, or the zone temperature at a given time once the ambient and zone disturbances are provided. Applying this method, the residential building model in TRNSYS can be represented as a thermal network to simulate the zone air temperature or to predict the sensible cooling load. The thermal network for the prototypical residential building is shown in Figure 3.4. In the network, the zone air is represented as a single node at the center. Five types of structures of building outside envelopes are included: the external wall, ceiling/roof, floor, and window. All the internal structures are neglected other than accounting for their thermal masses.

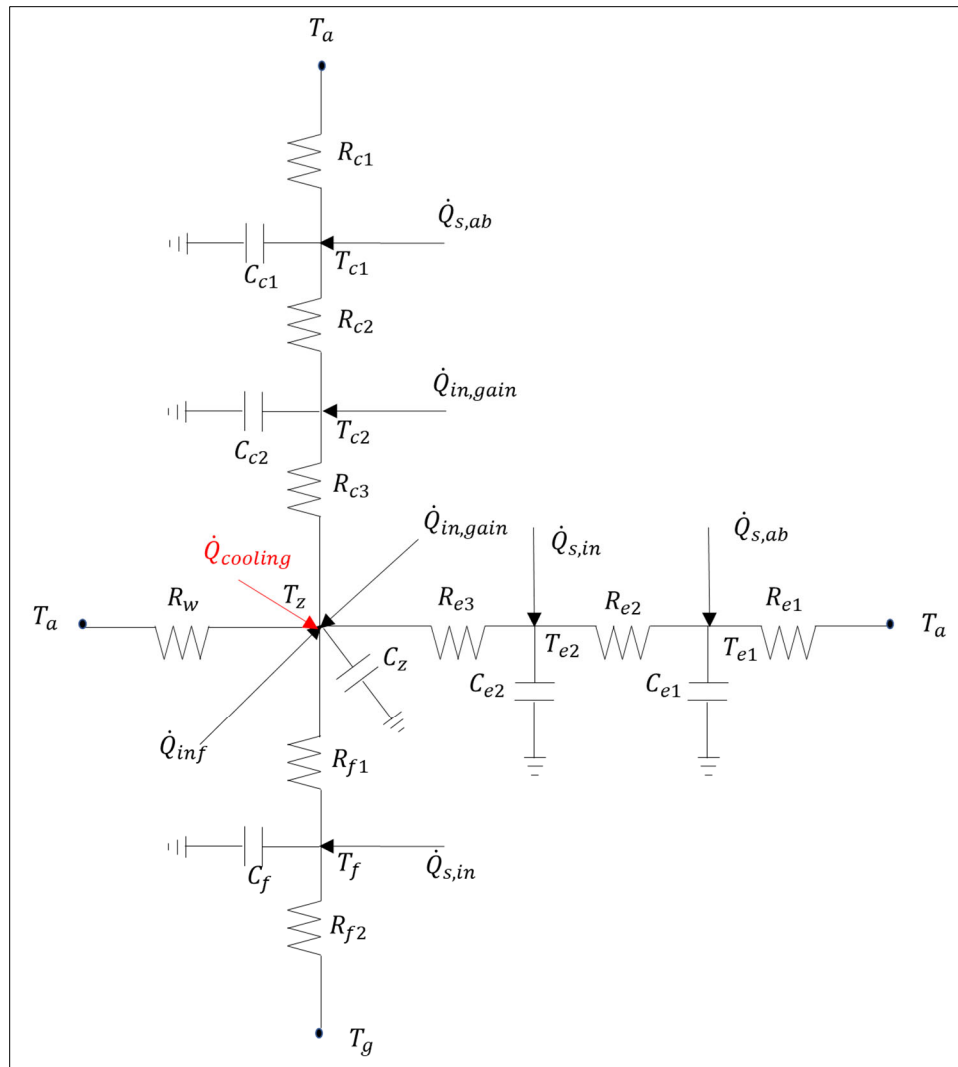


Figure 3.4. Thermal network for the prototypical residential building.

In Figure 3.4, the T , R and C represent the temperatures, resistances and capacitances of the building elements respectively with subscripts e, c, f, w, a, z, g representing the external wall, ceiling, floor, ambient (outdoor), zone (indoor), and ground, respectively. All these resistances and capacitances are assumed to be time invariant. Furthermore, considering the heat gain and loss of the building, the $\dot{Q}_{in,gain}$ represents the internal heat gain (including residents' activities and lighting), assuming 70% of which is on the top of roof and 30% is in the air node. \dot{Q}_{inf} represents the infiltration heat gain from outside, which is directly added to zone air. $\dot{Q}_{s,in}$ and $\dot{Q}_{s,ab}$ represent the solar radiation incident in the building through the windows, and solar radiation absorbed by the outside surface. It is assumed that 50% of solar incident heat gain is on the inside surface of external wall and the other 50% of that on the internal surface of floor. Similarly, 50% of absorbed solar gain is on the outside surface of roof and 50% of that is on the outside surface of external wall. The $\dot{Q}_{cooling}$ is heat removed by the air conditioner. All these heat gains are considered as disturbance inputs to the model, and data of which is collected from the (TMY-3) weather data. Then, the thermal network can be represented by the steady state equation by:

$$\begin{cases} \frac{dx}{dt} = \mathbf{A}x + \mathbf{B}u \\ y = cx + du \end{cases} \quad (3-47)$$

where the output y is zone temperature, the x is state vector and u is disturbance input vector described as below:

$$x^T = [T_{c1}, \quad T_{c2}, \quad T_{e1}, \quad T_{e2}, \quad T_g, \quad T_z] \quad (3-48)$$

$$u^T = [T_a, \quad T_g, \quad \dot{Q}_{s,in}, \quad \dot{Q}_{s,ab}, \quad \dot{Q}_{in,gain}, \quad \dot{Q}_{inf}, \quad \dot{Q}_{cooling}] \quad (3-49)$$

And A is a 6×6 Matrix and B is a 6×7 matrix shown below, c and d are vectors :

$$\mathbf{A} = \begin{bmatrix} A(1,1) & A(1,2) & 0 & 0 & 0 & 0 \\ A(2,1) & A(2,2) & 0 & 0 & 0 & A(2,6) \\ 0 & 0 & A(3,3) & A(3,4) & 0 & 0 \\ 0 & 0 & A(4,3) & A(4,4) & 0 & A(4,6) \\ 0 & 0 & 0 & 0 & A(5,5) & A(5,6) \\ 0 & A(6,2) & 0 & A(6,4) & A(6,5) & A(6,6) \end{bmatrix} \quad (3-50)$$

$$\mathbf{B} = \begin{bmatrix} B(1,1) & 0 & B(1,3) & 0 & 0 & 0 & 0 \\ 0 & 0 & 0 & 0 & B(2,5) & 0 & 0 \\ B(3,1) & 0 & B(3,3) & 0 & 0 & 0 & 0 \\ 0 & 0 & 0 & B(4,4) & 0 & 0 & 0 \\ 0 & B(5,2) & 0 & B(5,4) & 0 & 0 & 0 \\ B(6,1) & 0 & 0 & 0 & B(6,5) & B(6,6) & B(6,7) \end{bmatrix} \quad (3-51)$$

with the nonzero elements are listed in Table 3.6 and Table 3.7. $c = [0, 0, 0, 0, 0, 1]$ and $d = \vec{0}$.

Table 3.6. Non-zero element in matrix \mathbf{A} .

$A(1,1) = -\left(\frac{1}{C_{c1}R_{c1}} + \frac{1}{C_{c1}R_{c1}}\right);$	$A(1,2) = \frac{1}{C_{c1}R_{c2}};$
$A(2,1) = \frac{1}{C_{c2}R_{c2}};$	$A(2,2) = -\left(\frac{1}{C_{c2}R_{c2}} + \frac{1}{C_{c2}R_{c3}}\right);$
$A(2,6) = \frac{1}{C_{c2}R_{c3}};$	$A(3,3) = -\left(\frac{1}{C_{e1}R_{e1}} + \frac{1}{C_{e1}R_{e2}}\right);$
$A(3,4) = \frac{1}{C_{e1}R_{e2}};$	$A(4,3) = \frac{1}{C_{e2}R_{e2}};$
$A(4,4) = -\left(\frac{1}{C_{e2}R_{e2}} + \frac{1}{C_{e2}R_{e3}}\right);$	$A(4,6) = \frac{1}{C_{e2}R_{e3}};$
$A(5,5) = -\left(\frac{1}{C_{e2}R_{e2}} + \frac{1}{C_{e2}R_{e3}}\right);$	$A(5,6) = \frac{1}{C_g R_{f1}};$
$A(3,4) = \frac{1}{C_z R_{c3}};$	$A(6,4) = \frac{1}{C_z R_{e2}};$
$A(3,4) = \frac{1}{C_z R_{f1}};$	$A(6,6) = -\left(\frac{1}{C_z R_{f2}} + \frac{1}{C_z R_{e3}} + \frac{1}{C_z R_{e3}} + \frac{1}{C_z R_w}\right).$

Table 3.7. Non-zero element in matrix \mathbf{B} .

$B(1,1) = \frac{1}{C_{c2}R_{c2}};$	$B(1,3) = \frac{1}{C_{c1}};$	$B(2,5) = \frac{1}{C_{c2}};$
$B(3,1) = \frac{1}{C_{e1}R_{e1}};$	$B(3,3) = \frac{1}{C_{e1}};$	$B(1,1) = \frac{1}{C_{e1}};$
$B(5,2) = \frac{1}{C_f R_{f1}};$	$B(5,4) = \frac{1}{C_f};$	$B(1,1) = \frac{1}{C_z R_w};$
$B(6,5) = \frac{1}{C_z};$	$B(6,5) = \frac{1}{C_z};$	$B(1,1) = \frac{1}{C_z}.$

3.3.2 Moisture Model Simplification

For the moisture model, there are few related publications. In TRNSYS, there two types of moisture models are included (Kummert, 2007): the effective capacitance humidity Model (EC Model) and the buffer storage humidity model (BS model). In the EC model, the moisture buffering effect of the building envelopes can be lumped together, which is defined as the product of the zone air mass and the moisture capacitance ratio:

$$M_{eff,i} = Ratio \cdot M_{air,i} \quad (3-52)$$

where $M_{eff,i}$ is the effective moisture capacity of the zone, $M_{air,i}$ is the mass of air in the zone, and the *Ratio* is the multiplication factor that can be set from 1 to 10. The EC model in TRNSYS introduces a concept called "effective penetration depth" to represent the depth that moisture penetrates into a material. Based on this idea, the moisture model for a building can be treated as a lumped model, in which the moisture in the space transfers from a node of space zone to a node of building internal surface, and then transfer to a node of building deep walls or other structures. Kramer et al., (2013) applied this model as a resistance-capacitance (RC) network and used it to predict the indoor climate which is then validated by on-site measurements. And Cai & Braun (2016) also applied MB model to study the inverse hygrothermal model for multi-zone building.

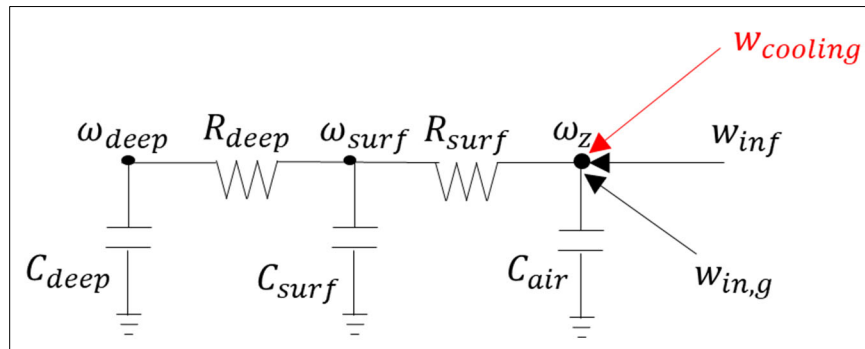


Figure 3.5. Moisture network for building model.

The simplified moisture model applied in this research is presented as the R-C moisture network shown in Fig. 3.5, in which ω_{deep} , ω_{surf} are the humidity ratio of the deep and surface of building interior envelopes, and ω_z is the humidity ratio of the space air. The unit for all the humidity ratio is [g/kg]. R and C represent the resistance and capacitance, and the subscript *deep*,

surf and *air* mean the envelop deep node, surface node and indoor zone node. Furthermore, moisture gain by infiltration (w_{inf}) and internal gain ($w_{in,g}$), as well as moisture removal by air conditioner ($w_{cooling}$) are inputs to the air nodes.

Based on the mass balance, the moisture network also can be represented as a steady state equation similar to Equation (3-47), where the output y is the indoor humidity ratio, x is state and u is disturbance input shown below:

$$x^T = [\omega_{deep}, \quad \omega_{surf}, \quad \omega_z], \quad (3-53)$$

$$u^T = [w_{inf}, \quad w_{in,g}, \quad w_{cooling}], \quad (3-54)$$

And \mathbf{A} is a 3×3 Matrix and \mathbf{B} is a 3×3 matrix described below:

$$A = \begin{bmatrix} -\left(\frac{1}{C_{deep}R_{deep}}\right) & \frac{1}{C_{deep}R_{deep}} & 0 \\ \frac{1}{C_{suf}R_{deep}} & -\left(\frac{1}{C_{surf}R_{deep}} + \frac{1}{C_{suf}R_{surf}}\right) & \frac{1}{C_{suf}R_{surf}} \\ 0 & \frac{1}{C_{air}R_{deep}} & -\left(\frac{1}{C_{air}R_{surf}}\right) \end{bmatrix}, \quad (3-55)$$

$$B = \begin{bmatrix} 0 & 0 & 0 \\ 0 & 0 & 0 \\ \frac{1}{C_{air}} & \frac{1}{C_{air}} & -\frac{1}{C_{air}} \end{bmatrix}, \quad (3-56)$$

$$c = [0,0,1] \text{ and } d = \vec{0}.$$

With these simplified thermal model and moisture model, the indoor space temperature and humidity can be well simulated coupled with the SSLC mode.

3.3.3 Simplified Residential Building Model Training

In the simplified residential building model, including the thermal and moisture model, the resistances (R) and capacitances (C) are trained by the simulation results from TRNSYS. The input quantities, including outdoor dry-bulb temperature, absolute humidity, heat gain from direct solar radiation incident, solar radiation absorbed on exterior surface, are observed from the TYM3 weather data directly. The other input quantities, such as internal heat and moisture gain, infiltration heat gain, are calculated depending on the methods described in section 3.2.

The initial value is calculated based on the building physical characteristics such as the building envelope's physical information, including wall thickness, surface area, thermal conductivity, specific heat and density, which is collected based on the setting in the TRNSYS building model in Table 3.3 and Table 3.4, to calculate the initial C-R values. Also, the maximum and minimum thermal conductivity, specific heat and density are used to set the bounds on R and C values.

It is assumed that all these R and C values are not time varying, and a nonlinear least-squares method is used to calculate the parameters of C and R by matching dry-bulb temperature and humidity ratio predicted from the simplified model to those from the TRNSYS simulated results. The numerical method for the nonlinear least square's method is the trust-region-reflective method (Coleman & Li, 1996), and the cost function is:

$$J = \sum_{k=1}^{N_{train}} (X_z - X_{trn})^2 \quad (3-57)$$

where N_{train} is the number of data points used in the training. X here can be the temperature or humidity ratio in the space, X_z are the simulated values from the simplified model, X_{trn} are data obtained from the TRNSYS simulation results for three summer months with one-minute time step.

To evaluate the impact of the different climates on the building performance under different control strategy, simulations coupling simple building model and SSLC system model are run with weather data for four different locations in United States. Figure shows the four locations representing different weather characteristics: (1) Phoenix, AZ; (2) Miami, FL; (3) Indianapolis, IN; (4) Denver; CO are selected to be representative of hot and dry, hot and humid, cold and humid; cold and dry climate zone.

simulation results for most of time. The largest RMSE value is found in plot of Phoenix (1.19 °C), whereas the smallest RMSE value is shown in the plot of Miami (0.43 °C).

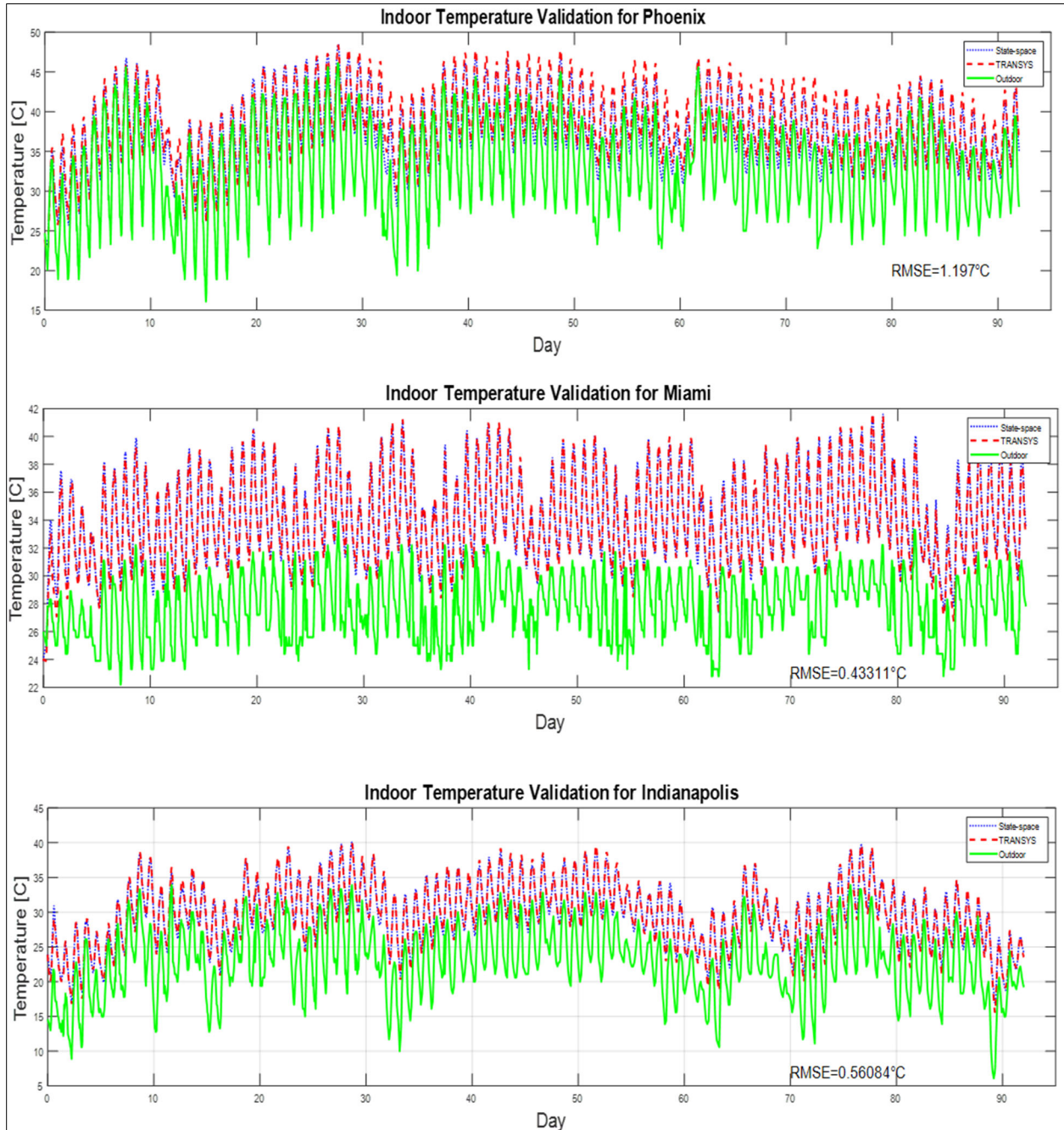


Figure 3.7. Indoor temperature comparison for state-space thermal model and TRNSYS in Phoenix, Miami, Indianapolis and Denver.

Figure 3.7 continued

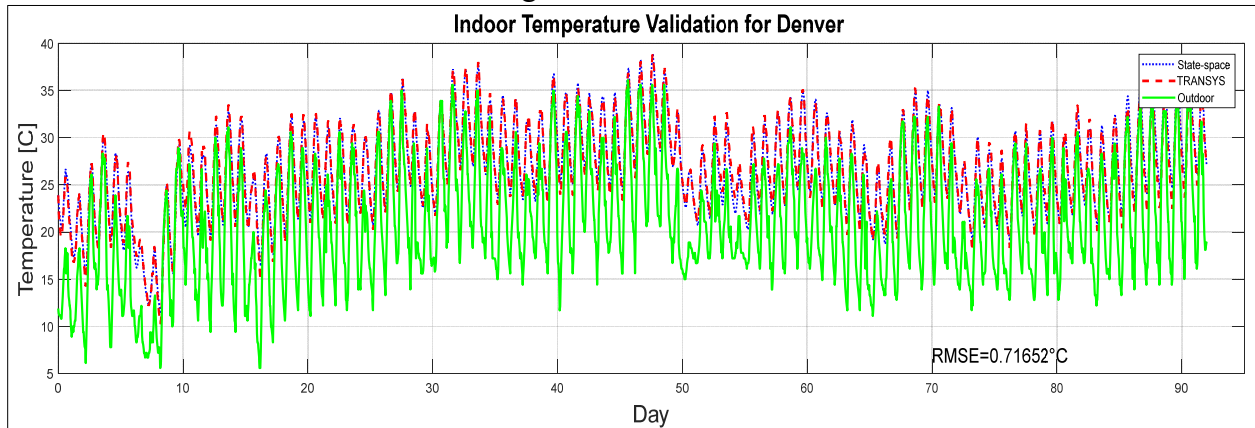


Figure 3.8 is another set of validation results for the moisture model. It can be seen that there is a good agreement between the absolute humidity (humidity ratio) predicted by the state-space moisture model and the results from the TRNSYS model. But for Miami and Denver, the prediction difference between state-space model and TRNSYS model is significantly larger, when the outdoor humidity fluctuates more dramatically. Except for Denver, the MAPE values are less than 10% for Phoenix, Miami and Indianapolis, since the weather in Denver is much drier as compared to the others.

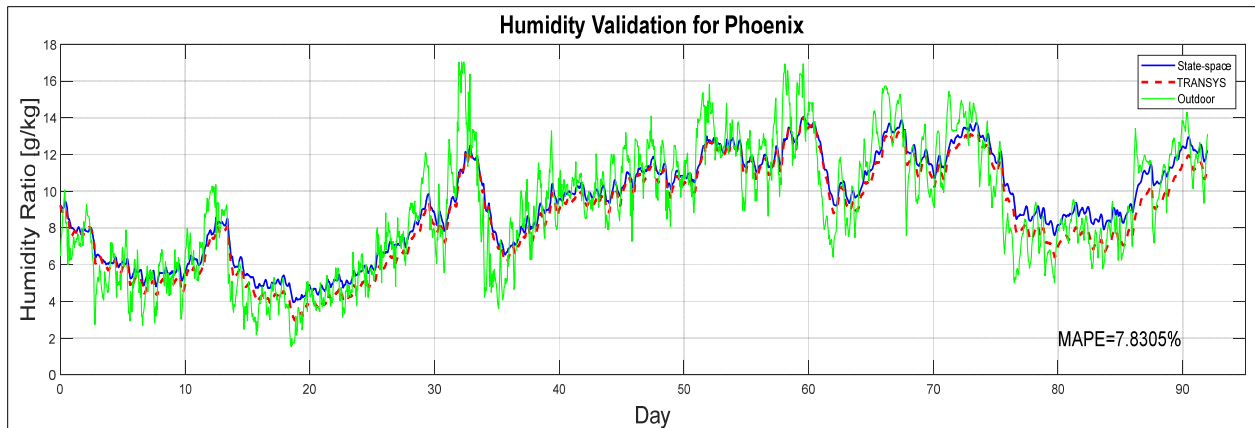
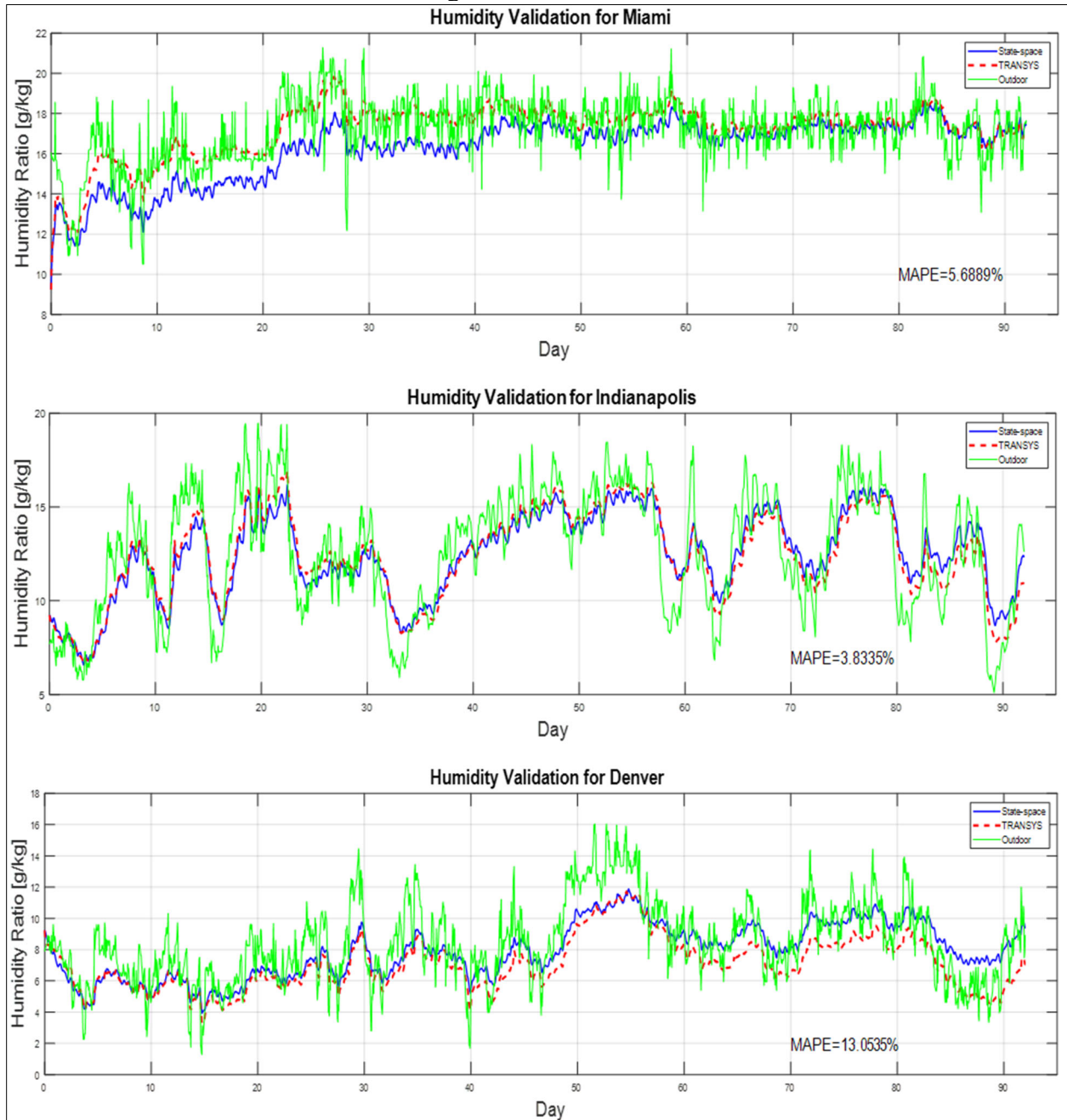


Figure 3.8. Indoor humidity ratio comparison for state-space moisture model and TRNSYS in Phoenix, Miami, Indianapolis and Denver.

Figure 3.8 continued



Since the thermal and moisture models in this research are used for building performance simulation corresponding to different SSLC control strategies, the error between state-space models and TRNSYS simulation results shown above is considered as acceptable.

3.4 Summary

In this chapter, a physics-based direct expansion A/C unit model is developed to predict the SSLC system performance, especially the system's cooling and dehumidification capacity and system overall power input, under various compressor and evaporator fan speeds. The developed SSLC system model contains four basic components: compressor, condenser, expansion valve and evaporator. The models of each component are developed separately, then each of them is connected as a cycle to become an integrated SSLC system model. Beside the SSLC system model, re-evaporation is considered in current work and the related numerical model is described in this chapter. Furthermore, in order to better understand the building responses to the implementation of SSLC system and SSLC control strategy, a prototype residential building is created in TRNSYS. To simplify the co-simulation between building space and SSLC system, the prototype residential building model in TRNSYS is transferred as a state-space thermal model and a state-space moisture model, which are validated by the simulation results from TRNSYS throughout the summer in four cities. In summary, the SSLC system model and the prototype building model is described in this chapter. In the following chapters, the SSLC system model will also be validated.

4. EXPERIMENTS AND MODEL VALIDATION

The sequential SSLC integrated model is developed in the previous chapter. In this chapter, the developed SSLC model is validated by experimental tests performed in laboratory environments. The heat pump used for the validation testing is a commercialized variable-speed heat pump with a nominal cooling capacity of 4-tons. The heat pump uses R410A as its working fluid and contains two units: (1) an outdoor unit mainly consisting of a variable speed scroll compressor (from 1800 rpm to 3500 rpm), a condenser coil, and a fan that blows ambient air through the condenser coil; (2) an indoor unit including a thermostatic expansion valve (TXV) to control pressure ratio and mass flow rate of the refrigerant, an evaporator coil, and a supply fan that is continuously controlled to provide an air flow rate ranging from 250 cfm (lowest speed) to 1600 cfm (full speed). To validate the integrated system model, the model for each component of the heat pump is validated first and then the whole integrated system is validated with all component model combined together. Besides the SSLC system model, the re-evaporation model described in Chapter 3 is also validated, the related parameters are trained. Furthermore, with the implementation of the SSLC system model, the performance of heat pump is predicted under varied equipment speeds, which also can be used to explain the potential of energy saving with the application of the proposed SSLC methodology.

4.1 Experimental Description

4.1.1 Experiment Set-up

The tested heat pump is set up in psychrometric chambers at the Herrick Labs at Purdue University. The indoor and outdoor units are placed in two insulated rooms with independent temperature and humidity control to set the rooms at the required indoor and outdoor operating conditions.

A schematic representation of the test unit is shown in Figure 4.1, where each component of the indoor and outdoor units, and the location of the sensors are indicated in the sketch.

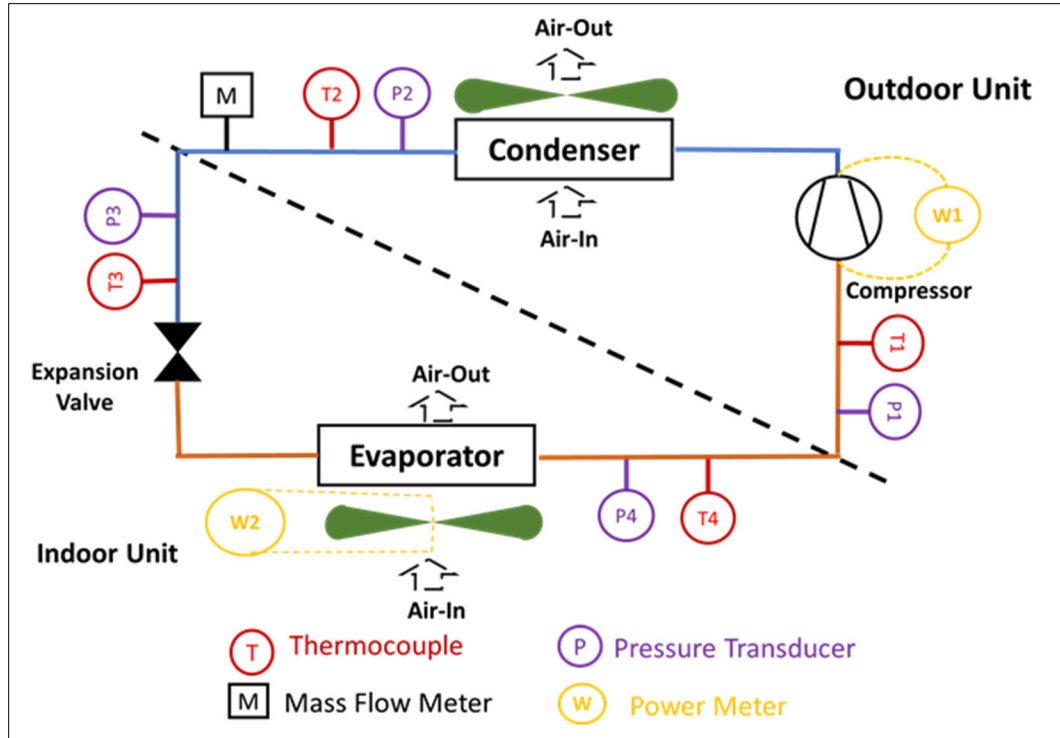


Figure 4.1. Testing system set-up at the refrigerant side.

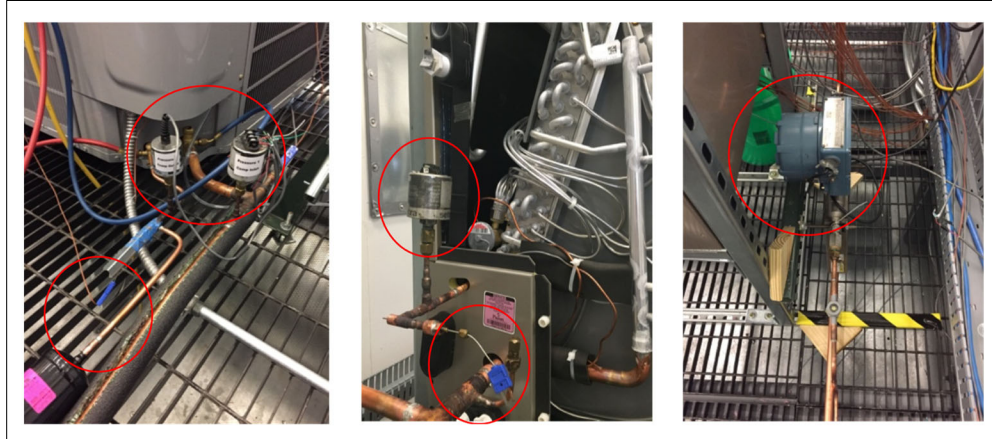


Figure 4.2. Location of sensors at refrigerant line: pressure transducer, thermocouple and mass flow meter.

As shown in Figure 4.1, four pressure transducers are installed along the refrigerant line: two of them are at the outlet of the outdoor unit (P2 in Figure 4.1) and inlet of the indoor unit (P3 in Figure 4.1), they are the high pressure transducers to measure the refrigerant pressure of condenser outlet ($P_{cond,out}$) and expansive valve inlet ($P_{TXV,in}$). The other two pressure transducers are along low pressure line: P4 in Figure 4.1 is used to measure the pressure of the

refrigerant flowing out of indoor unit ($P_{evap,out}$), and P1 is to measure the pressure of refrigerant entering the outdoor unit ($P_{comp,in}$). Through measuring the inlet and outlet refrigerant pressure of the two units, the evaporating and condensing pressure can be calculated, and the pressure drop along the refrigerant line between the two units can be obtained. Furthermore, temperatures of the refrigerant are measured by probe-type thermocouples (T type), with an accuracy of $\pm 0.5^\circ\text{C}$. There are four thermocouples (shown in Figure 4.1 as T1, T2, T3 and T4) installed along the refrigerant line, to measure the temperature of the refrigerant at the entrance and exit of the units. And then the evaporating and condensing temperature, as well as superheated and sub-cooled temperature can be calculated. A mass flow meter, labeled as M in Figure 4.1 is installed at the inlet of the TXV and the upstream of thermocouple and pressure transducer (P3), which is used to measure the refrigerant mass flow rate (\dot{m}_r).

At the air side of the indoor unit, a 3×3 wire-type thermocouple grid ($\pm 1^\circ\text{C}$ accuracy for each thermocouple) is installed in the air duct connecting the indoor unit outlet (shown in Figure 4.3) to measure the dry-bulb temperature ($T_{db,a,o}$) of air exiting the evaporator coil. Based on the ANSI/ASHRAE Standard 111-1988, the thermocouple grid is set at the height of 35 inches from the air-flow duct inlet, where the out-flowing air is considered to be effectively mixed. Moreover, a small amount of air at inlet and outlet of the indoor unit is extracted to a dew-point sensor, to measure the air dew-point temperature ($T_{dp,a,i}$; $T_{dp,a,o}$). At the indoor unit air inlet, the same 3×3 wire type thermocouple grid is also installed to measure dry-bulb temperature ($T_{db,a,i}$) of entering air. And the relative humidity is measured by the sensor in the psychometric room. Finally, the out-flowing air stream flows through the nozzle box, where the air mass flow rate ($\dot{m}_{e,a}$) and air atmospheric pressure (P_{atm}) are measured.

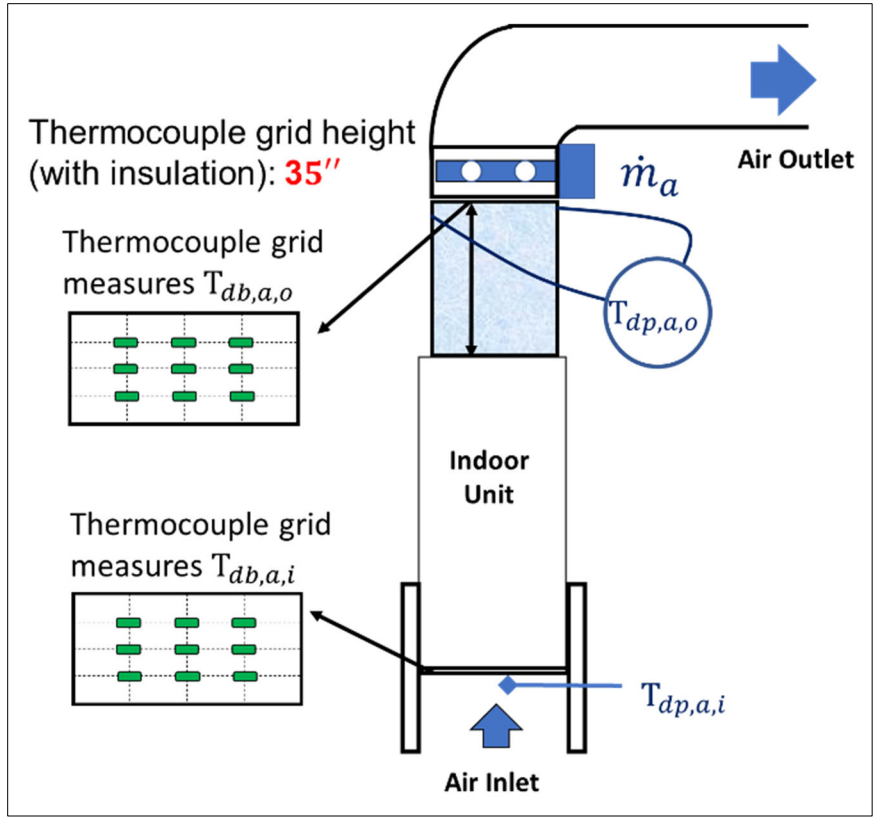


Figure 4.3. Experiment set-up on the air side.

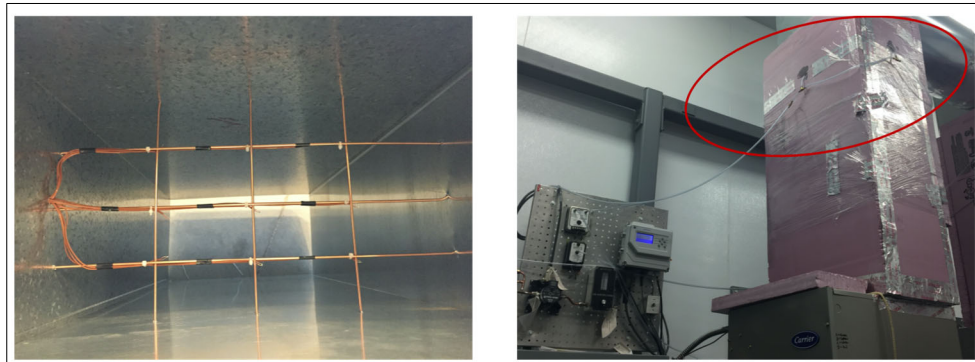


Figure 4.4. Sensors location on the air side: thermogrid for drybulb temperature, dew-point hygrometer.

Furthermore, there are two power meters installed to measure the power of the outdoor unit (including compressor and condenser fan) and indoor fan, respectively. Because the condenser fan speed is locked with the compressor speed and the power of condenser fan can be read from the software of the controller, the power of compressor can be obtained by subtracting the condenser

fan power from total outdoor unit power . The model and sensitivity of all sensors are listed in the Table 4.1.

Table 4.1. The model and uncertainty of measurement sensors.

	Sensor Model	Uncertainty (absolute/relative)
Temperature of refrigerant	Omega Thermocouple wire (T type)	$\pm 0.5^{\circ}\text{C}$
Pressure of refrigerant	Setra 206	$\pm 0.13\%$
Mass flow rate of refrigerant	Micro Motion Model DH025	$\pm 0.15\%$
Dry-bulb temperature of air	Omega Thermocouple Probe (T type)	$\pm 1^{\circ}\text{C}$
Dew-point temperature of air	D-2 OptiSonde General Eastern Chilled Mirror Hygrometer	$\pm 0.2^{\circ}\text{C}$
Mass flow rate of air	Ebtron GTx116-P+	$\pm 3\%$
Indoor fan power	DL5C5PAN7 of Scientific Columbus	$\pm 0.1\%$
Compressor power	PDM21331-A Multifunction	$\pm 0.1\%$

4.1.2 Testing Conditions

The primary purpose of the testing conducted in this research is to validate the SSLC system model in both operating modes (sensible-only and low-SHR) over a reasonable range of conditions. Thus, two regions were selected in the ASHRAE psychometric chart (shown in Figure 4.5) as the test regions of interest for the two modes of the SSLC system. The red area is bounded by the lines connecting the following four points, which are:

$$\begin{aligned}
 Point_{red} (1) &= (T_{red,1} = 15.56^{\circ}\text{C} (60^{\circ}\text{F}), RH_{red,1} = 60\%, P = P_{atm}) \\
 Point_{red} (2) &= (T_{red,2} = T_{red,1}, RH_{red,2} = 40\%, P = P_{atm}) \\
 Point_{red} (3) &= (T_{red,3} = 32.22^{\circ}\text{C} (90^{\circ}\text{F}), \omega_{red,3} = \omega_{red,2}, P = P_{atm}) \\
 Point_{red} (4) &= (T_{red,4} = T_{red,3}, RH_{red,4} = RH_{red,1}, P = P_{atm})
 \end{aligned} \tag{4-1}$$

In the blue area the equipment is tested in such a way that the SHR achieves its lowest possible value owing to the high relative humidity of the indoor air conditions. For the sensible

only region, the dry-bulb temperatures at points 1 and 2, and 3 and 4 are the same, and the relative humidities for points 1 and 4 are same. Point 3 is determined by choosing a point with the same humidity ratio as point 2 and the same dry-bulb temperature as point 4. The five points bounding the low-SHR (deep dehumidification) region are:

$$\begin{aligned}
 \text{Point}_{blue} (1) &= (T_{blue,1} = 15.56^{\circ}\text{C} (60^{\circ}\text{F}), RH_{blue,1} = 90\%, P = P_{atm}) \\
 \text{Point}_{blue} (2) &= (h_{blue,2} = h_{blue,1}, RH_{blue,2} = 40\%, P = P_{atm}) \\
 \text{Point}_{blue} (3) &= (T_{blue,3} = 32.22^{\circ}\text{C} (90^{\circ}\text{F}), RH_{blue,3} = RH_{blue,2}, P = P_{atm}) \quad (4-2) \\
 \text{Point}_{blue} (4) &= (T_{blue,4} = T_{blue,3}, RH_{blue,4} = 70\%, P = P_{atm}) \\
 \text{Point}_{blue} (5) &= (h_{blue,5} = h_{blue,4}, RH_{blue,5} = RH_{blue,1}, P = P_{atm})
 \end{aligned}$$

For the blue region, the enthalpy of points 1 and 2, and 4 and 5 are the same; the relative humidity of points 1 and 5 are the same, and the relative humidity of point 2 is equal to that of point 3.

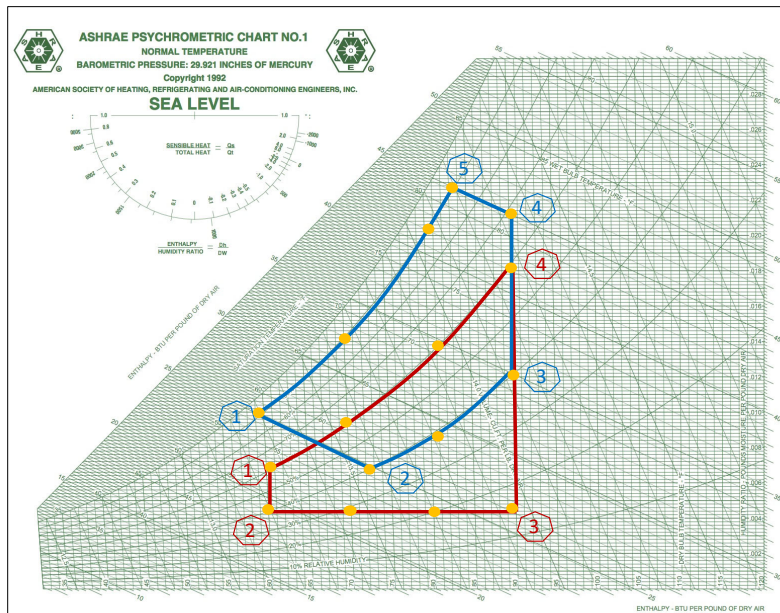


Figure 4.5. Testing conditions on the psychrometric chart.

The outdoor conditions selected for the tests include the following dry-bulb temperatures: 18.33 °C (65 °F), 23.89 °C (75 °F), 35.00 °C (95 °F) and 40.56 °C (105 °F). All outdoor conditions used in the tests involve the same relative humidity of 44%.

4.1.3 Test Data Calculation and Uncertainty Analysis

The measured quantities are calculated and converted to the parameters that can be directly input to each component model, and then the outputs of each component model are compared with the corresponding parameters predicted by the SSLC model. The related testing data calculations are described as follows.

Testing Data Calculation

For the compressor, the tested refrigerant mass flow rate and the compressor power are compared with those predicted by the simulation model. Because the compressor power and refrigerant mass flow rate are directly measured quantities by power meters and mass flow meter, there involves no further calculation.

Considering the refrigerant side of the condenser, the measured quantities are the pressure and temperature at the outlet. The condensing pressure is the value measured at the condenser coil outlet assuming the pressure drop along coil is neglected. Then, the condensing temperature is the average of saturated liquid and vapor temperature:

$$T_{cond} = \frac{T_{c,r,v} + T_{c,r,l}}{2} \quad (4-3)$$

where the $T_{c,r,l}$ and $T_{c,r,v}$ are the saturated liquid and vapor temperature of refrigerant corresponding to the condensation pressure, respectively. They can be calculated in EES or Matlab with Coolprop, and obtained by:

$$\begin{aligned} T_{c,r,v} &= T(P_{cond}, \phi = 1), \\ T_{c,r,l} &= T(P_{cond}, \phi = 0), \end{aligned} \quad (4-4)$$

here, the P_{cond} is the condensing pressure in the coil and ϕ is the refrigerant vapor quality. Moreover, the sub-cooled temperature (ΔT_{sc}) can be obtained by:

$$\Delta T_{sc} = T_{cond} - T_{cond,out} \quad (4-5)$$

The air flow rate ($m_{c,a}$) through condenser coil is obtained from the manufacturer's information. The condenser fan speed is locked with the compressor and changes with compressor speed.

For the indoor unit, the evaporating pressure is the quantity measured at the outlet of evaporator with the assumption that the refrigerant flows through the coil with constant pressure. Then, the evaporating temperature is calculated by:

$$T_{evap} = \frac{T_{e,r,v} + T_{e,r,l}}{2} \quad (4-6)$$

where the $T_{e,r,l}$ and $T_{e,r,v}$ are the saturated liquid temperature and saturated vapor temperature of the refrigerant corresponding to the evaporating pressure, respectively. Similarly, they can be calculated as follows:

$$\begin{aligned} T_{e,r,v} &= T(P_{evap}, \phi = 1), \\ T_{e,r,l} &= T(P_{evap}, \phi = 0), \end{aligned} \quad (4-7)$$

Also, the super-heat temperature (ΔT_{sh}) is calculated by:

$$\Delta T_{sh} = T_{evap,out} - T_{evap} \quad (4-8)$$

Furthermore, the enthalpy of refrigerant at the inlet and outlet of the evaporator is estimated to calculate the cooling capacity on the refrigerant side. The refrigerant enthalpy of coil outlet ($h_{evap,out}$) can be obtained by the measured temperature ($T_{evap,out}$) and refrigerant pressure ($P_{evap,out}$) at the corresponding location. For the inlet, the refrigerant enthalpy is approximately equal to the refrigerant enthalpy at the inlet of TXV ($h_{TXV,in}$), with assumption that the process in the TXV is isenthalpic.

$$\dot{Q}_{evap,r} = \dot{m}_r(h_{evap,out} - h_{TXV,in}) \quad (4-9)$$

where $\dot{Q}_{evap,r}$ is the cooling capacity on the refrigerant side of evaporator.

On the air side of the evaporator, the cooling capacity can be obtained by:

$$\dot{Q}_{evap,a} = \dot{m}_a(h_{e,a,i} - h_{e,a,o}) \quad (4-10)$$

where \dot{m}_a is the mass flow rate of the air stream, $h_{e,a,i}$ is the entering air enthalpy determined by the measured dry-bulb and dew-point temperatures at the inlet of the unit, $h_{e,a,o}$ is the out-flowing air enthalpy determined by the measured dry-bulb and dew-point temperatures at the outlet of the unit.

During the tests, the group of testing data is considered as valid when the cooling capacity at the air side matches that at the refrigerant side within a relative error of $\pm 10\%$. And the SHR (the ratio of sensible cooling capacity to the total cooling capacity) is provided by:

$$SHR = \frac{T_{e,a,i} - T_{e,a,o}}{h_{e,a,i} - h_{e,a,o}} \quad (4-11)$$

where $T_{e,a,i}$ and $T_{e,a,o}$ are the dry-bulb temperature of air stream at inlet and outlet respectively.

The coefficient of performance (COP) is then given as:

$$COP = \frac{\dot{Q}_{evap,r}}{\dot{W}_{OD} + \dot{W}_{Fan}} \quad (4-12)$$

where the \dot{W}_{OD} , \dot{W}_{Fan} are the power of outdoor unit and indoor unit fan.

Uncertainty Analysis

Uncertainty of the model quantifies the potential difference between the true values of output to model predicted values of output. The “Uncertainty Analysis” is conducted here to estimate the effect of the uncertainties in the individual measurement on the calculated results (Moffat, 1988).

In particular, Cheung and Wang (2018) break up overall uncertainty of a model into four contribution components: uncertainty due to inputs, uncertainty due to outputs, uncertainty due to numerical methods and uncertainty due to model random error. However, in the SSLC model, most parts are physics-based, the uncertainty of model is considerably small, thus, only the uncertainty due to experimental data and the variable uncertainty propagation are studied in the current work.

The uncertainty analysis in this work is based on Moffat’s (1988) and Moffat's (1988) work. And the uncertainties of each experimental data point is represented as error bars in the following work.

4.2 SSLC system Model Validation

During the experimental steady-state testing, a total of 30 different boundary conditions (i.e., combinations of different indoor temperature, indoor humidity, and outdoor temperature) were tested. In particular, each condition was tested under two combinations of equipment speeds: full compressor speed with the lowest evaporator fan speed; and the lowest compressor speed with full evaporator fan speed. A total of 60 steady-state data points were collected in this process. Validation of the SSLC system model was performed by comparing model-predicted quantities against those directly calculated from the measured results. The mean absolute percentage error (MAPE) of the quantity or root mean square error (RMSE) was used as an indicator of the model accuracy:

$$MAPE = \frac{100\%}{n} \sum \left| \frac{y_i^{actual} - y_i^{predict}}{y_i^{actual}} \right| \quad (4-13)$$

$$RMSE = \sqrt{\frac{1}{n} \sum (y_i^{actual} - y_i^{predict})^2} \quad (4-14)$$

The numerical model is validated component by component first (compressor model and evaporator model), and then validated as an integrated system.

4.2.1 Compressor Model Validation

As shown in Figure 4.6, the empirical constants (a_1, a_2, a_3, W_{loss} and $b_1, b_2, \delta p$) involved in the compressor model are trained by 30 out of the 60 total test points (red points in Figure 4.6), and then are validated using the remaining 30 points (blue points in Figure 4.6). The parameter values that were obtained through model training are listed in Table 4.2.

Table 4.2. Values of parameters used in compressor model.

a_1	a_2	a_3	W_{loss}	b_1	b_2	δp
278.45	1.94	1.41×10^3	226.85	4.99	-7.54×10^{-5}	0.993

The following set of figures represent the comparison of output results between experimental data and prediction values, where the horizontal axis is the experimental results and the vertical axis is the model predicted values. The dashed lines represent a $\pm 10\%$ relative error bound of the experimental value.

It can be observed that the tested refrigerant mass flow rate for full compressor speed or lowest compressor speed spans a wide range, which is from 30 g/s to nearly 110 g/s. In Figure 4.6, the points located at the top right represent the full speed compressor operation conditions, and points at the left bottom represent the conditions with the lowest compressor speed. It can be observed that most of the model predicted values lay within the dashed lines, and the MAPE of mass flow rate is 3.96%.

The MAPE of compressor power is slightly higher than 5%, which is 6.25%. It can be seen that the compressor power is predicted more accurate at full compressor speed but is over-predicted at lowest compressor speed. The compressor speed ratio of lowest compressor speed is the average

values during a period steady state time, since the compressor cannot run as stable as in its full speed operation condition. To some extent, it influences the model prediction results. It can be improved in the future work where more accurate compressor frequency data is collected.

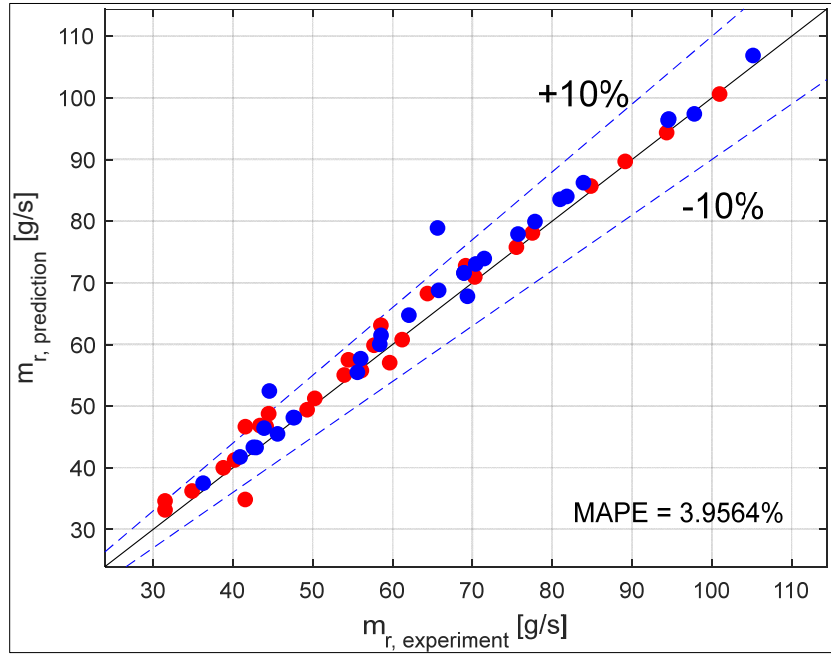


Figure 4.6. Compressor model validation of mass flow rate.

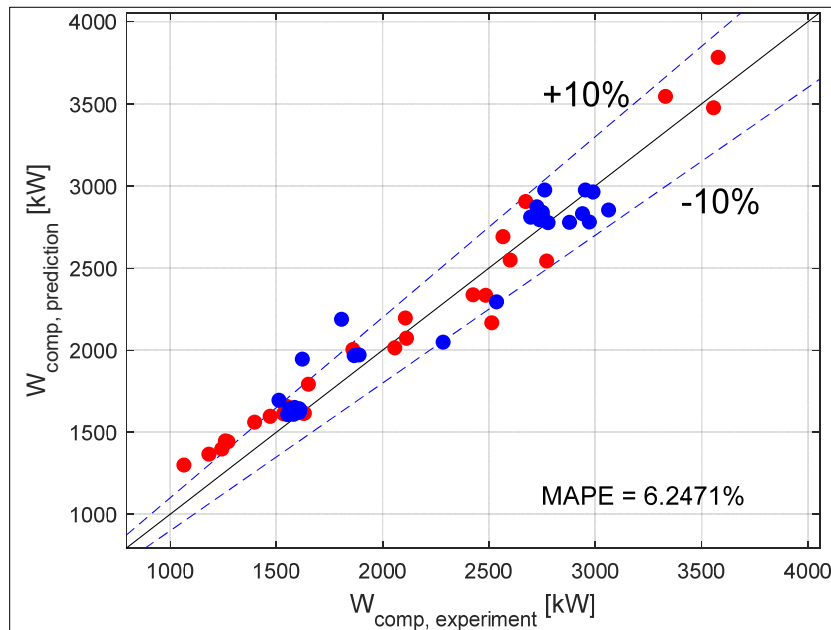


Figure 4.7. Compressor model validation of compressor power.

4.2.2 Evaporator Model Validation

In the evaporator model, the inputs are the refrigerant mass flow rate and superheat temperature on the refrigerant side, as well as entering air dry-bulb temperature, relative humidity and volume flow rate on the air side. All these inputs were measured during the tests, except the superheated temperature, which was calculated from the pressure and temperature measurements. Similarly, in Figure 4.8 and Figure 4.9, the dashed lines represent the $\pm 10\%$ relative error bounds of the tested value. In Figure 4.10, the dashed lines represent the $\pm 1^\circ\text{C}$ absolute error.

The values are input into the evaporator model to calculate the cooling capacity, SHR, and supply air temperature. The sensible and latent cooling capacity is related to the total cooling capacity and the SHR. In the cooling capacity validation, shown in Figure 4.8, the tested points expand a wide range from around 5kW to nearly 20kW and all points are located between the $\pm 10\%$ relative error bounds. In Figure 4.10, the predicted points of air out-flowing temperature also located between $\pm 1^\circ\text{C}$ absolute error bound. The lowest temperature of air existing the evaporator is 4.06°C , which nearly reaches the freezing temperature of the vapor in the air. The equipment SHR of experimental data changes from 0.3 to 1. In Figure 4.9, there are points with SHR equal to 1, which indicates that sensible-only mode is realized both in testing and in model prediction. In addition, the error of SHR between model prediction and testing data is larger than the other quantities; the SHR uncertainty (the uncertainty error bar) is also larger than the uncertainties for other quantities, since SHR is calculated by more input variables, in which more measurement uncertainties are transferred to SHR results. However, most data except one are within $\pm 10\%$ relative error, which is accepted in this case.

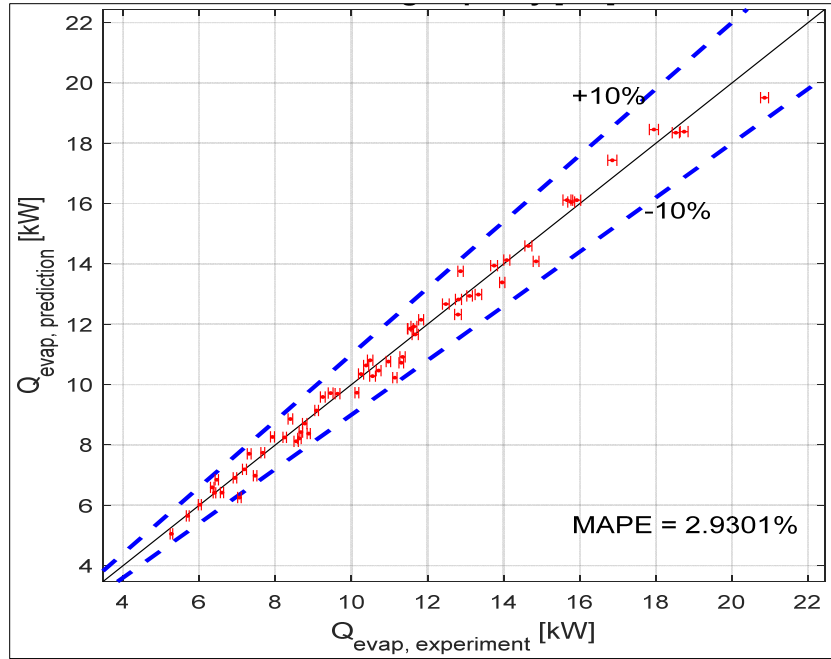


Figure 4.8. Evaporator model validation of cooling capacity.

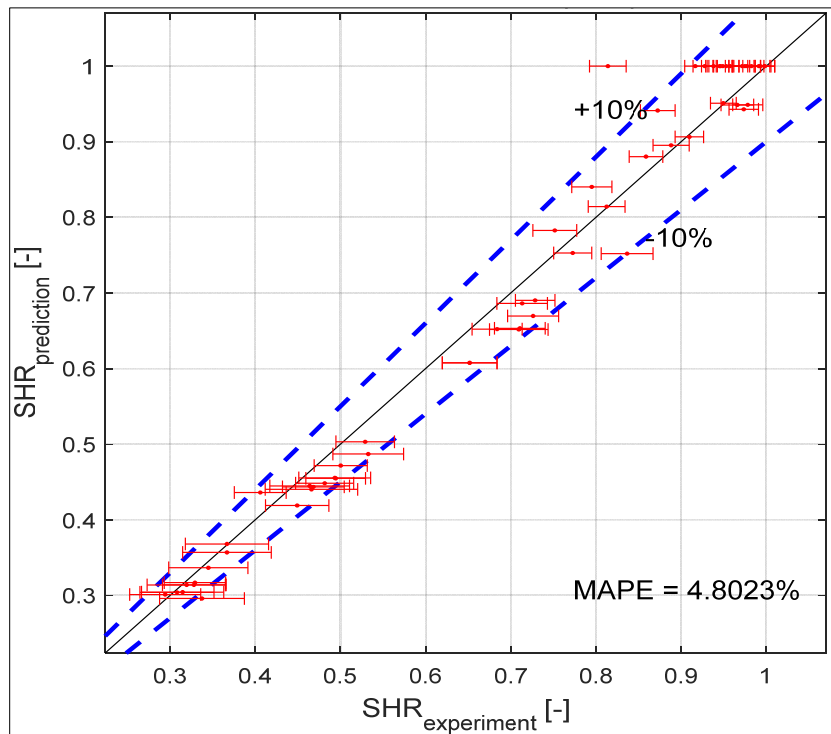


Figure 4.9. Evaporator model validation of SHR.

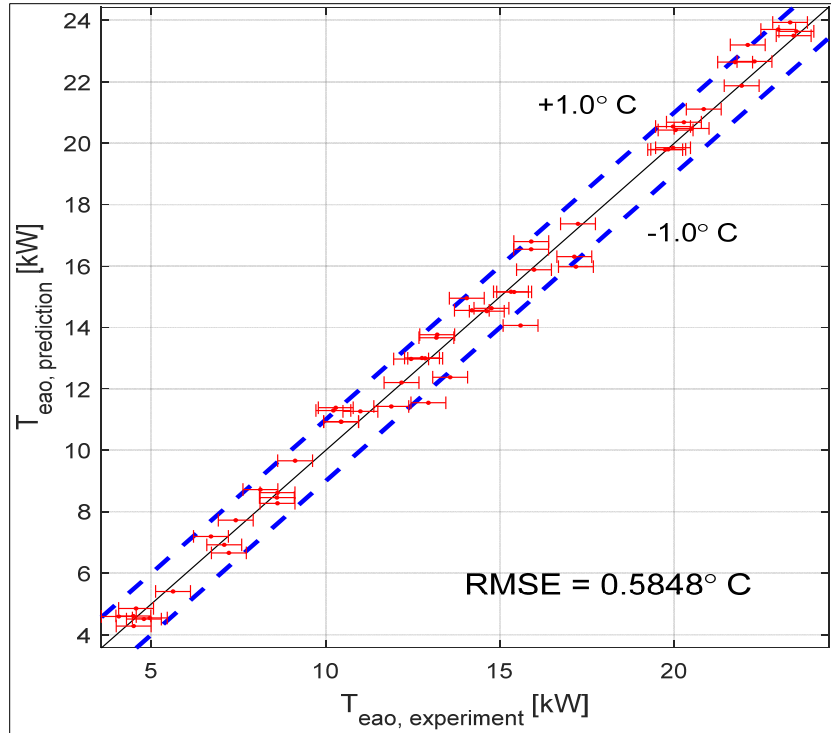


Figure 4.10. Evaporator model validation of air out-flowing temperature

4.2.3 SSLC System Model Validation

In the integrated SSLC system model validation, a comparison between the experimental and predicted data is conducted based on three outputs: cooling capacity, SHR and COP. In the following three figures, the predicted data are plotted on the vertical axes versus experimental data on the horizontal axes. The uncertainties of measured data are calculated based on the associated instrumentation uncertainties (listed in Table 4.1). As observed from the results, the model predicted values fall generally within $\pm 10\%$ error bounds of the experiential value in each plot. In Figure 4.11, the validated cooling capacities span a wide range that fully cover the part-load capacity and full capacity of the test unit operating at various air inlet conditions. The MAPE of cooling capacity validation is 3.4%. Figure 4.12 shows that in both experimental and model predictions, the lowest SHR that the equipment can reach is 0.3 and the highest value is 1, which implies that the deepest dehumidification rate that can be achieved by this equipment under the best set of conditions is an SHR of 0.3, and the sensible-only mode is achievable in both experimental and model predictions. To consider the ratio of cooling capacity to power input, Figure 4.13 shows that the COP varies significantly under different equipment speeds and air inlet

conditions, additionally a low MAPE value of 4.6% is achieved when comparing experimental with model prediction results.

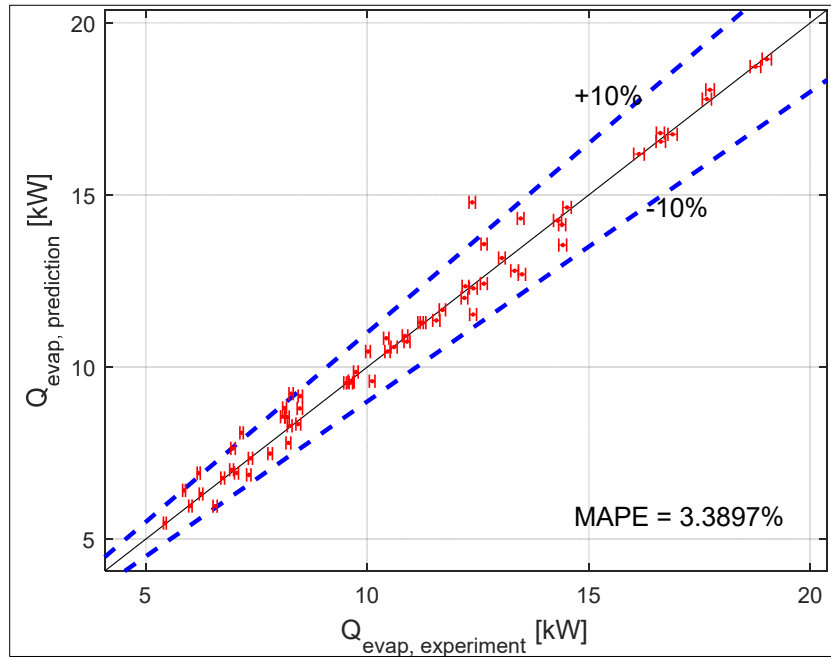


Figure 4.11. Integrated SSLC model validation of cooling capacity.

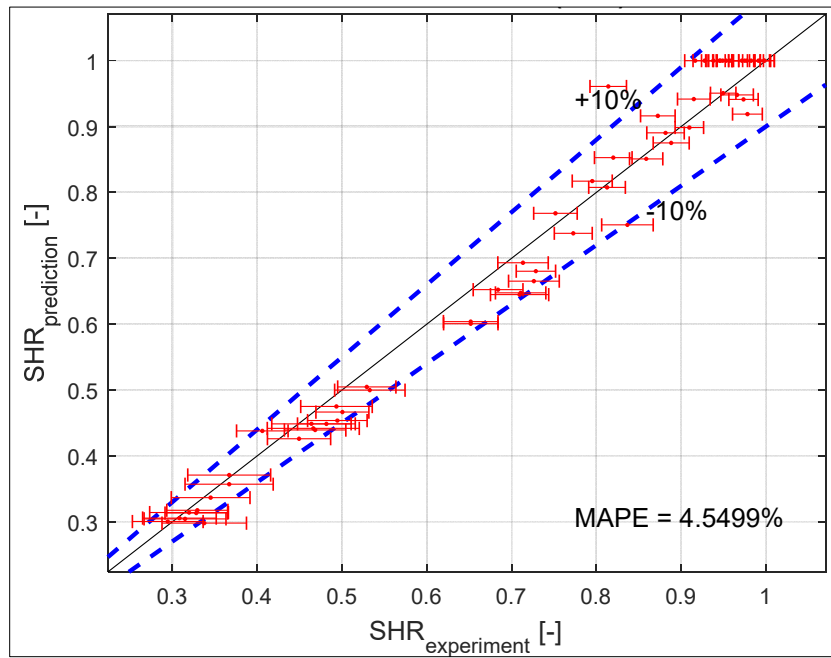


Figure 4.12. Integrated SSLC model validation of SHR.

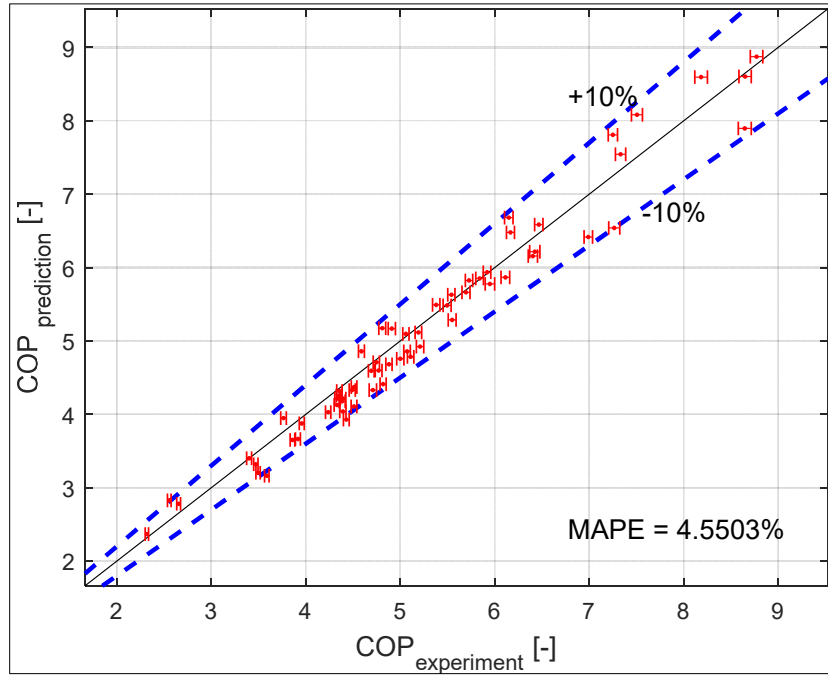


Figure 4.13. Integrated SSLC model validation of COP

4.2.4 Re-evaporation model validation

The re-evaporation model has already been described in the previous chapter and is validated in this section. In the re-evaporation model, to determine the correlation α and the maximum amount moisture hold by coil, an experimental testing is conducted. In the experiment, the entering air is at 32 °C (90.5 °F) dry-bulb temperature and 26.84 °C (80.3 °F) wet-bulb temperature. The dry-bulb temperature and dewpoint temperature of air at outlet are also measured. The experimental testing evaporation rate can be expressed as the difference of the humidity ratio between entering air ($\omega_{e,a,i}$) and existing air ($\omega_{e,a,o}$) multiplied by the mass flow rate of the air through:

$$\dot{q}_{evap,test} = \dot{m}_{ea}(\omega_{e,a,o} - \omega_{e,a,i}) \quad (4-15)$$

During the experimental testing, the fan in indoor unit is coupled with compressor so that both compressor and supply fan is turned on and off at the same step. The air flowing though the coil is extracted by the nozzle fan connecting with the outlet of indoor unit when the unit is turned from humidification state to OFF, and the air flow rate keeps as an average of 394.42 CFM. So, in this testing case, the correlation of β is -4.103.

In Figure 4.14, the horizontal axis represents the time from the unit turned off to the time that the difference of humidity ratio between entering air and existing air covers to a value close to zero. The vertical axis is the re-evaporation rate, i.e., the amount of moisture re-evaporating back to the flowing-through air stream. The blue dash-line is the experimentally measured evaporation rate.

When the unit stops running, the evaporator coil surface temperature increases gradually which leads to the evaporation rate changing from negative value to maximum value and then decreases. From 3 mins the unit stopped, the re-evaporation occurs and re-evaporation rate climbs up to the maximum value in approximately 12 mins and decreases to nearly zero in 25 mins. However, the testing data shows a significant fluctuation after 25 mins since the distribution of humidity from the inlet influences the testing results.

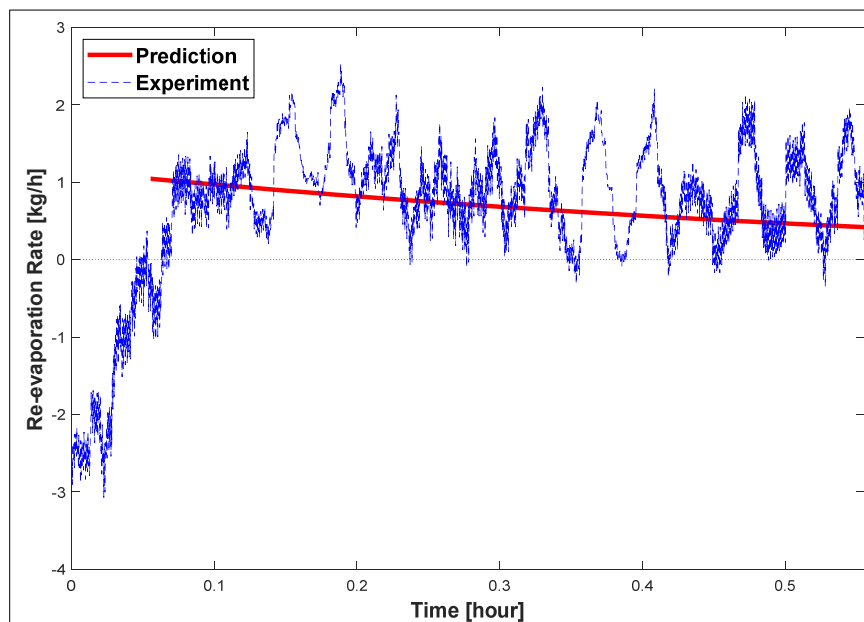


Figure 4.14. Re-evaporation model calibration.

Then, the experimental data is used for re-evaporation calibration. The maximum moisture that evaporator coil can hold (M_0) is 0.55 kg (1.28 lb), which is calculated by the integration of re-evaporation rate starting from the time that re-evaporation occurs to the time the humidity of entering air is nearly equal the humidity of existing air. The last step is to evaluate the correlation α . It is known that the total moisture re-evaporating back to air stream is a constant no matter which model is applied. Thus, it is assumed that the integration of the re-evaporation rate of the

testing data is equal to that obtained from the numerical model, both are integrated from 3 mins to 33 mins, which is expressed as follow:

$$\int_{3/60}^{33/60} -\beta \frac{e^{\alpha\beta t} \cdot (e^{\alpha M_s} - 1)}{e^{\alpha\beta t} \cdot (e^{\alpha M_s} - 1) + 1} dt = \int_{3/60}^{33/60} q_{\text{experiment}}(t) dt \quad (4-16)$$

where t is the time starts from the time when the unit is turned off. M_s is the amount of moisture on the coil surface at the end of time when compressor stops, which is equal to M_0 . And α is equal to 0.5348.

The developed re-evaporation model is plotted in Figure 4.14 in the red line. In comparison to the blue dashed-line (i.e., the experimental data), the predicted re-evaporation rate decreases exponentially with time. Different from the experimental line, the model predicted re-evaporation rate starts from the maximum value then decreases gradually. However, based on the numerical calculation, the moisture evaporating into the air stream between 3-min to 33-min are the same for both experimental testing and the developed model.

4.3 Modeling Results and Energy Saving Potential

4.3.1 Modeling Results under Special Boundary Conditions

After validating the numerical model of the sequential SSLC system, system characteristics such as cooling capacity, SHR, and COP can be predicted accurately given a set of boundary conditions. For example, Figure 4.15 to Figure 4.17 show a set of results of the tested heat pump under an outdoor temperature of 35°C (95°F), an indoor temperature of 23.89°C (75°F), and an indoor relative humidity of 45%. To identify the changes of system performance as the equipment speed varies, three outputs are plotted against compressor speed and air flow rate. Figure 4.15 shows that the total cooling capacity increases with an increase of either compressor speed or evaporator air flow, and, in general, the cooling capacity is more sensitive to a change in compressor speed than a change in air flow rate. However, in Figure 4.16, SHR increases as evaporator air flow rate climbs until the maximum SHR value, i.e., one, is reached, but it decreases with increasing compressor speed until it reaches the minimum SHR value, which is determined by equipment speed limitations and heat exchanger design. These trends in Figure 4.15 and Figure

4.16 clearly indicate that a cooling system provides more latent capacity but less sensible capacity with a higher compressor speed and lower indoor fan speed, this operating mode is referred to in the current work as the deep dehumidification mode. The system provides more sensible capacity if the compressor runs at a low speed, but the evaporator fan operates at a higher speed. It is even possible with the modeled equipment to achieve performance with no latent capacity, which is referred to as the sensible only mode in the current work.

Figure 4.17 shows the effects of compressor and fan speeds on system COP, which decreases with increasing compressor speed since the increase in compressor power consumption is faster than the associated increase of cooling capacity. On the other hand, when the evaporator fan speed increases, the system COP increases at first but then begins to drop off. The reason is that when operating in the high fan speed region, although cooling capacity increases with a higher air flow rate through the evaporator, the power consumption of the fan increases faster than the capacity increases.

These complicated non-linear relationships among COP, SHR and cooling capacity means that an optimal COP can be achieved, while providing the same sensible and latent capacities, by operating the system sequentially in multiple modes rather than continuously in a single mode.

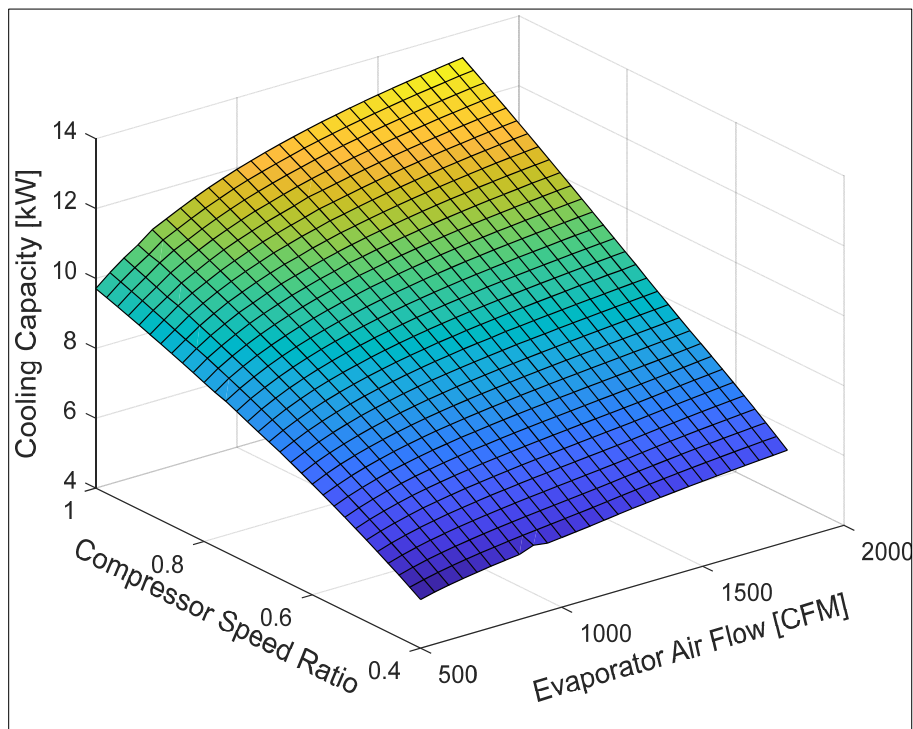


Figure 4.15. One case of developed SSLC model simulation for cooling capacity.

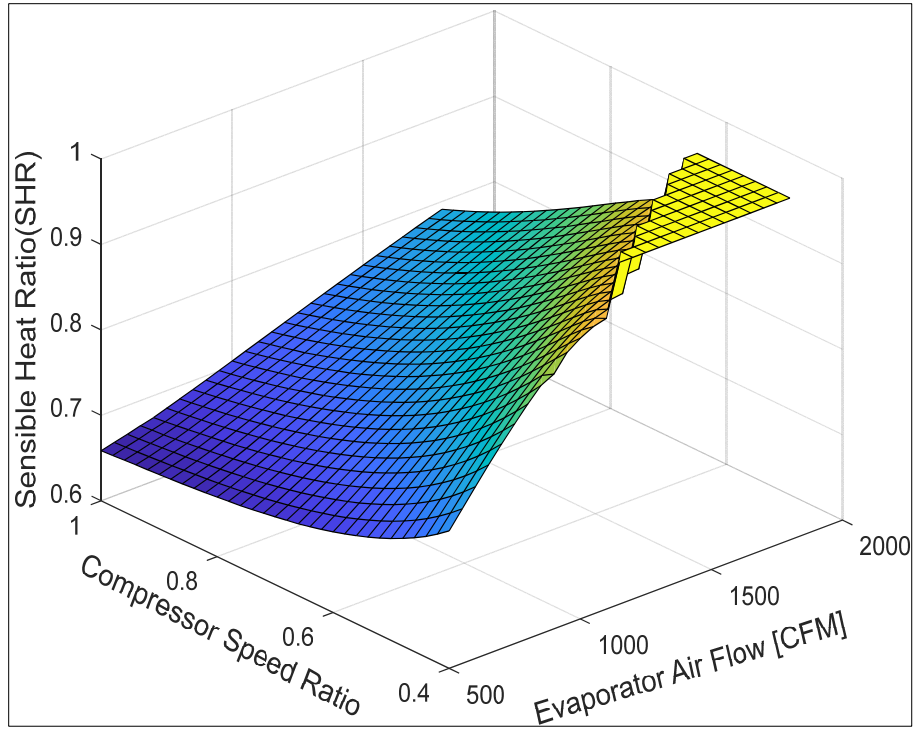


Figure 4.16. One case of developed SSLC model simulation for SHR.

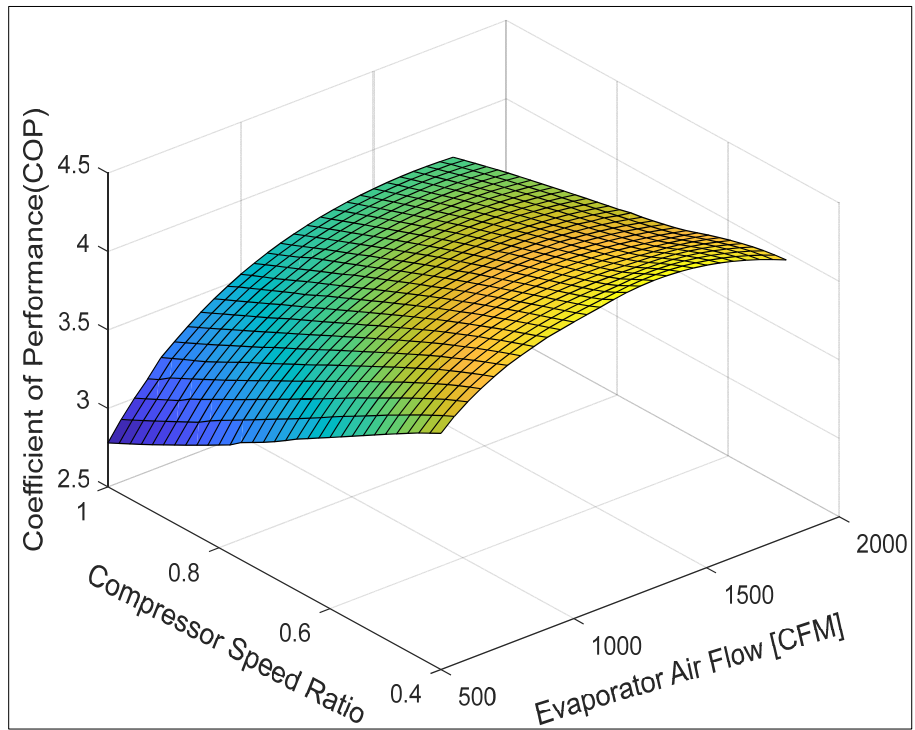


Figure 4.17. One case of developed SSLC model simulation for COP.

4.3.2 Energy Saving Potential

In the proposed sequential SSLC approach, energy can be saved by switching between the low-SHR (deep dehumidification) mode and the sensible-only mode with a suitable length of time spent in each mode. Specifically, a fixed time period is separated into two segments, the cooling system operates in the low-SHR mode in the first segment, within which the entire latent load and part of the sensible load of the space is satisfied; then, in the second time segment, the system switches to sensible only mode to only meet the remaining sensible load of the space. The compressor speed, fan speed, and the length of time for each mode segment need to be calculated based on system performance predicted by the numerical model, so that the total power consumption can be minimized while the required sensible and latent loads are satisfied by the system within this time period.

The fixed time period is chosen to be one hour as an example, and the transient processes that occur from mode switching are neglected. In the current approach, the system first operates in low SHR mode for a duration of t_{dh} , and then switches to sensible only mode for the remaining time, $(1 - t_{dh})$. For a particular choice of time ratio γ_{time} , the following optimization can be formulated:

Minimize:

$$W_{total}(\gamma_{comp_1}, \gamma_{fan_1}, \gamma_{comp_2}, \gamma_{fan_2}) = W_1 \cdot t_{dh} + W_2 \cdot (1 - t_{dh}), \quad (4-17)$$

subject to the constrains:

$$\sqrt{\left(\frac{Q_{sen_total} - Q_{sen1} \cdot t_{dh} - Q_{sen2} \cdot (1 - t_{dh})}{Q_{sen_total}}\right)^2} \leq 0.1, \quad (4-18)$$

$$\sqrt{\left(\frac{Q_{lat_total} - Q_{lat1} \cdot t_{dh}}{Q_{lat_total}}\right)^2} \leq 0.1, \quad (4-19)$$

$$SHR_2 = 1. \quad (4-20)$$

where, W_{total} is the total energy consumption for both modes, γ_{comp} and γ_{fan} are the speed ratio for compressor and evaporator fan, respectively. For each mode, the energy cost depends on the compressor and evaporator fan speed ratio. Q_{sen1} and Q_{lat1} are the sensible and latent capacity

produced in low-SHR mode respectively, and Q_{sen2} is the sensible capacity produced in sensible only mode. The sensible and latent capacities produced in the two modes also depend on the corresponding compressor and evaporator fan speed ratios in each mode. In addition, Equation(4-18) and Equation(4-19) represent that the difference between the sensible and latent capacity produced by the SSLC must match the total sensible and latent load within 10%. Equation(4-20) represents that only sensible cooling is involved in the second portion of the time segment.

By varying the compressor and evaporator fan speed between low-SHR mode and sensible only mode to hold the total capacity and SHR constant, a study has been performed that changes the dehumidification time from 0 minutes to 60 minutes (one hour). The corresponding energy cost for the SSLC system is shown in Figure 4.18. Three system performance conditions with the same sensible capacity are selected: 8kW, 9kW and 10kW total capacity with corresponding SHR's of 0.9, 0.8, 0.7, respectively. In particular, when the dehumidification time is 60 minutes, the equipment is operating at constant speed without switching modes with a total capacity and SHR that matches the load cooling demand and SHR. In Figure 4.18, the dehumidification cannot start from zero since when the dehumidification time is too short, the latent capacity requirement cannot be satisfied by operating in a low-SHR mode even when the compressor reaches its full speed and the evaporator fan is at its lowest speed.

For these three conditions, as the dehumidification time increases, the energy consumption first decreases to a minimum point, and then increases to the baseline point (i.e., the performance at constant speed operation). It is important to notice that the lowest energy consumption point for each example is the optimal point among all possible choices of dehumidification time. Comparing with constant speed operation as the baseline, the energy savings that the proposed sequential SSLC system can achieve is 11.5%, 7.8% and 6.9% respectively for the aforementioned conditions.

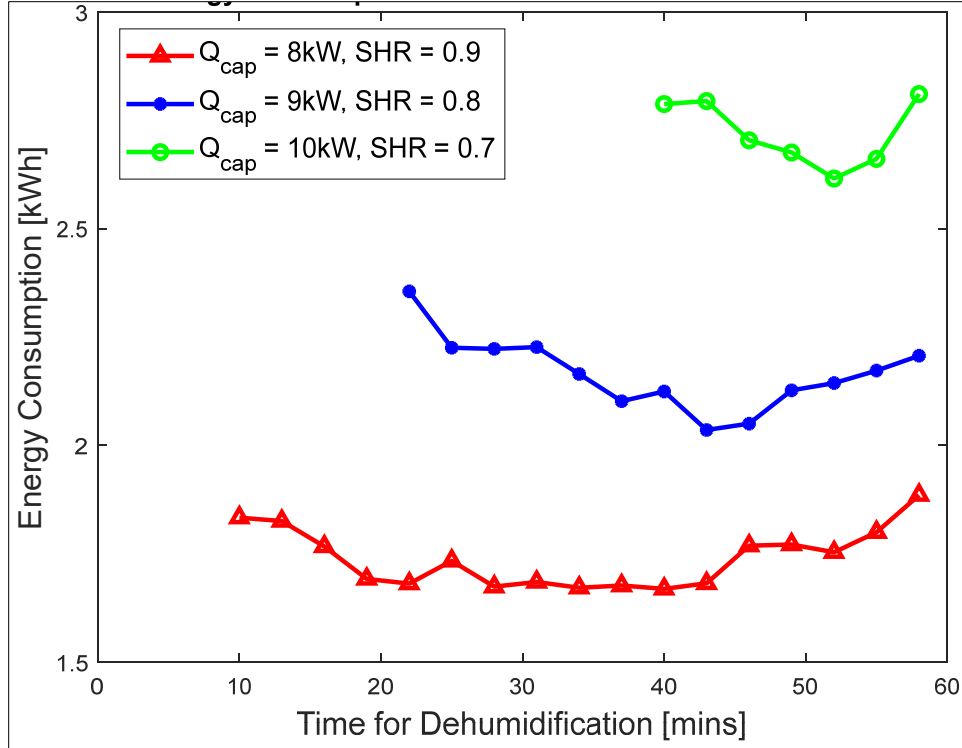


Figure 4.18. Energy consumption with different dehumidification times.

4.4 SSLC Model Simplification with Artificial Neural Network

The physics-based SSLC model developed in Chapter 3 is not well suited to be coupled with the building model to simulate heat pump performance under different control strategies due to the complexity of those detailed models. First, the convergence of the calculation involved in the physics-based SSLC model is highly dependent on the initial guesses, which cannot be guaranteed to work for different boundary conditions. Also, the physics-based SSLC model cannot find the minimum point in the optimization process of the future control co-simulation, since the A/C system performance mapping involves sudden changes when the evaporation coil switches from dry-coil to wet-coil, which means that no gradient exists at this sharp transition.

In recent years, machine-learning techniques are widely used in engineering areas to perform pattern recognition, function approximations, optimizations, simulations and classifications. More recently, deep-learning has been applied to cooling system performance mapping. Thus, an artificial neural network (ANN) modeling is developed to overcome the aforementioned limitations in this work. The general procedure for generating an ANN model can be summarized as follows:

- Define the input and output variables;
- Determine the number of layers and number of neurons in each layer;
- Identify the activated function between neurons;
- Training/test the network by comparing its results with physical model

4.4.1 Initial Neural Network Generation

The input variable is determined as the SSLC system model inputs, which include boundary conditions (outdoor temperature, indoor temperature and humidity), and equipment operation information (compressor and indoor fan speed ratio). Whereas the outputs from the ANN model are the cooling system capacity, sensible heat ratio (SHR) and total power, since the other outputs can be calculated based on these basic outputs.

Generally, the ANN model is affected by two critical characteristics such as the number of hidden layers and the number of neurons in hidden layer (Mohanraj et al,2009). The higher the number of hidden layers and neurons, the better the model can capture non-linearities, but also the higher the probability of overfitting (Ziviani et al., 2018). Overfitting occurs when the error of the objective function on the training dataset is driven to a very small value, but when the ANN model is used on the testing dataset, the error is large, meaning that the model has memorized the training dataset, but has not learned the general trend (Schikuta, 2008). Thus, in this work, the initial ANN model is constructed to be simple, it consists of a single input layer, a single hidden layer and a single output layer. The number of initial number of neurons in hidden layers can be determined by the following equation:

$$\text{Number of hidden neurons} = \frac{1}{2}(\text{inputs} + \text{outputs}) + \sqrt{\text{number of training data}} \quad (4-21)$$

Then, the structure of the ANN model is optimized by increasing or decreasing the number of neurons within a hidden layer at first, and then by adding hidden layers.

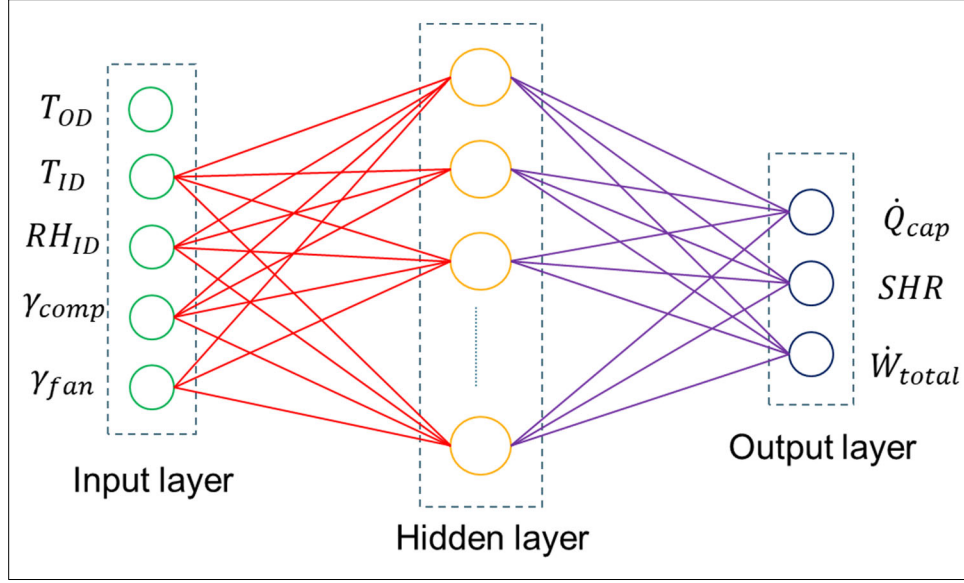


Figure 4.19. Neural network structure of developed SSLC system.

After the training samples are stored in the input layer, each neuron is characterized by a set of input signals, x_j , ($j = 1, \dots, J$), each of which has a certain weight, ω_{ij} , ($i = 1, \dots, I$). All the input signals weighted by the respective synaptic strengths of the neuron are summed by means of a linear combiner. Mathematically, the relationship between input nodes and first hidden layer nodes can be expressed by Equation(4-22).

$$\theta = W^{(1)}X + b^{(1)} = \begin{bmatrix} \omega_{11}^{(1)} & \cdots & \omega_{1j}^{(1)} & \cdots & \omega_{1J}^{(1)} & b_1^{(1)} \\ \vdots & \ddots & \vdots & \ddots & \vdots & \vdots \\ \omega_{i1}^{(1)} & \cdots & \omega_{ij}^{(1)} & \cdots & \omega_{iJ}^{(1)} & b_i^{(1)} \\ \vdots & \ddots & \vdots & \ddots & \vdots & \vdots \\ \omega_{I1}^{(1)} & \cdots & \omega_{Ij}^{(1)} & \cdots & \omega_{IJ}^{(1)} & b_I^{(1)} \end{bmatrix} \begin{bmatrix} X_1 \\ \vdots \\ X_J \\ 1 \end{bmatrix} \quad (4-22)$$

where each $\omega_{ij}^{(k)}$, ($k = 1, \dots, K$) is the weight multiplied by the j-th input node and mapping to i-th neuron in layer k and each $b_i^{(k)}$ is the bias unit mapping to i-th neuron in layer k. A non-linear activation function $\varphi(\cdot)$, a hyperbolic tangent function in the current work, has been chosen to limit the amplitude of the output of the neuron as given by Equation(4-23).

$$Z^{(1)} = \varphi(W^{(1)}X + b^{(1)}) \quad (4-23)$$

where $Z^{(1)}$ is the results from the activation function of the first layer.

Then, the network mapping from first hidden layer to next layer, no matter second hidden layer or output layer, takes the similar step shown in Equation (4-24) until it reaches the output layer.

$$W^{(k)}X + b^{(k)} = \begin{bmatrix} \omega_{11}^{(k)} & \cdots & \omega_{1j}^{(k)} & \cdots & \omega_{1J}^{(k)} & b_1^{(k)} \\ \vdots & \ddots & \vdots & \ddots & \vdots & \vdots \\ \omega_{i1}^{(k)} & \cdots & \omega_{ij}^{(k)} & \cdots & \omega_{iJ}^{(k)} & b_i^{(k)} \\ \vdots & \ddots & \vdots & \ddots & \vdots & \vdots \\ \omega_{I1}^{(k)} & \cdots & \omega_{Ij}^{(k)} & \cdots & \omega_{IJ}^{(k)} & b_I^{(k)} \end{bmatrix} \begin{bmatrix} Z_1^{(k-1)} \\ \vdots \\ Z_I^{(k-1)} \\ 1 \end{bmatrix} \quad (4-24)$$

Whereas, a linear activation function is selected for the output layer of neurons, which is given by Equation (4-25).

$$\hat{y} = W^{(K)}X + b^{(K)} \quad (4-25)$$

where \hat{y} is the output values predicted by the ANN model.

Based on the above mathematical explanation, the number of parameters including all weights and biases in each layer are determined by the numbers of neurons. For example, if the network has n_k neurons in layer k and n_{k+1} neurons in k+1 layer, the dimension of the parameter matrix is $n_{k+1} \times (n_k + 1)$ when input values are transferred from kth layer to k+1th layer. Hence, the total number of parameters trained in the entire network is the sum of dimension of weights and biases matrix. The signals are transferred through each intermediate layer till reaching the output layer. The ANN output results are compared with the training data y, and a loss function is defined as the mean square error according to Equation (4-26).

$$J = \frac{1}{n} \sum_{i=1}^n (y_i - \hat{y}_i)^2 \quad (4-26)$$

During the iteration process, the weights and biases are determined through updating the parameters until the loss function is less than the set convergence criteria. The AdaMax optimizer, an adaptive stochastic gradient descent method, is adopted for ANN model rapid convergence and all weights adjusting.

Since the input and output variables are of different types and have different orders of magnitude, all inputs and outputs parameters are normalized in the range of (0.1, 0.9) to ensure the equivalence:

$$x_n = 0.8 \frac{x - x_{min}}{x_{max} - x_{min}} + 0.1 \quad (4-27)$$

where x is the actual data point of one input, x_n is the normalized data point, x_{min} and x_{max} are the minimum and maximum values defined according to the variables.

To evaluate the accuracy of the trained ANN model, three well-known statistical quantities have been used introduced. The R^2 value is used to measure how statistically close the data are to the fitted regression line and is defined as:

$$R^2 = \frac{cov(y^{actual}, y^{predict})}{\sqrt{cov(y^{actual}, y^{actual})cov(y^{predict}, y^{predict})}} \quad (4-28)$$

where $cov(\cdot)$ denotes the covariance, y^{actual} is the actual experimental data, and $y^{predict}$ is the ANN model predicted data. Since the R^2 cannot determine whether the coefficient estimated and the predictions are biased, two additional indicators are introduced. The mean absolute percentage error (MAPE) in Equation (4-29) is selected to statistically measure how accurate the ANN model is.

$$MAPE = \frac{100\%}{n} \sum \left| \frac{y_i^{actual} - y_i^{predict}}{y_i^{actual}} \right| \quad (4-29)$$

4.4.2 ANN Model Training

In the ANN model training procedure, a large amount of data points are required, and it is impractical to obtain all of them via steady state experimental testing. Thus, all the data used for ANN model training is generated from the physics-based SSLC model described in Chapter 3. Prior to training the weights and bias in ANN model, the data set consisting of 1505 data points is split into two groups, i.e. the training and testing datasets (40% of 1505 data points) and validation datasets (60% of 1505 data points) as the training algorithm requires the two datasets to be provided separately. In the training and testing datasets, 80% data points are used for training and the other 20% data points are used for testing. Regarding to the network structure, it starts from a single input layer containing 5 input variables (the outdoor temperature, indoor temperature, indoor humidity, compressor speed ratio and fan speed ratio), a single hidden layer with eleven neural nodes, and a single output layer with three nodes representing total cooling capacity, SHR and total power consumption, respectively. Then, the number of neural nodes in hidden layer and the number of hidden layer is gradually increased until overfitting occurs.

4.4.3 ANN Model Training Results

The initial number of neural nodes in hidden layers is 14, which is determined by the Equation(4-21). To optimize the structure of neural network, the number of neural nodes in single hidden layer changes from 11 to 15, and number of hidden layers also increases from 1 to 2. As shown in Table 4.3, the accuracy of ANN model improves slightly when the neural nodes change from 11 to 13 and then becomes worse after it reaches to 15. Also, overfitting occurs when the number of hidden layers reaches to 2.

Table 4.3. Neural network training accuracy for different numbers of hidden layers and neural nodes.

	\dot{Q}_{cap}		SHR		\dot{W}_{tot}	
	R^2	MAPE	R^2	MAPE	R^2	MAPE
Hidden layer =1; Neural = 11	99.50%	1.40%	99.50%	1.20%	100.00%	0.90%
Hidden layer =1; Neural = 12	99.80%	0.90%	99.70%	1.00%	99.90%	0.70%
Hidden layer =1; Neural = 13	99.90%	0.80%	99.70%	0.90%	100.00%	0.60%
Hidden layer =1; Neural = 14	99.80%	1.00%	99.50%	1.20%	99.90%	0.70%
Hidden layer =1; Neural = 15	99.80%	1.10%	99.70%	1.20%	99.9%	1.00%
Hidden layer =2; Neural = 11; Neural = 9;	94.70%	4.70%	98.00%	2.80%	96.80%	0.50%
Hidden layer =2; Neural = 12;Neural = 10	94.60%	24.50%	98.00%	2.80%	96.80%	4.40%

Based on the regression results for the neural networks with different structure, it suggests the selection of a single hidden layer with 13 neural nodes, the weights and bias applied to transfer through each layer is listed in the Table 4.3.

From Figure 4.20 to Figure 4.22, the physical-based SSLC model predicted data are plotted on the vertical axis versus ANN model predicted data on the horizontal axis. The two dash lines in the figures are the $\pm 5\%$ relative error lines. In the set of figures, it indicates that almost all 1505 data points for three outputs fall in between $\pm 5\%$ relative error lines. The data points with SHR being equal to 1 predicted from two models has a larger difference compared with other data points

(with SHR being less than 1). But the differences for all data points are still less than 5% which is considered as acceptable in this study.

More specifically, the R-squares values are close to 100% and are 99.9%, 99.7%, and 100% with respect to system cooling capacity, SHR and total power consumption, respectively. The mean absolute percentage error (MAPE) values for three output variables are all lower than 1%. The developed ANN model is sufficiently accurate to be coupled with a building model and be applied in control strategy simulation in the future steps.

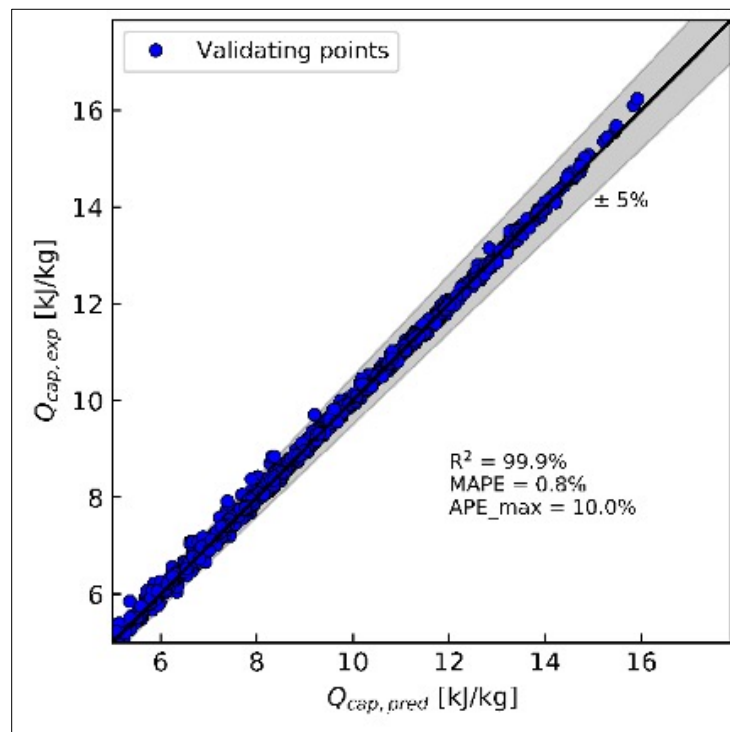


Figure 4.20. Comparison of validating data between ANN model and physical-based SSLC model for cooling capacity.

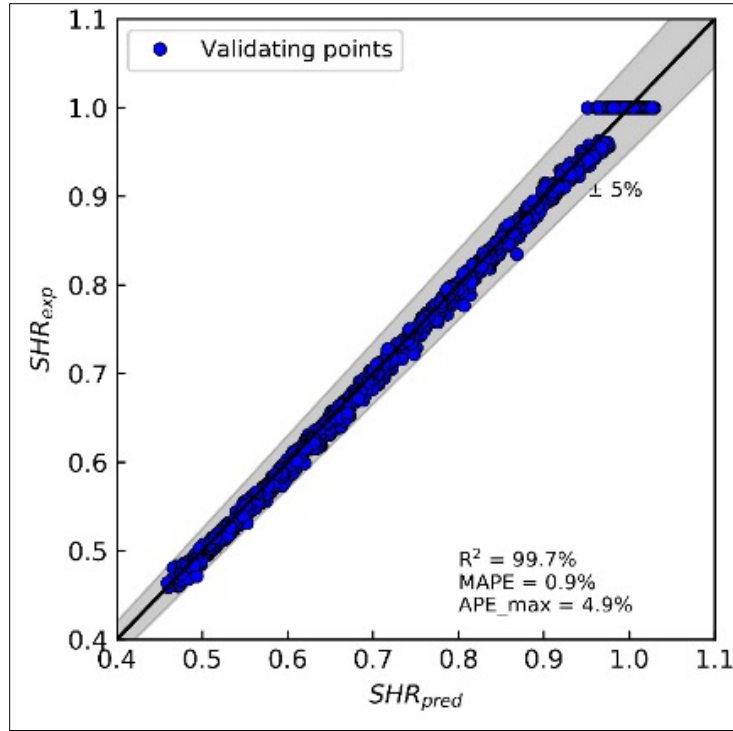


Figure 4.21. Comparison of validating data between ANN model and physical-based SSLC model for SHR.

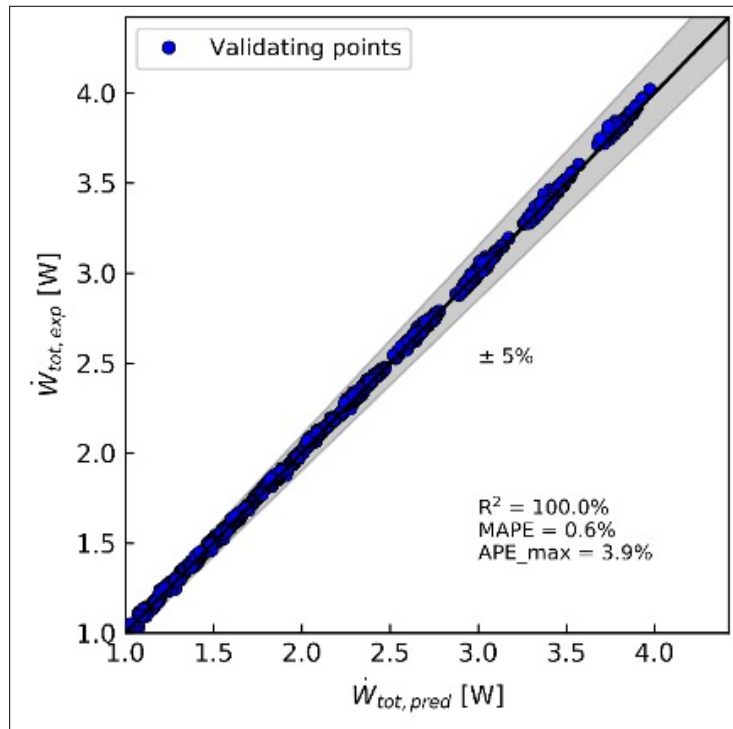


Figure 4.22. Comparison of validating data between ANN model and physical-based SSLC model for total power input.

4.5 Summary

In this chapter, the developed SSLC system model is experimentally validated by testing a commercialized variable-speed heat pump. In the process of model validation, the testing measurements are converted to the inputs and outputs of sub-models (including compressor, condenser and evaporator models). Through comparing the outputs from experimental results and model predictions with the same inputs, the accuracy of each sub-model is evaluated. Then, by combining all sub-models in a cycle, the integrated SSLC system model is also validated. The validated SSLC system model can be used to predict the SSLC system performance, including cooling capacity, SHR and system total power input, under different compressor and indoor fan speeds in typical indoor and outdoor conditions. It is demonstrated in this chapter that the non-linear relationship between delivering cooling capacity and power input provides a potential of energy saving through switching the heat pump in two different SSLC modes with carefully chosen switching times. Furthermore, in order to simplify the process of the co-simulation between SSLC system and prototype residential building, the SSLC system model is modeled as an ANN model with single input layer, single hidden layer and single output layer, which will be applied in the following chapters.

5. SSLC CONTROL STRATEGIES

To pursue the potential application of the developed sequential SSLC methodology, different control strategies to decide when and how to adjust the equipment speeds and operating modes are developed and described in this chapter. The control strategy introduced here mainly includes two methods: mode switch control with fixed equipment speeds in each mode and load prediction control to continuously adjust equipment speeds according to the space sensible cooling load. The mode switch control algorithm has a relatively lower computation complexity, it is referred to as the simplest two stage A/C unit control. The algorithm complexity is higher for the load prediction control, which requires a continuous estimation of the cooling load based on measurements of the space conditions to adjust the equipment speeds. However, both control strategies have their own benefits and limitations, which makes them suitable for different applications. The main purpose of this chapter is to describe the control logic for each strategy. In order to evaluate their performance through simulations, the control strategies are implemented on an A/C unit applying the SSLC approach, in which the numerical model used to predict A/C unit performance is combined with the simplified building thermal and moisture models. Furthermore, a baseline is proposed in the first section of this chapter to evaluate the energy efficiency improvements for SSLC systems. Based on this baseline, different control strategies developed in this work can be compared and evaluated.

5.1 Baseline Simulation

The energy consumption of an air conditioner is not only related to the mechanical characteristics of its components, but is also impacted by the equipment control logic. A fair baseline control strategy is critical for future SSLC system efficiency evaluation and justification. However, the widely used energy consumption baseline in previous works only considers temperature control, while it ignores the humidity requirement, in which situation only the space sensible load is handled. In comparison to SSLC system control strategies, both sensible load and latent load in the space are required to be met, in other words, both indoor temperature and humidity are controlled to be within a comfortable range. Thus, the previous baseline is not applicable to the SSLC energy consumption evaluation.

In the current work, a new baseline that meets both indoor sensible and latent load is proposed, and the energy consumption of the baseline is predicted and compared with the energy consumption of the SSLC system subjective to the evaluation. In the proposed baseline, the indoor temperature and relative humidity setpoint are 74°F (23.33°C), 50%. To maintain this setpoint, both sensible and latent loads in the building need to be handled by the A/C unit.

The building and A/C unit apply the sequential SSLC approach. The co-simulation framework of the baseline combining the prototype building with an SSLC A/C unit is presented in Figure 5.1. The simplified building thermal and moisture models predict both sensible and latent cooling loads for a constant time step (set as 1-min in this work) according to the provided weather data as well as the indoor temperature and relative humidity setpoints. Then, the developed SSLC system numerical model is used to determine equipment speed ratios, i.e., compressor speed ratio and indoor fan speed ratio, to match the provided cooling capacity with the estimated cooling loads as much as possible. The calculation algorithm used here is a least-square method that minimizes the square of the residual representing the difference between the space cooling loads and the cooling capacities provided by the air conditioner system. The residual is expressed as:

$$r = \begin{bmatrix} \dot{Q}_{sen,load} - \dot{Q}_{sen,cap} \\ \dot{Q}_{lat,load} - \dot{Q}_{lat,cap} \end{bmatrix} \quad (5-1)$$

where $\dot{Q}_{sen,load}$ and $\dot{Q}_{lat,load}$ are the sensible and latent load predicted from simplified thermal and moisture model of prototype residential building, $\dot{Q}_{sen,cap}$ and $\dot{Q}_{lat,cap}$ are the sensible and latent cooling capacity delivered by the A/C system, respectively.

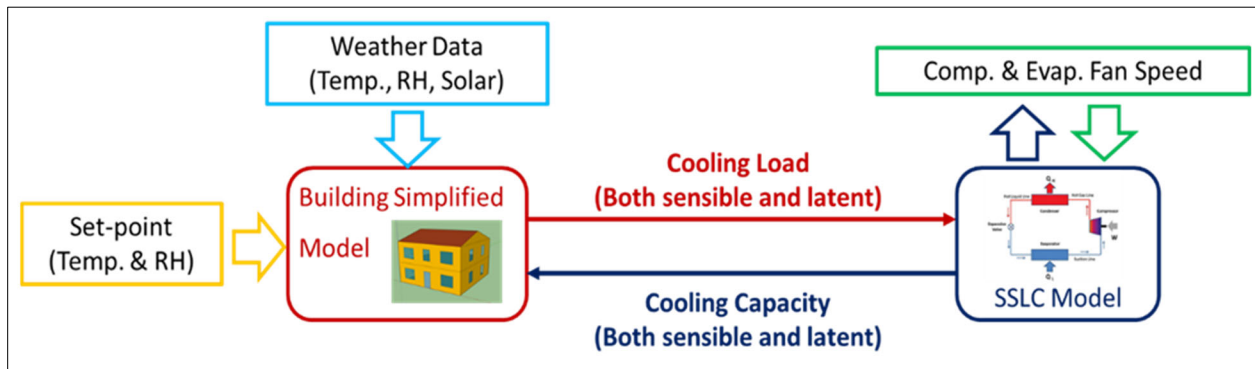


Figure 5.1. Building and SSLC system co-simulation framework of baseline

In practical applications of the baseline, some special issues need to be considered during the process of equipment speed determination:

- 1) The temperature and humidity cannot always be perfectly controlled at the same time since the building sensible and latent load do not occur at the same time during some time periods. When there is only sensible load in the conditioned space (i.e., with no latent load), the A/C unit can operate at proper compressor speed and indoor fan speed in a sensible only mode to meet the sensible load. However, if there is only latent load existing in space, the unit has to be operated for dehumidification which inevitably induces overcooling in room space. In the proposed baseline, the dehumidification can be activated only if the space temperature is higher than 73°F, i.e., +1°F of setpoint temperature, however, it has to stop dehumidifying the space if the indoor temperature is lower than 73°F to avoid too much sensible overcooling.
- 2) In some cases, the cooling capacity delivered by the A/C unit is constrained by equipment settings. In this work, the compressor speed is allowed to vary from 0.4 to 1.0 of full-speed and the air flow volume of supply fan changes from 500 CFM to 1800 CFM. The minimum overall capacity of this A/C unit occurs when the compressor speed ratio is 0.4, the indoor fan speed ratio is 0.27 (air flow rate is 500 CFM); the maximum overall capacity that A/C unit can deliver is the situation with the compressor speed ratio being 1.0 and the indoor fan speed ratio being 1.0 (air flow rate is 1800 CFM). When the predicted overall cooling load is lower than the minimum overall cooling capacity of tested unit, the A/C unit continues to cool down the space until the space temperature reaches temperature lower bound, i.e., 73°F in this baseline. When the predicted overall cooling load is higher than the maximum overall cooling capacity of A/C unit, the unit will run at highest equipment speeds, but the space temperature or humidity will increase freely.

To simulate the building performance under the baseline control strategy, the indoor temperature and relative humidity of two days (July 4th and July 26th) are simulated with Indianapolis weather data as examples to demonstrate how building thermal and moisture perform under baseline. These two days are selected because of their different outdoor conditions: the weather is warm and dry on July 4th but warm and humid on July 26th. These two days are also

simulated under proposed SSLC control strategies, in which the building thermal and moisture performance will be compared with baseline.

Figure 5.2 and Figure 5.3 represent the indoor temperature and relative humidity (RH) performance in a dry day and a humid day, respectively. In these two figures, the blue and red dash lines represent outdoor temperature and RH, respectively. The blue and red solid lines represent the indoor temperature and RH, respectively. It can observe from Figure 5.2 that from 9:00 in the morning to the end of the day, the space temperature maintains between $74^{\circ}\text{F} \pm 0.5^{\circ}\text{F}$ and the RH is below the set-point, i.e., 50%. However, in the early morning, between 4:00 and 7:30, since the indoor temperature is lower than 73°F , the A/C unit does not deliver either sensible or latent capacity to space, as a result, the RH in space exceeds the humidity set-point in this period. In Figure 5.3, the space temperature fluctuates between $73^{\circ}\text{F} \pm 0.5^{\circ}\text{F}$ from 00:00 to 5:00, as well as from 11:00 to 21:00, when the indoor RH is below the humidity setpoint. During the time between 5:00 and 11:00, and after 21:00, RH in space is higher than the setpoint, so the system controls the indoor temperature to decrease to 73°F to remove more latent load in space.

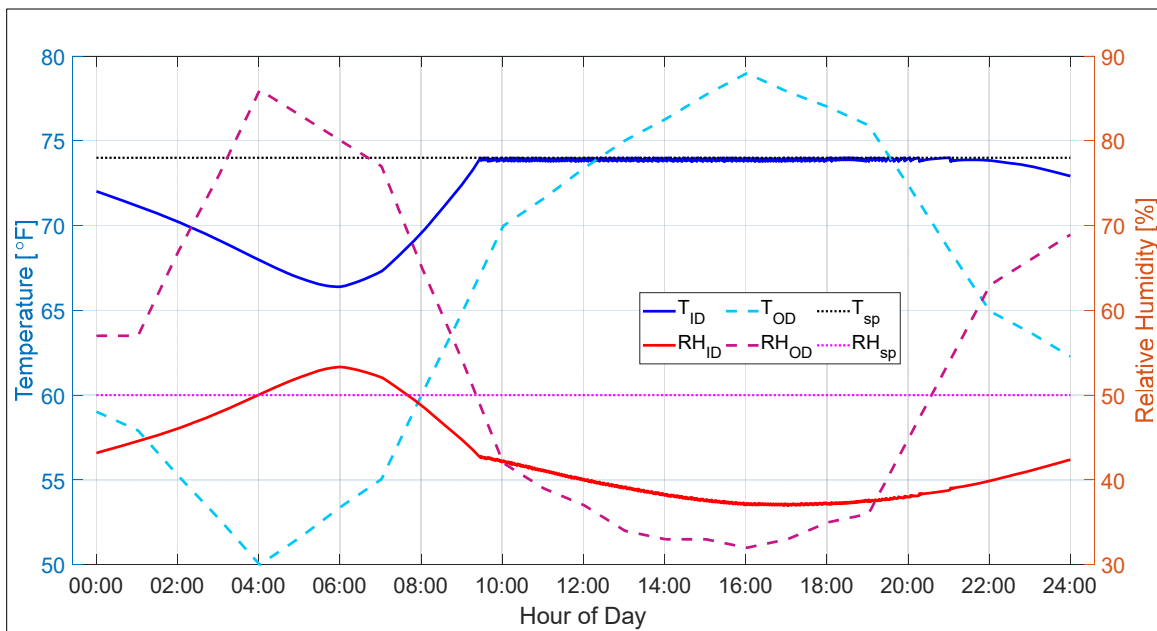


Figure 5.2. Indoor temperature and relative humidity simulation of baseline on July 4th.

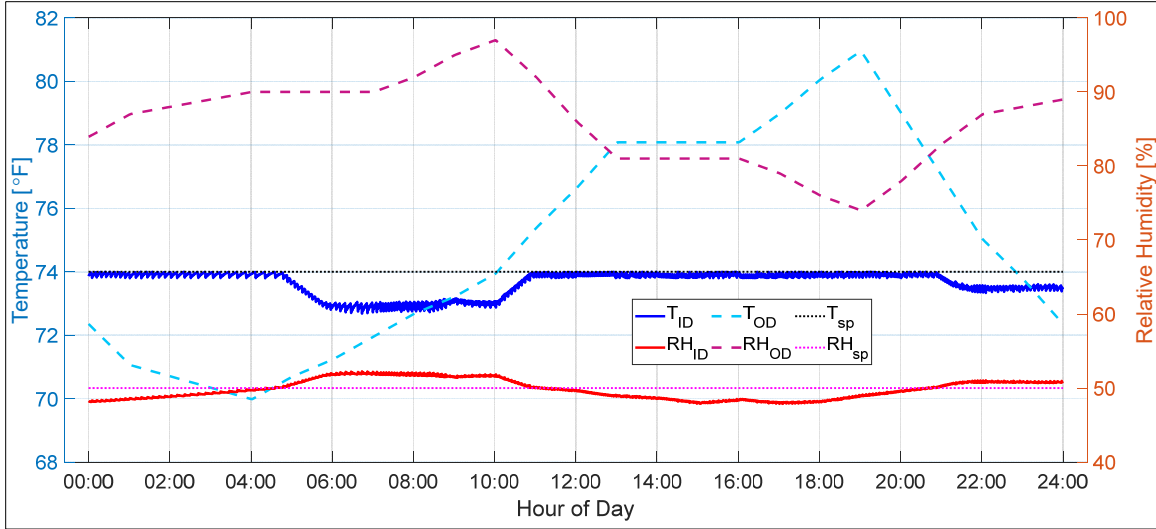


Figure 5.3. Indoor temperature and relative humidity simulation of baseline on July 26th.

In Figure 5.2 and Figure 5.3, the corresponding performance of space temperature and relative humidity is demonstrated in baseline simulation with two different weather conditions. To consider both temperature and humidity in a space and their coupling effect, the sensible and latent cooling capacity provided by an A/C unit to match both sensible and latent loads at the same time through varying both compressor speed and indoor evaporator fan speeds. During this process, the power consumption of the A/C unit is also predicted.

5.2 Co-Simulation of Cooling System and Building under SSLC Control Strategies

In the previous work, an ANN model of SSLC system and simplified steady-state building models are developed independently. Since the control strategy is the bridge connecting the cooling system model and building model, a co-simulation structure used to connect each model is constructed and the input and output variables of each module are identified. In general, the control strategy module is the core of the co-simulation, in which the system operation mode (sensible-only mode or deep-dehumidification mode) as well as the equipment speeds of A/C system are determined at each time step. Then the information determined by the SSLC control strategy is input to SSLC system model to predict its performance.

In more detail, the co-simulation coupling the ANN model of SSLC system and the simplified building thermal and moisture model is conducted as follows (shown in Figure 5.4):

- 1) The dry-bulb temperature and relative humidity in the space is input to the SSLC control strategy module to determine which mode the A/C system should operate in for the next time step: sensible only mode or deep dehumidification mode. For the first time step in the simulation, the initial indoor temperature and relative humidity are chosen to be the respective set-point values.
- 2) Besides determining the system operation mode, the equipment speeds, i.e., compressor speed and supply fan speed, are both calculated in the SSLC control strategy module which are sent to SSLC numerical model as input variables. The difference among different SSLC control strategies is that the SSLC mode determination and the equipment speed calculation are carried out via different approaches.
- 3) In the SSLC system model, the validated ANN model predicts the A/C unit behavior based on information including the indoor space conditions, outdoor weather conditions and the speed of compressor and supply fan. In this module, the A/C unit's deliverable sensible capacity and latent capacity is calculated, the power consumption of the whole unit is also estimated.
- 4) Finally, the sensible and latent cooling capacities are delivered to the building space. Integrating the information related to the delivered cooling capacities and building outdoor conditions, the indoor temperature and relative humidity for the next time step are predicted and saved for next time-loop calculation.

During this co-simulation, the cooling system behavior and energy consumption are estimated and thermal comfort conditions in building are predicted.

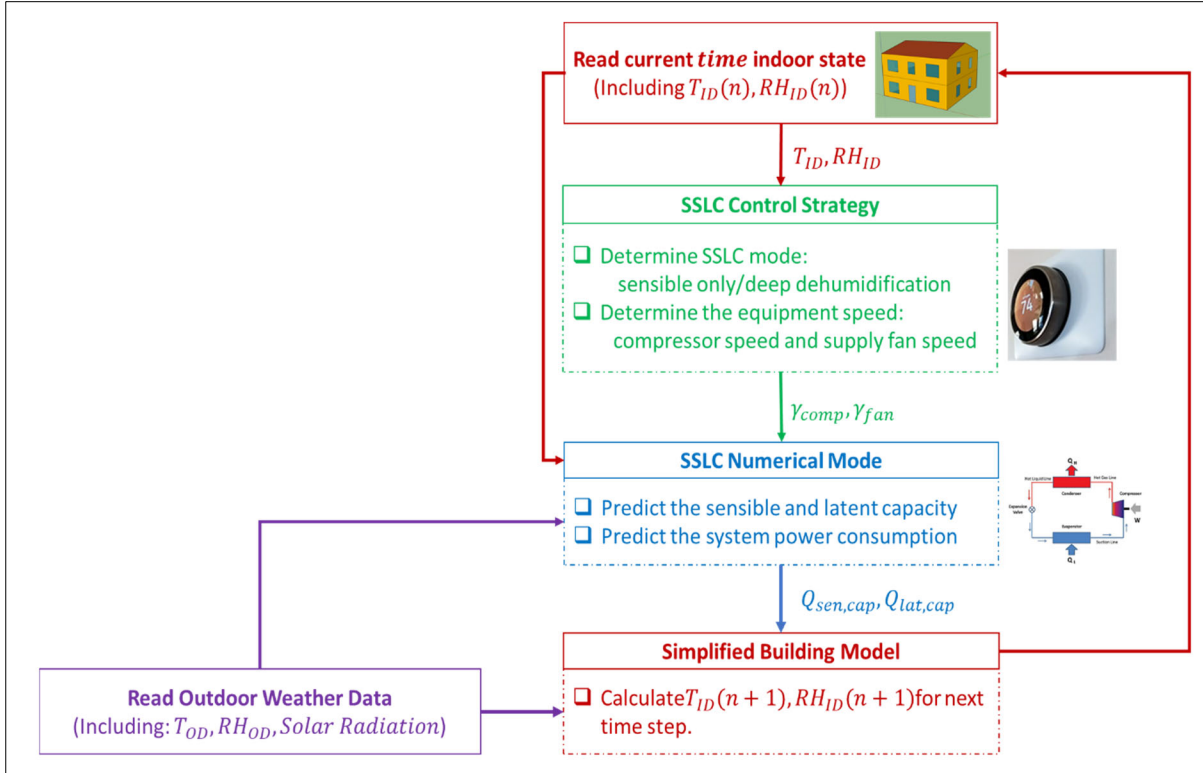


Figure 5.4. Co-simulation structure connecting SSLC system and prototype building under SSLC control strategies.

5.3 Control Strategy 1 – Mode Switch with Constant Equipment Speeds

In the SSLC system, there are two coupled variables that need to be controlled: temperature and humidity. In practice, the indoor air temperature and humidity cannot be perfectly controlled all the time. The first reason is that the sensible and latent loads in a space do not occur at the same time. For example, in the early summer of Indianapolis, the building contains high latent load but low sensible load because of the humid and cold outdoor weather conditions. In this situation, the dehumidification may lead to over-cooling, since it is impossible to remove the indoor moisture without cooling down the space. Furthermore, the equipment SHR (ratio of the deliverable sensible capacity to total capacity) is limited by the A/C system design and control logic, which cannot satisfy the various building load SHR (ratio of the sensible load to the total load). In other words, the indoor temperature and humidity cannot be both controlled to stay around setpoints all the time. To overcome these limitations, one variable is selected to be met in priority, this control strategy is referred to as priority control with constant equipment speed.

The priority control includes two different approaches: Thermostat Priority Control and Humidistat Priority Control. For the thermostat priority control, temperature is controlled as the priority. The A/C system is switched to dehumidification mode only when both sensible and latent load existing in space. For humidistat priority control, the A/C system controls the humidity first if the indoor temperature is higher than the dead bound. The A/C system changes to sensible only mode when no dehumidification is required in the space and only the sensible load needs to be met.

The equipment speeds are constant in each SSLC mode. More specifically, only two stages of speed are required for the compressor and the evaporator fan respectively: in the dehumidification mode, the compressor operates at the higher speed stage and the supply fan runs at lower speed stage to realize deep dehumidification, whereas, in the sensible only mode, the speed stages for the compressor and the evaporator fan need to be swapped so that compressor operates at low speed but the supply fan runs at a high speed.

5.3.1 Compressor Speed and Supply Fan Speed Determination

To meet both the sensible and latent cooling loads in a space, the compressor speed and supply fan speed are required to be determined properly. The sensible and latent loads are mainly determined by two factors: the outdoor weather conditions and indoor temperature and humidity setpoints. In this work, the indoor setpoints of temperature and relative humidity are 74°F and 50%, respectively. To estimate the cooling load, the sensible and latent hourly average load of the prototype building is shown in Figure 5.5, which is estimated by TRNSYS for the whole summer from June to August (2208 hours) with TMY3 weather data in Indianapolis.

The space sensible load is plotted against the outdoor temperature in Figure 5.6. And the load line shown in a red line in Figure 5.6 is generated by a linear regression approach. It can see that the sensible cooling load is 9.7kW, when the outdoor temperature is the A/C unit rating temperature (95°F). Thus, the SSLC system should deliver no less than 9.7kW cooling capacity, no matter in which SSLC mode, when the indoor conditions are 74°F and 50% and the outdoor temperature is 95°F.

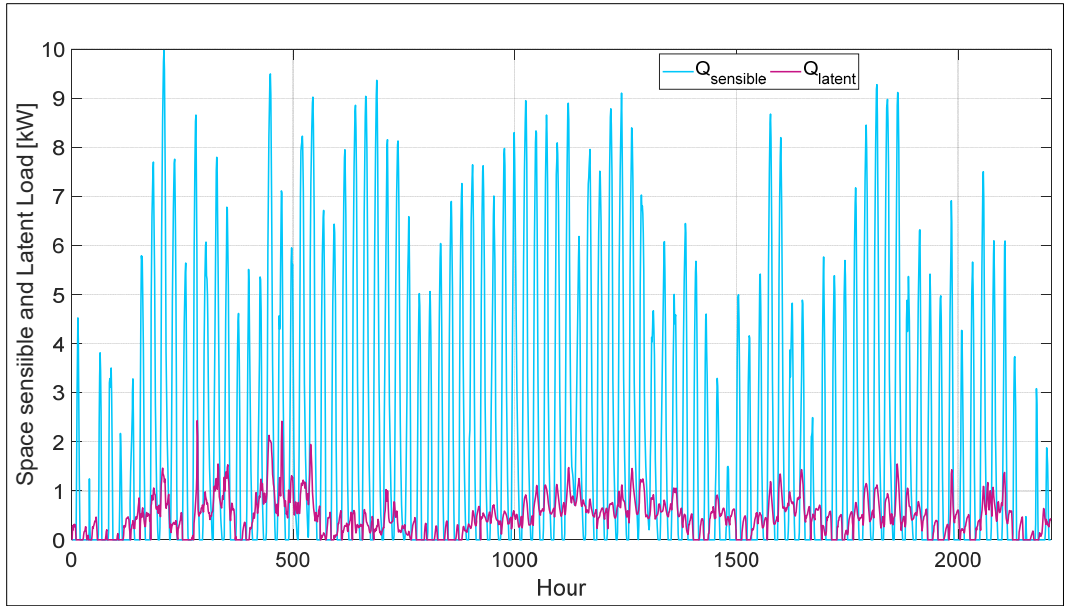


Figure 5.5. Sensible and latent hourly average load of prototype building throughout summer under Indianapolis weather conditions.

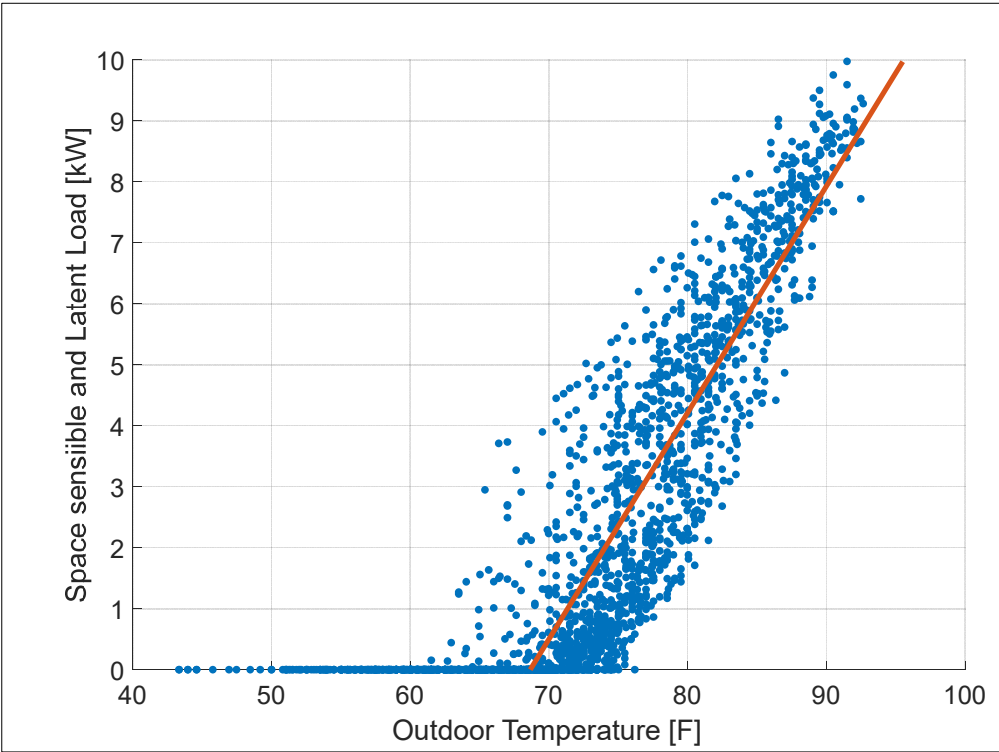


Figure 5.6. Sensible load line generation.

To determine the compressor speed and supply fan speed, the A/C system performance indicators including total capacity and SHR are mapped in Figure 5.7 under different equipment speeds at 23.3°C (74°F) and 50% indoor conditions and 35°C (95°F) outdoor temperature. The criteria of equipment speed-determination to realize sensible and latent cooling separately is that the equipment SHR is as low as possible in deep dehumidification mode and the equipment SHR reaches 1 in sensible-only mode.

It is observed in Figure 5.7 that the lowest equipment SHR occurs at top left corner, where system operates at full compressor speed with the lowest supply air flow rate. The highest equipment SHR is at bottom right, which equals to 1, indicating that the sensible only mode can be realized. Thus, for deep dehumidification mode, the compressor is at full-speed and the supply fan speed ratio is 0.28 (air flow rate is 500 CFM) which can deliver a total capacity of 9.61kW and a equipment SHR of 0.64. In the sensible only mode, the compressor speed ratio is 0.5 and the supply fan reaches full speed (1800 CFM) where the equipment SHR is over 0.9 (nearly equals 1). With this compressor speed and supply fan speed, the sensible cooling capacity delivered by the cooling system can still meet the building sensible load around 96% of the time in summer.

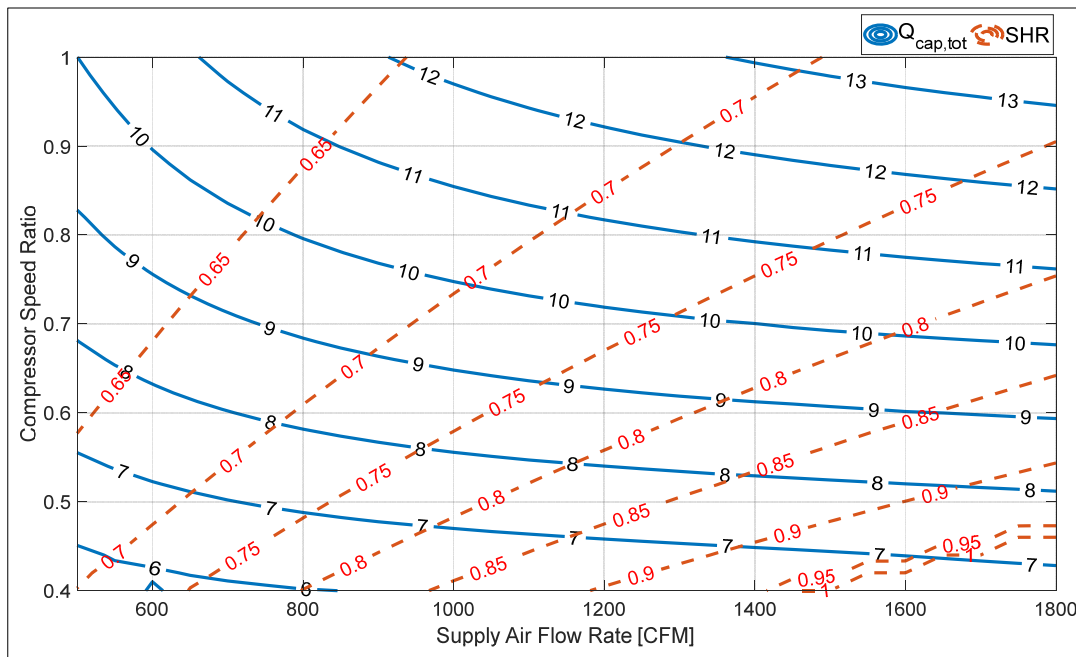


Figure 5.7. Total capacity and SHR contour under full ranges of compressor speed ratio and supply air flow rate.

5.3.2 Thermostat Priority Control

The control logic of thermostat priority control is shown in Figure 5.8. There are three statuses of the controlled A/C unit: OFF, (sensible-only) Cooling and (deep) Dehumidification. When the unit is in OFF status, both compressor and supply fan are deactivated, so there is not any sensible or latent capacity delivered to the space. But when the unit is switched to cooling (sensible only mode) status, the compressor operates at low speed while supply fan is at high speed to provide high sensible capacity and low latent capacity, or even no latent capacity at dry-warm indoor conditions. The last status is dehumidification, in which situation the compressor is switched to high compressor speed and low supply fan speed to remove as much latent load in the building as possible. After the three operation statuses are defined, the next critical step is to define the temperature and humidity conditions for targeting the unit to switch among the three statuses.

The set-point dry-bulb temperature of the simulated A/C system is set to be 74 °F (23.3 °C), and the upper and lower temperature bounds is ± 1 °F from the setpoint temperature. To avoid overcooling in deep dehumidification, a dead bound is set to be -3 °F from the set-point temperature. Based on the ANSI/ASHRAE Standard 55-2020 recommendations, a comfortable relative humidity (RH) in the space should be between 40% and 60%.

The unit statuses of previous time step (step n-1 as shown in Figure 5.8) is first back read and then go through the following logic for different status of the previous step:

- 1) Step(n-1) = OFF, the current indoor temperature is checked first. If the indoor temperature is higher than the upper bound (75°F), the indoor humidity is then read and a further step is required to choose between sensible cooling mode or dehumidification mode, otherwise (i.e., if the indoor temperature is lower than upper boundary), the cooling system stays OFF in current time step. If a further mode determination step is necessary, (i.e., choose whether sensible cooling mode or dehumidification mode is to be used), the indoor humidity is then compared with the control upper bound. In this mode determination step, if both indoor temperature and humidity exceeds the upper control bounds, the unit is switched to dehumidification mode; if only the temperature is higher than the upper bound, the unit is switched to sensible cooling mode.
- 2) Step(n-1) = (sensible) Cooling, the unit is turned off when the indoor temperature is below the low temperature bound. But if there is still a cooling requirement (the

temperature is still higher than the lower bound), the indoor humidity is checked to see whether it is higher than the upper bound, i.e., 60%. Similarly, the unit conducts dehumidification only if both temperature and humidity are required to be met.

- 3) Step (n-1) = (deep) Dehumidification, to have enough time for dehumidification, the indoor room dry-bulb temperature is compared with the deadband temperature. As long as the indoor dry-bulb temperature is higher than the deadband temperature and the room humidity does not reach the lower bound, the unit stays at the dehumidification mode.

The characteristics of thermostat priority control can be summarized as follows: the indoor dry-bulb temperature is measured, compared with its upper and lower bounds first, then the humidity is measured; as long as there is no sensible load removal requirement, the A/C unit stays OFF; only when there is both sensible and latent load removal requirement, the unit is turned to dehumidification mode.

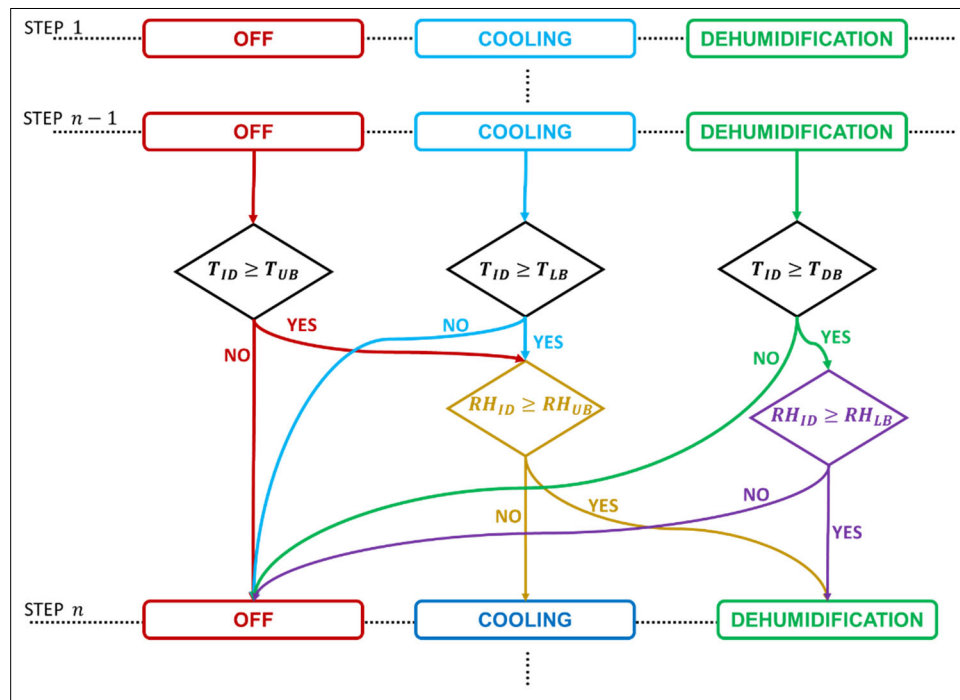


Figure 5.8. Control logic framework for thermostat priority control.

Based on the aforementioned control strategy, the A/C system is coupled with the simplified building model to simulate SSLC system performance and the building thermal and moisture response to the control strategy.

Figure 5.10 and Figure 5.10 represent the indoor dry-bulb temperature and absolute humidity response to thermostat priority control, as well as the corresponding A/C unit cooling capacity and equipment SHR on July 4th. Since the relative humidity also changes with the indoor temperature, the absolute humidity is a better humidity indicator to identify the moisture decrease in the space. In Figure 5.10, the blue solid line and light blue dash line represent the indoor and outdoor dry-bulb temperature, respectively. Two black dash lines are the lower and upper temperature bounds, i.e., 73°F and 75°F. The red solid line and dash line are the outdoor and indoor humidity ratio (absolute humidity). And two pink dash lines are corresponding absolute humidity bounds, which is calculated base on 74°F indoor setpoint temperature and 40% and 60% relative humidity, respectively.

In Figure 5.10, the A/C unit is switched between OFF and sensible only mode without entering the deep dehumidification mode, since the indoor humidity never reaches the up limitation throughout the day. Correspondingly, the indoor temperature is well controlled between the high and low bounds. The temperature in space increases when the A/C unit is turned off and decreases when the A/C unit is switched to sensible only mode. Regarding to the indoor humidity ratio, there are slight fluctuations with the outdoor humidity but no significant decrease caused by the dehumidification of A/C unit.

The fact is also verified in Figure 5.10, where the red and black solid lines are sensible and latent capacity delivered by the A/C unit, and the equipment SHR is represented as the blue dash line. It can be observed that the sensible capacity of the A/C unit is much higher than the latent capacity for most of unit operation time. The equipment SHR (defined as the ratio of sensible capacity to total capacity) is higher than 0.9 and nearly reaches 1 for all A/C unit cycles.

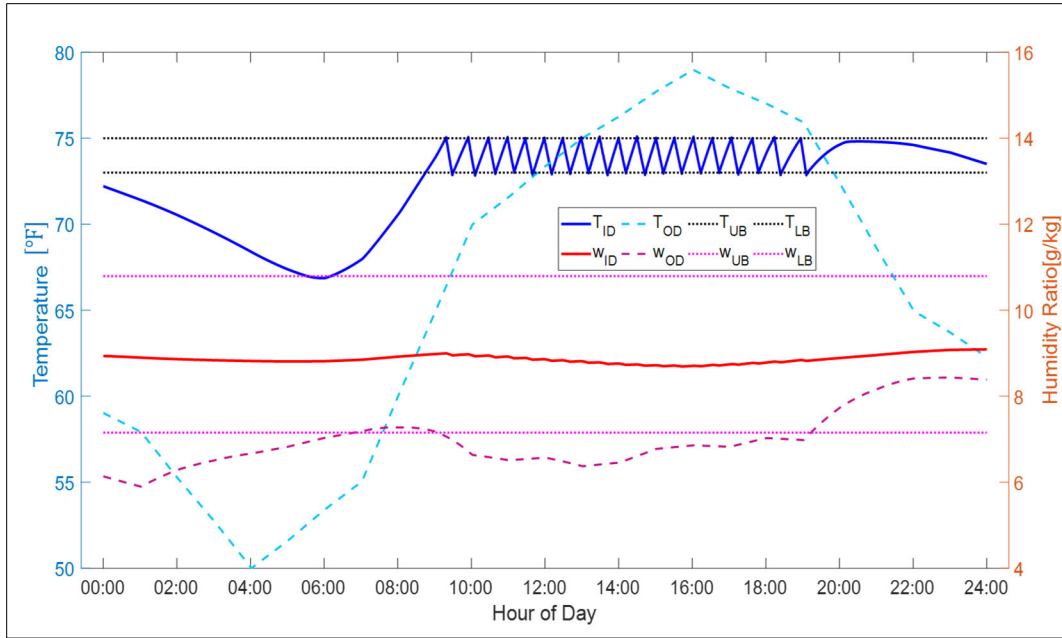


Figure 5.9. Indoor temperature and absolute humidity response to thermostat priority control on July 4th.

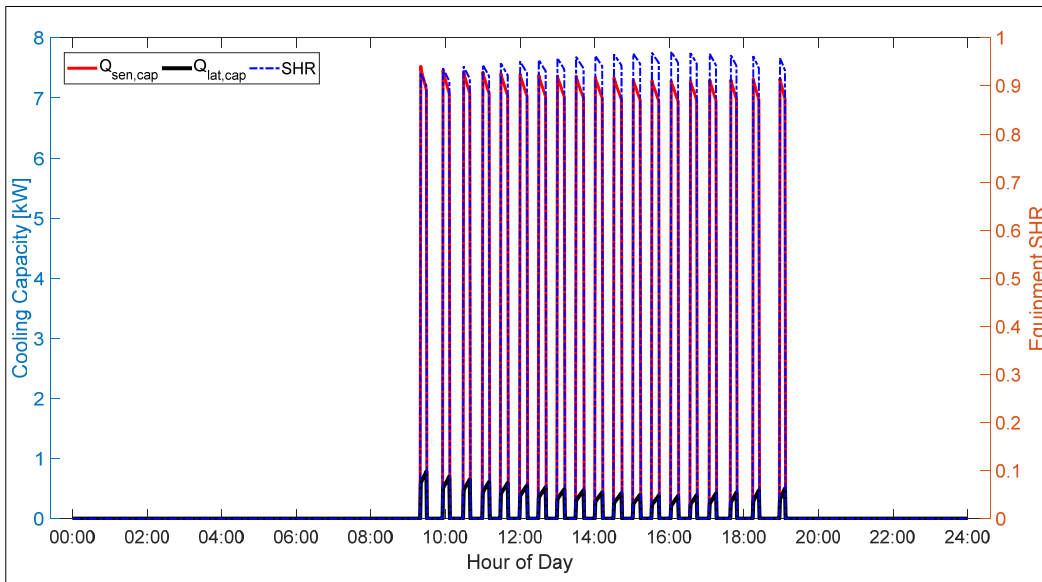


Figure 5.10. A/C unit performance under thermostat priority control on July 4th.

Figure 5.11 and Figure 5.12 show the indoor dry-bulb temperature and absolute humidity performance under the thermostat priority control as well as corresponding cooling capacity and equipment SHR in a humid day: July 26th. In Figure 5.11, the A/C unit is switched among three

different modes: OFF, sensible only and deep dehumidification. It suggests that when the A/C unit is turned into deep dehumidification mode at 5:00, 7:00 and 22:00, both the indoor dry-bulb temperature and absolute humidity decrease dramatically. During the deep dehumidification process, the unit is turned off even if the indoor humidity does not reach the lower bound. It is because the indoor dry-bulb temperature already reaches the deadband temperature (71°F). To avoid the room space being overcooled continuously, the A/C unit stops delivering cooling capacity. Furthermore, it can be observed in Figure 5.11 that the indoor humidity exceeds the upper bound around 5:00, but the A/C unit remains OFF until the indoor temperature reaches the upper bound. This is an indication of the one important characteristics of thermostat priority control: the A/C unit enter deep dehumidification mode only when there is sensible cooling requirement.

Besides the indoor dry-bulb temperature and absolute humidity response to thermostat priority control, the A/C unit performance is plotted in Figure 5.12. It illustrates that the sensible capacity delivered by A/C unit stays constant in each on/off cycle to deal with the indoor sensible load, but the latent capacity delivered by A/C unit is significantly high in deep dehumidification mode and low in sensible only mode. Furthermore, the equipment SHR nearly reaches 0.9 in sensible only mode but only around 0.62 in deep dehumidification.

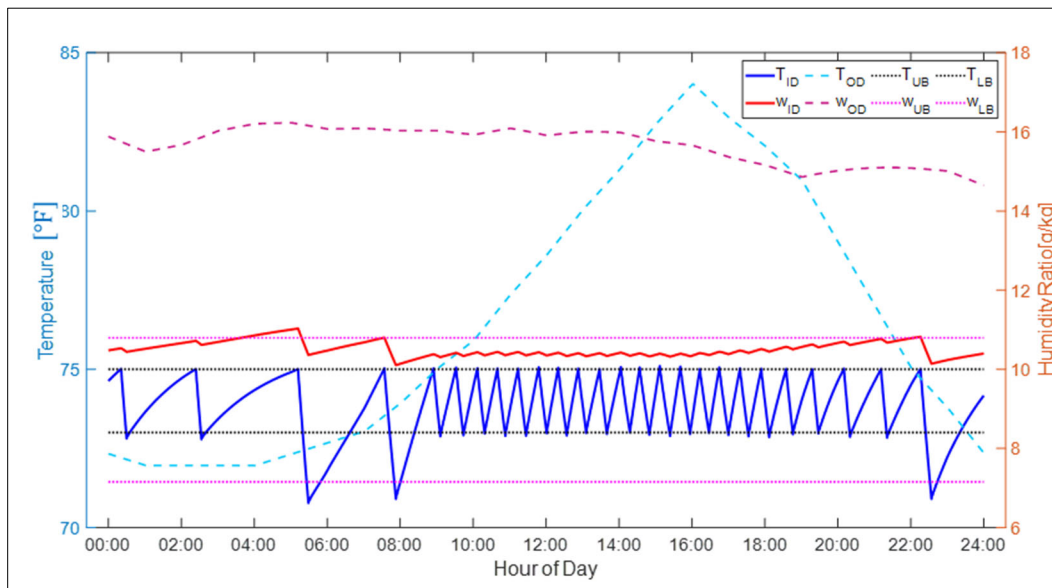


Figure 5.11. Indoor temperature and absolute humidity response to thermostat priority control on July 26th.

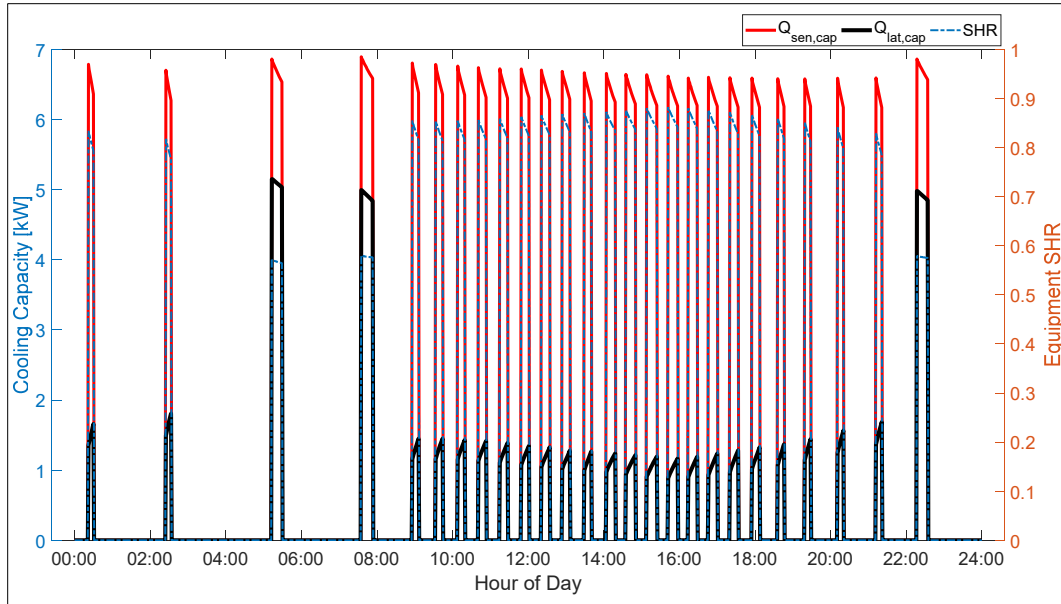


Figure 5.12. A/C unit performance under thermostat priority control on July 26th.

As a summary, the sensible and latent capacities of a variable speed A/C unit can be controlled through varying the compressor speed and supply fan speed to allow the unit to operate in two different operation modes: sensible only mode and deep dehumidification mode. More specifically, when operates in sensible only mode, the A/C unit is providing almost a constant sensible capacity to building and the latent capacity is decreased as close as zero, whereas, the delivered latent capacity can be 40% of total capacity in deep dehumidification mode. However, based on the simulation results in two typical days with different weather conditions, both the indoor dry-bulb temperature and absolute humidity are satisfied on the dry day. The absolute humidity is limited within the control boundaries in a cool and humid day, because little sensible load exists in the early morning and mid-nighttime. To improve this situation, humidistat priority control can be considered when there is a stricter humidity control requirement.

5.3.3 Humidistat Priority Control

Different from thermostat priority control, the humidistat priority control read the indoor humidity first, and then capture the indoor temperature before the A/C unit takes actions. The logic diagram for humidistat priority is shown in Figure 5.13. The first step is similar to thermostat priority control, the unit status of previous time step (step n-1 shown in Figure 5.13) is first back read and then follows the logic:

- (1) Step(n-1) = OFF, the indoor humidity is read first. If it is higher than the upper bound, the indoor dry-bulb temperature is then compared to the dead bound temperature. To avoid the overcool of room space, the A/C unit is turned off if the indoor temperature is lower than the deadband temperature, otherwise the unit switches to the dehumidification status. If the indoor absolute humidity is lower than the upper limit, the indoor temperature is checked to determine the A/C unit mode: OFF status or sensible only mode.
- (2) Step(n-1) = (sensible only) Cooling, the indoor humidity is also checked first. If it exceeds the upper humidity limit and the indoor dry-bulb temperature is higher than deadband, the A/C unit is switched to (deep) dehumidification status, but if there is no dehumidification requirement, sensible only cooling continues until the indoor dry-bulb temperature lower than the lower bound.
- (3) Step(n-1) = (deep) dehumidification, the A/C unit stays in dehumidification status until the indoor temperature reaches the dead bound, or the indoor humidity reaches the low boundary. However, if the indoor humidity load is satisfied but the indoor dry-bulb temperature is still higher than the low boundary, the A/C unit is switched to sensible only cooling.

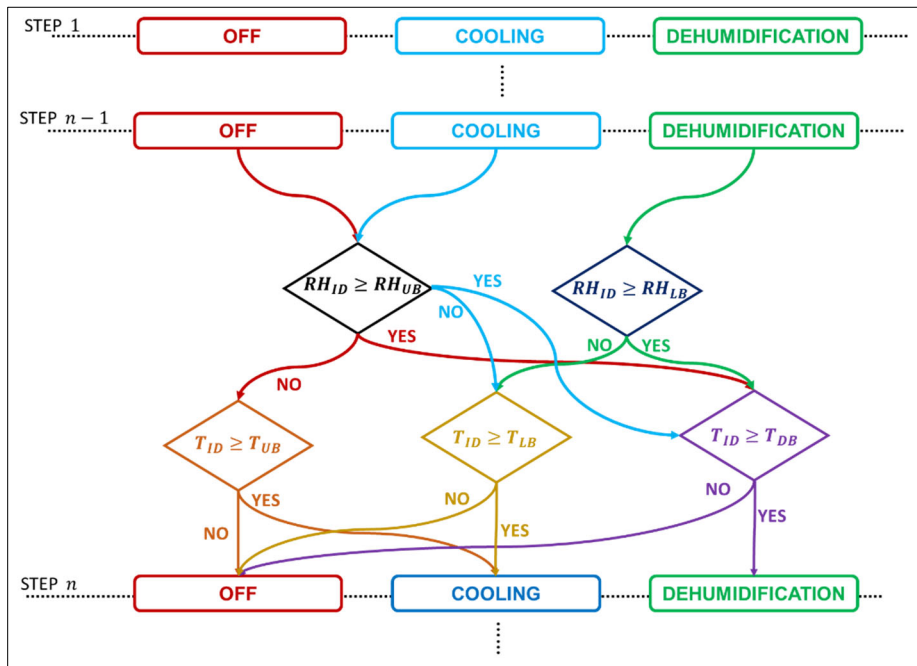


Figure 5.13. Control logic framework for humidistat priority control.

To summarize the characteristics of humidistat priority control, the indoor humidity is measured and compared with bounds first. If the indoor humidity is satisfied, then the temperature is considered. Furthermore, during the process of dehumidification, the indoor temperature is still stayed higher than dead band to avoid overcooling.

Based on the humidistat priority control logic, the A/C unit is coupled with the simplified building model to simulate the SSLC system performance and the building thermal and moisture response to this control strategy. In the simulation, all the parameters, including temperature and humidity setpoints, upper and lower bounds are consistent with those in the simulation of thermostat priority control. Two same days (July 4th and July 26th) is selected as samples to demonstrate the simulation results.

It can be seen from Figure 5.14 that the space temperature and humidity response to the humidistat priority control, as well as A/C unit performance are the same as the simulation results under thermostat priority control, which illustrates that there is no any difference between thermostat priority control and humidity priority control in a situation where no latent load excites in space.

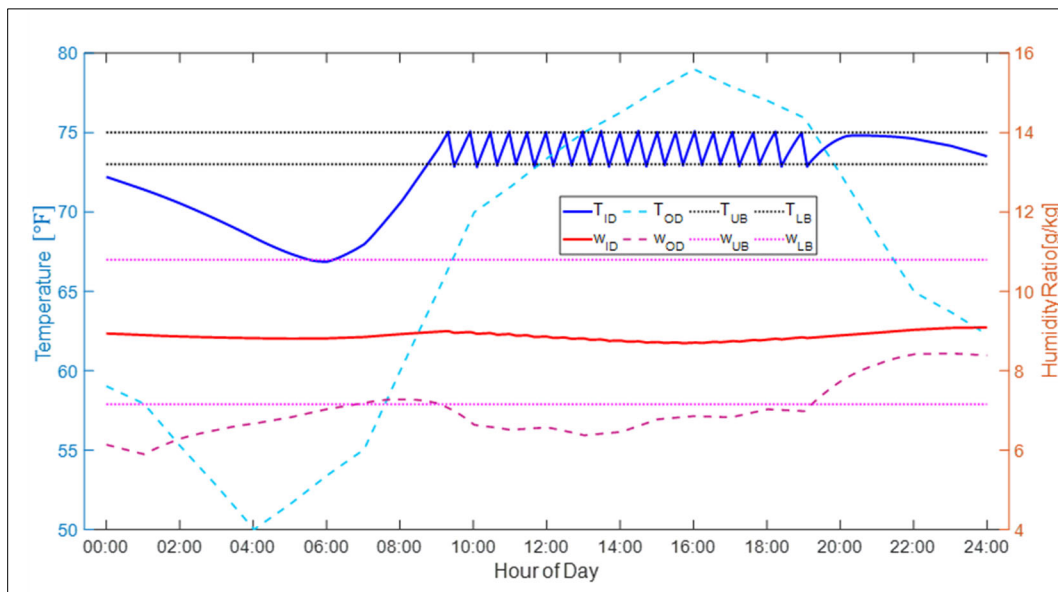


Figure 5.14. Indoor temperature and absolute humidity response to humidistat priority control on July 4th.

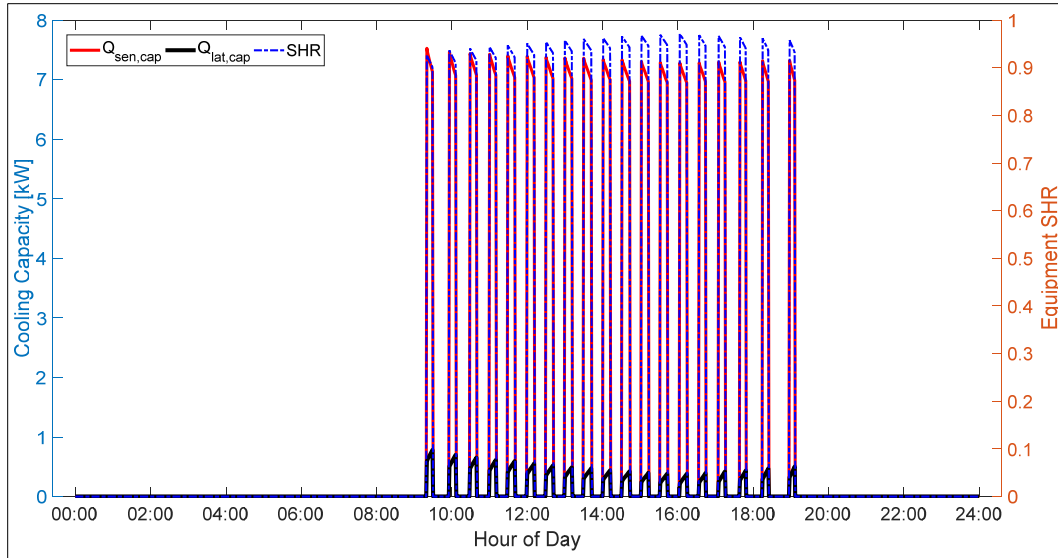


Figure 5.15. A/C system performance under humidistat priority control on July 4th.

On July 26th, the outdoor humidity is much higher than that on July 4th. In Figure 5.16 and Figure 5.17, the A/C unit is turned to deep dehumidification model multiple times. It can be observed that the A/C unit dehumidifies the space at 4:00 even though the indoor temperature is much lower than upper bound temperature. But in the simulation results of thermostat priority control, the indoor space is dehumidified until the indoor temperature reaches the upper bound at around 5:00. This situation also happens at around 7:00 and 22:00. This result indicates that with application of humidistat priority control in A/C system, the removal of latent load in space is more than that when applying the thermostat priority control. Since the indoor temperature and humidity is coupled and decreases at the same time, the dehumidification process is interrupted to avoid overcooling.

Beside the indoor and humidity response to humidistat priority control, it also can be verified from A/C unit capacity and equipment SHR in Figure 5.17 that the equipment SHR decreases to 0.62 in the deep dehumidification mode to deliver more latent capacity. In the sensible only mode, the equipment SHR of the A/C unit is between 0.8 and 0.9, which is much higher than that in the dehumidification mode. Since the equipment SHR is also influenced by the humid indoor air condition, the equipment SHR does not reach 1 to only deliver the sensible capacity.

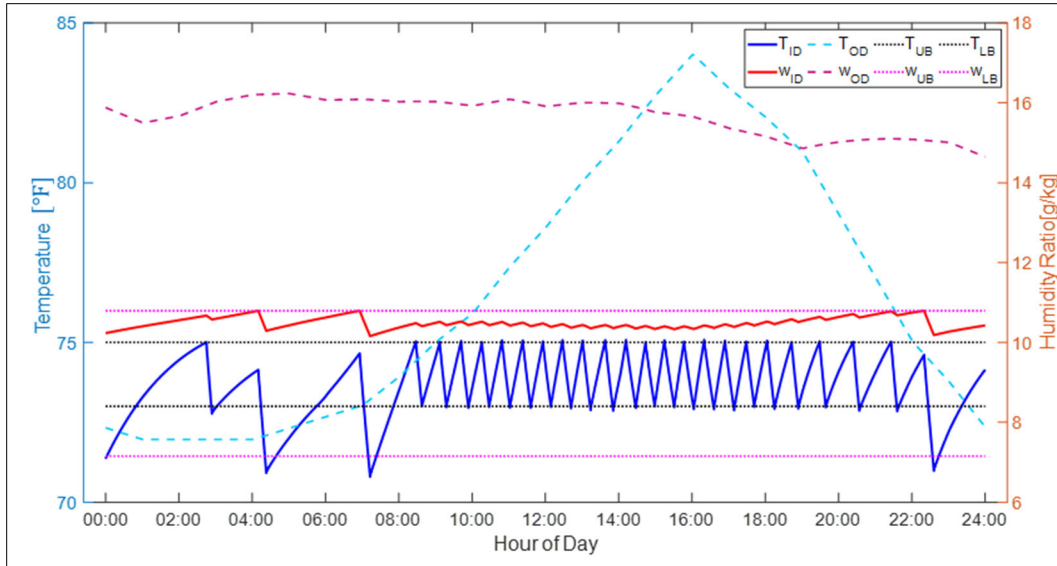


Figure 5.16. Indoor temperature and absolute humidity response to humidistat priority control on July 26th.

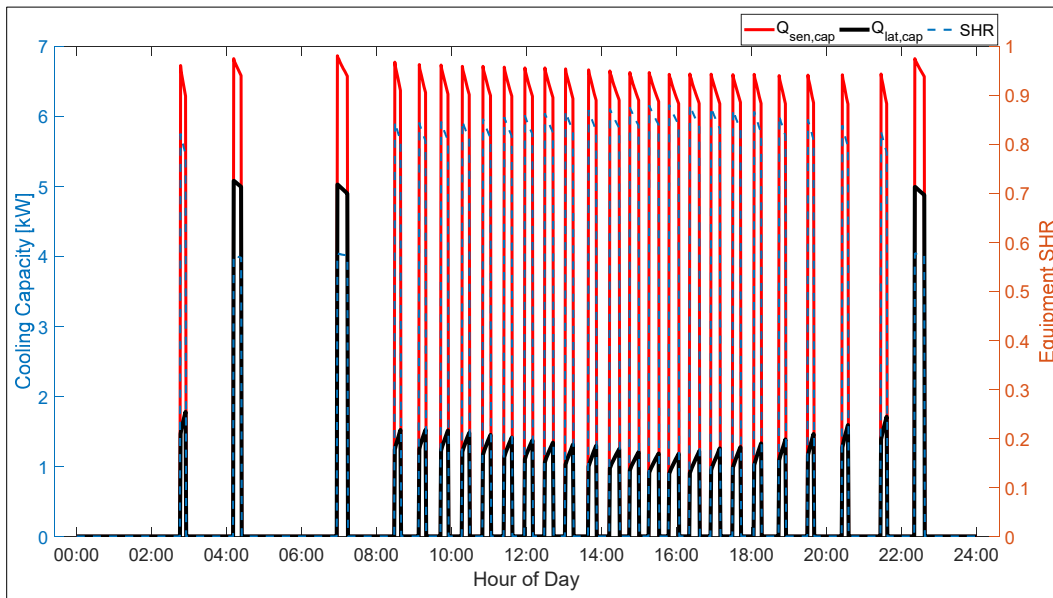


Figure 5.17. A/C system performance under humidistat priority control on July 26th.

5.4 Control Strategy 2 – Load Prediction Control with Variable Equipment Speeds

The logic of load prediction control with variable equipment speed is based on the thermostat priority control mentioned earlier. In the thermostat priority mode switch control, the A/C unit is turned off whenever the building sensible load is zero or extremely small. In contrast, the A/C unit is turned into sensible only mode or deep dehumidification mode, only when the

predicted sensible load is greater than zero or a small threshold. If the measured indoor humidity exceeds upper bound, the A/C unit then operates in dehumidification mode with its lowest equipment SHR until the indoor humidity reaches its lower bound or the space temperature reaches the deadband. But if the measured humidity does not exceed the upper bound, the A/C unit runs at the sensible-only mode or stays in OFF status. Different from the mode switch control with constant equipment speed, the idea of the load prediction with variable equipment speed control is to use the previous indoor measurement data, including the measured temperature and humidity in the space, to predict the sensible cooling load and SHR for the upcoming time step. When the unit is in the sensible only mode, the sensible cooling capacity delivered by the A/C unit is approximately equal to the predicted sensible cooling load and the equipment SHR is as close to 1 as possible. However, when the unit is in deep dehumidification mode, the equipment SHR reaches the minimum value, providing a sensible cooling capacity that also equals the predicted sensible cooling load.

Thus, an estimation of sensible load for the upcoming time step for the compressor speed and supply fan speed determination is critical in the application of the proposed load prediction control strategy.

5.4.1 Sensible Load Estimation

To estimate the sensible load in a space, the transient response of the temperature within a conditioned space is simulated by applying the simple energy balance principle to a lumped capacitance building model:

$$C_z \frac{dT_z}{dt} = \dot{Q}_{load,s} - \dot{Q}_{cool,s} \quad (5-2)$$

where T_z is the temperature of the conditioned space and C_z is the lumped thermal capacitance of the conditioned space. $\dot{Q}_{load,s}$ is the sensible cooling load, which includes internal heat gains due to building occupants, electrical plug loads and other internal heat source, as well as the external heat gain/loss driven by the temperature difference between the conditioned space and the surrounding environment. $\dot{Q}_{cool,s}$ is the sensible cooling capacity delivered by the A/C unit. It is indicated in Equation (5-2) that the rate of change in the indoor room temperature is increased when there is a significant imbalance between cooling capacity and cooling load.

To predict the indoor temperature at each time step, Equation (5-12) is transformed as a first-order forward difference formula to estimate the derivative term:

$$C_z \frac{T_z(n+1) - T_z(n)}{\Delta t} = \dot{Q}_{load,s}(n) - \dot{Q}_{cool,s}(n) \quad (5-3)$$

where $T_z(n)$ is the indoor temperature at the starting point of time step from n to $n+1$ and $T_z(n+1)$ is the temperature at the end point of time step from n to $n+1$. $\dot{Q}_{load,s}(n)$ and $\dot{Q}_{cool,s}(n)$ are the sensible cooling load and the sensible cooling capacity delivered by the A/C unit respectively, between the time-step of n and $n+1$. The cooling capacity delivered by A/C unit can be determined after the thermal capacitance (C_z) and sensible cooling load are estimated.

The prediction process starts from two continuous time-steps, at which the A/C unit is turned off at the first time-step but is switched on at the second time-step. At time-step 1, $\dot{Q}_{cool,s}(1)$ is zero since the air conditioner is off, as shown in Equation (5-4):

$$C_z \frac{T_z(2) - T_z(1)}{\Delta t} = \dot{Q}_{load,s}(1) \quad (5-4)$$

Then, at the time-step 2, the A/C unit operates at a known initial compressor and supply fan speeds: minimum compressor speed and minimum supply fan speed. During this time-step, the sensible cooling capacity ($\dot{Q}_{cool,s}(2)$) can be calculated from the SSLC performance mapping with known compressor and supply fan speed.

$$C_z \frac{T_z(3) - T_z(2)}{\Delta t} = \dot{Q}_{load,s}(2) - \dot{Q}_{cool,s}(2) \quad (5-5)$$

In order to predict the thermal capacity of the building, it is assumed that in a short period of time, specifically, in the continuous two time-steps, the sensible cooling load is constant, which means that:

$$\dot{Q}_{load,s}(1) = \dot{Q}_{load,s}(2) \quad (5-6)$$

To combine previous equations from Equation (5-2) to Equation (5-6) together, it is easy to obtain the thermal capacitance and sensible cooling load during the second time step:

$$C_z = \frac{\dot{Q}_{cool,s}(2) \cdot \Delta t}{2T_z(2) - T_z(1) - T_z(3)} \quad (5-7)$$

$$\dot{Q}_{load,s}(2) = C_z \frac{T_z(3) - T_z(2)}{\Delta t} + \dot{Q}_{cool,s}(2) \quad (5-8)$$

Then, the sensible cooling capacity needed to drive the indoor temperature to the setpoint temperature is estimated from Equation (5-6) by assuming that $\dot{Q}_{load,s}(3)$ is equal to $\dot{Q}_{load,s}(2)$:

$$\dot{Q}_{cool,s}(3) = \dot{Q}_{load,s}(3) - C_z \frac{T_{sp} - T_z(3)}{\Delta t} \quad (5-9)$$

The compressor speed and supply fan speed of the A/C unit can be calculated based on sensible cooling load estimation and SSLC operation mode determination, which will be explained in the next section. It is noted that, due to practical equipment constraints, the actual cooling capacity that can be delivered by the equipment cannot always match the demanded capacity as expressed in Equations (5-9). After the equipment speeds are determined, the actual cooling capacity delivered to the space is calculated based on the SSLC performance map, and the actual space temperature at the end of third time-step ($T_z(4)$) can be measured.

However, it is necessary to update the sensible cooling load in each time step since the deviation may exist between the actual value and the predicted value. The actual sensible cooling load is estimated based on the measured indoor temperature and actual delivered cooling capacity ($\dot{Q}_{cool,s,actual}$, the capacity calculated from the A/C unit performance map based on equipment speeds, not the value obtained by Equations (5-9)) as shown below:

$$\dot{Q}_{load,s}(3) = \dot{Q}_{cool,s,actual}(3) + C_z \frac{T_z(4) - T_z(3)}{\Delta t} \quad (5-10)$$

With C_z being estimated from Equation (5-7) and assumed to be constant, Equations (5-9) and (5-10) can be applied to following time-steps. Therefore, the sensible cooling load in the n th time step is estimated by:

$$\dot{Q}_{cool,s}(n) = \dot{Q}_{load,s}(n) - C_z \frac{T_{sp} - T_z(n)}{\Delta t} \quad (5-11)$$

and the actual sensible cooling load in the time-step n is updated by:

$$\dot{Q}_{load,s}(n) = \dot{Q}_{cool,s,actual}(n) + C_z \frac{T_z(n+1) - T_z(n)}{\Delta t} \quad (5-12)$$

However, further modifications need to be applied to Equation (5-11) to accommodate some practical concerns: (1) when the current temperature is above the setpoint temperature for less than 1 °F but more than 0.5 °F, the numerator in Equation (5-11) is replaced by 0.5 °F (i.e., cool down 0.5 °F in one time step) in order to avoid too frequent ON/OFF switching of the system; (2) when the current temperature is above the set point temperature for more than 1 °F, the

numerator in Equation (5-11) is replaced by 1 °F (i.e., cool down 1 °F in one time step), which is for the purpose of having a relatively rapid cooling but still ensuring the required cooling capacity being within the deliverable range of the actual equipment.

Now the whole process of sensible load prediction can be carried out by applying Equations (5-11) and Equation (5-12). The sensible cooling load is re-estimated in each time step and updated in the next time step when the A/C unit is cycled on. The thermal capacitance C_z is updated on each on/off cycle. Since the sensible load in space changes with weather data and internal gain profile smoothly without abrupt changes, the sensible load does not change in two adjacent steps and the thermal capacitance C_z is estimated accurately.

5.4.2 Compressor and Supply Fan Speed Determination

To deliver a given sensible cooling capacity to the conditioned space, the compressor speed and supply fan speed are required to be determined.

In deep dehumidification mode, the required sensible cooling capacity needs to match the predicted sensible cooling load in the current time-step, and, ideally, the equipment SHR can reach its minimum value.

$$\dot{Q}_{load,s} = \dot{Q}_{cool,s} \quad (5-13)$$

$$SHR_{equipment} = SHR_{minimum} \quad (5-14)$$

As shown in Figure 5.7 that the lowest equipment SHR occurs at the top left corner, where the compressor runs at full speed and supply fan operates at lowest speed; the highest equipment SHR is at the bottom right, where the supply fan is at full speed but the compressor runs at minimum speed. The equipment SHR increases with the decrease of compressor speed and the increase of supply fan speed. To obtain a minimum equipment SHR, the sensible cooling capacity is estimated using full compressor speed and lowest supply air flow rate under current indoor and outdoor conditions first. Then, this sensible cooling capacity with the lowest equipment SHR is compared with the required sensible cooling load. If the sensible cooling capacity with the lowest equipment SHR is lower than the required sensible cooling load, the compressor runs at highest speed and the supply air flow rate is calculated by looking up the system performance map together with Equation (5-13). In contrast, if the sensible cooling capacity with lowest equipment SHR is

higher than the sensible cooling load, the supply air fan maintains lowest speed and the compressor speed is calculated by performance map look up with the condition described in Equation (5-13) satisfied. Based on the aforementioned method, it can guarantee that the sensible cooling capacity delivered by A/C unit matches the sensible cooling load with minimum equipment SHR. However, there could be a special case that the deliverable sensible capacity cannot perfectly match the required cooling load because of the compressor and supply fan speed limitations. In this case, both the compressor and the supply fan are controlled to stay at full speed, when the maximum deliverable cooling capacity is still lower than the required cooling load; or both compressor and supply fan are control to stay at minimum speeds when the minimum deliverable capacity is still higher than the required load.

In the sensible-only mode, the sensible cooling capacity delivered by the A/C unit to conditioned space is equal to the sensible cooling load predicted from the previous time step but the equipment SHR is as close to one as possible.

$$\dot{Q}_{load,s} = \dot{Q}_{cool,s} \quad (5-15)$$

$$SHR_{equipment} = 1 \quad (5-16)$$

Based on the performance characteristic of A/C unit, the sensible cooling capacity with maximum SHR occurs at the right bottom in Figure 5.7, where the A/C unit operates at lowest compressor speed but highest supply air fan speed under the current indoor and outdoor conditions. If this sensible cooling capacity with maximum SHR is higher than the cooling load, the compressor will run at minimum speed. In contrast, if sensible cooling capacity with maximum SHR is lower than the predicted sensible cooling load, the supply fan will run at maximum speed. Based on aforementioned method, one equipment speed, either compressor or supply fan, is determined.

In addition to the general equipment determination method described above, several different situations are considered:

- 1) As an example, shown in Figure 5.18, the A/C unit performance mapping at full range of compressor speed ratio and supply air flow rate is predicted under 74°F indoor temperature and 55% indoor relative humidity, 95 °F outdoor temperature. In Figure 5.18, the equipment SHR calculated at full supply fan speed and highest supply air flow rate is still less than 1, which means A/C unit cannot realize the sensible only cooling

because of the equipment speeds limitation. In this situation, the method to determine the other equipment speed is the same as what is explained in deep dehumidification mode. The other equipment speed is determined by looking up the performance map to solve Equation (5-15).

- 2) The other situation is shown in Figure 5.19, in which the A/C unit performance mapping at full range of compressor speed ratio and supply air flow rate is predicted under 74 °F indoor temperature and 45% indoor relative humidity, 95 °F outdoor temperature. It is shown in Figure 5.19 that the equipment SHR calculated at lowest compressor speed and highest supply fan speed is equal to 1, and the sensible only cooling mode is realized.

In the second situation, the sensible cooling capacity of two points located on A/C unit performance mapping are calculated: the first point is labeled as Point A, where the supply air flow rate is maximum and equipment SHR is equal to 1; the second point is labeled as Point B, where the compressor is at minimum speed and the equipment SHR is equal to 1. Point A and Point B are both shown in Figure 5.19. Then the sensible cooling load ($\dot{Q}_{load,s}$) is compared with the sensible cooling capacity at point A and point B (i.e., $\dot{Q}_{A,s}$ and $\dot{Q}_{B,s}$):

If $\dot{Q}_{B,s} \leq \dot{Q}_{load,s} \leq \dot{Q}_{A,s}$, the sensible cooling load value is between the sensible capacity value calculated at Point A and Point B, the point on A/C unit performance mapping is obtained though minimizing the overall power input of A/C unit and, at the same time, requiring the equipment SHR being 1:

$$\text{Minimize:} \quad \dot{W}_{total} \quad (5-17)$$

$$\text{Constrains:} \quad \left| \frac{\dot{Q}_{cool,s} - \dot{Q}_{load,s}}{\dot{Q}_{load,s}} \right| \leq 10\%; \quad (5-18)$$

$$SHR_{equipment} > 0.99;$$

If $\dot{Q}_{load,s} \leq \dot{Q}_{B,s}$ or $\dot{Q}_{load,s} \geq \dot{Q}_{A,s}$, the method determining the other equipment speed is same with the situation 1.

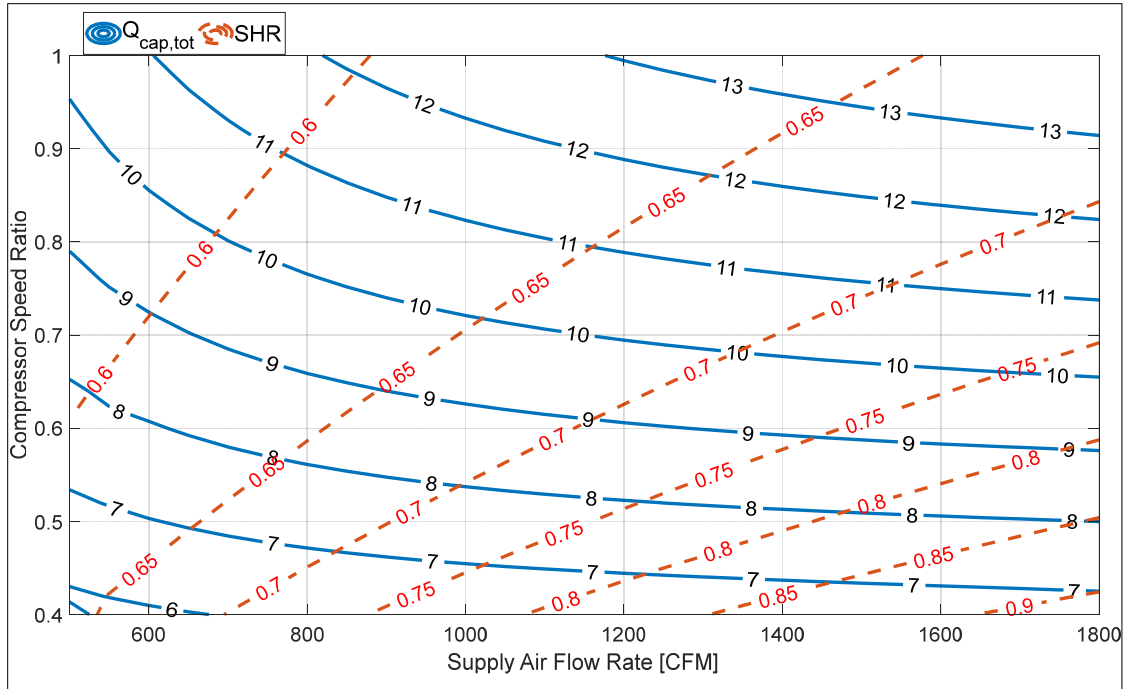


Figure 5.18. Total capacity and SHR contour under full ranges of equipment speeds in the situation that no SHR equals to 1.

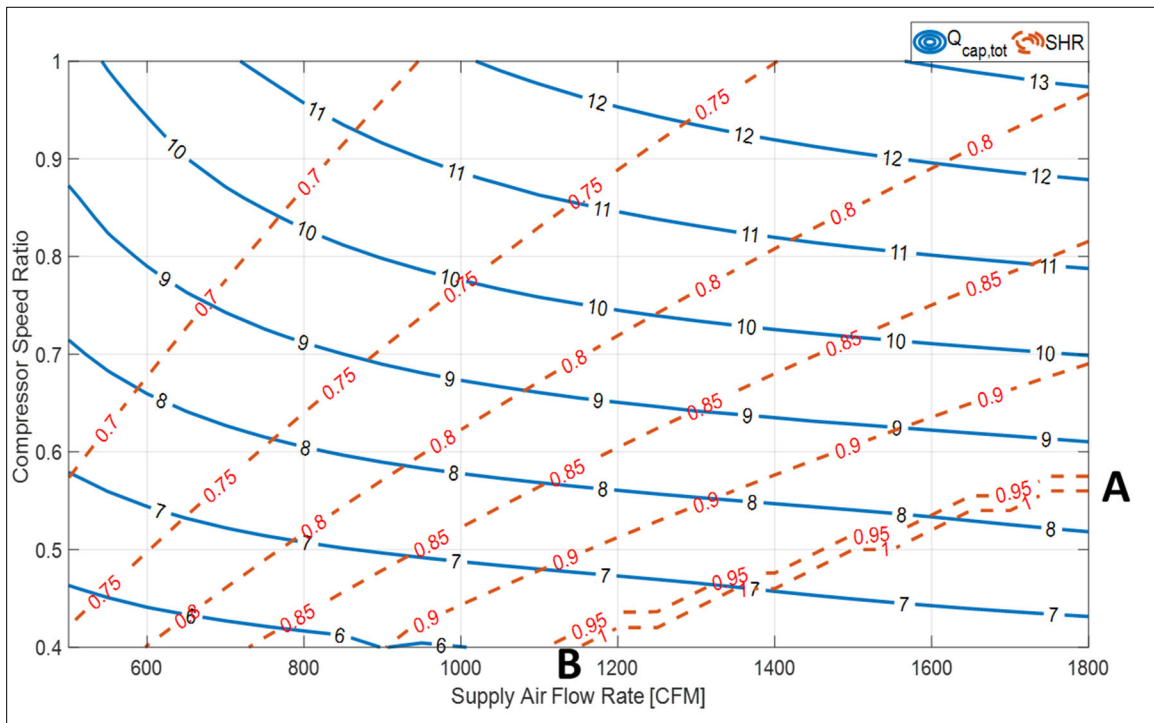


Figure 5.19. Total capacity and SHR contour under full ranges of equipment speeds in the situation that larges region shows SHR equals to 1.

5.4.3 Simulation Results

The same two days (July 4th and July 26th) are selected as examples to show the results of both building and A/C unit performance under the load prediction control strategy with variable speeds. In Figure 5.20, the blue and red dashed lines represent outdoor temperature and RH, respectively. The blue and red solid lines represent the indoor temperature and RH, respectively. Since on July 4th the humidity is lower than the upper bound during the whole day, the cooling system is never switched to deep dehumidification mode.

It is observed from Figure 5.20 that the equipment SHR is between 0.7 and 0.8 from 9:00 to 11:00 when the sensible cooling load in space is low but the latent is high. At this time, even though the compressor and supply fan operate at lowest speed, the cooling capacity delivered by A/C unit is still higher than the sensible cooling load in space. The equipment SHR shown in Figure 5.20 between 9:00 and 11:00 is simulated at lowest compressor speed ratio and minimum supply air flow rate. However, the sensible cooling load significantly increases, and the outdoor humidity ratio decreases during the daytime, the equipment SHR reaches 1 and only sensible cooling capacity is delivered to the space.

Furthermore, in Figure 5.20, the equipment SHR is lower at the beginning of on/off cycle, and then increase to 1 immediately, since, during the initial time step for the estimation of building thermo capacitance and the cooling load, the compressor and supply fan are set to operate at their lowest speeds. After this initial time step, the equipment starts to operate under the load prediction control strategy. It is also indicated in Figure 5.20 that when the A/C unit is cycled on, the equipment SHR changes from 1 to 0.75. The reason is that when the indoor temperature decreases, the cooling load also decreases gradually which can be lower than the minimum capacity that A/C unit will deliver. In this situation, the compressor and supply fan operate at minimum speeds and the equipment SHR at these equipment speeds are around 0.75.

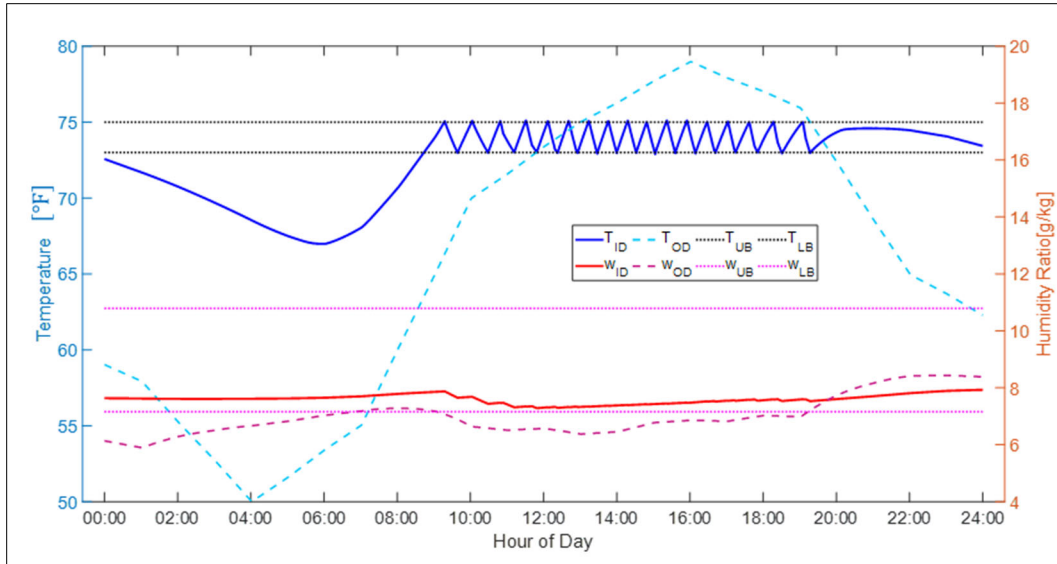


Figure 5.20. Indoor temperature and absolute humidity response to load prediction control on July 4th.

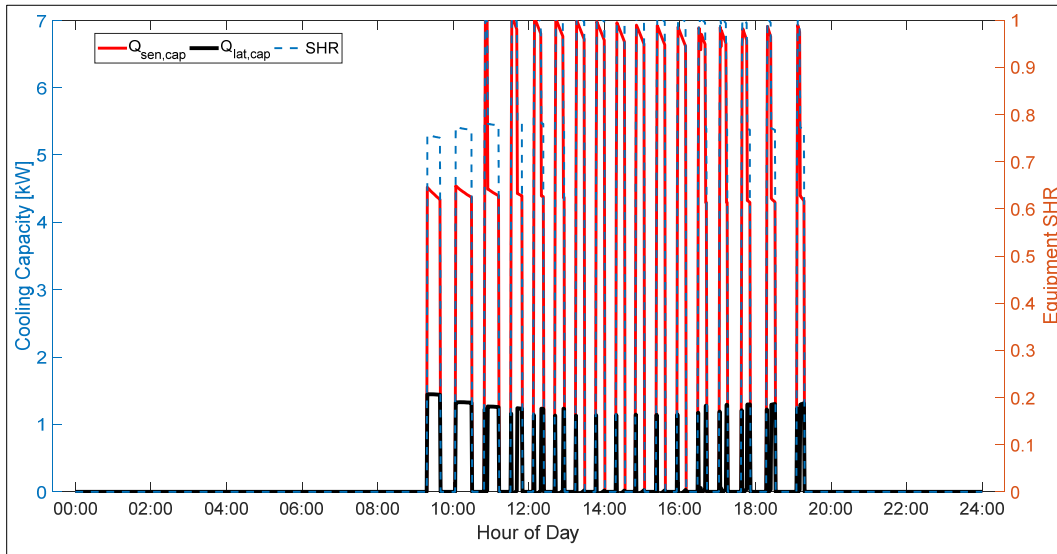


Figure 5.21. A/C system performance under load prediction control on July 4th.

The outdoor weather is cool and humid on July 25th. In Figure 5.22, between 3:30 and 7:00, the indoor temperature and humidity ratio significantly reduces to dead bound, i.e. 71°F and the indoor humidity also decreases, which indicates that the A/C unit is turned into deep dehumidification when the unit is cycled on. In Figure 5.23, the equipment SHR does not reach 1 even though the A/C unit is operating in “sensible only mode”. It is because that indoor space is

humid and the equipment SHR is less than 1 even when the equipment speeds reach the required limitations.

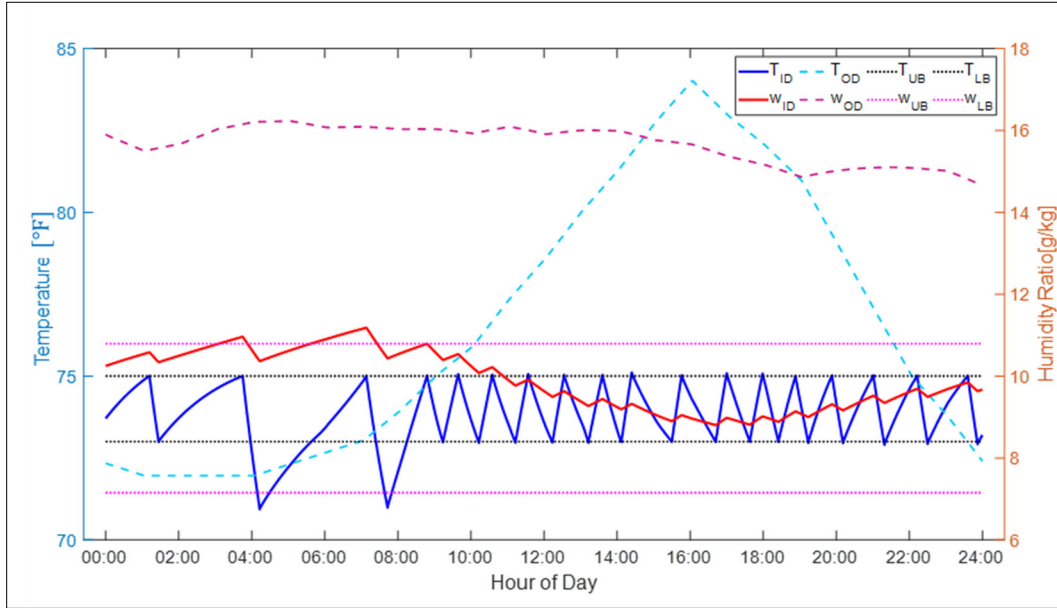


Figure 5.22. Indoor temperature and absolute humidity response to load prediction control on July 26th.

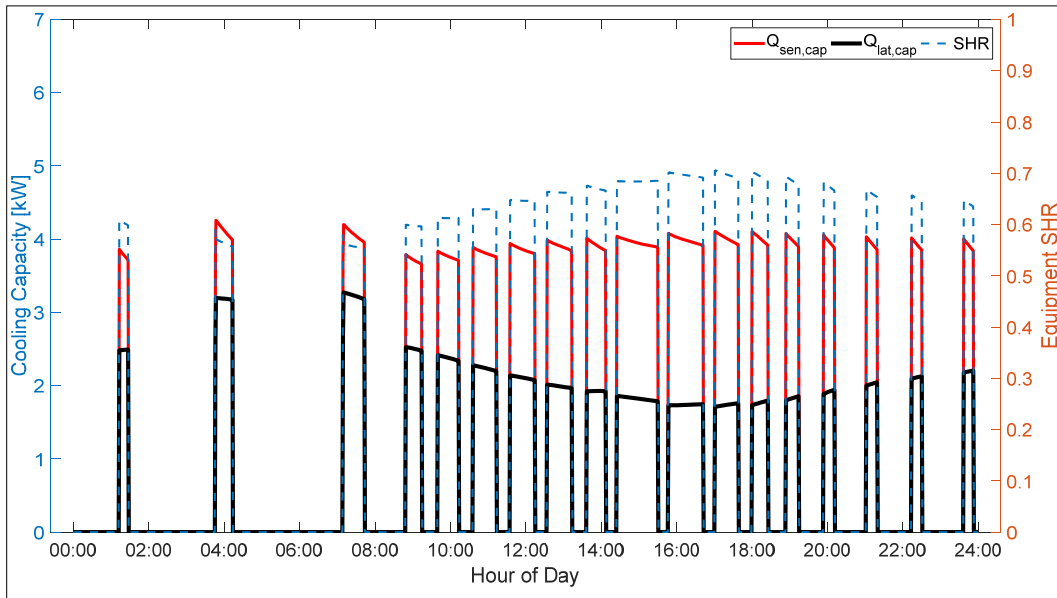


Figure 5.23. A/C system performance under load prediction control on July 26th.

5.5 Summary

This chapter mainly explains control methods to realize sequential separate sensible and latent cooling. Two SSLC control strategies are described. With the application of these SSLC control strategies, SSLC operation mode, i.e., sensible only cooling mode or deep dehumidification mode, is selected depending on the indoor temperature and humidity conditions first, and then the compressor speed and supply speed is determined depending on the specific logic in different control strategies. In the first proposed SSLC control strategy, the equipment speeds are pre-determined and maintained constant in each A/C unit on/off cycle. But in the second proposed SSLC control strategy, the equipment speeds are varied to match the delivered sensible cooling capacity with building sensible cooling load.

Furthermore, in this chapter, a baseline simulation that controls indoor temperature and humidity ideally is proposed and described. To understand the benefit and limitations of two SSLC control strategy, the building and A/C unit performance under each SSLC control strategy will be evaluated and compare with the baseline.

6. ENERGY PERFORMANCE AND COMFORT DELIVERY ANALYSIS

The numerical model of an SSLC system is developed and validated in Chapter 3 and Chapter 4, and can be used to predict the A/C unit performance under various indoor/outdoor conditions and equipment speeds. Furthermore, different control strategies for SSLC applications are proposed in Chapter 5. In this chapter, the control strategies proposed in previous chapter are applied to space cooling of a prototype residential building in five cities representing various typical weather characteristics. Cities included in this study are Indianapolis, Denver, Miami, Phoenix and Seattle, which are in cool and humid zone, cool and dry zone, hot and humid zone, hot and dry zone, and marine zone, respectively. In a cool and humid zone or in a cool and dry zone, the outdoor temperature is low so that the A/C unit cycles on and off from time to time (does not stay on for a long time as is likely to happen under hot outdoor conditions). Thus, Indianapolis and Denver are selected to investigate SSLC system performance in a dry and a humid environment when frequent A/C unit on/off cycles are expected. Different from Indianapolis and Denver, the outdoor temperature in Miami and Phoenix is extremely high throughout the summer so that the A/C unit will stay on for a long time. In these two cities, the SSLC system behavior can be observed in the situation that A/C unit operates continuously. Seattle is a special example selected in this work since the sensible and latent loads in room space do not occur in the same time duration in this case. The energy performance and comfort delivery performance of the A/C unit with different control strategies throughout a summer season (June, July and August) can be analyzed by comparing with the performance of the proposed baseline control with the same simulation duration, outdoor weather conditions and building models.

6.1 Case Study for Cool and Humid Climate Zone — Indianapolis

Indianapolis is an example to illustrate the difference between the various SSLC system control strategies proposed in Chapter 5. In this chapter, both the mode switch control strategy with fixed equipment speeds (also referred to as SSLC control strategy 1) and load prediction control with variable equipment speeds (also referred to as SSLC control strategy 2) are applied in co-simulation of a SSLC system integrated with a prototype residential building model. Indianapolis has a warm and humid summer, and the humidity varies significantly between day

and night. The humidity decreases in the daytime while the dry-bulb temperature increases. In other words, the sensible and latent loads of the building do not occur at the same time.

Based on the co-simulation results of SSLC system integrated with a building model under various control strategies in Indianapolis, different A/C unit performance indicators, including integrated sensible and latent capacity delivered to building space, as well as the total energy consumption of SSLC system, are summarized in Table 6.3. In addition, an average coefficient of performance (COP) through three months (June, July and August) of summer is defined as:

$$\text{Average COP} = \frac{\sum \dot{Q}_{sen,cap} + \sum \dot{Q}_{lat,cap}}{\sum \dot{W}_{tot}} \quad (6-1)$$

where $\sum \dot{Q}_{sen,cap}$ and $\sum \dot{Q}_{lat,cap}$ are the integrated sensible and latent capacity delivered from SSLC system, respectively. $\sum \dot{W}_{tot}$ is the total energy consumption of the SSLC system.

Table 6.1. Energy performance under different control strategies in Indianapolis throughout summer.

	Integrated Sensible Capacity	Integrated Latent Capacity	Energy Consumption	Average COP
	[kWh]	[kWh]	[kWh]	[-]
Baseline	3084.5	1025.1	848.7	4.84
Thermostat Priority	3343.8	658.7	746.3	5.36
Humidistat Priority	3382.2	390.5	775.1	5.25
Control Strategy 2	3329.6	1005.8	873.1	4.96

It is observed from Table 6.3 that in the baseline simulation, the A/C unit delivers 4109.6kWh total integrated cooling capacity and consumes 848.7 kWh energy in those three months. The SSLC system under the mode switch control (control strategy 1) delivers higher integrated sensible capacity but lower integrated latent capacity in comparison to the baseline simulation results. It is recalled that two specific control strategies, thermostat priority control and humidistat priority control, are proposed in the category of mode switch control. The average COPs of A/C unit under thermostat priority control and humidistat priority control are 5.36 and

5.25, respectively, which are improved for 10.7% and 8.4% in comparison to the average COP simulated in the baseline. The average COP under control strategy 2 (i.e., the load prediction control with variable equipment speeds) increases 2.4%.

Besides the energy performance of the heat pump, the comfort delivery performance is also considered. In the current work, since the indoor setpoint temperature is 74°F and the upper and lower temperature deadband are $\pm 1^\circ\text{F}$ from setpoint temperature, the upper comfort temperature bound representing a well-controlled indoor environment is defined as 75.5°F. Regarding to humidity, the indoor relative humidity upper bound is 60%, the comfort relative humidity limit is defined as 65%. However, the lower limits of temperature and humidity involving thermal comfort is not defined in current work, since the heating and humidification is not considered in this research.

In Table 6.2, the maximum temperature and relative humidity (RH) are listed for baseline, two control strategies in the category of control strategy 1 and SSLC control strategy 2. Additionally, it also calculated the accumulated time that the indoor temperature or relative humidity is beyond the upper comfort bound, which is Temperature Comfort Violation and Humidity Comfort Violation in Table 6.2. It is worth mentioning that, because sensible and latent load do not occur at the same time, the humid comfort violation is accumulated only when the SSLC system is cooling the room space.

Table 6.2. Comfort Delivery under different control strategies in Indianapolis throughout summer.

	Max. Indoor Temp. [°F]	Max. Indoor RH [%]	Temperature Comfort Violation [hour]	Humidity Comfort Violation [hour]
Baseline	74	58.1	0	0
Thermostat Priority	75.2	66.1	0	0.15
Humidistat Priority	75.2	64.7	0	0.13
Control Strategy 2	75.2	57.1	0	0

The set of plots from Figure 6.1 to Figure 6.4 presents the simulation results involving indoor temperature and humidity fluctuation for the whole summer with different control strategies: baseline, thermostat priority of SSLC control strategy 1, humidistat priority of SSLC control strategy 1 and SSLC control strategy 2. In the upper plot of Figure 6.1, the indoor temperature, shown as blue line, flows freely with outdoor temperature when the A/C unit is turned off, but is well-controlled no more than the set-point temperature (74°F), represented as red dash line in Figure 6.1. In the lower plot of Figure 6.1, the indoor relative humidity swings between the upper and lower humidity bounds, i.e., 60% and 40%, respectively. The indoor relative humidity is higher than upper bound only when the indoor temperature is overcooled for 1°F.

The indoor temperature and relative humidity simulation results in Figure 6.1 and Figure 6.4 are different from the baseline in Figure 6.1. In Figure 6.1 and Figure 6.4, the indoor temperature fluctuates between the upper and lower temperature bounds when the SSLC is in the sensible only mode, but the indoor temperature reaches dead bound (71°F) when the SSLC system is in the deep dehumidification mode. It can be observed that under control strategy 1, the indoor relative humidity exceeds the upper bound more frequently than that in the baseline simulation and the SSLC system simulation under control strategy 2. However, in Figure 6.4, the relative humidity is well-controlled below upper bound.

As a summary, to co-simulate the SSLC system integrated with the building model under Indianapolis weather conditions, the SSLC system gives a higher energy efficiency when control strategy 1 (mode switch control with fixed equipment speed) is applied, in this control strategy category, the energy efficiency performance under thermostat priority control and humidistat priority control are similar. The indoor relative humidity is not well-controlled between the pre-setting humidity bounds. However, under control strategy 2 (load prediction control with variable equipment speeds), the relative humidity is better controlled although the SSLC system average COP is higher than that under control strategy 1.

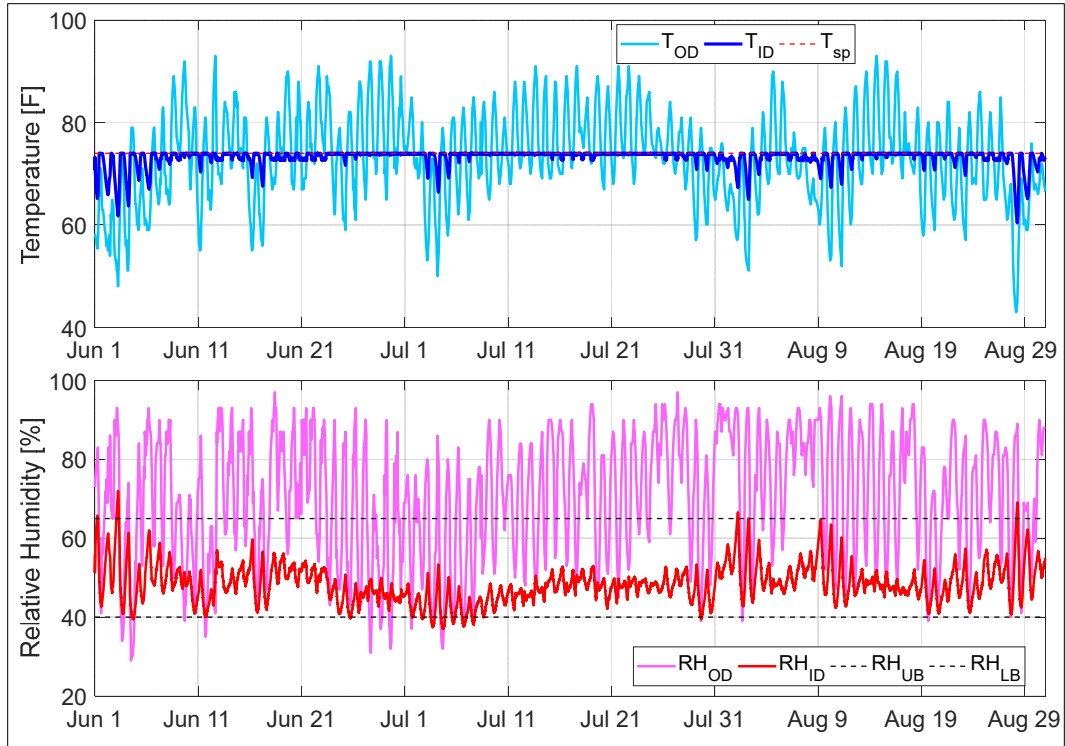


Figure 6.1. Indoor temperature and humidity simulation for baseline in Indianapolis.

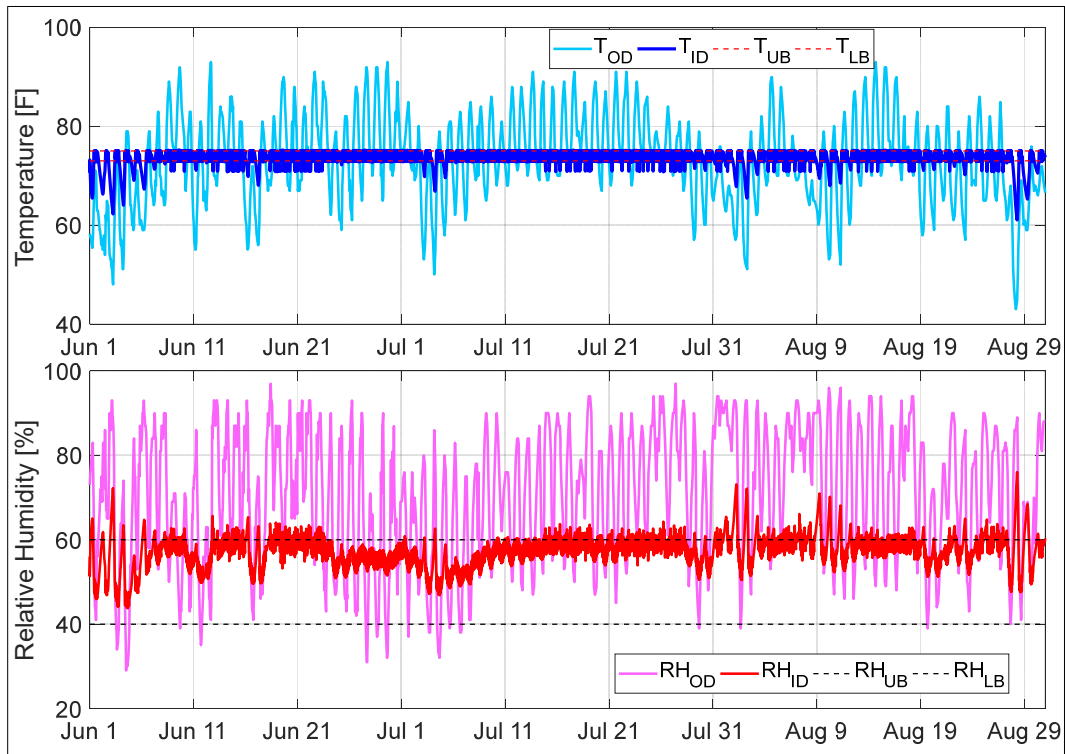


Figure 6.2. Indoor temperature and humidity response to thermostat priority control in Indianapolis.

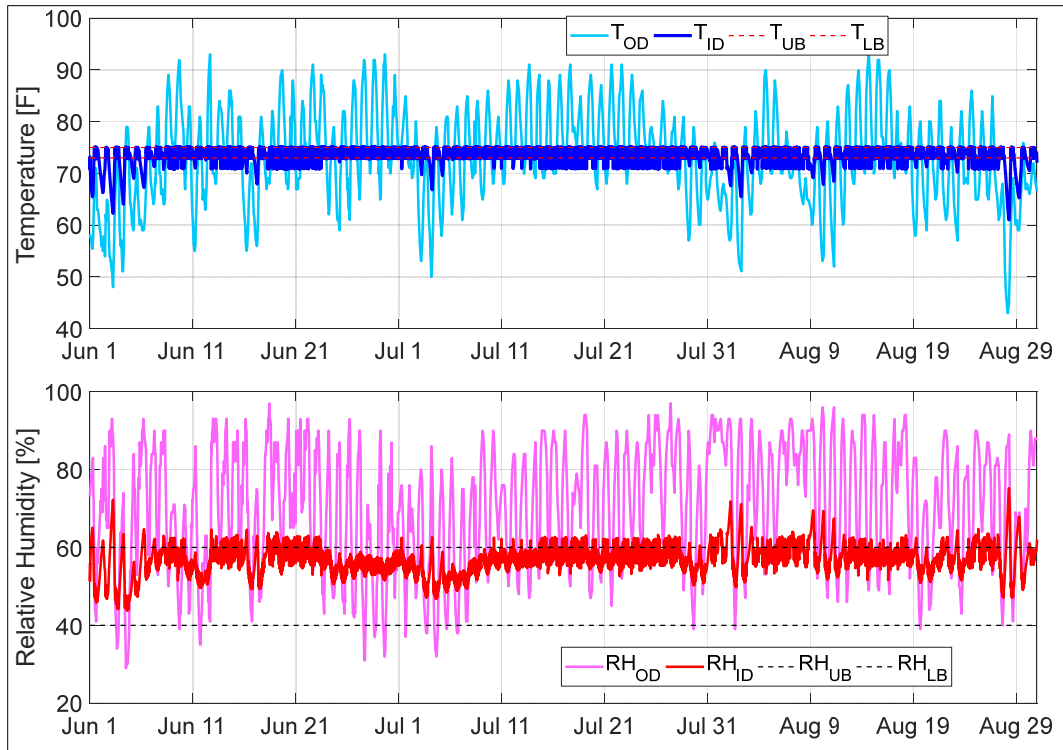


Figure 6.3. Indoor temperature and humidity response to humidistat priority control in Indianapolis.

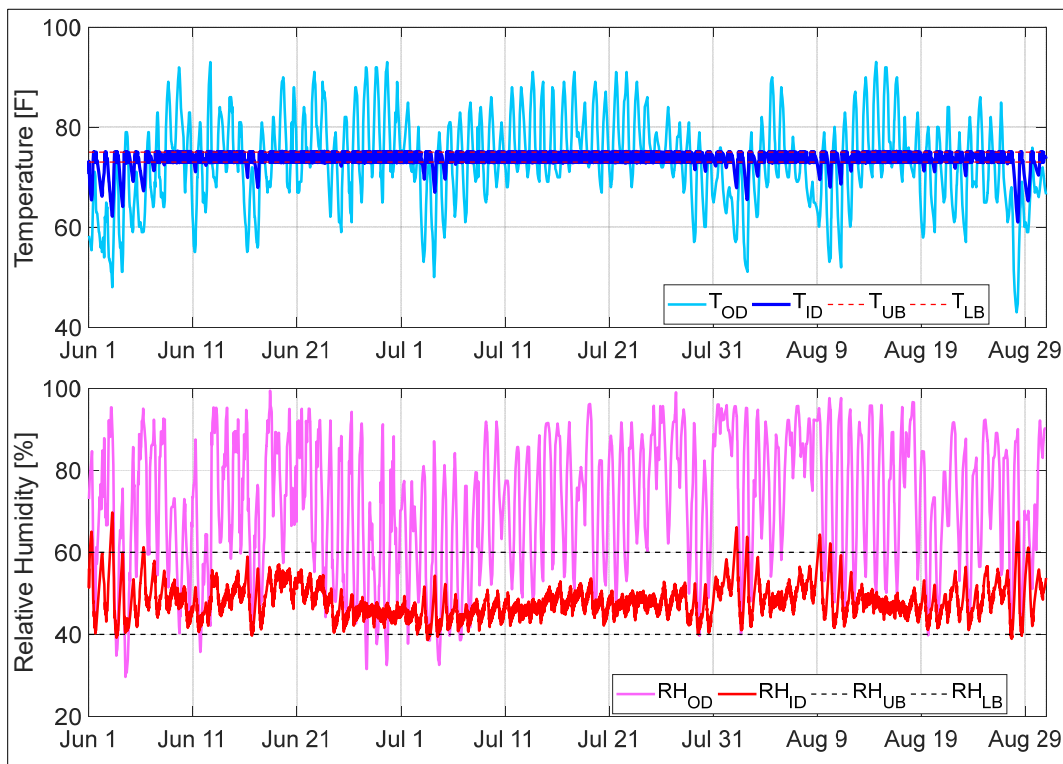


Figure 6.4. Indoor temperature and humidity response to SSLC control strategy 2 in Indianapolis.

6.2 Case Study for Cool and Dry Clime Zone — Denver

Denver is a typical city in the cold and dry climate zone, where the humidity remains very low through the whole year. In summer seasons, the outdoor environment is cool at night and hot during the day, the humidity remains low although it can occasionally be high after raining. After applying various control strategies in the co-simulation of SSLC numerical model and prototypical residential building model under Denver weather conditions, the energy performance of the SSLC system is summarized in Table 6.3.

It can be observed from Table 6.3 that the A/C unit delivered 2429.0 kWh integrated sensible capacity and 517.4 kWh integrated latent capacity but consumes 656.2 kWh energy in the baseline. The average COP of the three months in summer is 4.49. The A/C unit under two SSLC control strategies deliver higher integrated sensible capacity but lower integrated latent capacity in comparison to the situation in the baseline. The thermostat priority control and humidistat priority control deliver 2721.1kWh and 2732.1kWh integrated sensible capacity respectively, but only 165.2kWh and 171.0kWh integrated latent capacity respectively. However, under SSLC control strategy 2, the cooling system delivers an integrated latent capacity of 394 kWh, which is much higher than that resulted from SSLC control strategy 1 but is still less than that in the baseline.

Table 6.3. Energy performance under different control strategies in Denver throughout summer.

	Integrated Sensible Capacity	Integrated Latent Capacity	Energy Consumption	Average COP
	[kWh]	[kWh]	[kWh]	[-]
Baseline	2429.0	517.4	656.2	4.49
Thermostat Priority	2721.1	165.2	543.9	5.31
Humidistat Priority	2732.1	171.0	547.2	5.30
Control Strategy 2	2723.1	394.0	623.5	5.00

During the simulation, the average COPs of the unit are improved with application of SSLC control strategies. The system average COP obtained by applying SSLC control strategy 1

(thermostat priority and humidistat priority) increases 18.3% compared with that in the baseline, and the average COP of SSLC system with control strategy 2 increases 11.3%.

With regard to comfort delivery in baseline, the indoor temperature and humidity are both controlled well within the acceptable range, which is implied by results in Table 6.4 that there is no temperature or humidity comfort violation. The indoor temperature does not exceed the setpoint temperature (74°F), the maximum indoor relative humidity reaches 63.5% in baseline simulation. For SSLC control strategies 1, the indoor temperature is controlled well below 75.2°F but the maximum RH reaches 68.2% and 67.5% respectively for thermostat priority control and humidistat priority control strategies, which is beyond the humidity comfort limit for 0.48 hour and 0.42 hour, respectively. However, under SSLC control strategy 2, compared with the SSLC control strategy 1, the maximum indoor RH is only 61.7% and it meets the RH comfort throughout the simulation time.

To summarize, with the application of the SSLC control strategy 1, the A/C unit energy performance is improved but it sacrifices the thermal comfort to some extent. However, the SSLC control strategy 2 makes a good trade-off between the energy efficiency and thermal comfort.

Table 6.4. Comfort Delivery under different control strategies in Denver throughout summer.

	Max. Indoor Temp. [°F]	Max. Indoor RH [%]	Temperature Comfort Violation [hour]	Humidity Comfort Violation [hour]
Baseline	74.0	63.5	0	0
Thermostat Priority	75.2	68.2	0	0.48
Humidistat Priority	75.2	67.5	0	0.42
Control Strategy 2	75.2	61.7	0	0

Plots from Figure 6.5 to Figure 6.8 present the simulation results involving indoor temperature and relative humidity performance for the whole summer with different control strategies in Denver. In the baseline (shown in Figure 6.5), it can be seen that the indoor humidity is lower than the upper bound (60%), except in several cold and humid days. When thermostat and

humidistat priority control are applied, it can be observed in Figure 6.6 and Figure 6.7 that the unit runs in sensible only mode for large amount of time, since the indoor RH is lower than 60% and only sensible capacity is required to be delivered to the space. When the indoor RH is over 60% and there is sensible cooling requirement in space, the unit operates in low-SHR mode (deep dehumidification mode), such as in Aug 16th. However, the unit stays off when there is no sensible cooling requirement even if the indoor RH exceeds the upper bound. Compared with the baseline, the indoor RH controlled under SSLC control strategy 1 is higher, which indicates that the moisture removal is lower, and the unit under SSLC control strategy 1 gives a higher COP by running in sensible only mode.

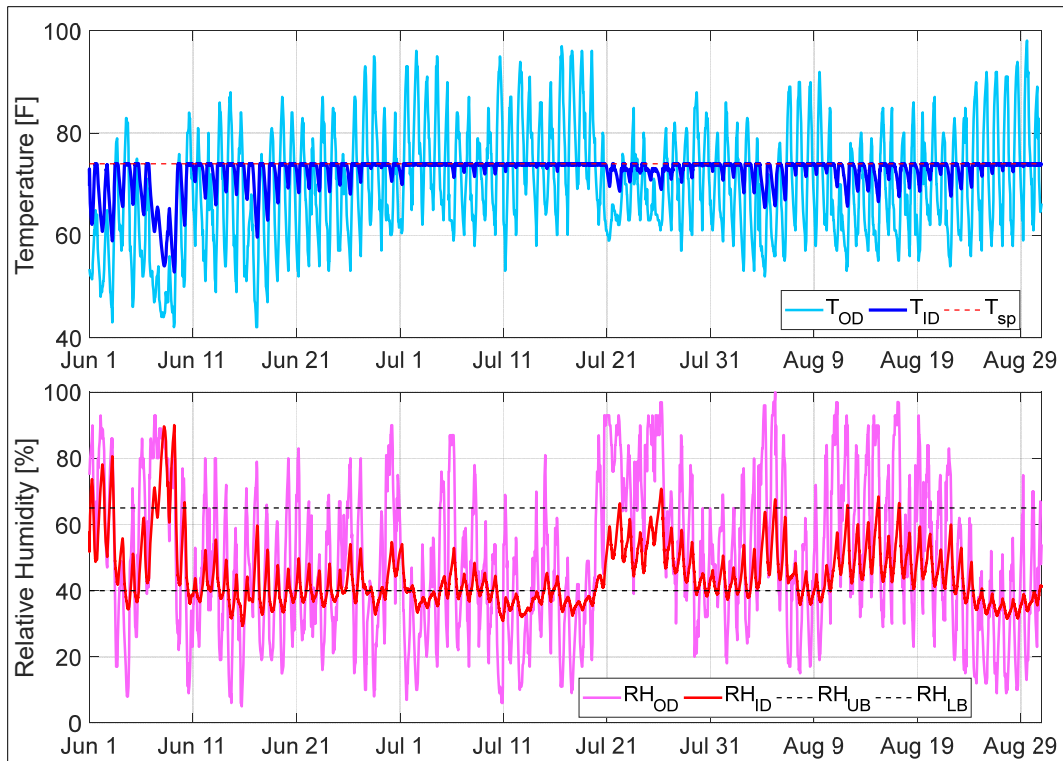


Figure 6.5. Indoor temperature and humidity simulation for baseline in Denver.

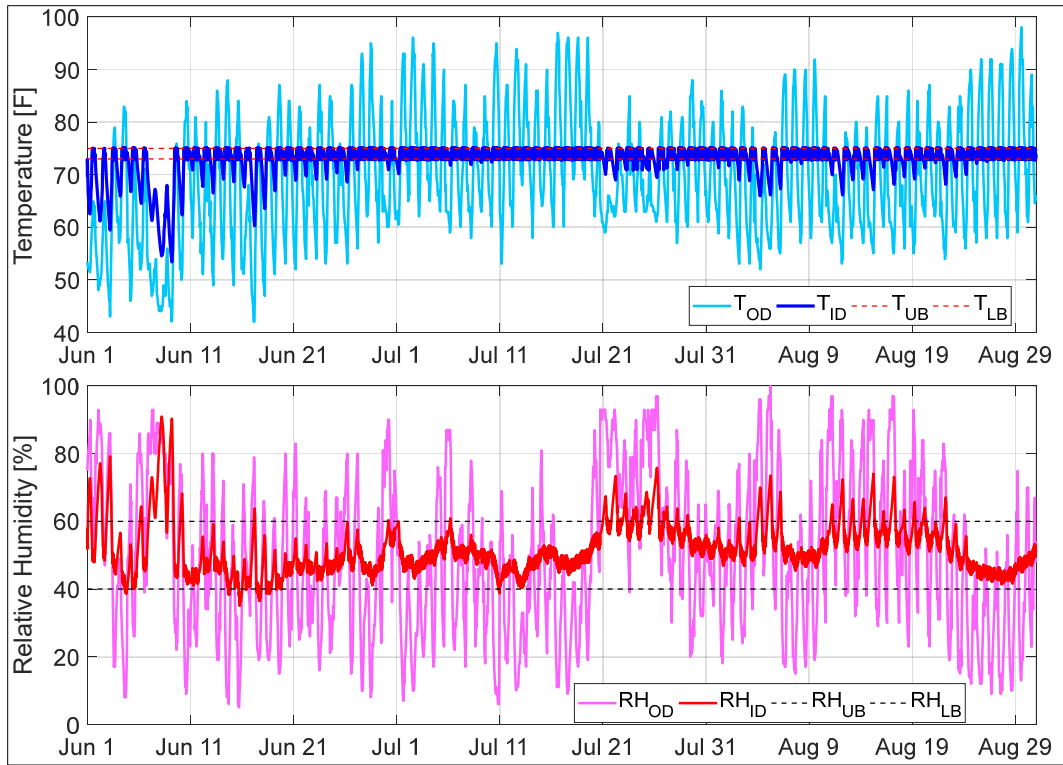


Figure 6.6. Indoor temperature and humidity response to thermostat priority control in Denver.

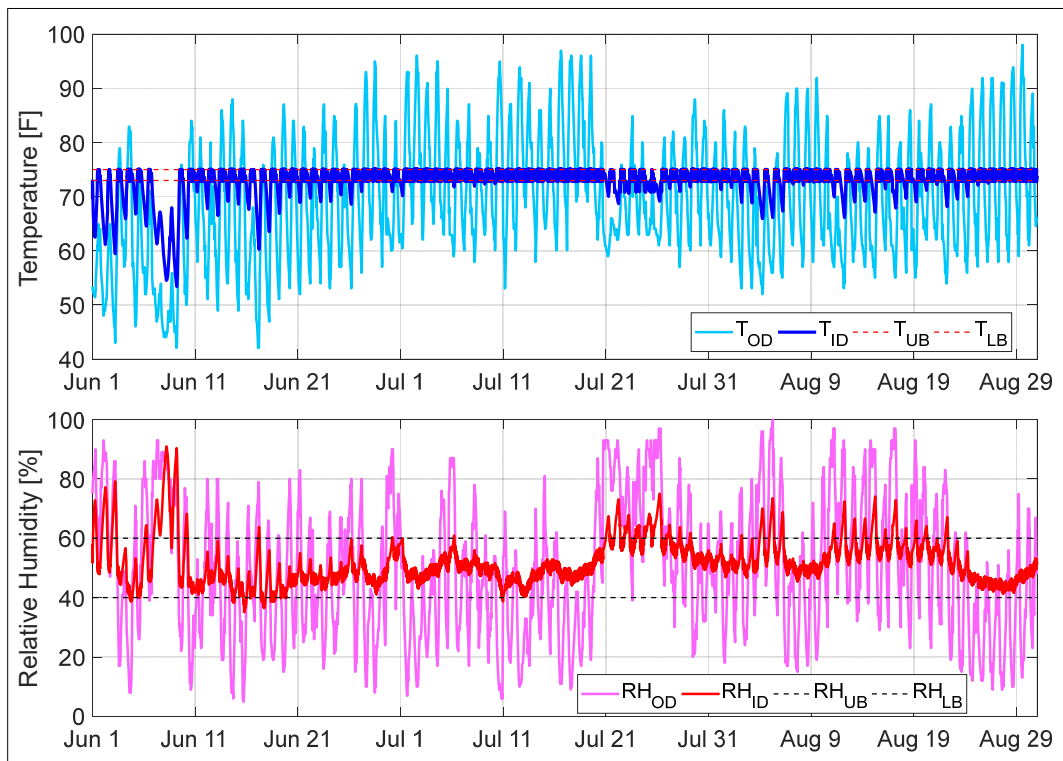


Figure 6.7. Indoor temperature and humidity response to humidistat priority control in Denver.

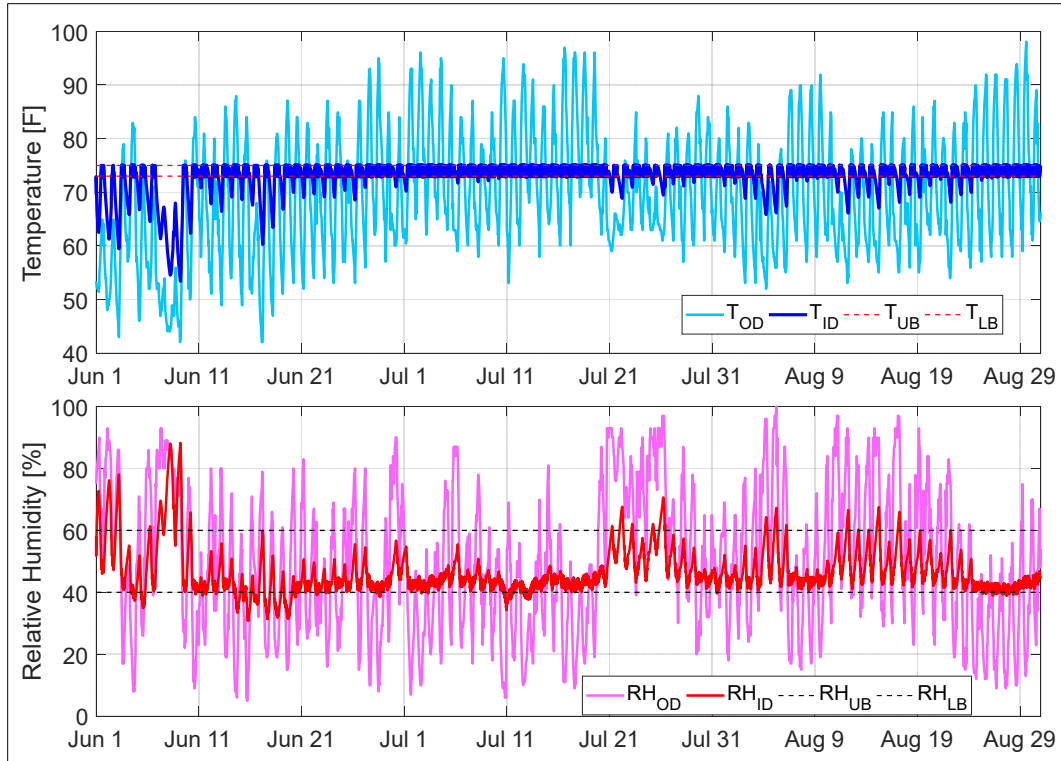


Figure 6.8. Indoor temperature and humidity response to SSLC control strategy 2 in Denver.

6.3 Case study for Hot and Humid Clime Zone — Miami

Miami is in a hot and humid zone where the weather is extremely hot and is usually accompanied by high humidity during the summer. There is a considerable amount of sensible and latent cooling load that needs to be removed. Thus, it can be seen in Table 6.5 that the integrated sensible capacity and latent capacities delivered to space throughout summer are 5100 kWh and 2220 kWh which is at the cost of 1615 kWh energy. With the application of SSLC control strategies, the delivered sensible capacity is slightly higher but the latent capacity is lower than those delivered in baseline. The energy consumption of cooling system after applying SSLC control strategy is lower than that in baseline. However, compared with the average COP in the baseline, the average COP of thermostat priority control and humidistat priority only has an improvement of 2.2% and 0.4%. With the application of control strategy 2, the average COP is improved by 7.2%, which is better than the improvement resulted from control strategy 1.

Table 6.5. Energy performance under different control strategies in Miami throughout summer.

	Integrated Sensible Capacity	Integrated Latent Capacity	Energy Consumption	Average COP
	[kWh]	[kWh]	[kWh]	[-]
Baseline	5100	2220	1615	4.53
Thermostat Priority	5256	1839	1531	4.63
Humidistat Priority	5339	1885	1587	4.55
Control Strategy 2	5159	2097	1494	4.86

Regarding to comfort delivery (shown in Table 6.6), the baseline meets both temperature and humidity comfort requirement under given weather conditions throughout the whole summer season. But in the cases where SSLC control strategies are applied, the indoor humidity exceeds the humidity comfort limit. When the A/C unit applies thermostat priority control and humidistat priority control, the maximum relative humidity in room space even reaches 66.6% and 65.5% and the time for humidity comfort violation is 0.21 hours and 0.16 hours. Thus, in hot and humid weather conditions the SSLC control strategies seems to be not as efficient as their applications in other types of weather conditions. The improvement on A/C unit performance is limited.

Table 6.6. Comfort Delivery under different control strategies in Miami throughout summer.

	Max. Indoor Temp.	Max. Indoor RH	Temperature Comfort Violation	Humidity Comfort Violation
	[°F]	[%]	[hour]	[hour]
Baseline	75.0	63.2	0	0
Thermostat Priority	75.2	66.6	0	0.21
Humidistat Priority	75.2	65.9	0	0.16
Control Strategy 2	75.2	65.4	0	0.10

To provide more details, Figures from Figure 6.9 to Figure 6.12 present the indoor temperature and humidity responses under different SSLC control strategies and under the benchmark control logic. It is seen from Figure 6.9 that the indoor temperature swings between 73°F and 74°F in the baseline, which illustrates that the latent load in space room is large so that the space is slightly overcooled by 1°F. Under thermostat priority control and humidistat priority control, it is observed that the indoor space is overcooled to 71°F and the A/C unit operates in deep dehumidification mode in nearly every on/off cycle, in which situation the COP of A/C unit stays low. However, with application of SSLC control strategy 2, the indoor relative humidity is much better controlled than that under SSLC control strategy 1. The reason is that part of the latent load is met by the A/C unit even though the A/C unit is in the sensible only mode.

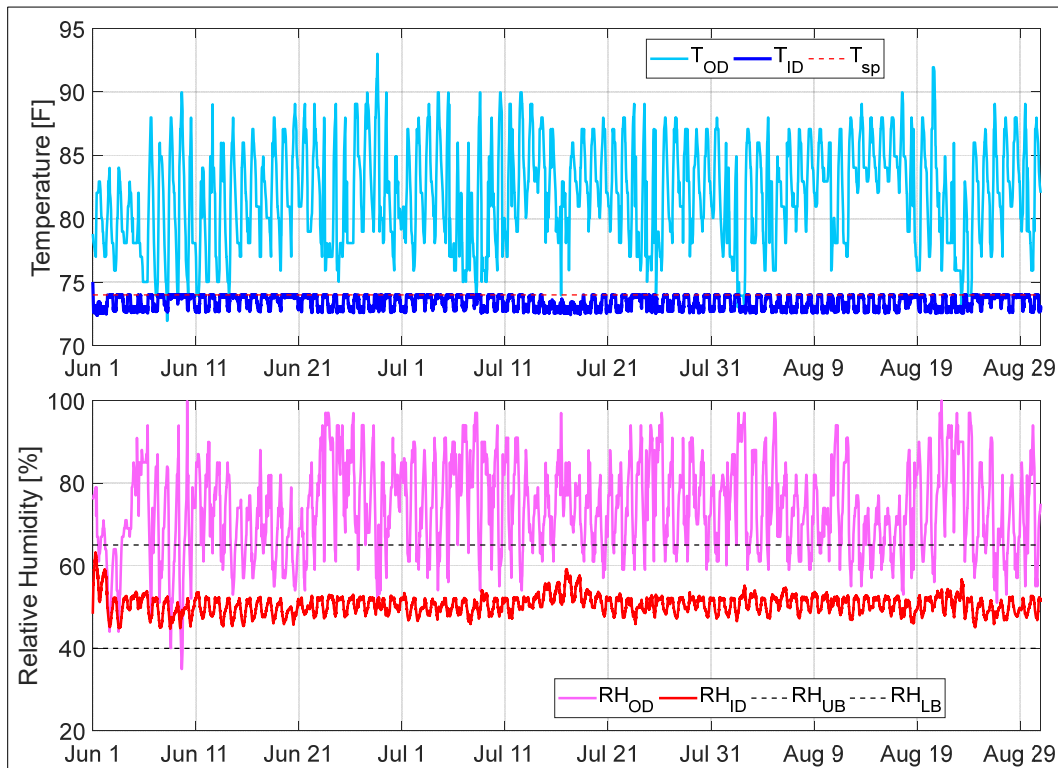


Figure 6.9. Indoor temperature and humidity simulation for baseline in Miami.

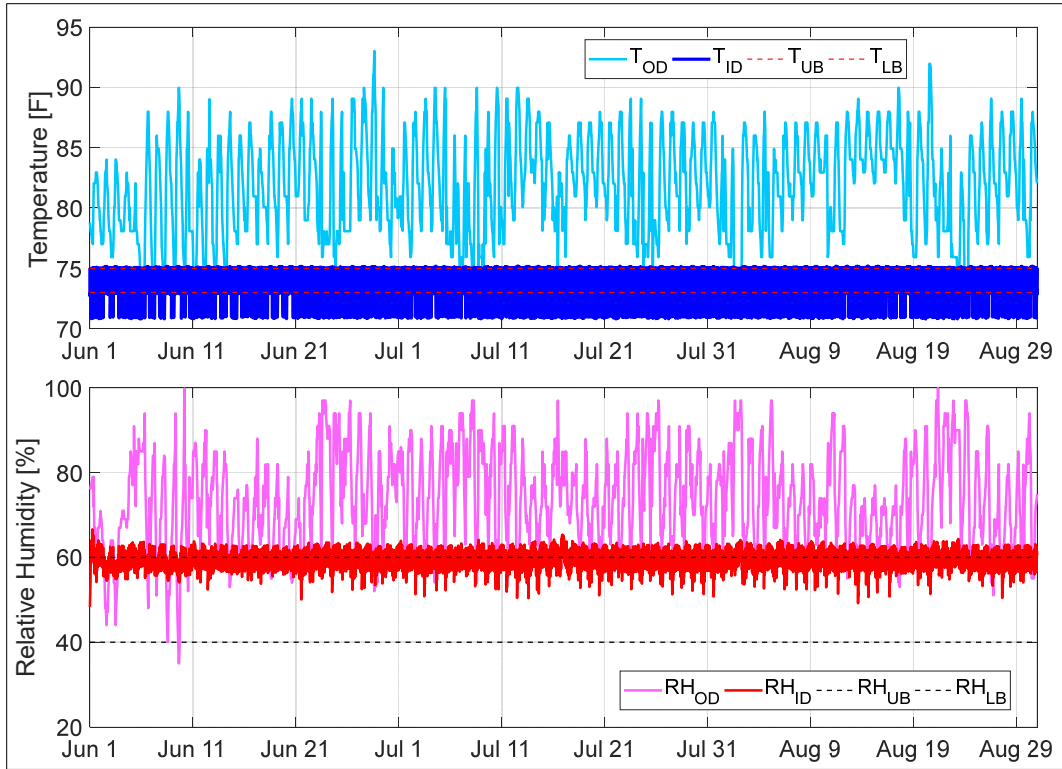


Figure 6.10. Indoor temperature and humidity response to thermostat priority control in Miami.

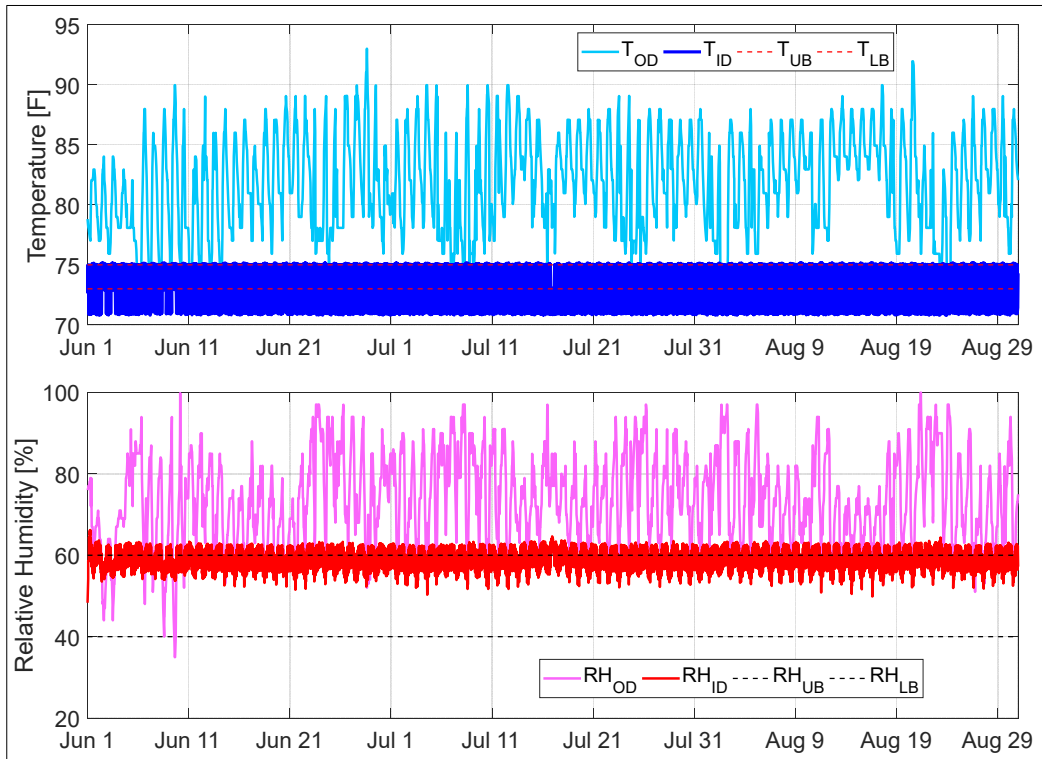


Figure 6.11. Indoor temperature and humidity response to humidistat priority control in Miami.

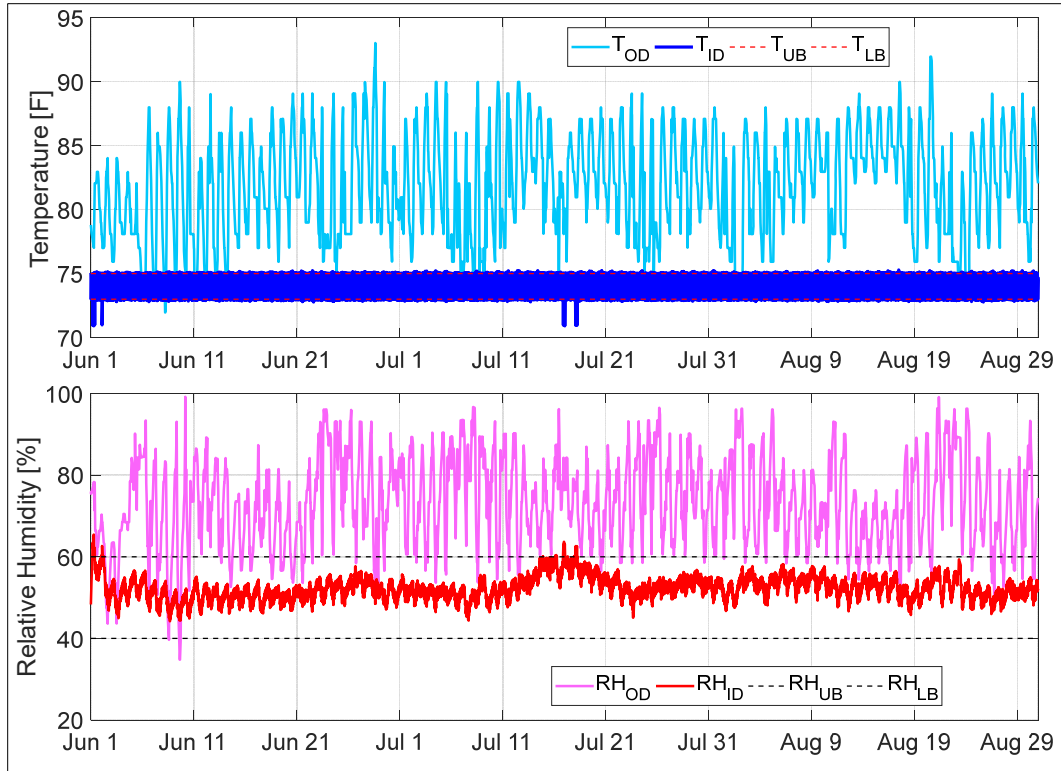


Figure 6.12. Indoor temperature and humidity response to SSLC control strategy 2 in Miami.

6.4 Case study for Hot and Dry Clime Zone — Phoenix

Phoenix has long, extremely hot summers. The sensible load of the prototype building simulated in Phoenix is significantly higher than the other cases, during certain time periods, it is even higher than the maximum deliverable sensible capacity of the A/C unit modeled in previous chapters. In order to match the A/C unit deliverable capacities with the existence of the high cooling loading in the prototype building in Phoenix, the cooling capacity and energy consumption in previous A/C unit model are scaled up by 50% (i.e., it is 50% oversized).

It is observed from Table 6.7 that in the baseline simulation, the A/C unit delivers 7931.4 kWh integrated sensible cooling capacity and 707 kWh integrated latent capacity with a consumption of 2328.3 kWh energy in those three months. The SSLC system under the mode switch control (control strategy 1) delivers higher integrated sensible capacity but lower integrated latent capacity in comparison to the baseline simulation results. The average COPs of A/C unit under SSLC control strategy 1 and SSLC control strategy 2 are 4.22 and 4.13, respectively, which are improved by 13.7% and 11.3% in comparison to the average COP simulated in the baseline. It can be observed that the average COPs of A/C unit under the two priority controls of SSLC control

strategy 1 equal each other and is close to the average COP of A/C unit under SSLC control strategy 2.

Table 6.7. Energy performance under different control strategies in Phoenix throughout summer.

	Integrated Sensible Capacity	Integrated Latent Capacity	Energy Consumption	Average COP
	[kWh]	[kWh]	[kWh]	[-]
Baseline	7931.4	707.2	2328.3	3.71
Thermostat Priority	8077.0	292.3	1982.1	4.22
Humidistat Priority	8077.8	293.2	1983.0	4.22
Control Strategy 2	8079.9	614.1	2103.9	4.13

Table 6.8. Comfort Delivery under different control strategies in Phoenix throughout summer.

	Max. Indoor Temp.	Max. Indoor RH	Temperature Comfort Violation	Humidity Comfort Violation
	[°F]	[%]	[hour]	[hour]
Baseline	74.5	52.9	0	0
Thermostat Priority	75.3	62.2	0	0
Humidistat Priority	75.3	62.2	0	0
Control Strategy 2	75.3	50.9	0	0

With regard to comfort delivery in the baseline, the indoor temperature and humidity are both controlled well within the acceptable range throughout the simulation time, which is implied by results in Table 6.8 that there is no temperature or humidity comfort violation. Since the outdoor weather is extremely dry, the maximum indoor relative humidity reaches 52.9% in baseline simulation. For SSLC control strategies 1, the maximum RH reaches 62.2% and for

thermostat priority control and humidistat priority control strategies. Under SSLC control strategy 2, compared with the SSLC control strategy 1, the maximum indoor RH is only 50.9% and it meets the RH comfort throughout the simulation time.

Plots from Figure 6.13 to Figure 6.16 present the simulation results involving indoor temperature and relative humidity performance for the whole summer in Phoenix with different control strategies. It can be seen from the baseline simulation that the indoor relative humidity is even lower than the lower bound from June 1st to July 11th since the outdoor environment is very dry. During July, the indoor humidity increases above the humidity setpoint occasionally and the dehumidification is required only in this situation. It is observed from Figure 6.14 and Figure 6.15 that the indoor temperature swings between upper and lower bounds for a majority of time and A/C unit is switched to deep dehumidification mode several times throughout summer. In Figure 6.16, the A/C unit operates in sensible only mode for the whole summer without switching to the deep dehumidification mode.

In this case, the A/C unit perform in sensible only mode with a high COP for a long time and the time duration required for dehumidification is limited as the indoor humidity fluctuates between 40% and 60%.

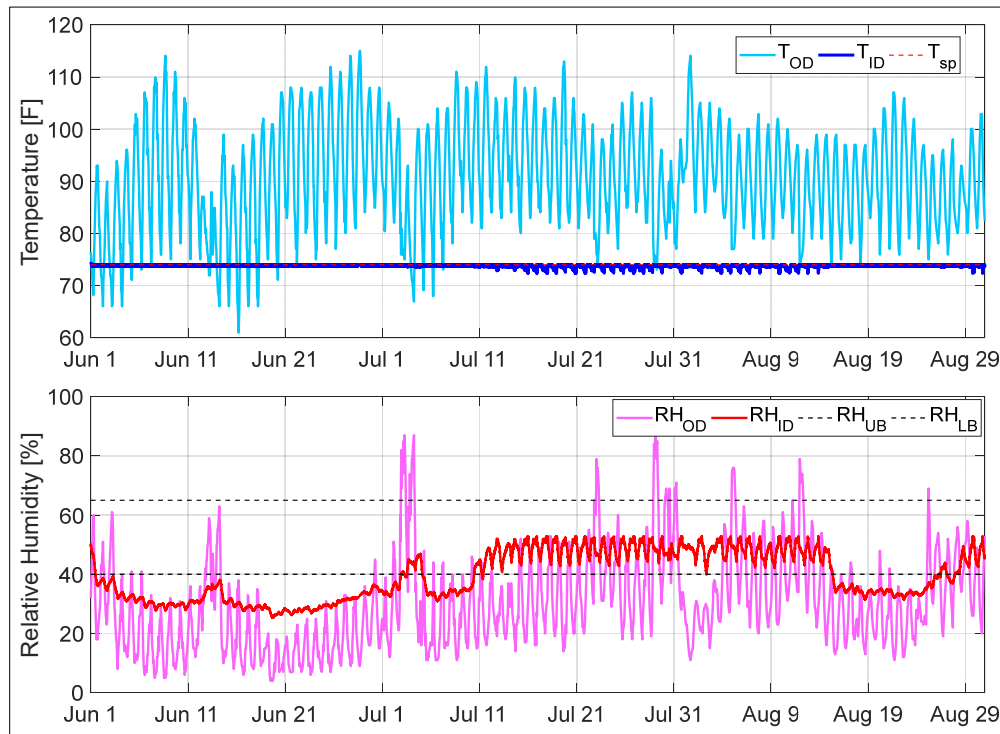


Figure 6.13. Indoor temperature and humidity simulation for baseline in Phoenix.

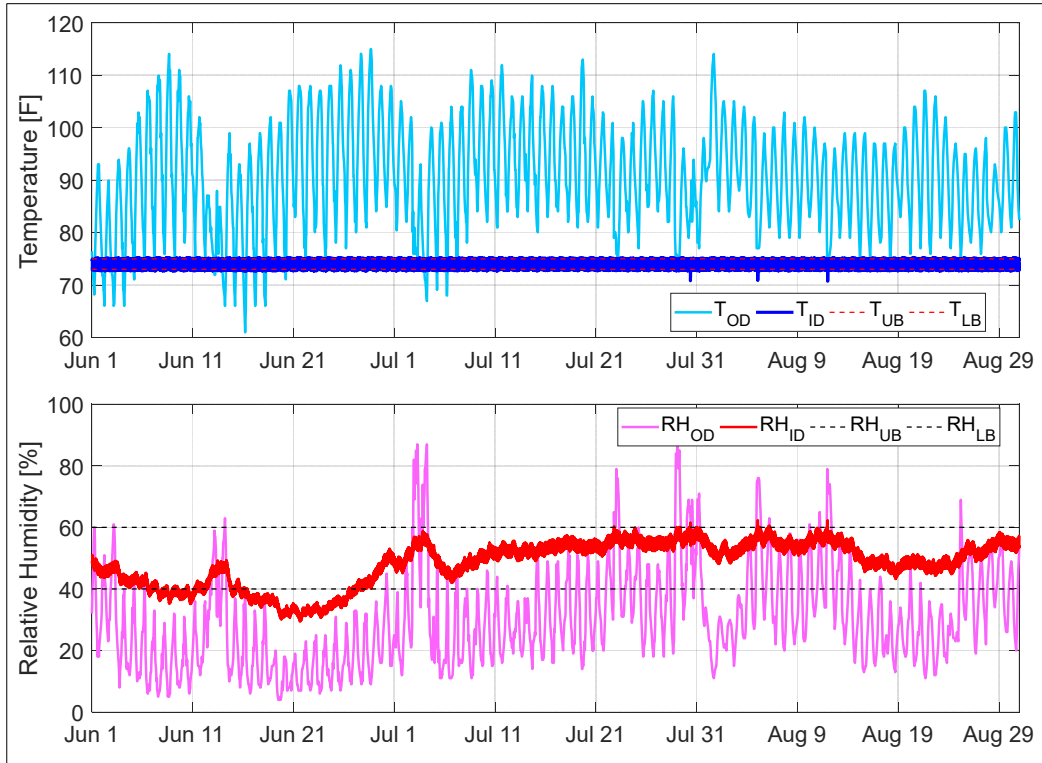


Figure 6.14. Indoor temperature and humidity response to thermostat priority control in Phoenix.

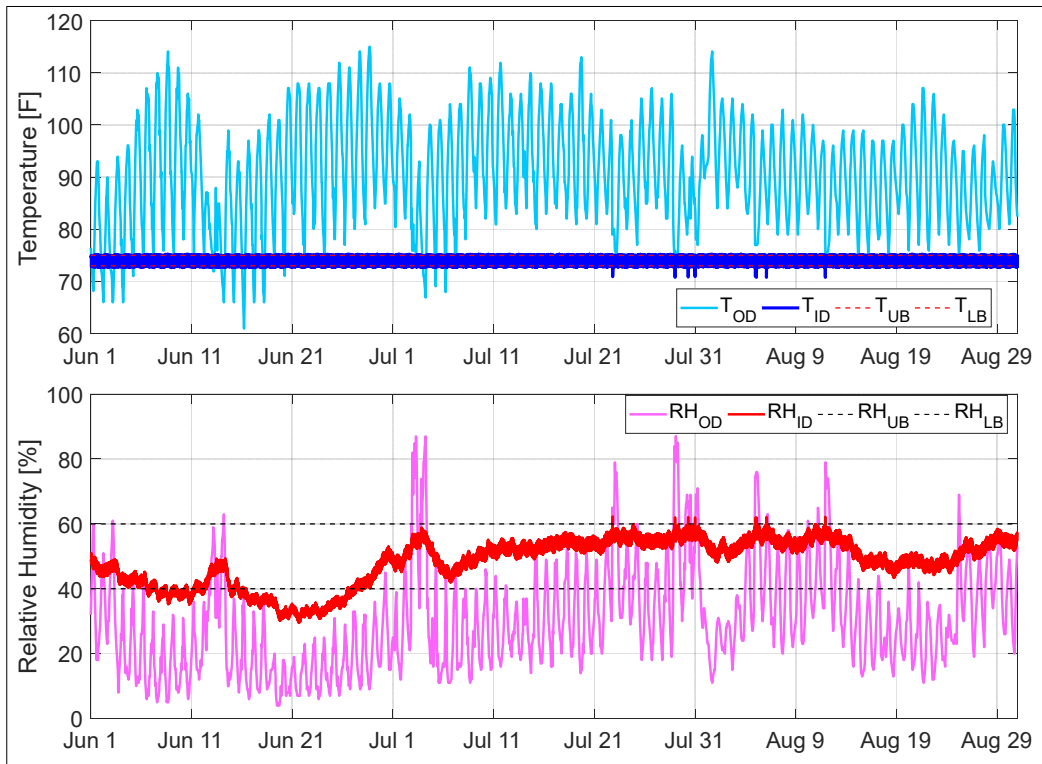


Figure 6.15. Indoor temperature and humidity response to humidistat priority control in Phoenix.

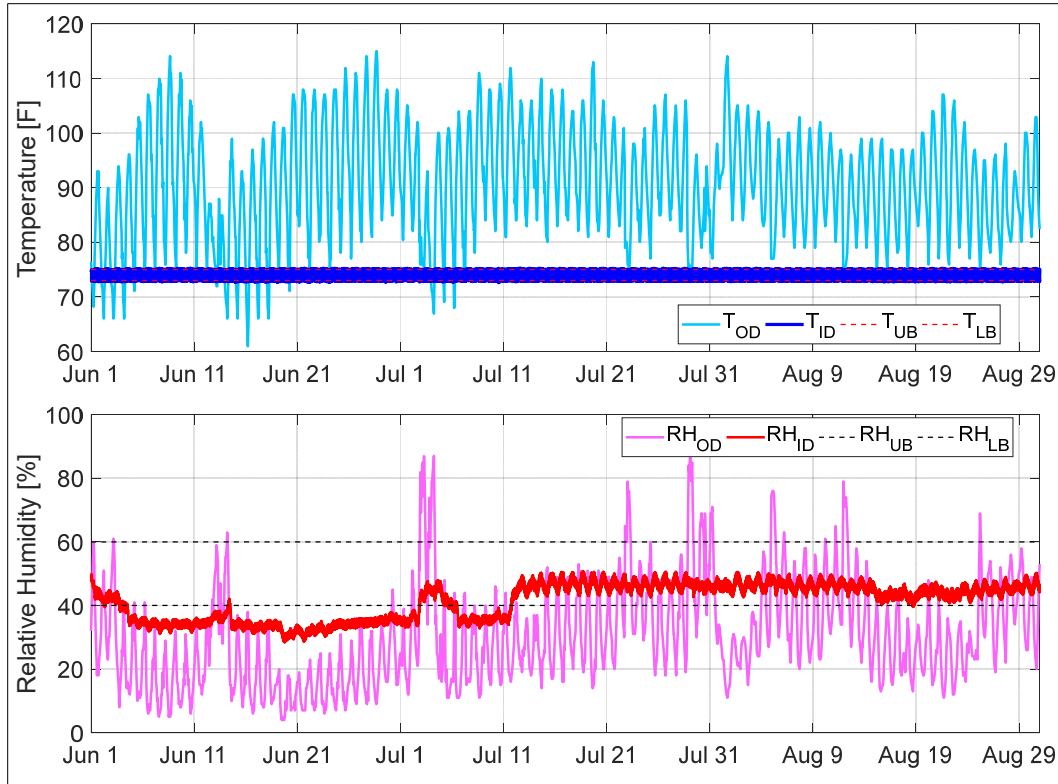


Figure 6.16. Indoor temperature and humidity response to SSLC control strategy 2 in Phoenix.

6.5 Case study for Marine Climate Zone—Seattle

Seattle has a cool climate and is classified as in the Marine climate zone, the cooling season in this climate zone is relatively short. Based on the simulation results in the baseline, which are listed in Table 6.9, the integrated sensible and latent capacities delivered by the A/C unit are 960.06kWh and 287.77kWh with costing 243.25kWh energy. And the average COP for the baseline is 5.13. However, with the application of the thermostat priority or humidistat priority control strategies, the average COP of A/C unit can be increased to 5.99, which is improved by 16.8%. And the average COP of A/C unit is 5.39 when the A/C unit is controlled by SSLC control strategy 2, which is improved by 5.07%. Furthermore, the integrated latent capacity delivered by A/C unit with SSLC control strategies is much less than that in baseline. Especially for thermostat and humidistat priority control, the delivered latent capacity is only 89.86kWh. Since the sensible and latent load in room space does not occur at the same time while the indoor humidity is lower than its upper bound when there is a cooling requirement. But the space temperature is lower than its dead bound when there is a dehumidification requirement, for this reason, the deep dehumidification mode is not triggered in both thermostat and humidistat priority control strategy

simulations. This is the reason for the energy performance with an application of thermostat priority control is the same as the with humidistat priority control.

Table 6.9. Energy performance under different control strategies in Seattle throughout summer.

	Integrated Sensible Capacity	Integrated Latent Capacity	Energy Consumption	Average COP
	[kWh]	[kWh]	[kWh]	[-]
Baseline	960.06	287.77	243.25	5.13
Thermostat Priority	1245.0	89.86	222.75	5.99
Humidistat Priority	1245.0	89.86	222.75	5.99
Control Strategy 2	1044.3	242.8	238.8	5.39

Regarding to the building comfort characteristic simulation, it can be seen from Table 6.10 that both the temperature and humidity are well controlled within the comfort limits. When under thermostat and humidistat priority control, the indoor maximum relative humidity is 59.3%, which also indicates that the deep dehumidification mode in this climate case is not triggered.

Table 6.10 Comfort Delivery under different control strategies in Seattle throughout summer.

	Max. Indoor Temp.	Max. Indoor RH	Temperature Comfort Violation	Humidity Comfort Violation
	[°F]	[%]	[hour]	[hour]
Baseline	74.0	57.5	0	0
Thermostat Priority	75.1	59.3	0	0
Humidistat Priority	75.1	59.3	0	0
Control Strategy 2	75.1	54.7	0	0

Plots from Figure 6.17 to Figure 6.20 present the simulation results involving indoor temperature and humidity performance for the whole summer with different control strategy: benchmark, thermostat priority control, humidistat priority control and SSLC control strategy 2. It can be observed from these figures that the indoor relative is much lower than the upper bound when the A/C unit is cooling down the room space. And the dehumidification requirement happens at nighttime while the indoor humidity is relatively low. To avoid overcooling in room space, the latent load in room space is not dealt with. In this case, the situation is special since the sensible and latent load removal requirement happen at different times, so the latent load in room space has to be ignored and indoor humidity is relatively high during this time.

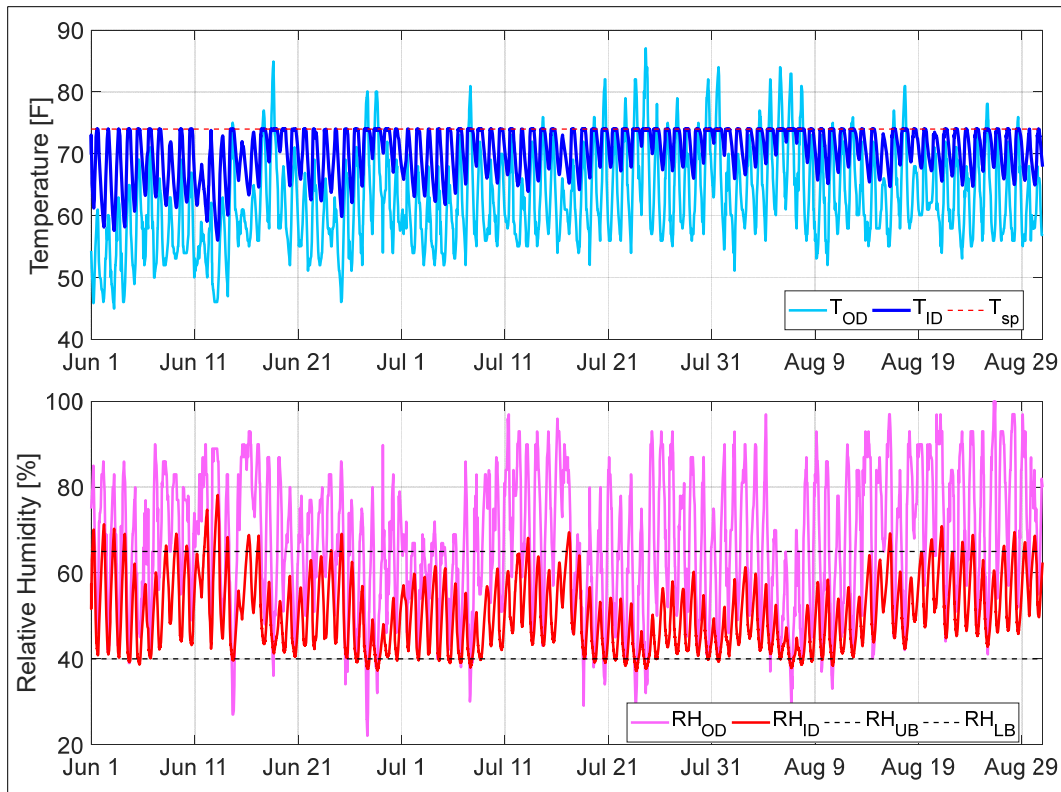


Figure 6.17. Indoor temperature and humidity simulation for baseline in Seattle.

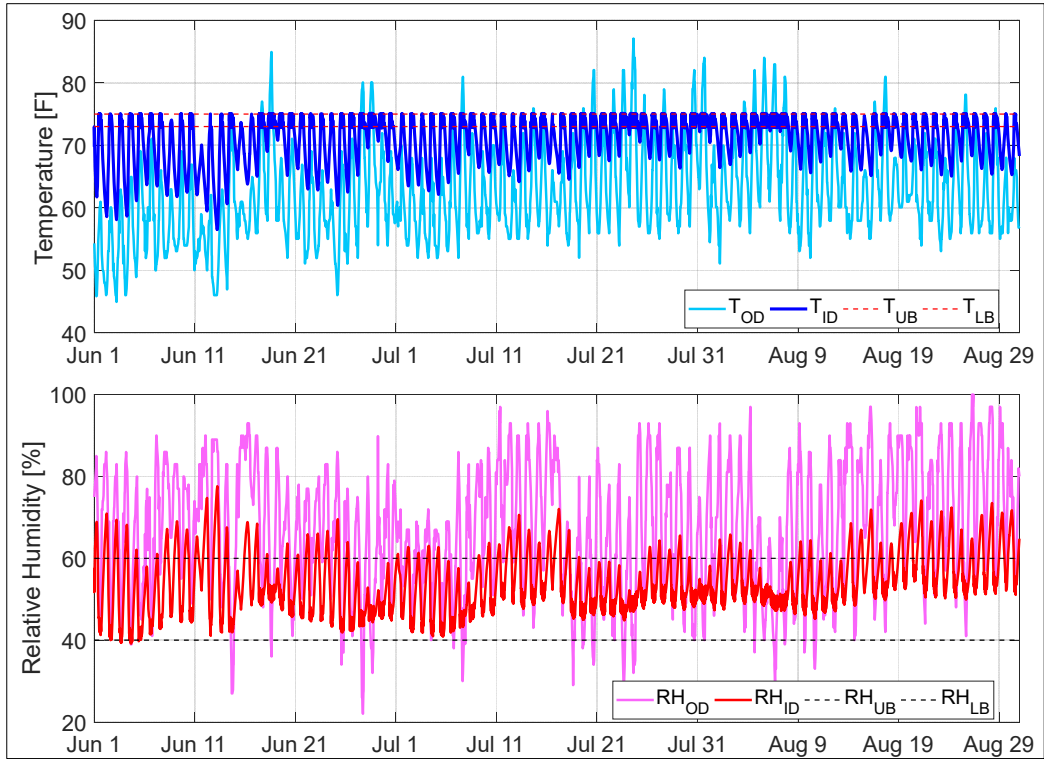


Figure 6.18. Indoor temperature and humidity response to thermostat priority control in Seattle.

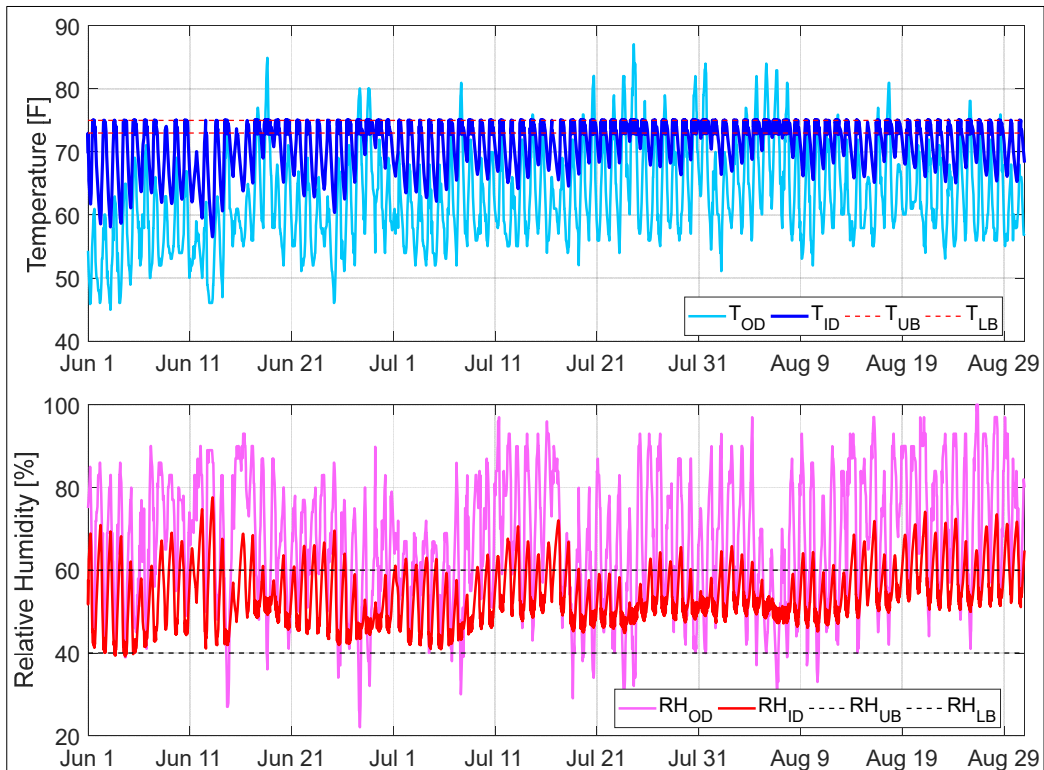


Figure 6.19. Indoor temperature and humidity response to humidistat priority control in Seattle.

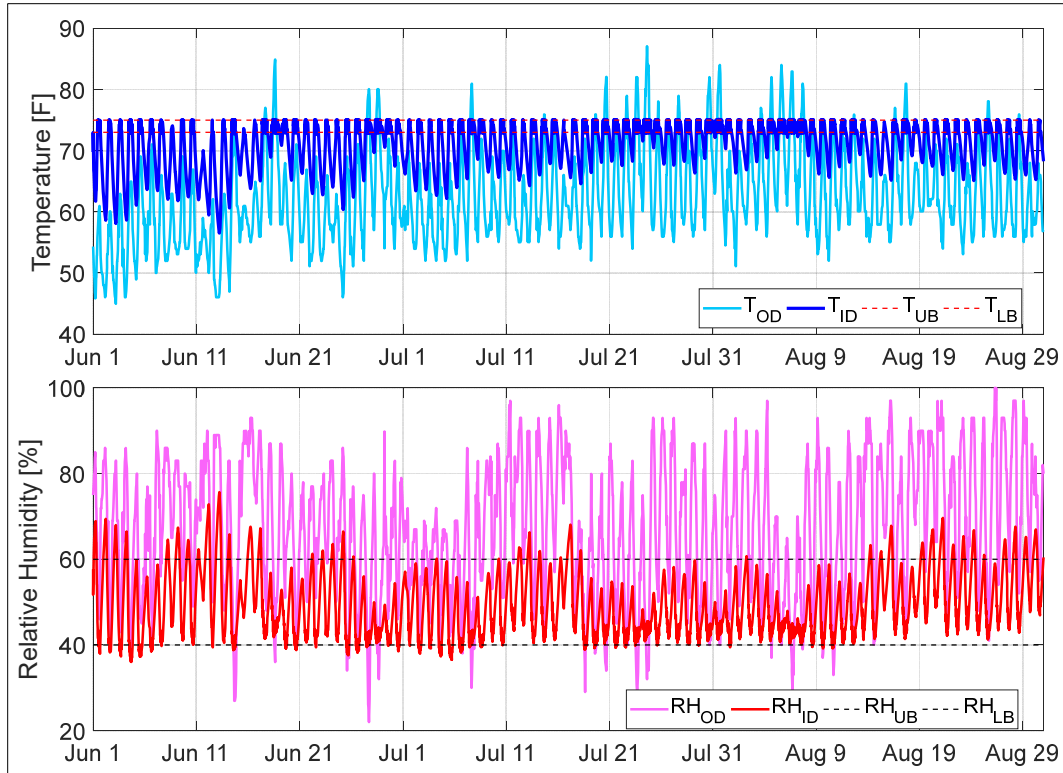


Figure 6.20. Indoor temperature and humidity response to SSLC control strategy 2 in Seattle.

6.6 Summary

In this chapter, the SSLC control strategies proposed in Chapter 5 are applied in five cities (Indianapolis, Denver, Miami, Phenix and Seattle) to investigate the SSLC system behavior in various typical climate zones. Through evaluating the A/C unit energy performance and observing building response to these SSLC control strategies the characteristics of each control strategy are demonstrated.

In general, the A/C unit energy performance is significantly improved with the application of SSLC control strategy 1, no significant energy performance difference is observed between thermostat priority control and humidistat priority control, especially in relatively dry weather conditions. For example, with the application of thermostat priority control, the average COP of the A/C unit throughout summer is improved by 18.3% in Denver and 13.7% in Phoenix. For these weather conditions, the A/C unit operates in sensible only mode for a majority of the time with high system COP, and the unit only switches to deep dehumidification mode during rainy days while latent load in space is required to be removed. But when it is applied in hot and humid weather conditions, such as Miami, the energy performance improvement is limited, since the A/C

unit must maintain a deep dehumidification model for a long time in which the unit COP is much lower. Furthermore, it shows impressive average COP improvement in Indianapolis and Seattle when the A/C unit is performed under SSLC control strategy 1. The reason is that in these climate zones, sensible and latent loads occur at different times, so that the A/C unit can operate in sensible only mode to only deliver sensible capacity at low indoor humidity for most of the time. But when the indoor humidity is high and the latent load is required to remove from space, the indoor temperature is lower than the deadband so that the A/C unit is turned off to avoid overcooling. It also shows that the energy efficiency improvement is limited with the application of control strategy 2.

The humidity in the space is not always well-controlled under SSLC control strategy 1. In other words, the energy performance improvement in SSLC control strategy 1 cases sacrifices the indoor thermal comfort to some extent. However, the SSLC control strategy 2 achieves a good tradeoff between energy efficiency and thermal comfort. Even though the unit is operating in sensible only mode, part of latent load is met through adjusting the equipment speed. For this reason, the improvement of energy performance for an A/C unit is less in comparison with SSLC control strategy 1.

Based on simulation results in five typical cities, it can be concluded that the SSLC control strategy 1 is appropriate to be applied in dry climate zones, where the energy efficiency of A/C system is significantly improved, and the indoor humidity requirement is also satisfied. In hot and humid climate zones, such as Miami, the SSLC system does not produce obvious improvement in A/C unit energy performance. And in humid and cool or marine climate zones, the SSLC control strategy 1 also can improve the A/C system efficiency but with a sacrifice of indoor thermal comfort. However, the SSLC control strategy 2 is more suitable to be applied in these kinds of climate zones to have a tradeoff between energy efficiency and indoor thermal comfort.

7. SUMMARY AND FUTURE WORK

7.1 Summary

The purpose of this research is to propose a sequential approach to achieve separate sensible and latent cooling with the application of variable speed technologies and independent speed control of both the compressor and supply fan, so that a single air conditioning system can be operated in two different modes sequentially based on properly developed SSLC control strategies to meet both sensible and latent loads which, in turn can realize energy savings without sacrificing occupant comfort.

In this research, a numerical SSLC system model is developed in Chapter 3 to predict A/C unit performance in two SSLC operation modes (the latent-load-removal mode and sensible load-removal mode). This physical-based numerical model is based on a direct expansion cooling model for its four basic components: compressor, condenser, expansion valve and evaporator. The SSLC system model constructed by building a sub-model for each individual component separately and then integrating them together as a cycle. This system model can be used to characterize the SSLC system performance, such as delivered cooling capacity, equipment SHR and power input, at various compressor and supply fan speeds, as well as different indoor and outdoor conditions.

In order to investigate the accuracy and reliability of the developed SSLC system model, steady state tests were conducted on a 4-ton split heat pump under different combinations of equipment speeds, as well as indoor and outdoor operating conditions. In Chapter 4, measurements from these experimental tests are used to validate the developed SSLC system model. In the process of validation, each component model is validated individually first and then the SSLC model is validated as an integrated system. It is also shown in Chapter 4 that the mean absolute percentage errors for three critical performance indicators, cooling capacity, SHR and COP are 3.39%, 4.55% and 4.55%, respectively, which suggests a good agreement between model prediction and measurement results. When this validated SSLC system model is applied to simulate an A/C unit performance at 95°F outdoor temperature, 75°F indoor temperature and 45% indoor relative humidity, the following phenomena can be observed: 1) the A/C unit delivers more latent capacity but less sensible capacity with a higher compressor speed and lower indoor fan speed, in contrast, the A/C unit provides more sensible capacity if the compressor runs at a lower

speed, but the evaporator fan operates at a higher speed. 2) The unit COP decreases with the increase of compressor speed; moreover, COP increases with the increase of supply fan speed at when the fan is in its low speed range, but COP begins to drop when the fan speed continues to increase beyond certain speed. The relationships among COP, SHR and cooling capacity are complicated and non-linear, which indicates that potential optimization for energy performance and efficiency can be achieved through control the SSLC system properly.

Thus, to realize the proposed SSLC methodology on a real A/C unit, two types of control strategies are proposed in this research: 1) mode switch control with constant equipment speeds in each mode; 2) load prediction control with variable equipment speeds. In the first type of SSLC control strategy, the equipment speeds are pre-determined and maintains constant in each A/C unit on/off cycle. But in the second proposed SSLC control strategy, the equipment speeds are continuously adjusted to match the delivered sensible cooling capacity with building sensible cooling load.

To evaluate the A/C unit performance with the implementation of the proposed sequential SSLC methodology and the building temperature and humidity response to different SSLC control strategies, a prototype residential building model for space thermal performance is developed and simulated in TRNSYS with given weather conditions in Chapter 3. In the TRNSYS simulation, heat gain/loss from building envelop, infiltration and internal heat gain are considered, similarly, moisture flux due to infiltration and internal gains are considered.

However, in the process of co-simulation between A/C unit and prototype building, it is found that both SSLC numerical model and TRNSYS building model are computationally so cumbersome that the whole co-simulation programming is too time consuming and suffers from insufficient numerical robustness. Thus, both prototype building model and SSLC numerical model are simplified before it is applied in the co-simulation. For the prototype building model, it is simplified to two steady state networks: a thermal network and a moisture network. The simplified thermal network and moisture network models are validated by the simulation results from TRNSYS in four cities, respectively. For the SSLC numerical mode, it is simplified to an artificial neural network model, which is trained and validated by 1505 simulation data points from the physical-based SSLC system model. It is shown in Chapter 4 that the ANN model performs well in predicting the A/C unit performance, in which the R-squares values for three output variables, i.e., total cooling capacity, SHR and power input, are 99.9%, 99.7%, and 100%, respectively.

Furthermore, the re-evaporation issue is also considered in the situation where, when the A/C unit is transiting from deep dehumidification mode to sensible only mode, the evaporator coil surface temperature increases and the moisture on coil surface evaporates back to air stream.

Finally, energy performance and comfort delivery performance of an A/C unit with the application of the proposed SSLC approach is simulated under different SSLC control strategies. Simulations are conducted using five cities representing various typical weather characteristics: Indianapolis, Denver, Miami, Phoenix and Seattle throughout three months of the summer season. To characterize the performance of each SSLC control strategy and evaluate the corresponding energy saving potential, a baseline control strategy is proposed in this work which realizes both temperature and humidity control in a room space. Such a baseline control is proposed because control logics currently implemented in industry and in commercialized A/C products only consider the temperature as the target variable and ignores the humidity in room space, it is not a reasonable comparison if the performance of these widely used control strategies is compared with the performance of SSLC control strategies where both temperature and humidity conditions are to be controlled. The baseline control strategy proposed in this work is an ideal situation that is not applied for practical applications, since it assumes that both temperature and humidity are perfectly controlled at every time step. Through comparing energy performance and comfort delivery of A/C unit with SSLC approach with those when applying the benchmark control strategy, it is concluded in Chapter 6 that the SSLC is suitable in a relatively dry climate, such as Denver and Phoenix, since the A/C unit could operate at sensible only mode with high COP for a majority of the cooling time and only switches to the deep dehumidification during the rainy days where the indoor humidity exceeds the thermal comfort limit occasionally. But for a hot and humid climate such as Miami, the A/C unit operates at deep dehumidification mode for a majority of the cooling time with low COP, in which situation the energy efficiency improvement is limited. In humid and cool or marine climate zones, the SSLC control strategy 1 also can improve the A/C system efficiency but with a sacrifice of indoor thermal comfort. However, the SSLC control strategy 2 is more suitable to be applied in these kinds of climate zones to have a tradeoff between energy efficiency and indoor thermal comfort.

As a summary, the following research objectives are achieved in this work:

- a) A numerical SSLC system model was proposed to characterize SSLC system performance in the two operation modes.

- b) The physics-based SSLC system model was experimentally validated and shown to be accurate for simulations of system performance and energy efficiency .
- c) The variable-speed A/C unit performance map was described by an ANN model, which is a necessary simplification of the physical based models to allow the co-simulation of equipment-building interactions.
- d) Two appropriate control strategies for sequential SSLC systems were developed, whose performance were compared with that with the proposed baseline control strategy.
- e) The performance and energy efficiency of an SSLC A/C unit and the associated building response are evaluated in various climate zones under different SSLC control strategies.

7.2 Future Work

Based on the methodologies and the results presented in this document, some suggestions of possible future works are discussed here which can further improve the results or extend the application of the proposed SSLC methodology. The first problem requiring further investigation is the re-evaporation occurring while the A/C unit switches from deep dehumidification mode to sensible only mode. The current re-evaporation model was validated in an experiment where the dew-point monitor used for humidity measurement cannot respond fast enough to capture the humidity change in the evaporator air-flowing streams so that the dynamic process of re-evaporation was not accurately included in the testing data. Another reason is that the sensible only mode or the deep dehumidification mode cannot be realized on the tested heat pump since the equipment speeds are controlled by its embedded control logic and cannot be changed independently. Thus, it is suggested that the re-evaporation model can be validated in the future with measurements focusing on this dynamic process. Also, the influence of re-evaporation on SSLC system performance can be further investigated.

The proposed SSLC methodology with its control strategies can be applied on an actual heat pump that the compressor and evaporator fan can be controlled independently to realize two typical SSLC modes so that the unit performance characteristics can be more clearly observed. Experimental tests can be conducted to analyze the implementation potential of SSLC control strategies in addition to the simulation studies presented in this document. For example, load-

based testing approach or field testing can be applied in the future to test and evaluate the performance of the SSLC control strategies when they are implemented in an actual heat pump.

Currently, all the work in this research is based on residential air conditioner system applications. In the future, the potential of applying SSLC technologies in commercial buildings could be discussed and investigated.

REFERENCES

- AHRI. (2015). NATIONAL STANDARD CAN / ANSI / AHRI 540-2015 , Performance Rating of Positive Displacement Refrigerant Compressors and Compressor Units.
- Bahman, A. M., Ziviani, D., & Groll, E. A. (2018). Vapor injected compression with economizing in packaged air conditioning systems for high temperature climate. *International Journal of Refrigeration*, 94, 136–150. <https://doi.org/10.1016/j.ijrefrig.2018.07.024>
- Bell, I. (2012). Welcome to ACHP's documentation! — ACHP 1.4 documentation. <http://achp.sourceforge.net/>
- Bell, I.H., Wronski, J., Quoilin, S., Lemort, V., 2014. Pure and pseudo-pure fluid thermophysical property evaluation and the open-source thermophysical property library coolprop. *Ind. Eng. Chem. Res.* 53,
- Bell, I. H., Ziviani, D., Lemort, V., Bradshaw, C. R., Mathison, M., Horton, W. T., Braun, J. E., & Groll, E. A. (2020). PDSim: A general quasi-steady modeling approach for positive displacement compressors and expanders. *International Journal of Refrigeration*, 110, 310–322. <https://doi.org/10.1016/j.ijrefrig.2019.09.002>
- Braun, J. E., & Chaturvedi, N. (2002). An inverse gray-box model for transient building load prediction. *HVAC and R Research*, 8(1), 73–99. <https://doi.org/10.1080/10789669.2002.10391290>
- Burns, P. R., Mitchell, J. W., & Beckman, W. A. (1985). Hybrid desiccant cooling systems in supermarket applications. *ASHRAE transactions*, 91(1), 457-468.
- Byrd, R. H., Schnabel, R. B., & Shultz, G. A. (1988). Approximate solution of the trust region problem by minimization over two-dimensional subspaces. *Mathematical Programming*, 40(1–3), 247–263. <https://doi.org/10.1007/BF01580735>
- Cai, J., & Braun, J. (2016). An inverse hygrothermal model for multi-zone buildings. *Journal of Building Performance Simulation*, 9(5), 510–528. <https://doi.org/10.1080/19401493.2015.1108999>

- Cai, J., & Braun, J. E. (2015). A generalized control heuristic and simplified model predictive control strategy for direct-expansion air-conditioning systems. *Science and Technology for the Built Environment*, 21(6), 773–788. <https://doi.org/10.1080/23744731.2015.1040327>
- Chen, T., Yin, Y., & Zhang, X. (2016). Applicability and energy efficiency of temperature and humidity independent control systems based on dual cooling sources. *Energy & Buildings*, 121, 22–31. <https://doi.org/10.1016/j.enbuild.2016.04.001>
- Cheung, H., & Wang, S. (2018). A comparison of the effect of empirical and physical modeling approaches to extrapolation capability of compressor models by uncertainty analysis: A case study with common semi-empirical compressor mass flow rate models. *International Journal of Refrigeration*, 86, 331–343. <https://doi.org/10.1016/j.ijrefrig.2017.11.020>
- Churchill, S. W. (1977). Friction-Factor Equation Spans All Fluid-Flow Regimes. *Chemical Engineering (New York)*, 84(24), 91–92.
- Coleman, T. F., & Li, Y. (1996). An interior trust region approach for nonlinear minimization subject to bounds. *SIAM Journal on Optimization*, 6(2), 418–445. <https://doi.org/10.1137/0806023>
- Dabiri, A. E., & Rice, C. K. (1981). Compressor-simulation model with corrections for the level of suction gas superheat. February 2017.
- Dai, Y. J., Wang, R. Z., Zhang, H. F., & Yu, J. D. (2001). Use of liquid desiccant cooling to improve the performance of vapor compression air conditioning. *Applied Thermal Engineering*, 21(12), 1185–1202. [https://doi.org/10.1016/S1359-4311\(01\)00002-3](https://doi.org/10.1016/S1359-4311(01)00002-3)
- Dhar, P. L., & Singh, S. K. (2001). Studies on solid desiccant based hybrid air-conditioning systems. *Applied Thermal Engineering*, 21(2), 119–134. [https://doi.org/10.1016/S1359-4311\(00\)00035-1](https://doi.org/10.1016/S1359-4311(00)00035-1)
- Fischer, S. K., & Rice, C. K. (1981). a Steady-State Computer Design Model for Air-To-Air Heat Pumps. Department of Energy, August 1983. <https://doi.org/10.2172/814817>
- Gholamrezaei, M., & Ghorbanian, K. (2010). Compressor map generation using a feed-forward neural network and rig data. *Proceedings of the Institution of Mechanical Engineers, Part A: Journal of Power and Energy*, 224(1), 97–108. <https://doi.org/10.1243/09576509JPE792>

- Gray, D. L., & Webb, R. L. (1986). Heat Transfer and Friction Correlations for Plate Finned-Tube Heat Exchangers Having Plain Fins. *Heat Transfer, Proceedings of the International Heat Transfer Conference*, 6, 2745–2750. <https://doi.org/10.1615/ihtc8.1200>
- Gungor, K. E., & Winterton, R. H. S. (1986). A general correlation for flow boiling in tubes and annuli. *International Journal of Heat and Mass Transfer*, 29(3), 351–358. [https://doi.org/10.1016/0017-9310\(86\)90205-X](https://doi.org/10.1016/0017-9310(86)90205-X)
- Guo, Y., Li, G., Chen, H., Hu, Y., Shen, L., Li, H., Hu, M., & Li, J. (2017). Développement d'un capteur de puissance de compresseur virtuel à vitesse variable pour un système de conditionnement d'air à débit de frigorigène variable. *International Journal of Refrigeration*, 74, 71–83. <https://doi.org/10.1016/j.ijrefrig.2016.09.025>
- Han, X., & Zhang, X. (2011). Experimental study on a residential temperature-humidity separate control air-conditioner. *Energy and Buildings*, 43(12), 3584–3591. <https://doi.org/10.1016/j.enbuild.2011.09.029>
- Henderson, H. I., & Rengarajan, K. (1996). A model to predict the latent capacity of air conditioners and heat pumps at part-load conditions with constant fan operation (No. CONF-960254-). American Society of Heating, Refrigerating and Air-Conditioning Engineers, Inc., Atlanta, GA (United States).
- Huang, J., & Gu, L. (2002). Prototype Residential Buildings to Represent the US Housing Stock. Draft LBNL Report. Berkeley, CA: Lawrence Berkeley National Laboratory.
- Jahnig, D. I., Reindl, D. T., & Klein, S. A. (2000). Semi-empirical method for representing domestic refrigerator/freezer compressor calorimeter test data. *ASHRAE Transactions*, 106(January).
- Jia, C. X., Dai, Y. J., Wu, J. Y., & Wang, R. Z. (2007). Use of compound desiccant to develop high performance desiccant cooling system. *International Journal of Refrigeration*, 30(2), 345–353. <https://doi.org/10.1016/j.ijrefrig.2006.04.001>
- Jiang, Y., Ge, T., & Wang, R. (2013). Performance simulation of a joint solid desiccant heat pump and variable refrigerant flow air conditioning system in EnergyPlus. *Energy and Buildings*, 65, 220–230. <https://doi.org/10.1016/j.enbuild.2013.06.005>

- Katejanekarn, T., & Kumar, S. (2008). Performance of a solar-regenerated liquid desiccant ventilation pre-conditioning system. *Energy and Buildings*, 40(7), 1252–1267. <https://doi.org/10.1016/j.enbuild.2007.11.005>
- Khalid, O., Ali, M., Sheikh, N. A., Ali, H. M., & Shehryar, M. (2016). Experimental analysis of an improved Maisotsenko cycle design under low velocity conditions. *Applied Thermal Engineering*, 95, 288–295. <https://doi.org/10.1016/j.applthermaleng.2015.11.030>
- Klein, S. A., Beckman, W. A., Mitchell, J. W., Duffie, J. A., Duffie, N. A., Freeman, T. L., ... & Kummert, M. (2004). TRNSYS 16–A TRaNsient system simulation program, user manual. Solar Energy Laboratory. Madison: University of Wisconsin-Madison.
- Kneifel, J. (2012). Prototype Residential Building Designs for Energy and Sustainability Assessment. Report NIST Technical Note 1765, National Institute of Standards and Technology, US Department of Commerce, 1–62. <http://dx.doi.org/10.6028/NIST.TN.1765>
- Kramer, R., van Schijndel, J., & Schellen, H. (2013). Inverse modeling of simplified hygrothermal building models to predict and characterize indoor climates. *Building and Environment*, 68, 87–99. <https://doi.org/10.1016/j.buildenv.2013.06.001>
- Krakow, K I, Lin, S, & Zeng, Z S. Analytical determination of PID coefficients for temperature and humidity control during cooling and dehumidifying by compressor and evaporator fan speed variation. United States.
- Kummert, M. (2007). Trnsys 16. Program, 5, 1–11.
- Li, N., Xia, L., Shiming, D., Xu, X., & Chan, M. Y. (2012). Dynamic modeling and control of a direct expansion air conditioning system using artificial neural network. *Applied Energy*, 91(1), 290–300. <https://doi.org/10.1016/j.apenergy.2011.09.037>
- Li, W. (2013a). Simplified steady-state modeling for variable speed compressor. *Applied Thermal Engineering*, 50(1), 318–326. <https://doi.org/10.1016/j.applthermaleng.2012.08.041>
- Li, W. (2013b). Simplified steady-state modeling for variable speed compressor. *Applied Thermal Engineering*, 50(1), 318–326. <https://doi.org/10.1016/j.applthermaleng.2012.08.041>

- Li, Z., & Deng, S. (2007a). A DDC-based capacity controller of a direct expansion (DX) air conditioning (A/C) unit for simultaneous indoor air temperature and humidity control - Part I: Control algorithms and preliminary controllability tests. *International Journal of Refrigeration*, 30(1), 113–123. <https://doi.org/10.1016/j.ijrefrig.2006.06.007>
- Li, Z., & Deng, S. (2007b). An experimental study on the inherent operational characteristics of a direct expansion (DX) air conditioning (A/C) unit. *Building and Environment*, 42(1), 1–10. <https://doi.org/10.1016/j.buildenv.2005.08.021>
- Ling, J., Hwang, Y., & Radermacher, R. (2010). Theoretical study on separate sensible and latent cooling air-conditioning system. *International Journal of Refrigeration*, 33(3), 510–520. <https://doi.org/10.1016/j.ijrefrig.2009.11.011>
- Ling, J., Kuwabara, O., Hwang, Y., & Radermacher, R. (2011). Experimental evaluation and performance enhancement prediction of desiccant assisted separate sensible and latent cooling air-conditioning system. *International Journal of Refrigeration*, 34(4), 946–957. <https://doi.org/10.1016/j.ijrefrig.2010.12.008>
- Ling, J., Kuwabara, O., Hwang, Y., & Radermacher, R. (2013). Enhancement options for separate sensible and latent cooling air-conditioning systems. *International Journal of Refrigeration*, 36(1), 45–57. <https://doi.org/10.1016/j.ijrefrig.2012.09.003>
- McQuiston, F. C., & FC, M. (1975). Fin efficiency with combined heat and mass transfer.
- Moffat, R. J. (1988). Describing the uncertainties in experimental results. *Experimental Thermal and Fluid Science*, 1(1), 3–17. [https://doi.org/10.1016/0894-1777\(88\)90043-X](https://doi.org/10.1016/0894-1777(88)90043-X)
- Mohanraj, M., Jayaraj, S., & Muraleedharan, C. (2012). Applications of artificial neural networks for refrigeration, air-conditioning and heat pump systems - A review. *Renewable and Sustainable Energy Reviews*, 16(2), 1340–1358. <https://doi.org/10.1016/j.rser.2011.10.015>
- NIST, Simulation models for finned-tube heat exchangers—EVAP-COND, National Institute of Standards and Technology, Gaithersburg, MD, 2003
- Piotr, A. (1989). SIMULATION MODEL ACCOUNTING FOR REFRIGERANT AND ONE ka. August.

- Qi, Q., & Deng, S. (2009). Multivariable control of indoor air temperature and humidity in a direct expansion (DX) air conditioning (A / C) system. *Building and Environment*, 44(8), 1659–1667. <https://doi.org/10.1016/j.buildenv.2008.11.001>
- Schmidt, T. E. (1945). La production calorifique des surfaces munies d'ailettes. *Annexe Du bulletin De L'Institut International Du Froid*, Annexe G-5.
- Seem, J. E., Klein, S. A., Beckman, W. A., & Mitchell, J. W. (1989). Transfer functions for efficient calculation of multidimensional transient heat transfer. *Journal of Heat Transfer*, 111(1), 5–12. <https://doi.org/10.1115/1.3250659>
- Sekhar, S. C., & Tan, L. T. (2009). Optimization of cooling coil performance during operation stages for improved humidity control. *Energy and Buildings*, 41(2), 229–233. <https://doi.org/10.1016/j.enbuild.2008.09.005>
- Shah, M. M. (1979). A general correlation for heat transfer during film condensation inside pipes. *International Journal of Heat and Mass Transfer*, 22(4), 547–556. [https://doi.org/10.1016/0017-9310\(79\)90058-9](https://doi.org/10.1016/0017-9310(79)90058-9)
- Sherman, M. H. (1987). Estimation of infiltration from leakage and climate indicators. *Energy and Buildings*, 10(1), 81–86. [https://doi.org/10.1016/0378-7788\(87\)90008-9](https://doi.org/10.1016/0378-7788(87)90008-9)
- Shirey, D., Henderson, H., & Raustad, R. (2006). Understanding the Dehumidification Performance of Air-Conditioning Equipment at Part-Load Conditions. 0641(321), 655–1063.
- Trcka, M., Wetter, M., & Hensen, J. (2007). COMPARISON OF CO-SIMULATION APPROACHES FOR BUILDING AND HVAC / R SYSTEM SIMULATION Technische Universiteit Eindhoven , Eindhoven , The Netherlands , Simulation Research Group , Building Technologies Department , Environmental Energy Technologies Division. *Proceedings of the Building Simulation*, May 2014, 3–5. http://www.bwk.tue.nl/bps/hensen/publications/07_BS07_trcka.pdf
- US Energy Information Administration. (2016). How much electricity is used for lighting in the United States? - FAQ - U.S. Energy Information Administration (EIA). [Www.Eia.Gov](http://www.Eia.Gov). <https://www.eia.gov/tools/faqs/faq.cfm?id=99&t=3>

- Wang, C. C., Tsai, Y. M., & Lu, D. C. (1998). Comprehensive study of convex-louver and wavy fin-and-tube heat exchangers. *Journal of Thermophysics and Heat Transfer*, 12(3), 423–430. <https://doi.org/10.2514/2.6354>
- Xia, Y., Deng, S., & Chan, M. Y. (2017). Inherent operational characteristics and operational stability of a variable speed direct expansion air conditioning system. *Applied Thermal Engineering*, 113, 268–277. <https://doi.org/10.1016/j.applthermaleng.2016.10.073>
- Xu, X., Deng, S., & Chan, M. (2008). A new control algorithm for direct expansion air conditioning systems for improved indoor humidity control and energy efficiency. *Energy Conversion and Management*, 49(4), 578–586. <https://doi.org/10.1016/j.enconman.2007.07.040>
- Xu, X., Xia, L., Chan, M., & Deng, S. (2010). Inherent correlation between the total output cooling capacity and equipment sensible heat ratio of a direct expansion air conditioning system under variable-speed operation (XXG SMD SHR DX AC unit). *Applied Thermal Engineering*, 30(13), 1601–1607. <https://doi.org/10.1016/j.applthermaleng.2010.03.016>
- Yadav, Y. K. (1995). Vapour-compression and liquid-desiccant hybrid solar space-conditioning system for energy conservation. *Renewable Energy*, 6(7), 719–723. [https://doi.org/10.1016/0960-1481\(95\)00009-9](https://doi.org/10.1016/0960-1481(95)00009-9)
- Zhou, X., Hong, T., & Yan, D. (2014). Comparison of HVAC system modeling in EnergyPlus, DeST and DOE-2.1E. *Building Simulation*, 7(1), 21–33. <https://doi.org/10.1007/s12273-013-0150-7>
- Ziviani, D., Bahman, A., & Groll, E. (2019). Multi-input multi-output (MIMO) artificial neural network (ANN) models applied to economized scroll compressors. 2016. <https://doi.org/10.18462/iir.icr.2019.1321>
- Ziviani, D., Bell, I. H., Zhang, X., Lemort, V., Paepe, M. De, Braun, J. E., & Groll, E. A. (2020). PDSim: Demonstrating the capabilities of an open-source simulation framework for positive displacement compressors and expanders. *International Journal of Refrigeration*, 110, 323–339. <https://doi.org/10.1016/j.ijrefrig.2019.10.015>